Aeroelastic rotor design minimizing the loads

Døssing, Mads; Bak, Christian

Published in:
Presentations from the Aeroelastic Workshop – latest results from AeroOpt

Publication date:
2011

Document Version
Publisher's PDF, also known as Version of record

Risø DTU

Presentations from the Aeroelastic Workshop – latest results from AeroOpt

Risø-R-Report

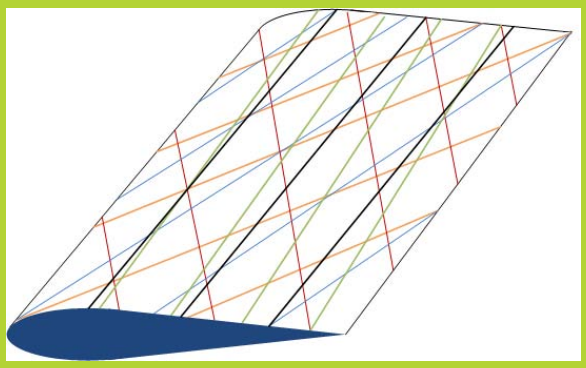

$$\begin{Bmatrix} F_x \\ F_y \\ F_z \\ M_x \\ M_x \\ M_x \end{Bmatrix} = \begin{bmatrix} S_{11} & S_{12} & & S_{14} & & \\ & S_{22} & & & S_{25} & \\ & & S_{33} & & & S_{36} \\ & & & S_{44} & S_{45} & \\ & & & & S_{55} & \\ & & & & & S_{66} \end{bmatrix} \begin{Bmatrix} \varepsilon_x \\ \varepsilon_y \\ \varepsilon_z \\ \kappa_x \\ \kappa_y \\ \kappa_z \end{Bmatrix}$$

Morten Hartvig Hansen (Ed.)
Risø-R-1769(EN)
February 2011

Risø DTU
National Laboratory for Sustainable Energy

Author: Morten Hartvig Hansen (Ed.)
Title: Presentations from the Aeroelastic Workshop – latest results from AeroOpt
Division: Wind Energy Division

Risø-R-1769(EN)
February 2011

Abstract (max. 2000 char.):

This report contains the slides of the presentations at the Aeroelastic Workshop held at Risø-DTU for the wind energy industry in Denmark on January 27, 2011. The scientific part of the agenda at this workshop was

- Anisotropic beam element in HAWC2 for modelling of composite lay-ups (Taeseong Kim)
- Nonlinear beam element in HAWC2 for modelling of mooring systems (Bjarne Kallesøe)
- Enhanced BEM including wake expansion and swirl (Christian Bak)
- Unsteady viscous-inviscid interactive airfoil code for wind turbines (Néstor Ramos García)
- PIV measurements on model scale wind turbine in water channel (Robert Mikkelsen)
- Potential of fatigue and extreme load reductions on swept blades using HAWC2 (David Verelst)
- Aeroelastic modal analysis of backward swept blades using HAWCStab2 (Morten H. Hansen)
- Aeroelastic rotor design minimizing the loads (Christian Bak)
- A small study of flat back airfoils (Niels N. Sørensen)
- Status of airfoil design and plans for wind tunnel tests of new thick airfoils (Christian Bak)

The presented results are mainly obtained in the EUDP project “Aeroelastic Optimization of MW Wind Turbines (AeroOpt)” funded under contract no. 63011-0190.

ISSN 0106-2840
ISBN 978-87-550-3885-1

Contract no.:
EUDP 63011-0190

Group's own reg. no.:
1110073

Sponsorship:

Cover :

Pages:204
Tables:0
References:0

Information Service Department
Risø National Laboratory for Sustainable Energy
Technical University of Denmark
P.O.Box 49
DK-4000 Roskilde
Denmark
Telephone +45 46774005
bibl@risoe.dtu.dk
Fax +45 46774013
www.risoe.dtu.dk

Contents

Preface

This report contains the slides of the presentations at the Aeroelastic Workshop held at Risø-DTU for the wind energy industry in Denmark on January 27, 2011. The scientific part of the agenda at this workshop was

- Anisotropic beam element in HAWC2 for modelling of composite lay-ups (Taeseong Kim)
- Nonlinear beam element in HAWC2 for modelling of mooring systems (Bjarne Kallesøe)
- Enhanced BEM including wake expansion and swirl (Christian Bak)
- Unsteady viscous-inviscid interactive airfoil code for wind turbines (Néstor Ramos García)
- PIV measurements on model scale wind turbine in water channel (Robert Mikkelsen)
- Potential of fatigue and extreme load reductions on swept blades using HAWC2 (David Verelst)
- Aeroelastic modal analysis of backward swept blades using HAWCStab2 (Morten H. Hansen)
- Aeroelastic rotor design minimizing the loads (Christian Bak)
- A small study of flat back airfoils (Niels N. Sørensen)
- Status of airfoil design and plans for wind tunnel tests of new thick airfoils (Christian Bak)

The presented results are mainly obtained in the EUDP project “Aeroelastic Optimization of MW Wind Turbines (AeroOpt)” funded under contract no. 63011-0190.

1 Anisotropic beam element

Anisotropic Beam Element in HAWC2 for Modeling of Composite lay-ups

Taeseong Kim

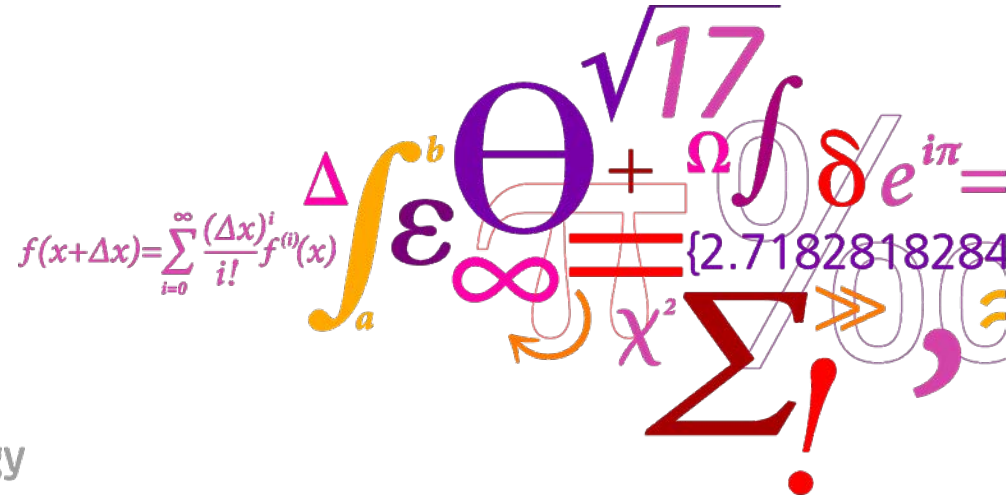

Risø DTU
National Laboratory for Sustainable Energy

Introduction

- All of composite blades have anisotropic material properties due to different layup angles.
  - It introduces addtional bending-bending and bending-twist couplings.
- The existing beam model in HAWC2 is capable for modeling of geometric couplings e.g the offset between elastic axis and shear center
  - The offset introduces the bending and torsion couplings
- Aeroelastic codes such as HAWC2, Bladed, FAST, and Flex are using classical engineering beam models.
- Classical beam models are derived by assuming isotropic material beam properties.
  - Anisotropic material properties of composite beam cannot be modeled with those classical beam models.

Typical layup conditions

±45deg layup angle

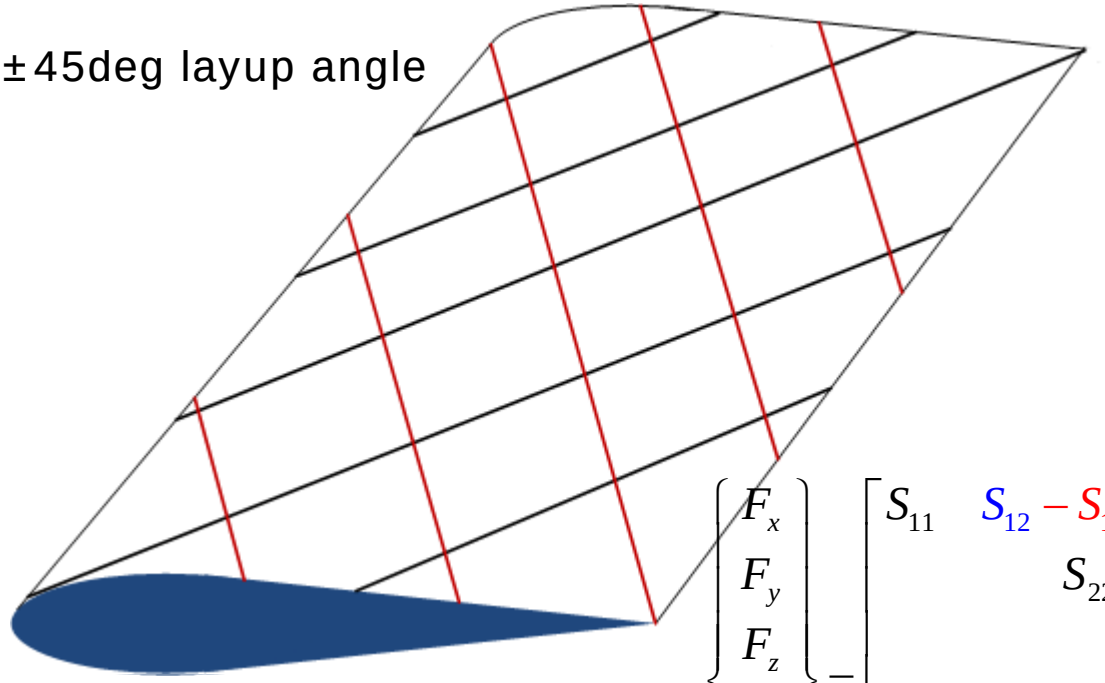

$$\begin{Bmatrix} F_x \\ F_y \\ F_z \\ M_x \\ M_x \\ M_x \end{Bmatrix} = \begin{bmatrix} S_{11} & S_{12}-S_{12}=0 & & & & \\ & S_{22} & & & & \\ & & S_{33} & & & \\ & & & S_{44} & S_{45}-S_{45}=0 & \\ & & & & S_{55} & \\ & & & & & S_{66} \end{bmatrix} \begin{Bmatrix} \varepsilon_x \\ \varepsilon_y \\ \varepsilon_z \\ \kappa_x \\ \kappa_y \\ \kappa_z \end{Bmatrix}$$

Possible new layup conditions

$[\theta_1/\theta_2/\theta_3/\theta_4/\theta_5]_T$

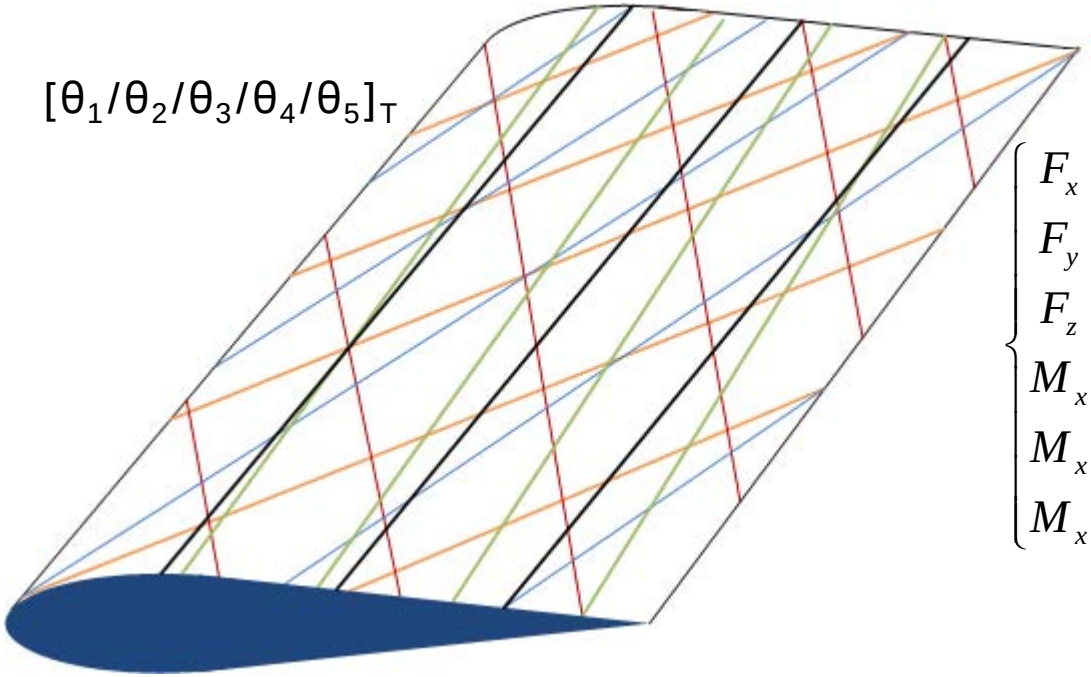

$$\begin{Bmatrix} F_x \\ F_y \\ F_z \\ M_x \\ M_x \\ M_x \end{Bmatrix} = \begin{bmatrix} S_{11} & S_{12} & & S_{14} & & \\ & S_{22} & & & S_{25} & \\ & & S_{33} & & & S_{36} \\ & & & S_{44} & S_{45} & \\ & & & & S_{55} & \\ & & & & & S_{66} \end{bmatrix} \begin{Bmatrix} \varepsilon_x \\ \varepsilon_y \\ \varepsilon_z \\ \kappa_x \\ \kappa_y \\ \kappa_z \end{Bmatrix}$$

- To analyze anisotropic composite blade ***anisotropic beam model*** should be introduced.

Method

- General FEM approach is considered to develop new a Timoshenko beam model.
- 2 nodes element is fixed for structural elements.
  - 2 nodes element is used for aerodynamic elements.
  - Linear shape function is available.
  - Linear shape function needs to have more elements.
  - Time cost is increased.
- 2 nodes element with higher order of the polynomial shape function is developed.
- Steady deflections are compared.
- Natural frequencies (Hz) for box beams are compared.
- Mode shapes are compared.
- Cross-sectional stiffness and mass matrix are given from the references.

Cases

- CASE 1: Wenbin Yu (2007)
  - Length of the beam: 7.5*in*
  - Graphite-Epoxy $[30°]_T$, rectangular box beam

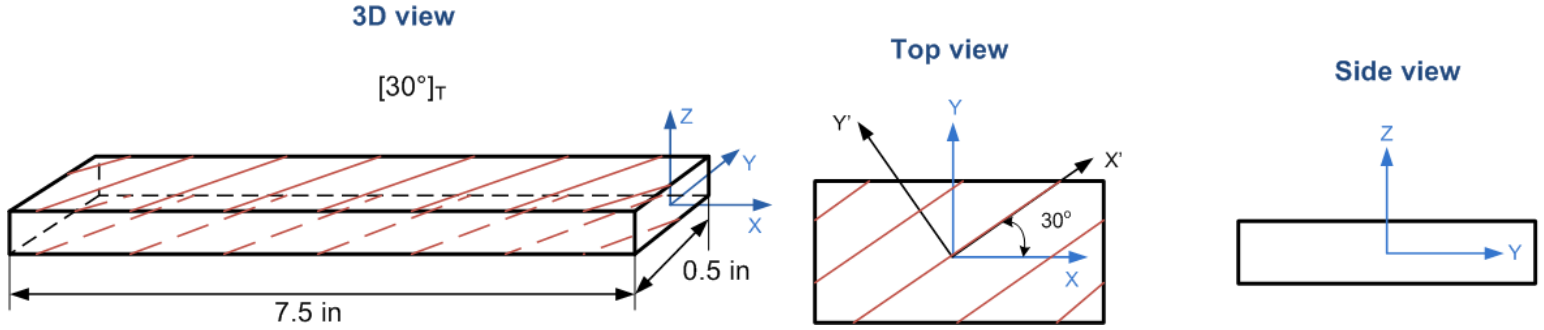

- CASE 2: Hodges *et al.* (1991)
  - Length of the beam: 100*in*
  - Graphite-Epoxy $[20°/-70°/20°/-70°/-70°/20°]_T$, rectangular box beam

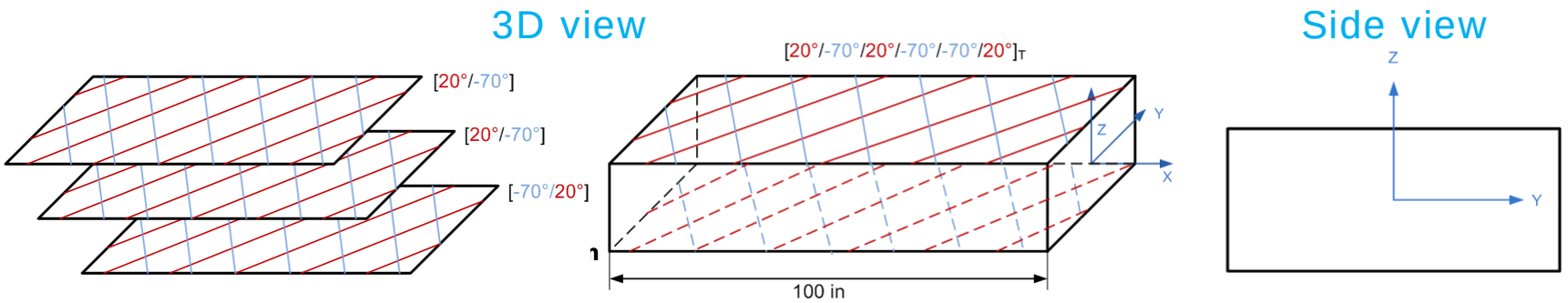

Results (case 1)

- Graphite-Epoxy $[30°]_T$, rectangular box beam

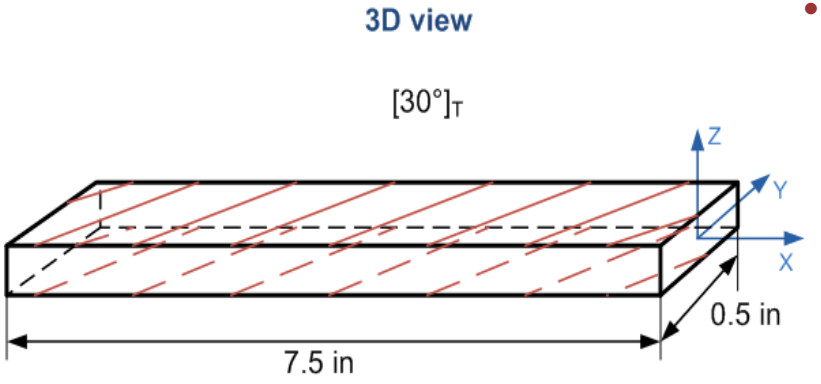

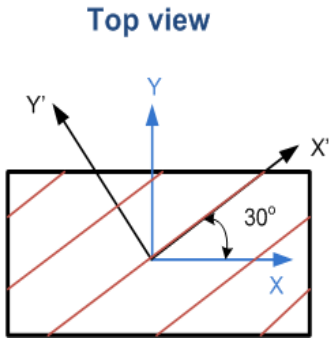

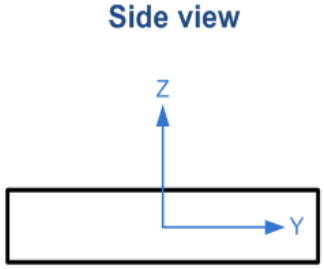

- The material properties and the dimensions of the structure

E_{11}	18.73×10^{6} psi
E_{22}, E_{33}	1.364×10^{6} psi
G_{12}	0.7479×10^{6} psi
G_{13}	0.6242×10^{6} psi
G_{23}	0.3686×10^{6} psi
$\nu_{12}, \nu_{13}, \nu_{24}$	0.3
ρ	1.450×10^{-4} lb.sec^2/in.^{4}
Width	0.5 in
Thickness	0.125 in
Length	7.5 in

Static analysis with cantilever beam (case 1)

- 2 nodes with 6th order polynomial

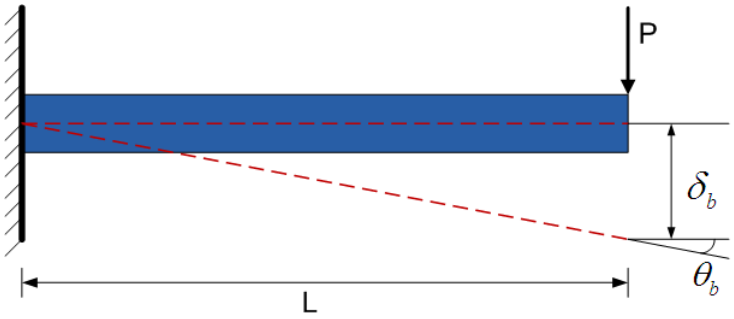

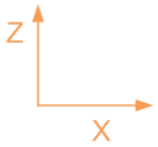

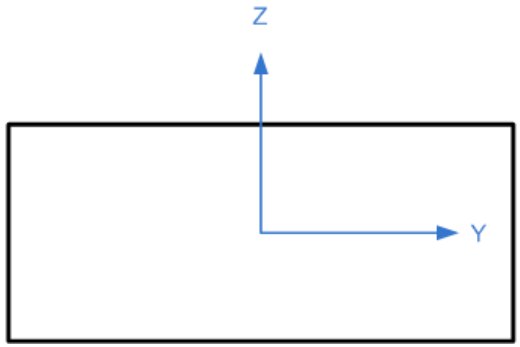

where L = 7.5in, P = -1lb

$$[s] = \begin{bmatrix} S_{11} & S_{12} & 0 & 0 & 0 & 0 \\ S_{12} & S_{22} & 0 & 0 & 0 & 0 \\ 0 & 0 & S_{33} & 0 & 0 & 0 \\ 0 & 0 & 0 & S_{44} & S_{45} & 0 \\ 0 & 0 & 0 & S_{45} & S_{55} & 0 \\ 0 & 0 & 0 & 0 & 0 & S_{66} \end{bmatrix}$$

- Anisotropic stiffness properties
  - Axial-lateral coupling
  - Torsion-flapwise bending

Static analysis with cantilever beam (case 1)

- 2 nodes with 6th order polynomial

Axial deflection

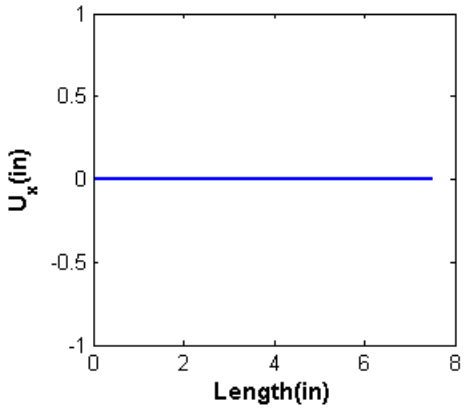

Edgewise deflection

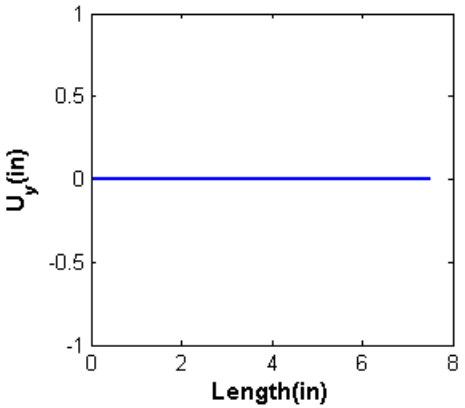

Flapwise deflection

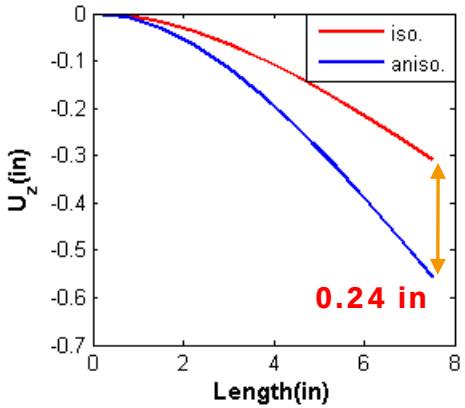

Torsion

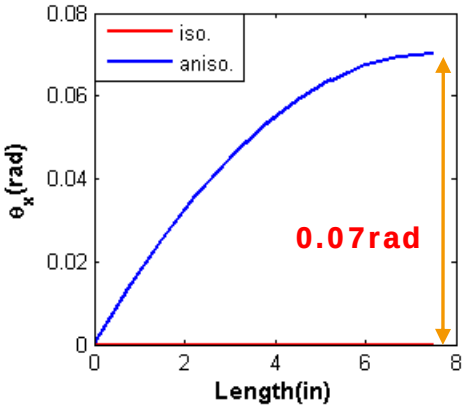

Edgewise bending

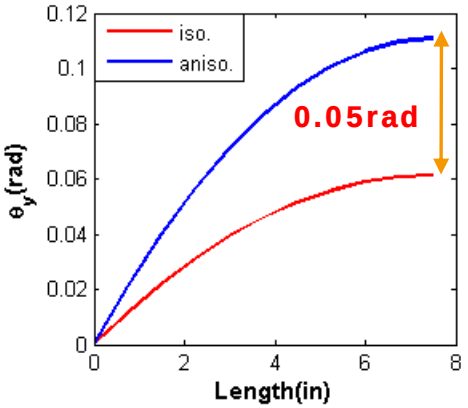

Flapwise bending

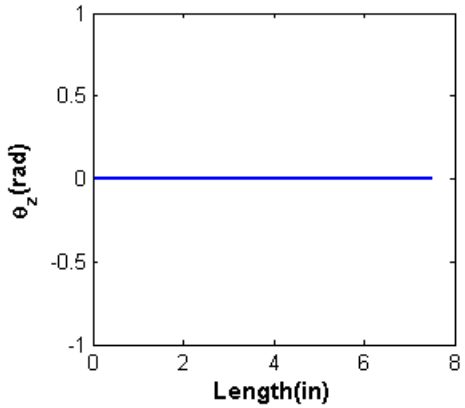

Comparisons of the natural frequencies (case 1)

Mode	Isotropic [Hz]	Anisotropic [Hz]
1(Flap)	70.6	52.6
2(Edge)	210.3	209.9
3(Flap)	436.5	327.3
4(Flap)	1197.9	906.7
5(Edge)	1304.8	1292.5
6(Flap)	2282.9	1752.9

Comparisions of the mode shapes (case 1)

1st Flap mode

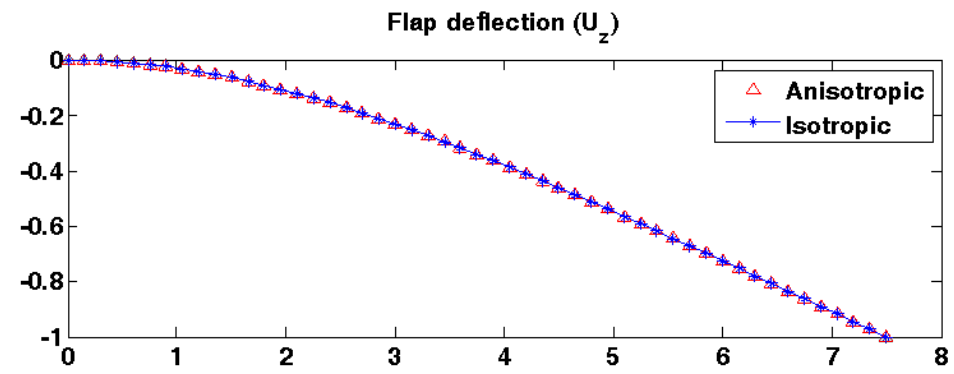

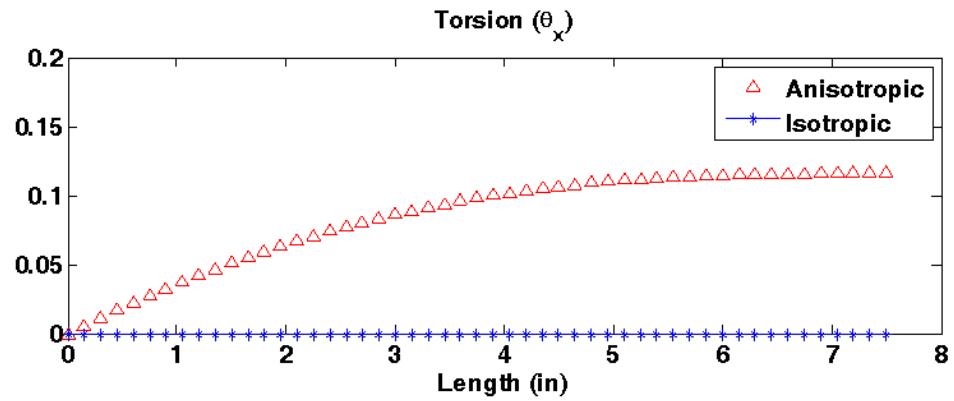

2nd Flap mode

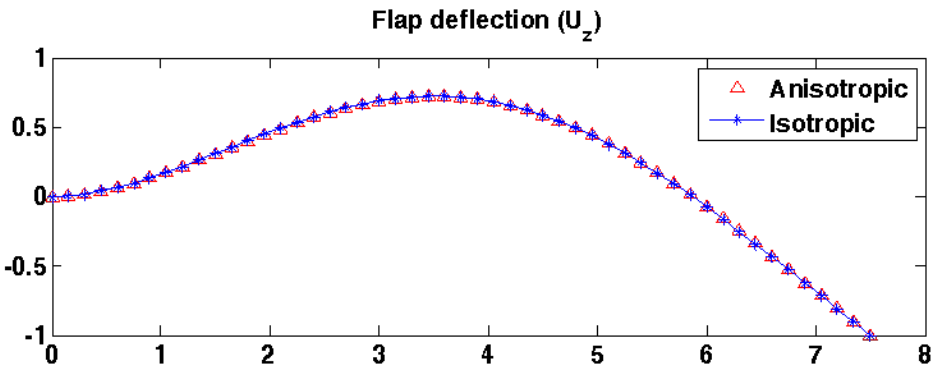

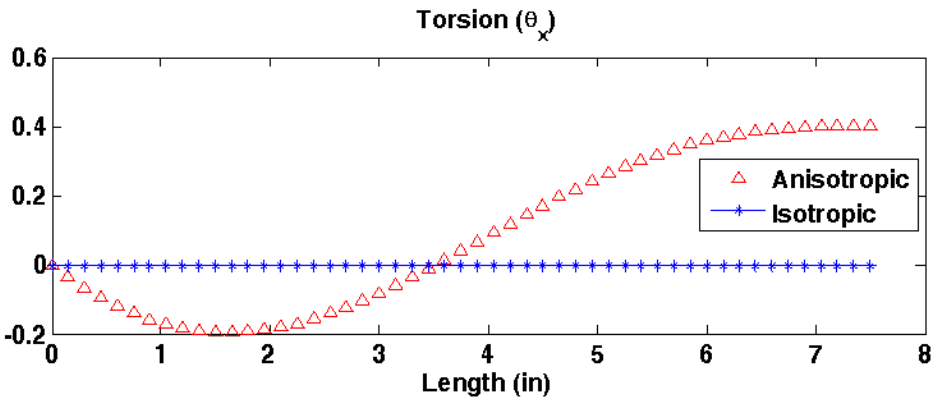

Results (case 2)

- Graphite-Epoxy $[20°/-70°/20°/-70°/-70°/20°]_T$, rectangular box beam

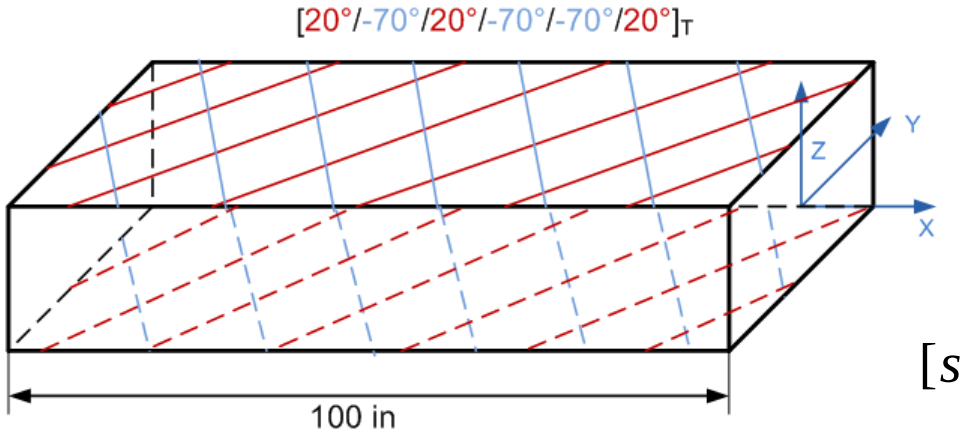

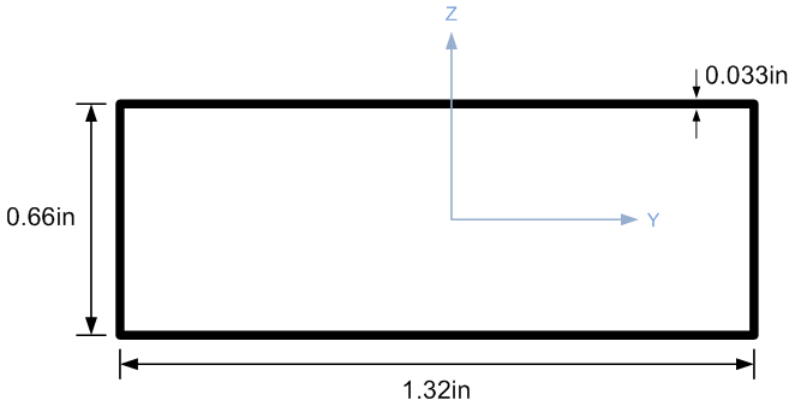

$$[s] = \begin{bmatrix} S_{11} & 0 & 0 & S_{14} & 0 & 0 \\ 0 & S_{22} & 0 & 0 & S_{25} & 0 \\ 0 & 0 & S_{33} & 0 & 0 & S_{36} \\ S_{14} & 0 & 0 & S_{44} & 0 & 0 \\ 0 & S_{25} & 0 & 0 & S_{55} & 0 \\ 0 & 0 & S_{36} & 0 & 0 & S_{66} \end{bmatrix}$$

where [s]: sectional stiffness matrix

Static analysis with cantilever beam (case 2)

- 2 nodes with 6th order polynomial

Axial deflection

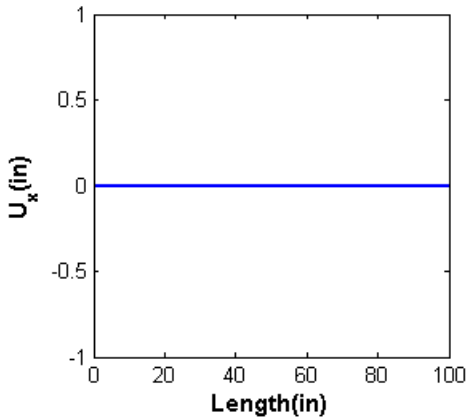

Edgewise deflection

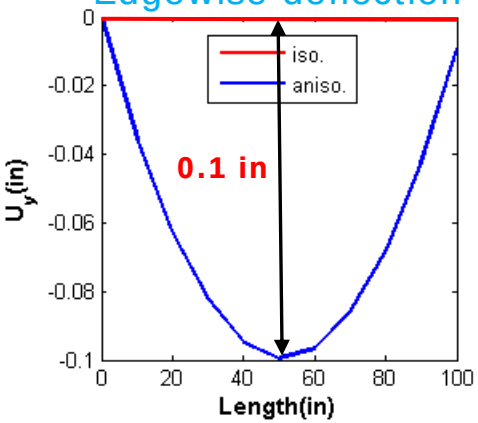

Flapwise deflection

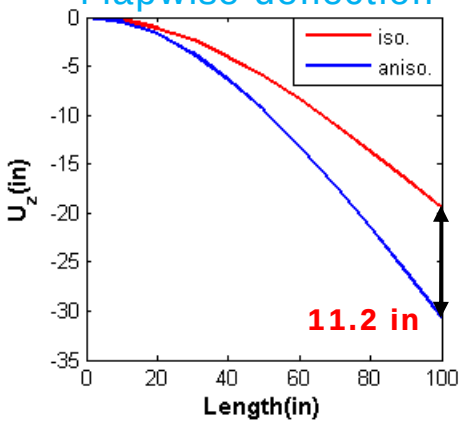

Torsion

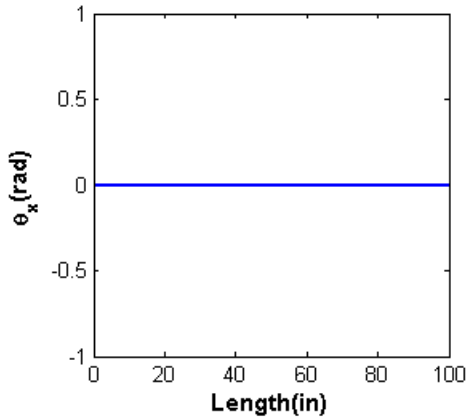

Edgewise bending

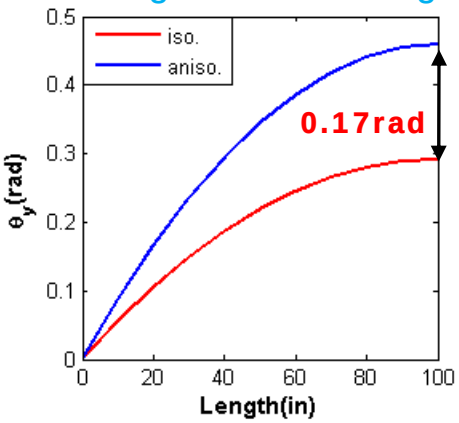

Flapwise bending

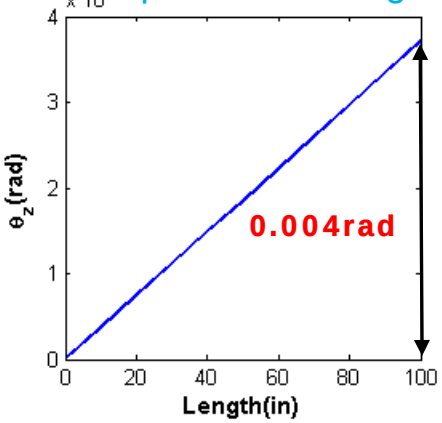

Comparisons of the natural frequencies (case 2)

	Isotropic [Hz]	Anisotropic [Hz]
1(Flap)	3.69	2.95
1(Edge)	6.43	5.09
2(Flap)	23.12	18.44
2(Edge)	40.23	31.84
3(Flap)	64.53	51.59
3(Edge)	112.22	87.95

Comparisions of the mode shapes (case 2)

3rd Flap mode

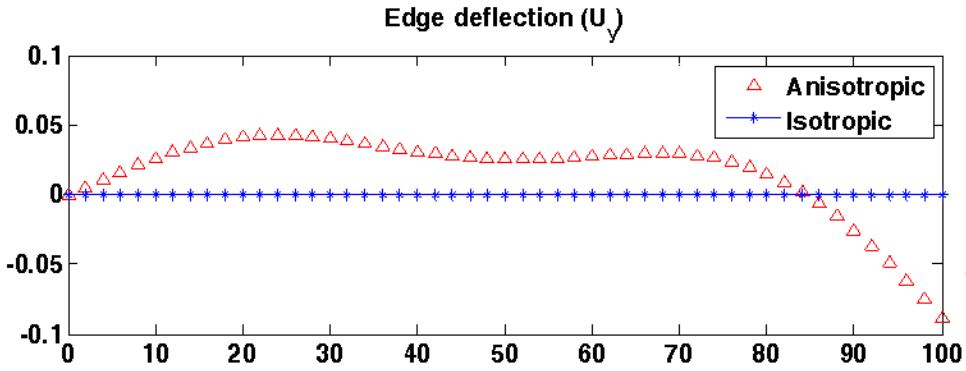

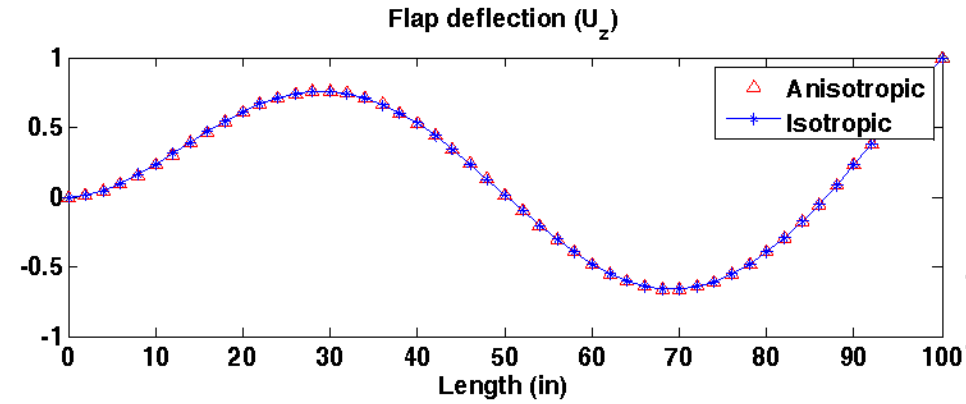

3rd Edge mode

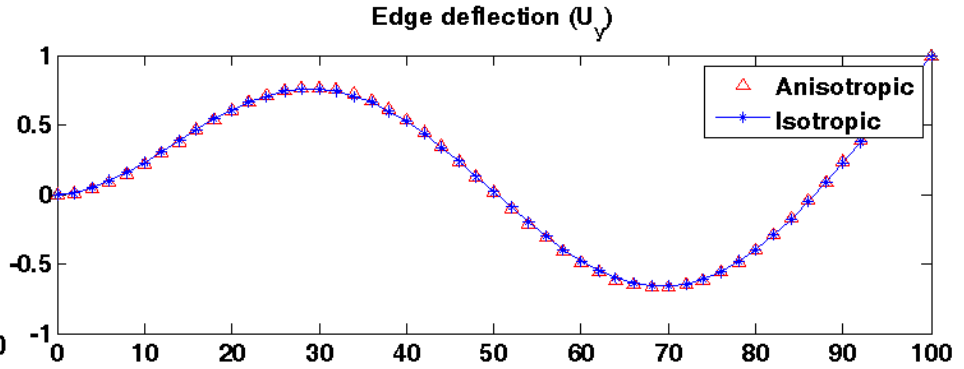

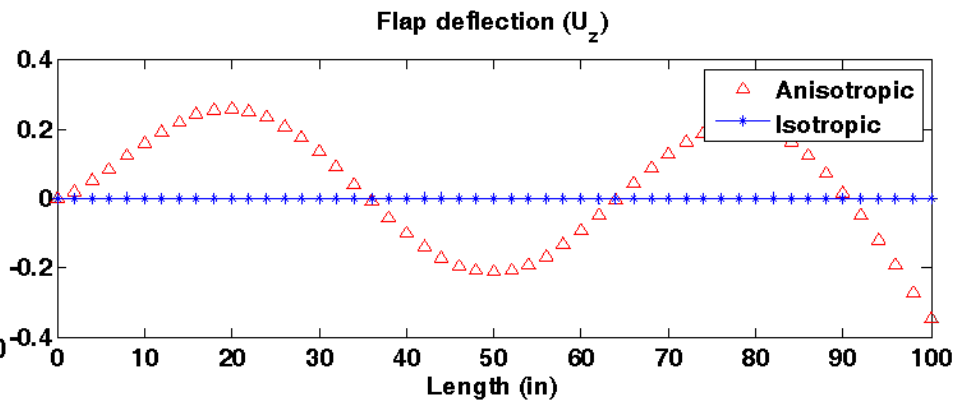

Conclusions

- Steady deflections for isotropic and anisotropic cases
  - Anisotropic beam deflects more than isotropic beam.

- Natural frequencies
  - Natural frequencies with isotropic material are higher than the frequencies for anisotropic material.

- Mode shapes
  - More coupling effects are illustrated when anisotropic materials are considered.
    - For the case 1, torsion mode is coupled with flap mode.
    - For the case 2, edge mode is coupled with flap mode.

Future works

- Future works
  - New element is going to be added in HAWC2.
  - More validations
    - Simple static analysis
    - Dynamic analysis
  - Tailoring study
    - Designing composite blade
  - What are the effects of anisotropic beam properties on loads ????

Thank you for your attention

2 Nonlinear beam element

Nonlinear beam element in HAWC2 for modeling of mooring systems

Bjarne S. Kallesøe, Risø DTU
Anders M. Hansen, Siemens Wind Power A/S

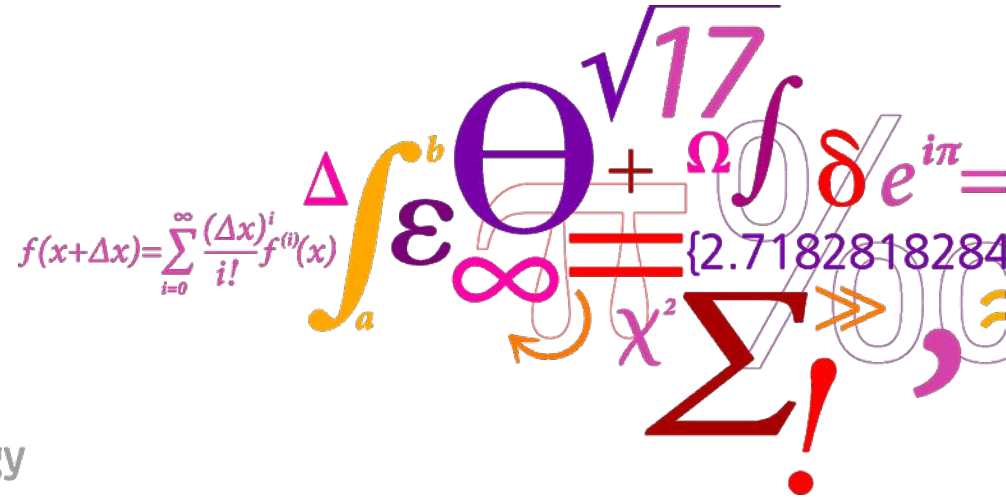

Risø DTU
National Laboratory for Sustainable Energy

Background and motivation

- Increasing focus on floating turbine concepts
- Mooring system an integrated part of the overall system dynamic
- Present mooring modeling in HAWC2
  - Quasi-static nonlinear stiffness based on pre-computed mooring line characteristic
  - Pros
    - Fast computations, based on well known mooring model
  - Cons
    - Quasi-static, symmetric mooring forces, complicated modeling based on external program
- Develop new mooring system model that:
  - Includes dynamic mooring lines to:
    - Analyze the effect and importance of such on overall system dynamic
    - Analyze loads on mooring systems
  - Is capable of modeling different mooring layouts

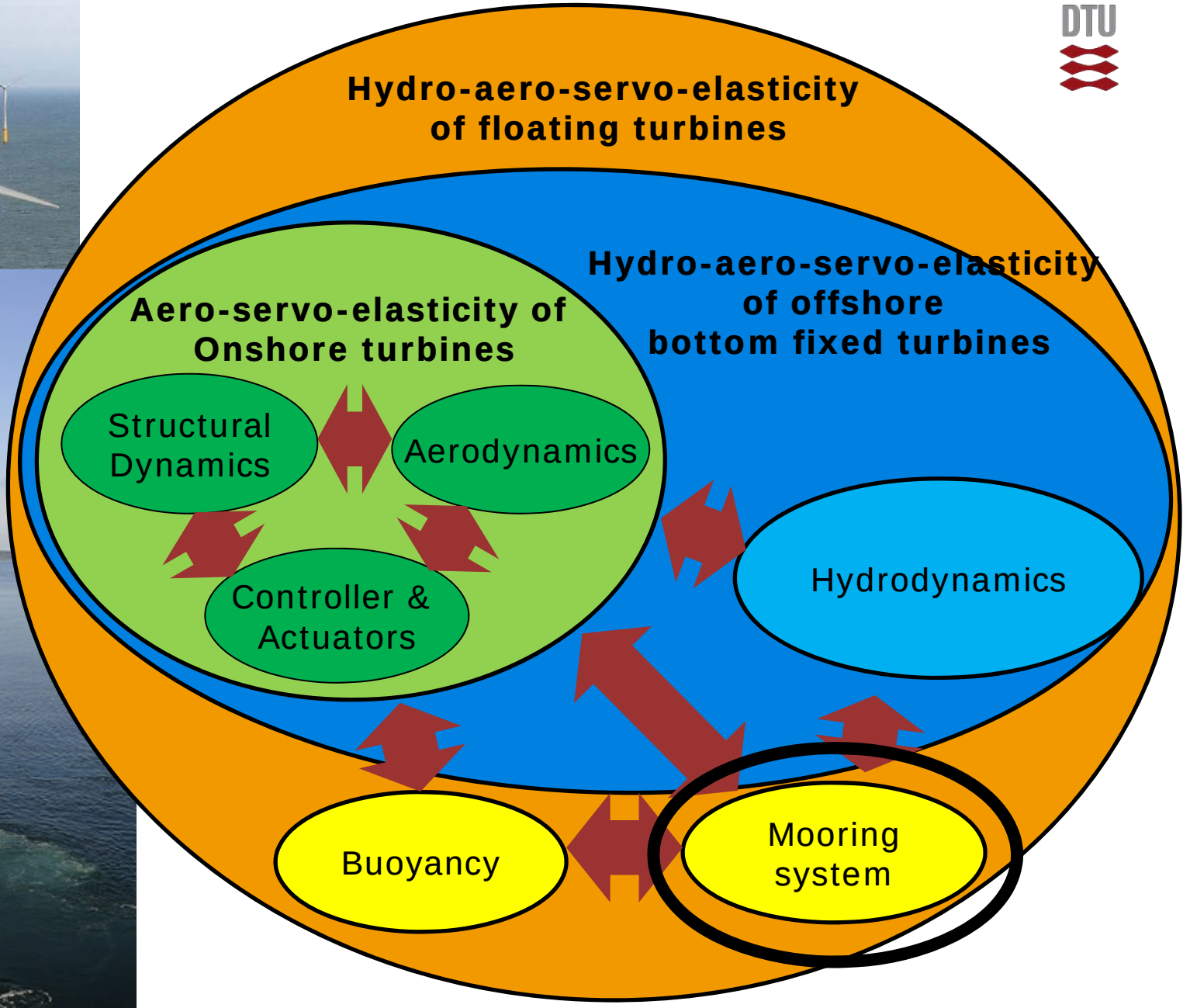
Hydro-aero-servo-elasticity
of floating turbines
Hydro-aero-servo-elasticity
of offshore
bottom fixed turbines
Aero-servo-elasticity of
Onshore turbines
Structural
Dynamics
Aerodynamics
Controller &
Actuators
Hydrodynamics
Buoyancy
Mooring
system

Mooring system

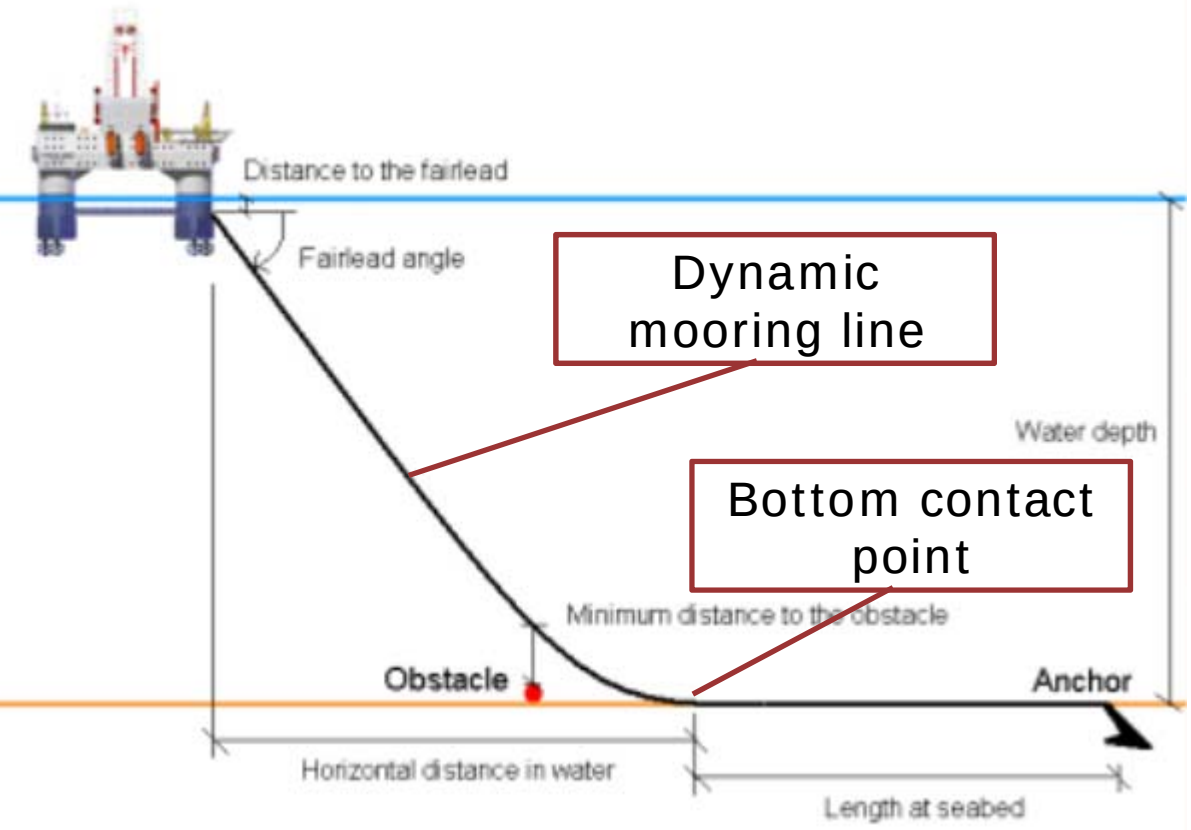

•Modeling split into two sections:

1) Bottom contact section; 2D inelastic quasi-static solution to determine bottom connection point
2) Dynamic mooring line section; nonlinear element with longitudinal flexibility and no bending stiffness. Includes drag, buoyancy and concentrated masses

Bottom contact section

- Bottom section model quasi-static in 2D, determine the radius to bottom contact point and the height and radius at the connection point to the mooring line
- Highly nonlinear problem

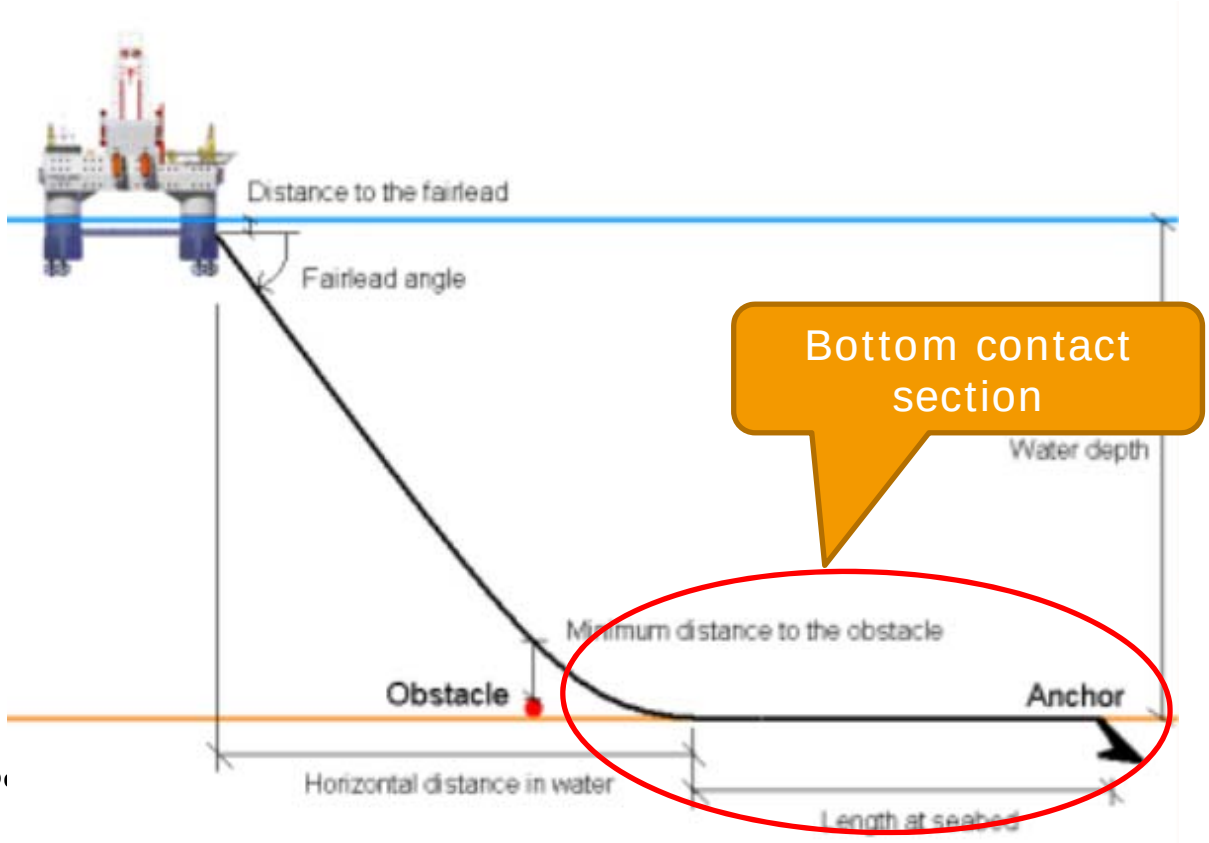

Bottom contact section

- Problem: given a connection point from the main solver, find the bottom contact point, line force and angle at connection point
- Solution scheme
  1. Get a guess on connection point from main solver
  2. Compute the bottom contact point by an iterative solution of the quasi-static equilibrium between free anchor chain and angle at connection point
  3. Compute vertically line force component by weight of floating anchor chain
  4. Compute horizontal line force component by angle at connection point
  5. Return line forces as residual of unconstrained equations to main solver

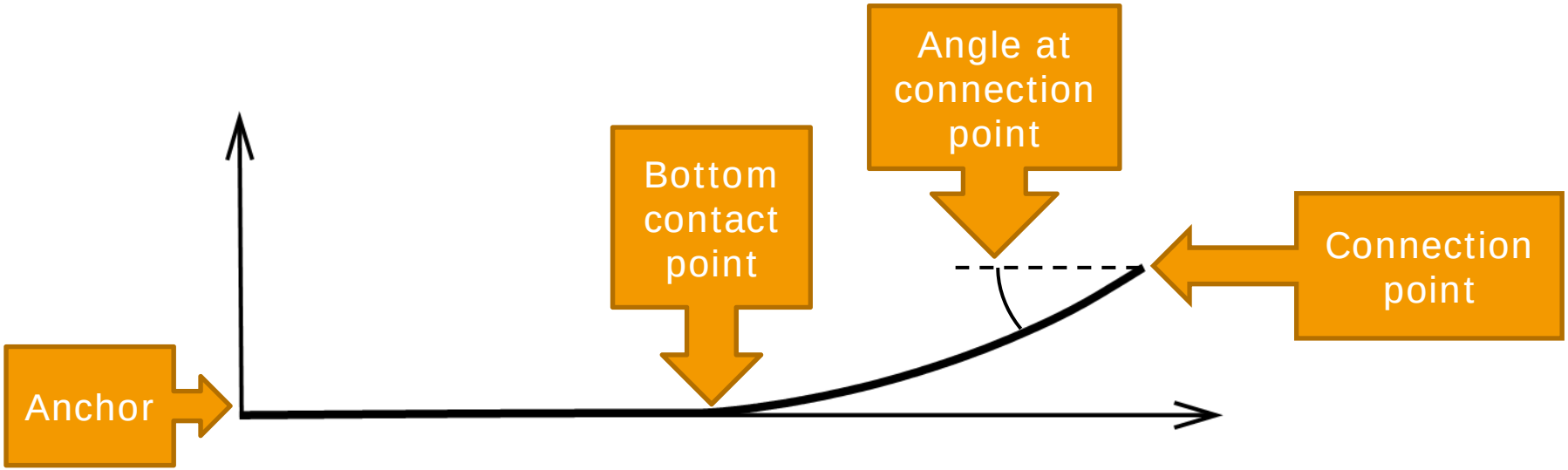

Dynamic mooring line section

- Mooring line divided into sections with uniform stiffness, mass and hydrodynamic characteristic
- Each section divided equidistantly into a number of 2 node elements
- Concentrated masses and drag points can be added to any node

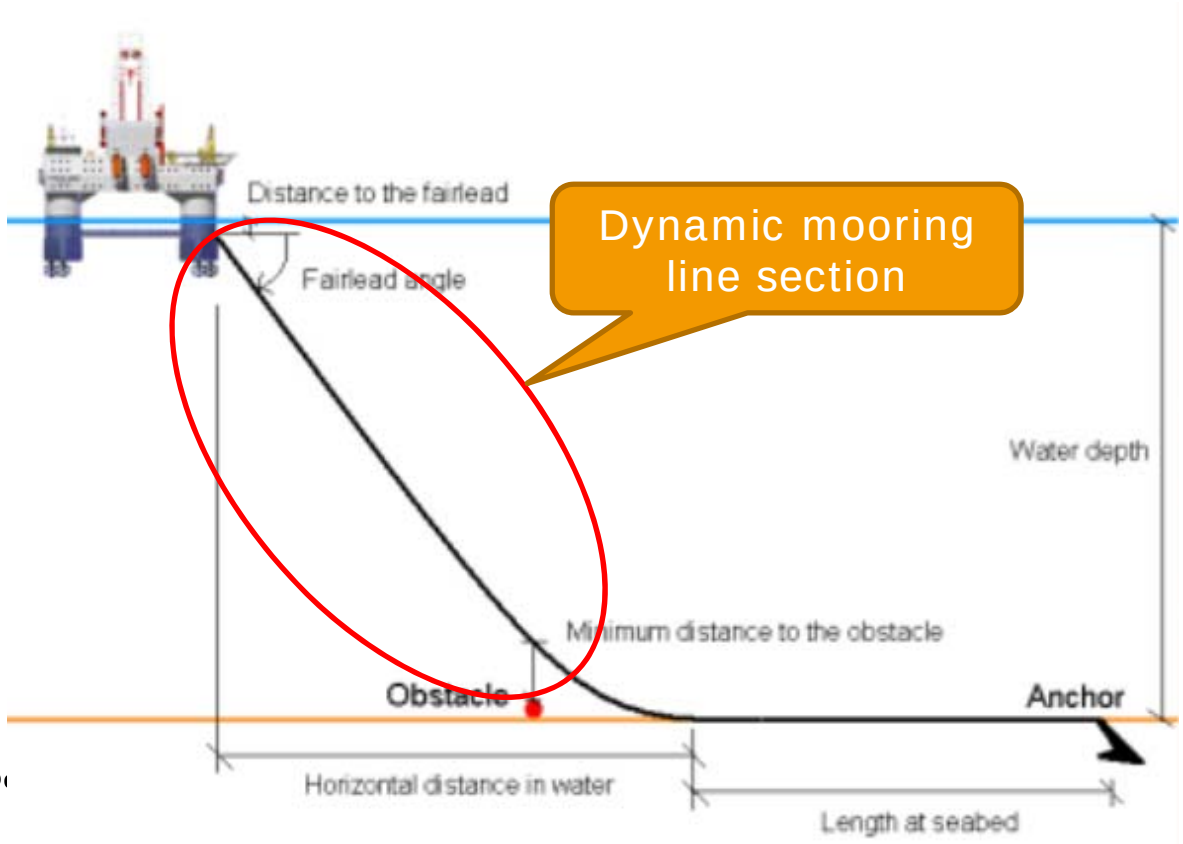

Nonlinear stiffness term

One line segment with uniform properties

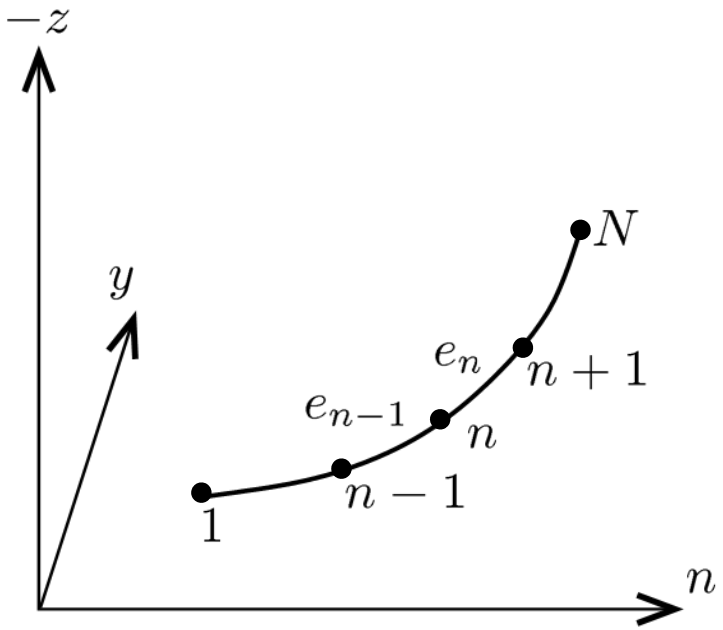

Length of element:

$$L_n = (x_{n-1} - x_n)^2 + (y_{n-1} - y_n)^2 + (z_{n-1} - z_n)^2$$

Green strain:

$$\epsilon_G = \frac{L_n^2 - L_{n,0}^2}{2L_{n,0}^2}$$

Axial force in element:

$$f = EA\epsilon_G$$

Element stiffness matrix:

$$K_e = f/L_n \begin{bmatrix} 1 & 0 & 0 & -1 & 0 & 0 \\ 0 & 1 & 0 & 0 & -1 & 0 \\ 0 & 0 & 1 & 0 & 0 & -1 \\ -1 & 0 & 0 & 1 & 0 & 0 \\ 0 & -1 & 0 & 0 & 1 & 0 \\ 0 & 0 & -1 & 0 & 0 & 1 \end{bmatrix}$$

Nodal elastic forces:

$$K_e \begin{bmatrix} \mathbf{x}_n \\ \mathbf{x}_{n+1} \end{bmatrix} = \begin{bmatrix} -f\delta \\ f\delta \end{bmatrix}, \quad \delta = \begin{bmatrix} \frac{x_{n+1}-x_n}{L_n} \\ \frac{y_{n+1}-y_n}{L_n} \\ \frac{z_{n+1}-z_n}{L_n} \end{bmatrix}$$

Equations of motion

Unconstrained equation of motion:

$$\mathbf{M}\ddot{\mathbf{x}}(t) + \mathbf{K}(\mathbf{x}, t)\mathbf{x}(t) - F_{gravity} - F_{buoyancy} - F_{drag}(\mathbf{x}, \dot{\mathbf{x}}, t) = \text{residual}$$

One line segment with uniform properties

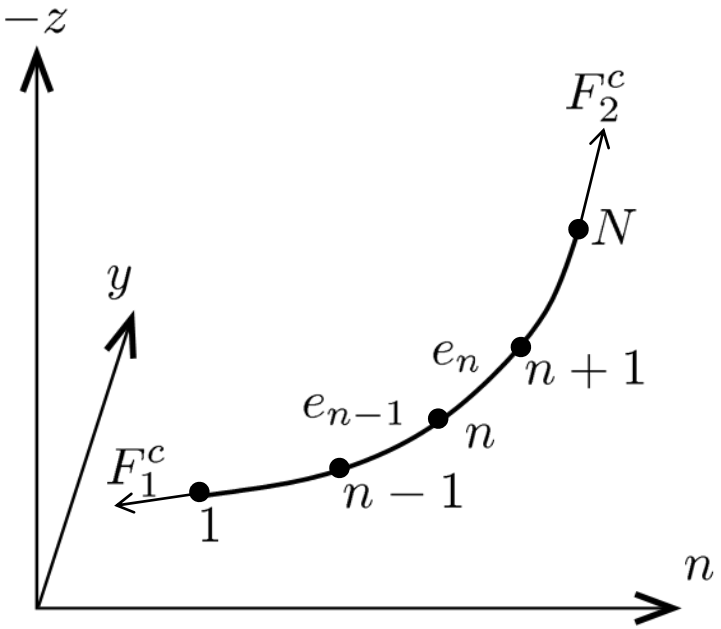

Constrain forces from constrain conditions:
1) distance from end of 2D bottom contact section to node 1 of first line segment = 0
2) distance from node N of one line segment to node 1 of the next segment = 0
3) distance from node N of last line segment to node n on a HAWC2 body = 0

Implementation in HAWC2

- The mooring system model is implemented in HAWC2 by an external system DLL interface that couples external systems with its one degrees of freedom to the HAWC2 model in a tightly coupled manner.

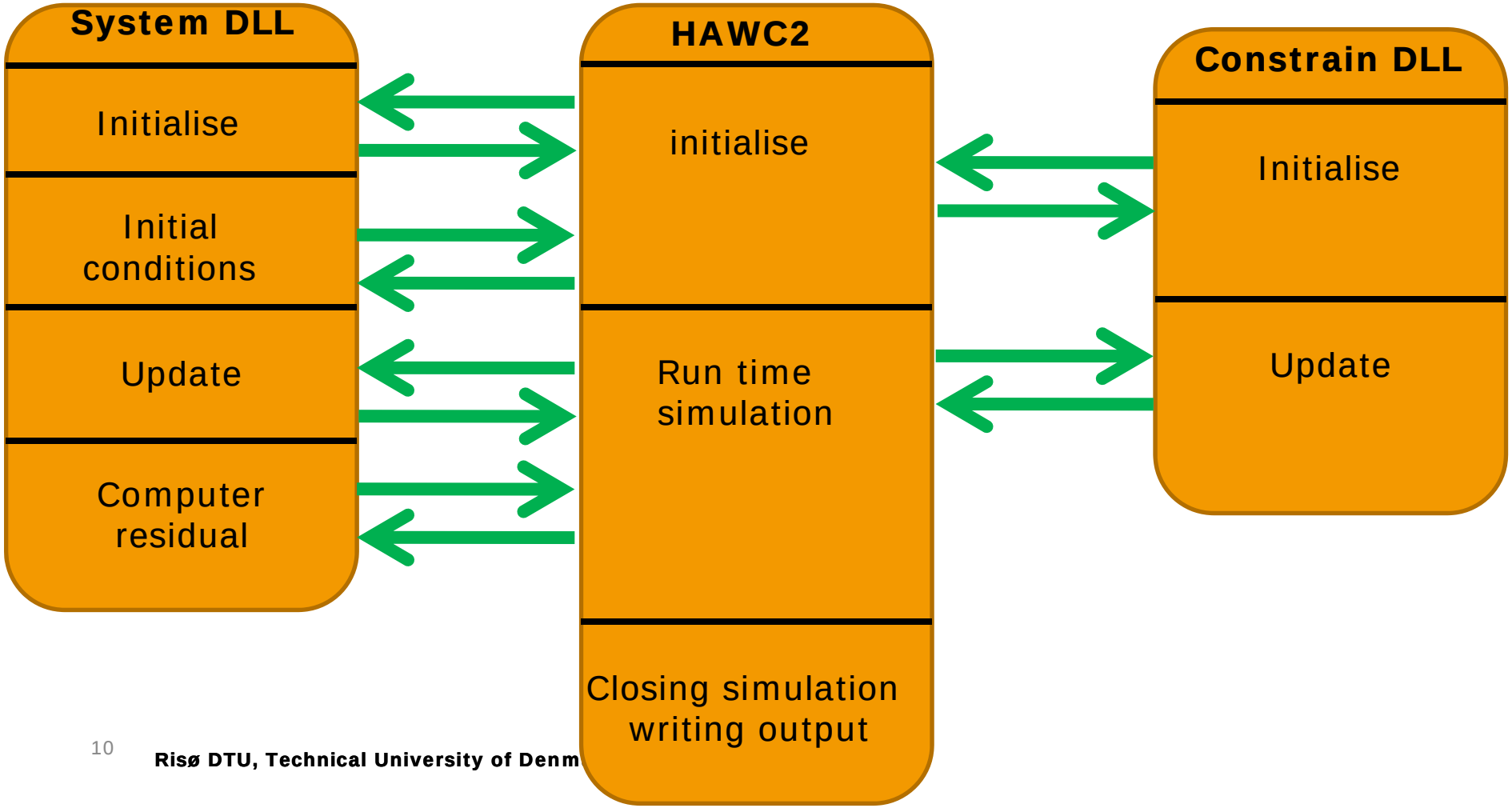

Mooring system model with one line

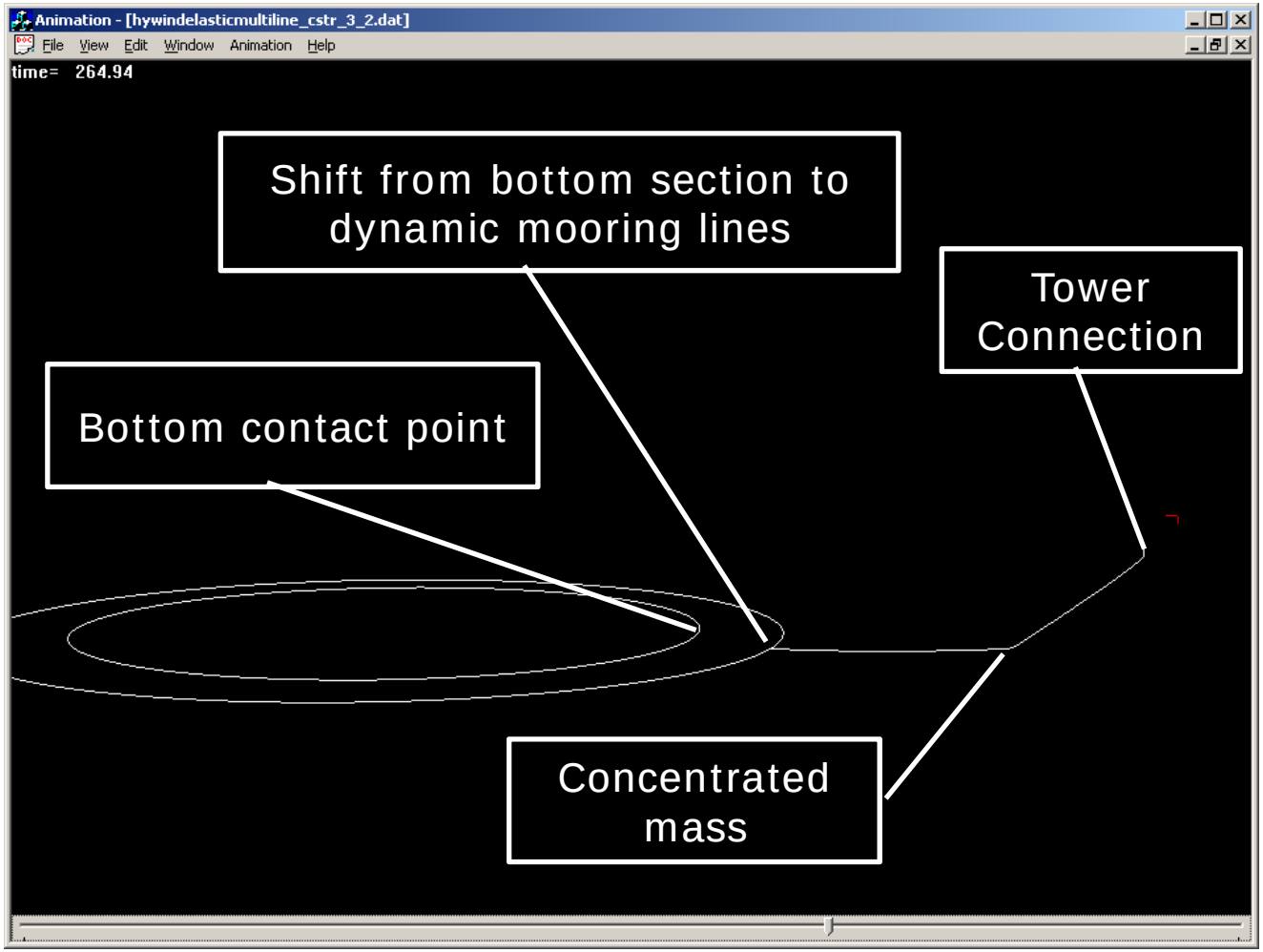

Quasi-static results (one line)

- Quasi-static results by moving tower connection point slowly back and forth
- Fits well to MIMOSA results

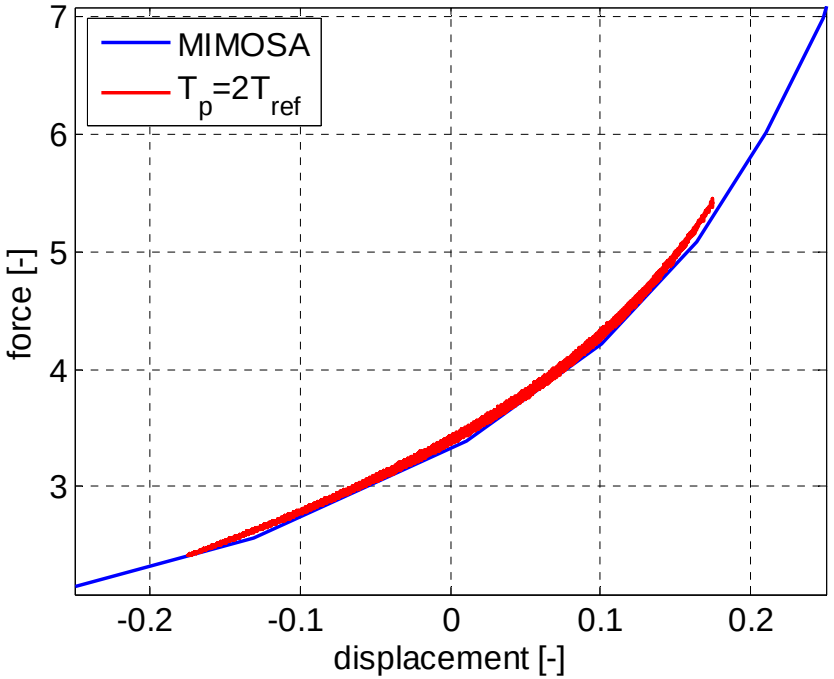

Result normalized by:
•Aerodynamic trust at rated power
•Rotor diameter and
•Systems natural surge period

Dynamic results (one line)

- Increasing oscillation frequency opens the loop

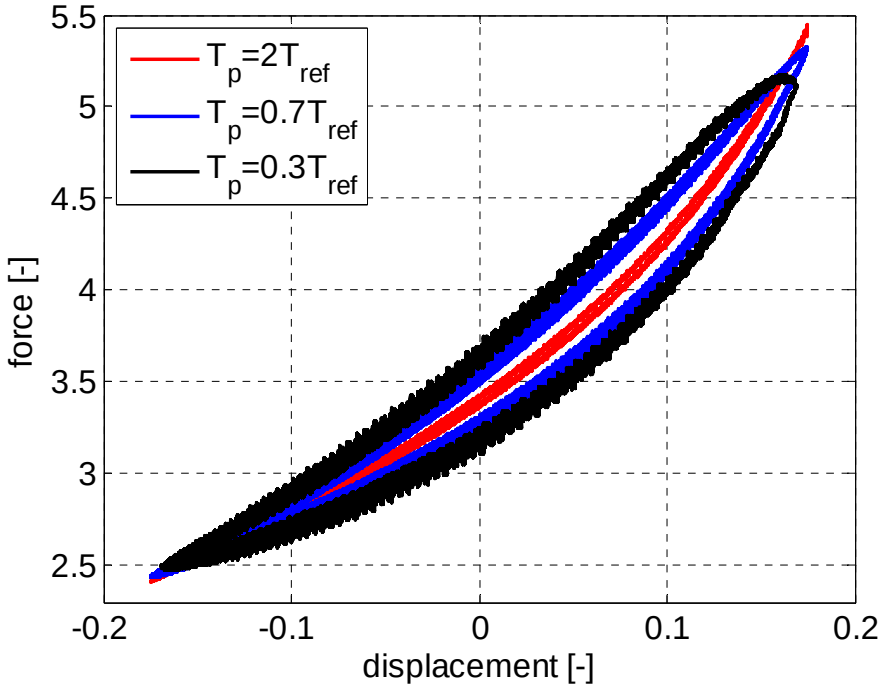

Result normalized by:
- Aerodynamic trust at rated power
- Rotor diameter and
- Systems natural surge period

Three line mooring system

- Mooring system as the one used in the OC3 project
- Three mooring lines, each with a concentrate mass to increase stiffness

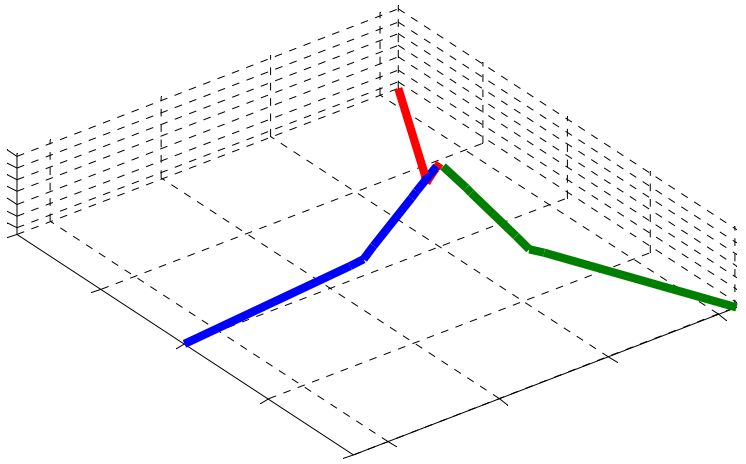

Quasi-static results (three lines)

- Results for 90 degrees direction fits well with MIMOSA results
- Different response for different direction because of unsymmetrical line setup; this effect is not included in the quasi-static implementation in HAWC2

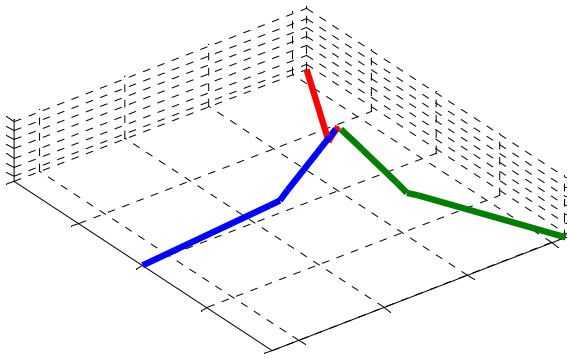

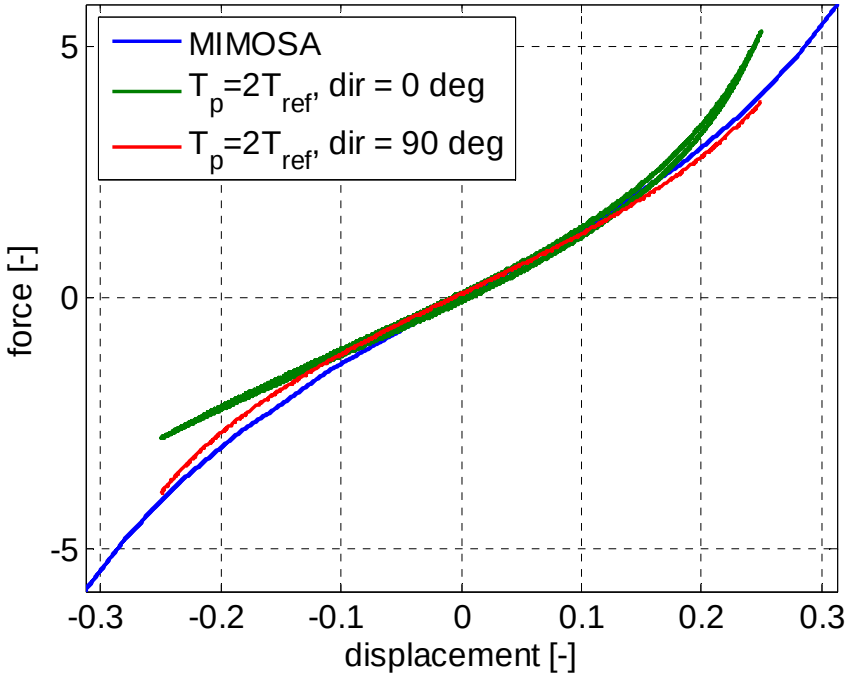

Result normalized by:
•Aerodynamic trust at rated power
•Rotor diameter and
•Systems natural surge period

Dynamic results (three lines)

- Increasing oscillation frequency opens the loop

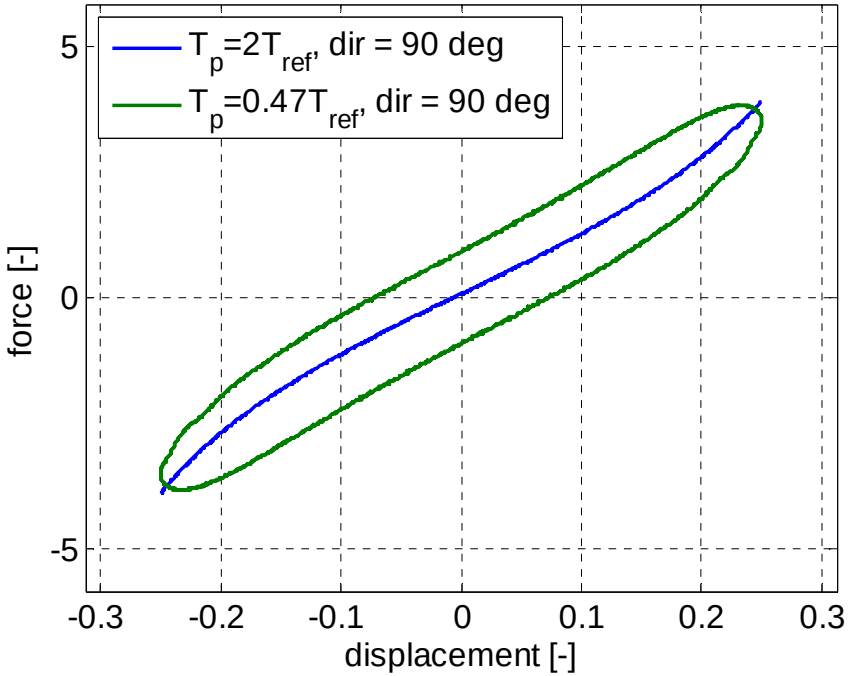

Result normalized by:
•Aerodynamic trust at rated power
•Rotor diameter and
•Natural surge period

Conclusion

- A nonlinear element that can model a cable with no bending stiffness but longitudinal flexibility has been developed
- A 2D bottom contact section that determine a quasi-static bottom contact point for the mooring system has been developed
- Quasi-static results shows good agreement with MIMOSA results

Further work

- Run selected load cases with detailed mooring model to analysis the mooring system behavior
- Run selected load cases with different model complexities to determine necessary model complexity for different modeling purposes
  - Mooring modeling necessary to determine turbine loads
  - Turbine modeling necessary to determine mooring line loads

3 Enhanced BEM

Enhanced BEM including wake expansion and swirl

Mads Døssing, Christian Bak, Helge A. Madsen

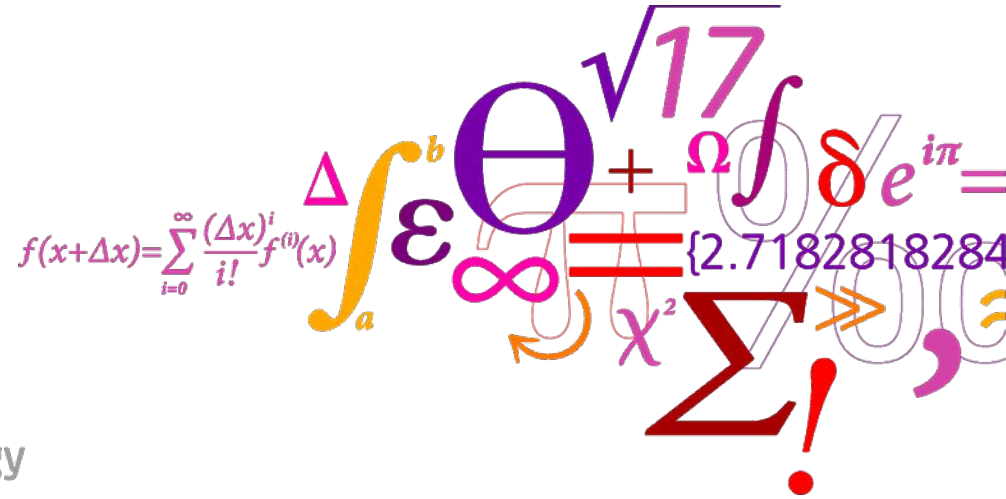

Risø DTU
National Laboratory for Sustainable Energy

Background
Reporting high aerodynamic efficiency

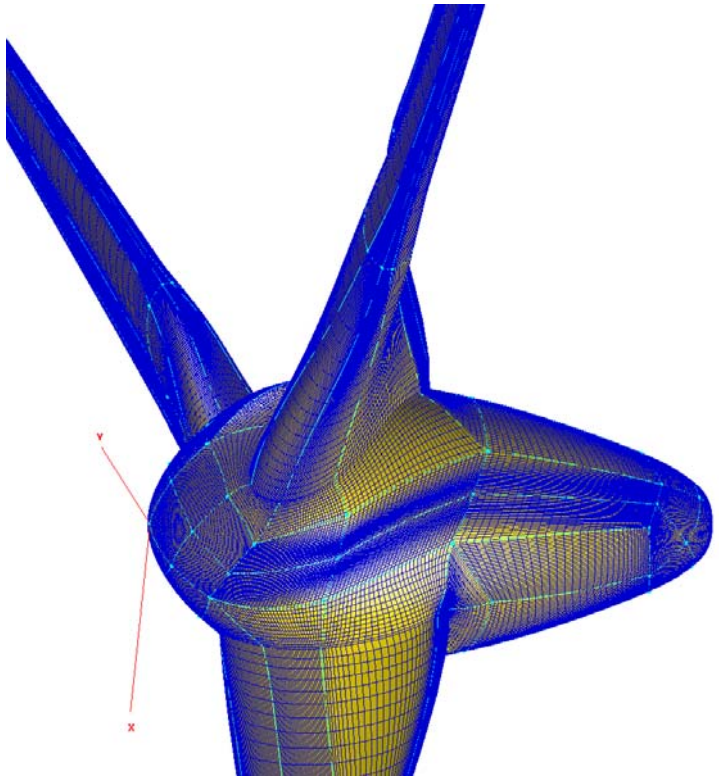

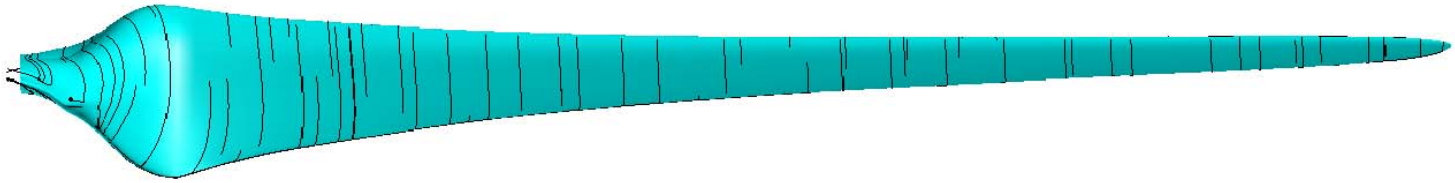

Background
Design of rotors: Max CP incl. swirl

Pressure

Axial velocity

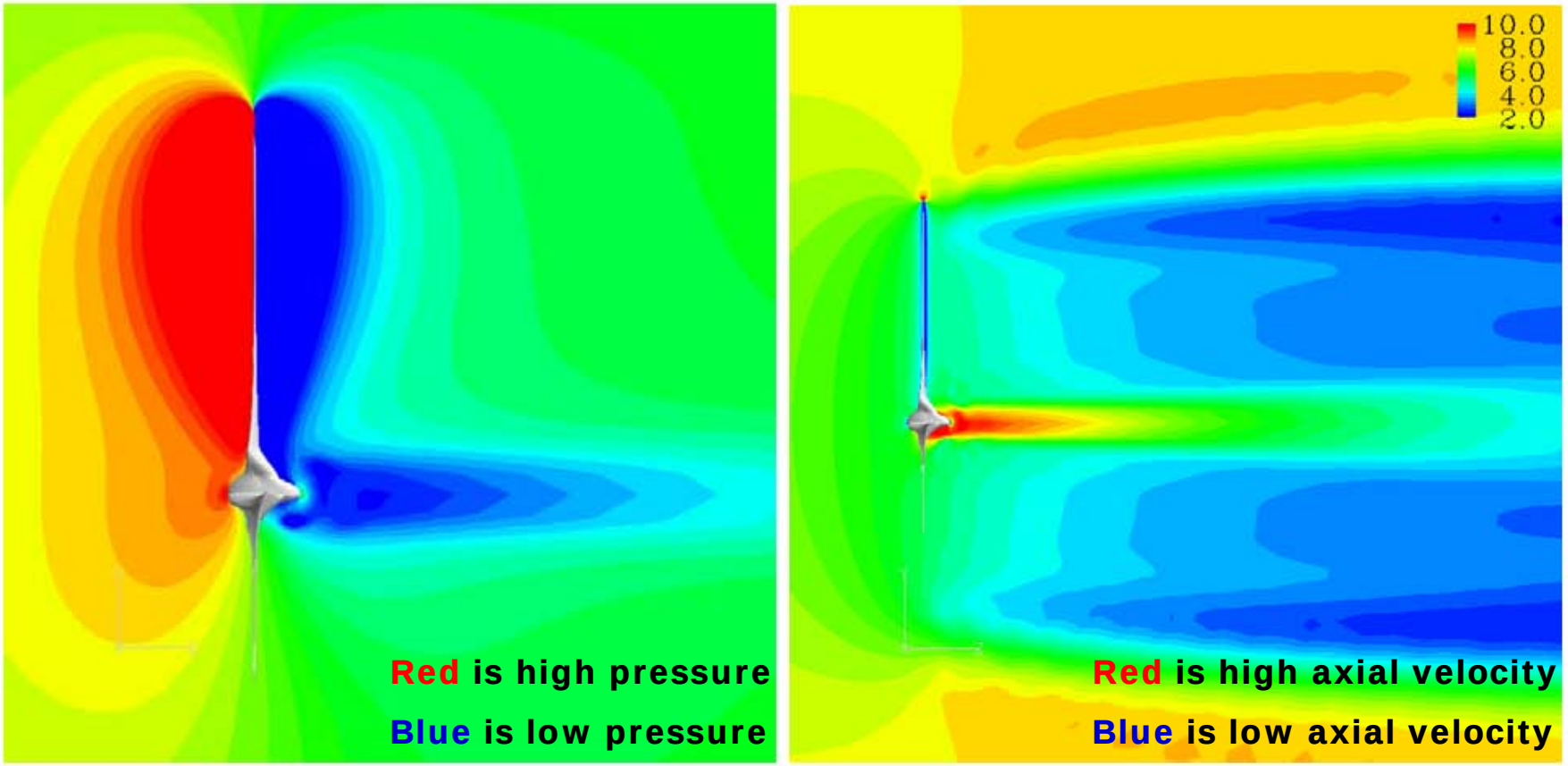

Figure 13. Contour plots of pressure (left) and axial velocity (right) in a vertical plane through the rotor.

Background
Design of rotors: Max CP incl. swirl

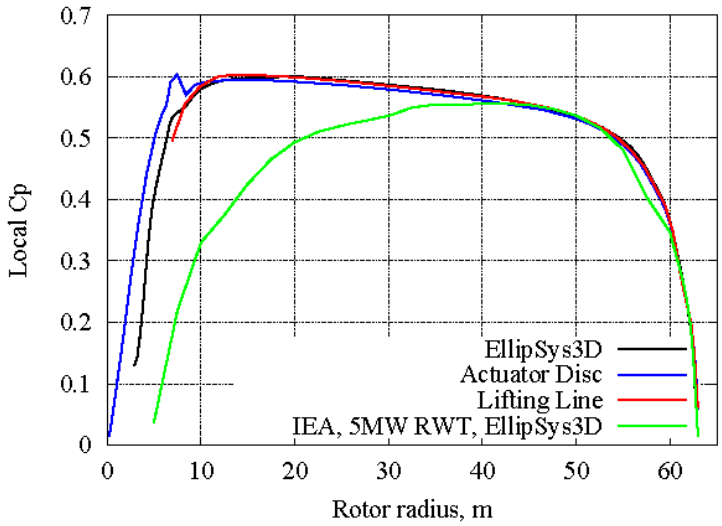

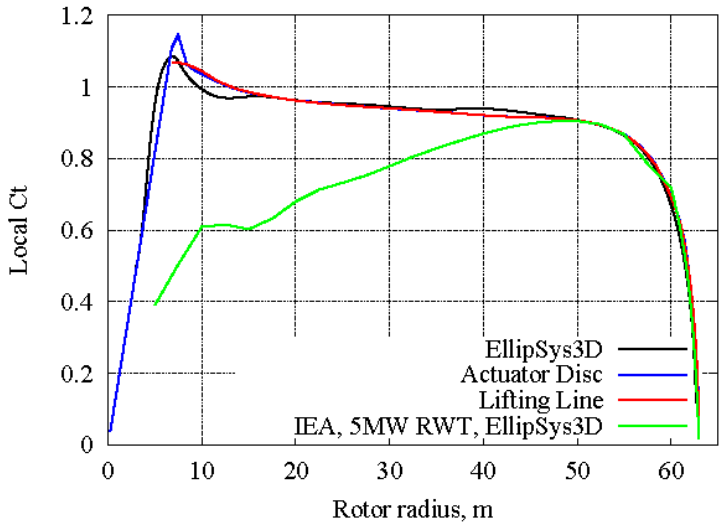

Table 1: Mechanical power and Thrust force for the present rotor. The IEA, 5MW RWT is included for comparison

	Mechanical power, P [MW]	Thrust force, T [kN]	CP	CT
EllipSys3D	**2.015**	**426**	**0.515**	**0.872**
Lifting Line	**2.011**	**424**	**0.514**	**0.868**
Actuator Disc	**1.995**	**425**	**0.510**	**0.870**
IEA, 5MW RWT EllipSys3D	**1.867**	**382**	**0.477**	**0.782**

BEM correction
Axial velocity in rotorplane

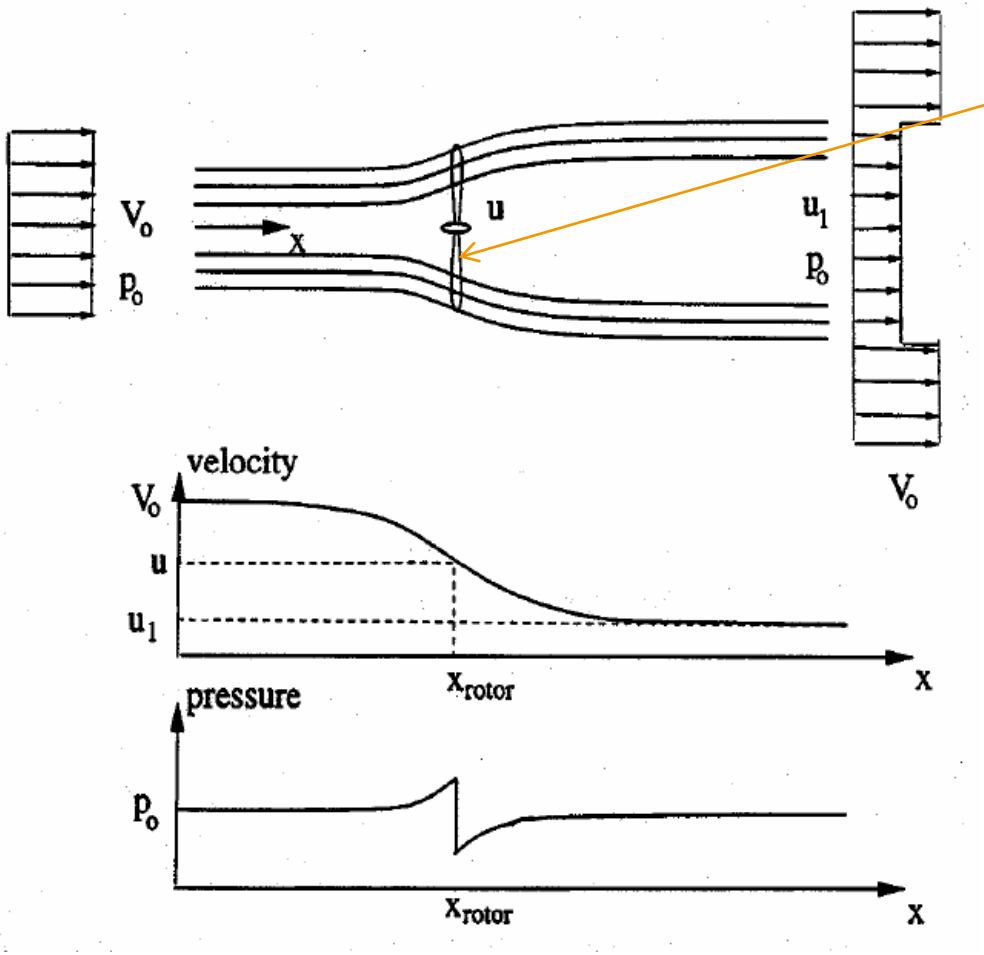

NEW

$$v_a = (1 - a + \Delta v_w - \Delta v_e)V_0$$

Δv_w correction for wake rotation

Δv_e correction for wake expansion

a axial induction factor

BEM correction
The model

- Expansion

$$\Delta v_e = \Delta v1_e - \Delta v2_e$$

$$\Delta v1_e = f(r, v_r) = l_1(r)v_r^3 + l_2(r)v_r^2 + l_3(r)v_r$$

$$\Delta v2_e = f(v_r(r/R = 0.9)) = k_1 v_r^2 + k_2 v_r + k_3$$

$$v_r = \frac{1}{2.24}\frac{C_{Tav}}{4\pi}\ln\left[\frac{0.04^2 + (r+1)^2}{0.04^2 + (r-1)^2}\right]$$

$$C_{Tav} = \frac{\int_0^r C_T 2\pi r dr}{\pi r^2}$$

- Swirl

$$\Delta v_w = 0.7\, p_w$$

$$p_w = \int_1^r \frac{v_t^2}{r} dr$$

$$v_t = 2a'\lambda_r$$

H. Madsen, C. Bak, M. Døssing, R. Mikkelsen, S. Øye, "**Validation and modification of the Blade Element Momentum theory based on comparisons with actuator disc simulations",** WIND ENERGY *Wind Energ. 2010;* ***13:373–389***

Application of BEM corrections

- How does the BEM corrections influence the rotor performance?
- Rotor designs are carried out to
  - investigate the influence of the the BEM corrections and
  - investigate how rotors should be designed when corrections for swirl and expansion are included

Validation of implementation in HAWTOPT

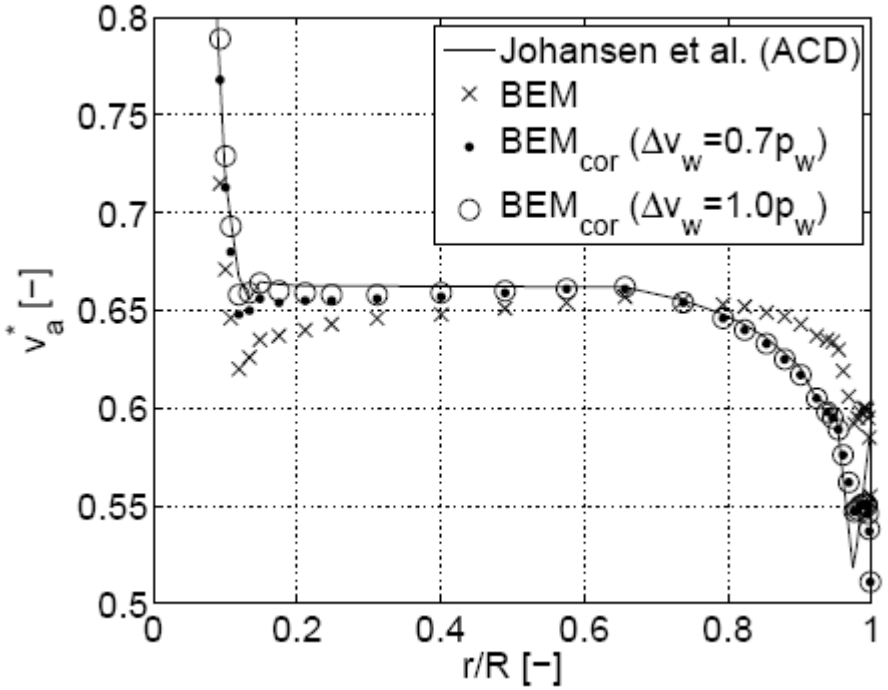

Axial velocity

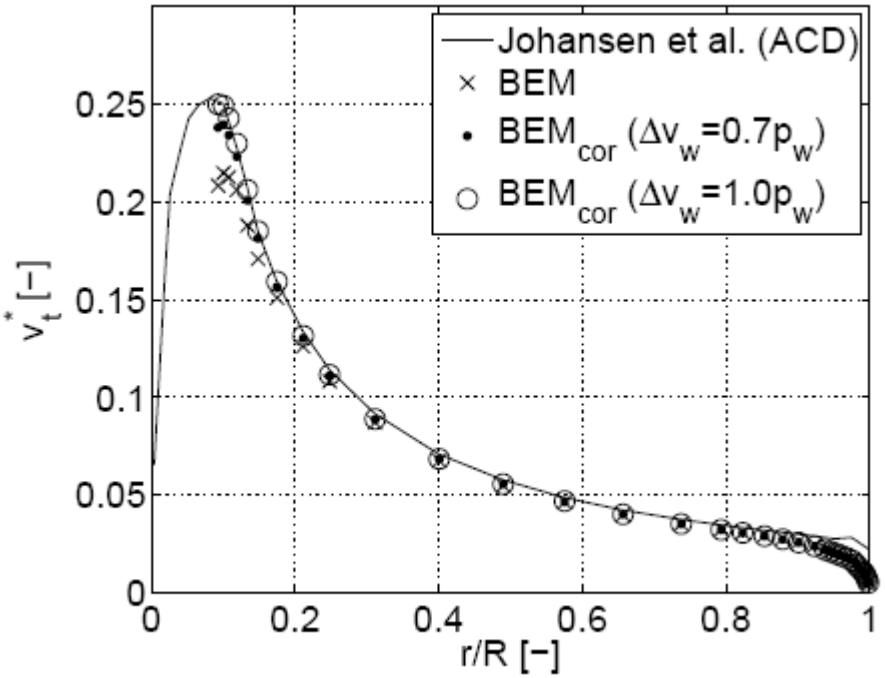

tangential velocity

Rotors optimized for maximum power

Tip speed ratio

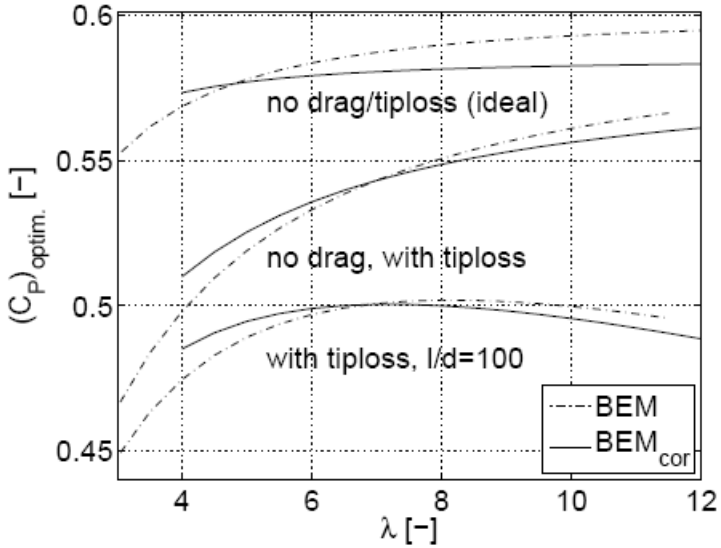

Chord

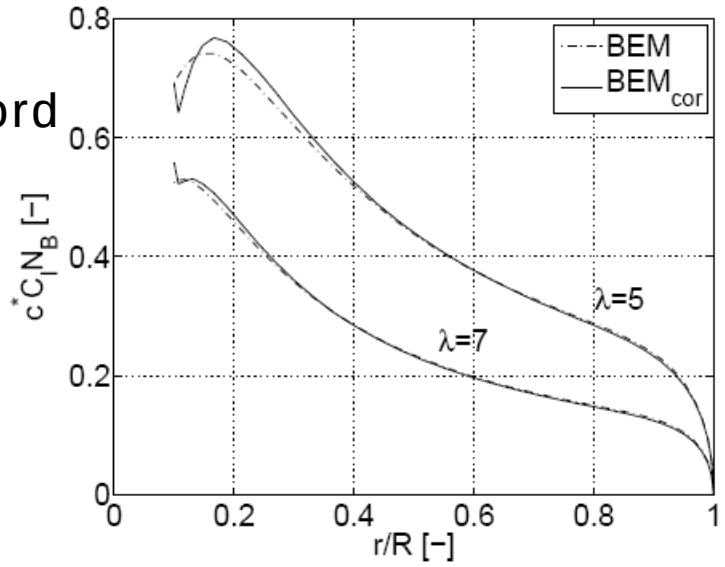

Inflow angle

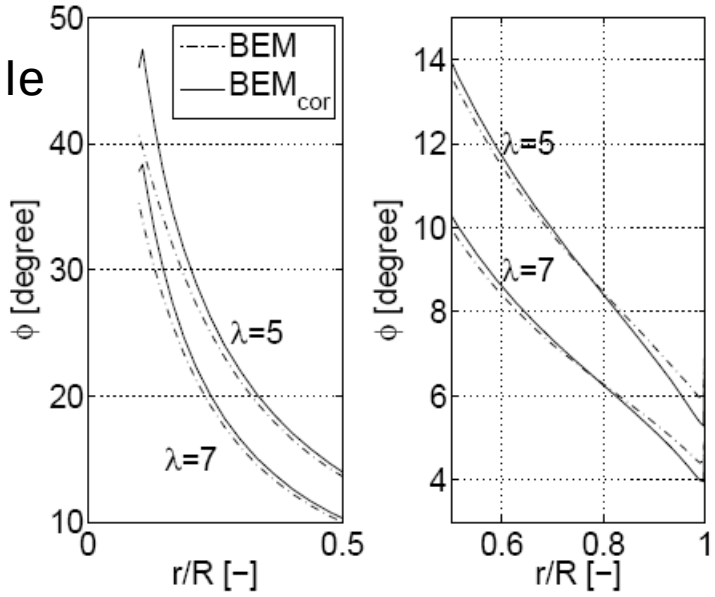

Root bending moments
Optimization for low thrust at reduced CP

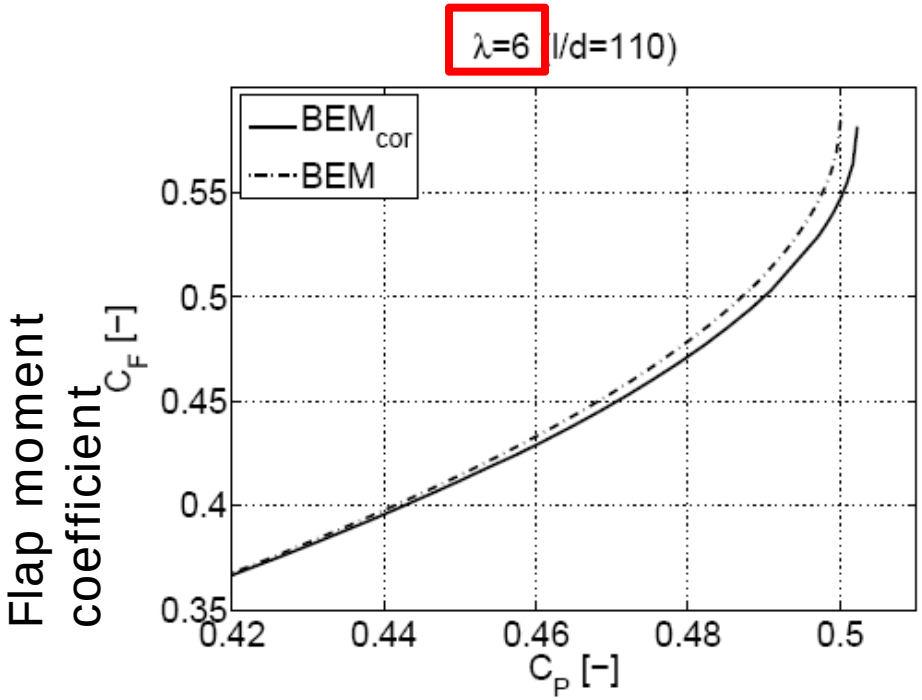

Flap moment coefficient

Power coefficient

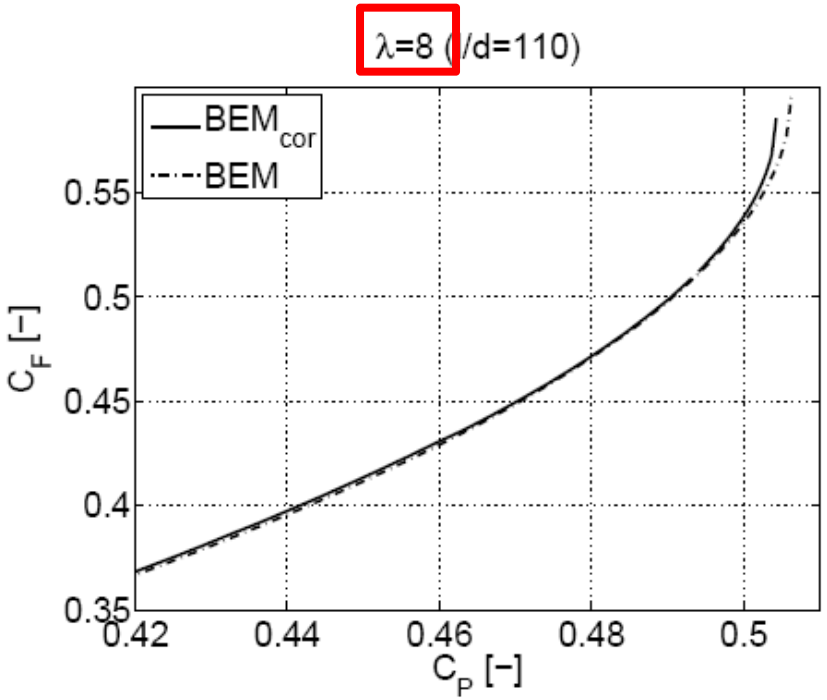

Power coefficient

Conclusion

- Rotor designs are carried out using BEM with correction for swirl and expansion
- No significant differences in designs are seen if λ_{design} is appr. 7-8, when comparing tradtinal BEM to corrected BEM.
- If λ_{design} is below 7-8
  - Chord lengths and twist close to the root should be increased
  - Power efficiency increased
- If λ_{design} is beyond 7-8
  - Power efficiency decreased

4 Unsteady viscous-inviscid airfoil code

Unsteady Viscous-Inviscid Interactive Airfoil Code for Wind Turbines

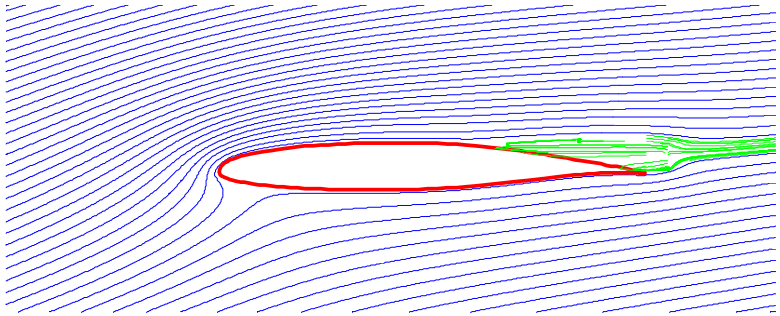

Néstor Ramos García
Jens Nørkær Sørensen
Wen Zhong Shen

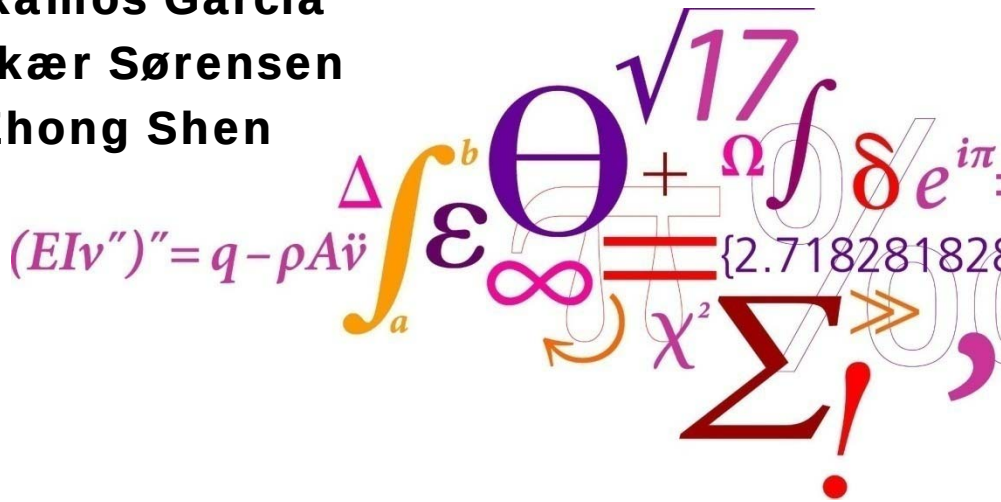

DTU Mekanik
Institut for Mekanisk Teknologi

PRESENTATION LAYOUT

- INTRODUCTION
- VISCOUS-INVISCID INTERACTION
- INTEGRAL BOUNDARY LAYER SOLVER via VI INTERACTION
  - STEADY 2D.
  - UNSTEADY 2D, SINGLE WAKE.
  - STEADY QUASI3D
- POTENTIAL DOUBLE WAKE SOLVER
- CONCLUSIONS

INTRODUCTION

- Blade-Element Momentum theory is often used for the design of wind turbines. Required Input: Lift and Drag force coefficients.
- Computer resources are getting more powerful with the years, but it is still behind our limits to realize an active design of airfoils and blades using Navier-Stokes solvers. High cost in computational time.
- The first HAWT Aerodynamics Specialists meeting, Wichita State University, 1983, concluded:
  - Inboard regions are producing more power than predicted.
  - Rotor is producing more power at high angles of attack due to secondary outward flow, caused by centrifugal pumping.

INTRODUCTION

- A code has been developed during the last three years that can fit our needs:
  - It has to compute accurately steady/unsteady airfoil forces.
  - It has to be fast in order to use it as a design method.
  - It has to take into account rotational effects. Centrifugal and Coriolis forces.

- The code uses the already known concept of UNSTEADY VISCOUS-INVISCID STRONG INTERACTION via transpiration velocity.

  - Inviscid flow → Unsteady potential flow, panel method.
  - Viscous flow → Quasi 3-D integral BL equations + Closures.

QUASI-3D BOUNDARY LAYER EQUATIONS

- The boundary layer equations are used with all the necessary assumptions in order to reduce them into the integral quasi-3D ones.

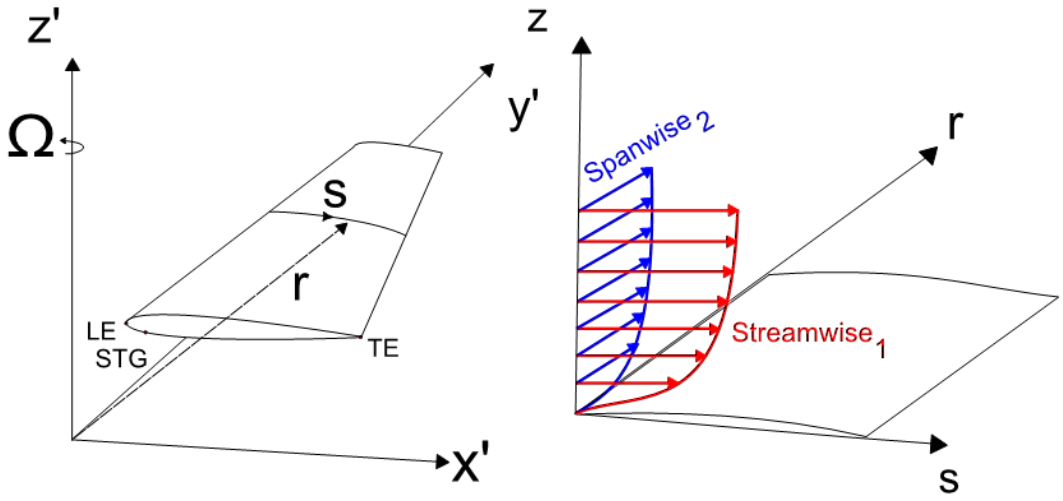

Integral θ -momentum

$$\frac{\partial \theta_1}{\partial s} = -\frac{\theta_1}{u_e}\frac{\partial u_e}{\partial s}(2+H) + \frac{C_f}{2} + s_w p_r \frac{2Ro \cdot ls}{u_{2D} c}\delta_2 - \frac{1}{u_e}\frac{\partial u_e}{\partial s}(2\theta_2 - \delta_2) - \frac{ls}{c}(2\theta_2 - \delta_2)$$

Integral r-momentum

$$\frac{\partial \theta_2}{\partial s} = -\frac{2\theta_2}{u_e}\frac{\partial u_e}{\partial s} + \tan\beta_w \frac{C_f}{2} + \frac{ls}{c}\left(\theta_1 + \delta_1 - \delta - \delta_3 + s_w p_r \frac{2Ro}{u_{2D}}(\delta - \delta_1)\right) - \frac{1}{u_e}\frac{\partial u_e}{\partial r}(2\delta_3 + \delta)$$

A set of 3D turbulent closure equations are used in order to close the system (semi-empirical)

VISCOUS-INVISCID STRONG INTERACTION

- ASSUMPTION OF AN EQUIVALENT FLOW, where the effects of real flow can be added. Transpiration velocity will take into account the effects of the real flow in the potential flow solver.

$$v_T = \frac{d}{dx}\int_0^\infty (u_e - u)dz = \frac{d}{dx}(u_e \delta_1)$$

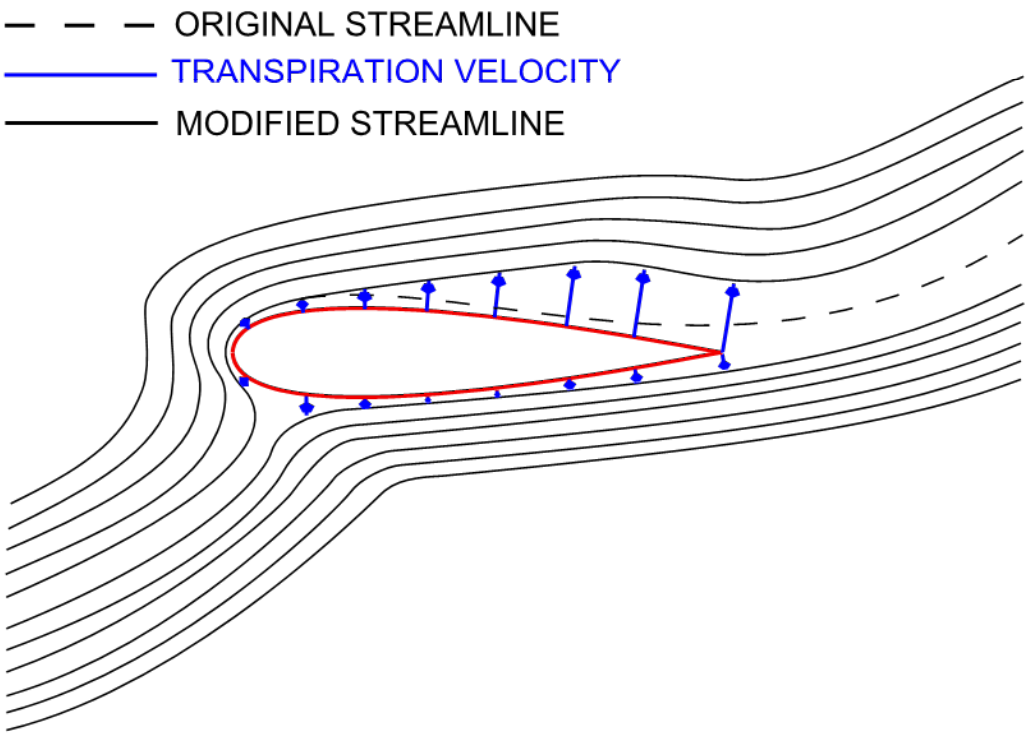

STEADY VISCOUS INVISCID SOLVER

STEADY VI

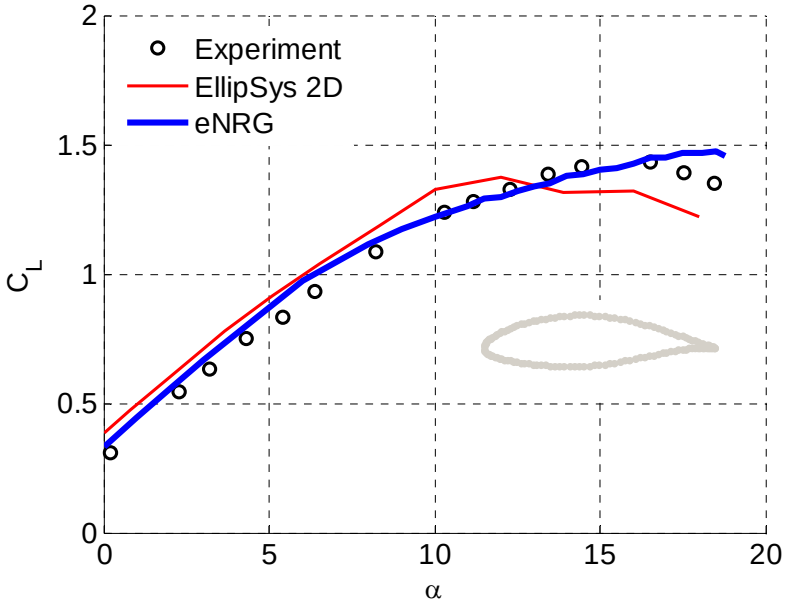

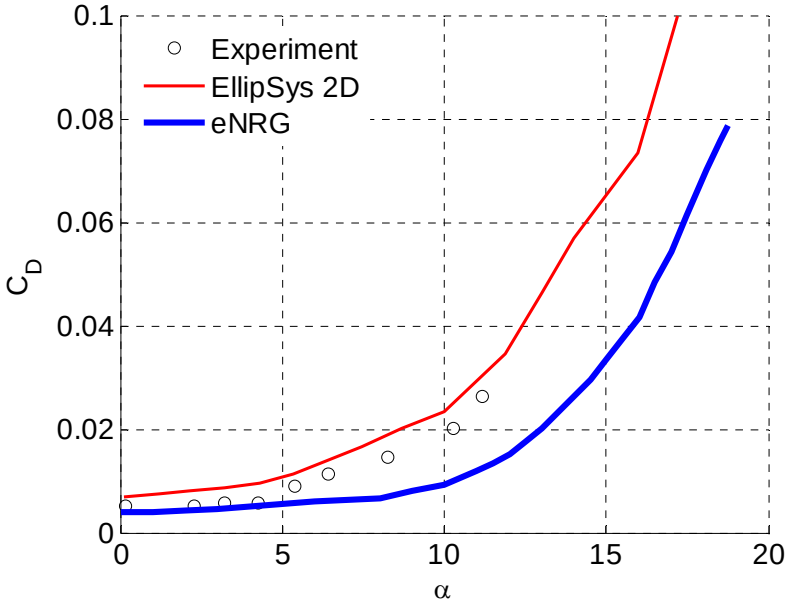

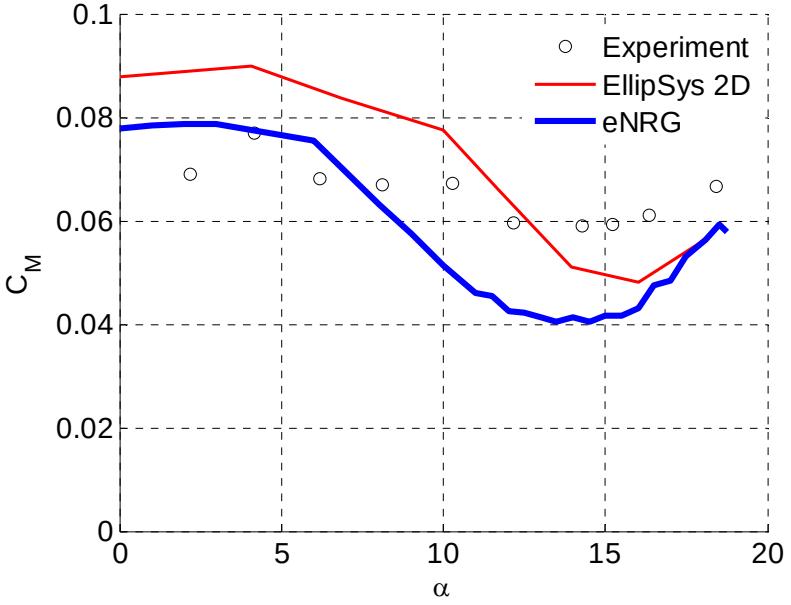

Comparison in between: **Experiments**, EllipSys2D, and the VI code: lift, drag and pitch moment coefficients in function of the angle of attack for the *NACA 65415* at *Re = 3e6*

The measurements were performed at NASAs low-turbulence pressure tunnel and reported in the book by Abbott and von Doenhoff.

STEADY VI, REYNOLDS VARIATION

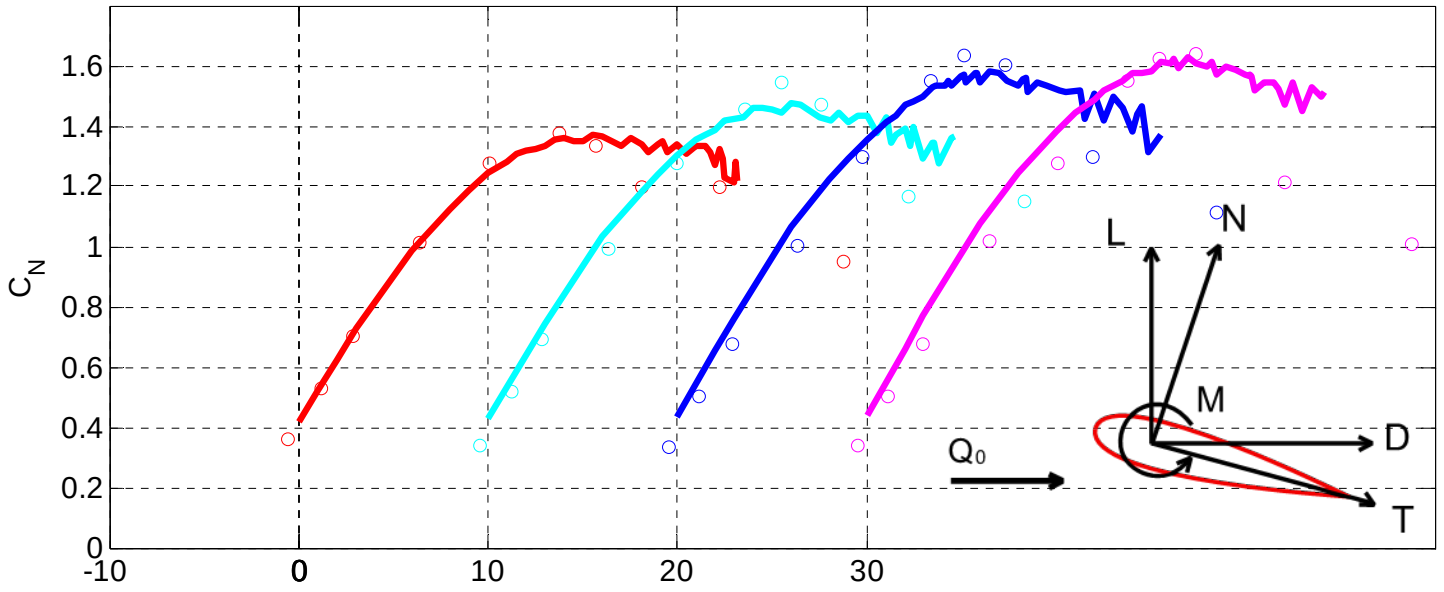

EXP Re 1.8e6
EXP Re 3.4e6
EXP Re6.3e6
EXP Re 8.2e6
eNRG Re 1.8e6
eNRG Re 3.4e6
eNRG Re 6.3e6
eNRG Re 8.2e6

NACA 4412

N.A.C.A Variable-Density Wind Tunnel.

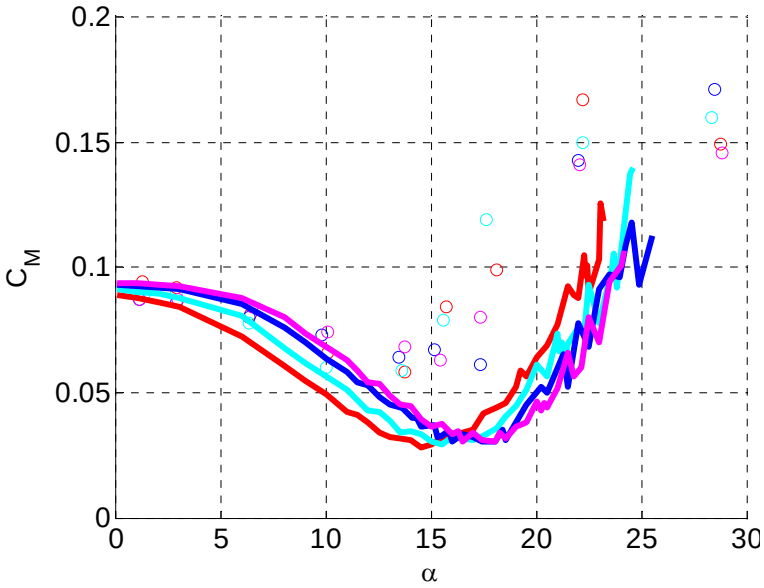

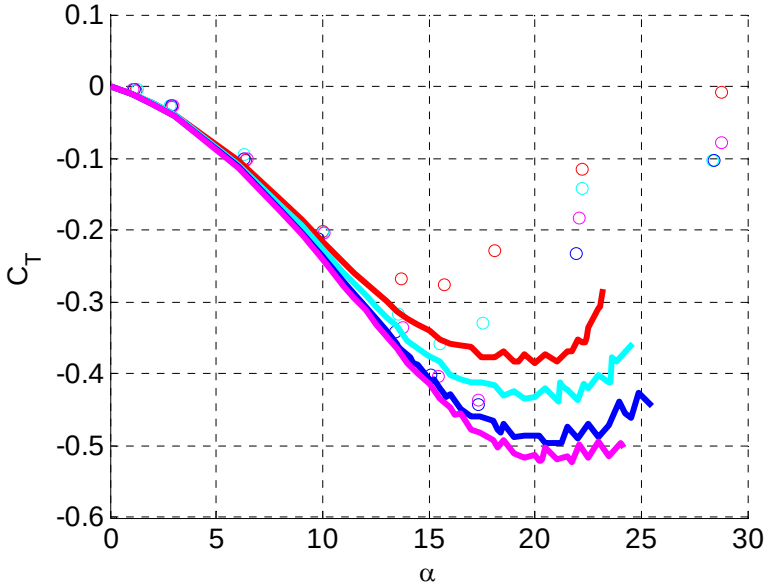

UNSTEADY VISCOUS INVISCID SOLVER SINGLE WAKE

UNSTEADY VISCOUS COMPUTATIONS, SINGLE WAKE

- **NACA 0015**
- **Re = 1.5e6**
- **k = 0.1**
- **α= 13.37 A = 7.55**

- Unsteady experiments, *University of Glasgow, G.U Aero Report 9221.*

- Vorticity formulated Navier-Stokes equation running a Spallart Allmaras turbulent model. *J.N. Sørensen and P.J. Nygreen, Computers & Fluids 30 (2001).*

- Unsteady Viscous-Inviscid strong coupling code.

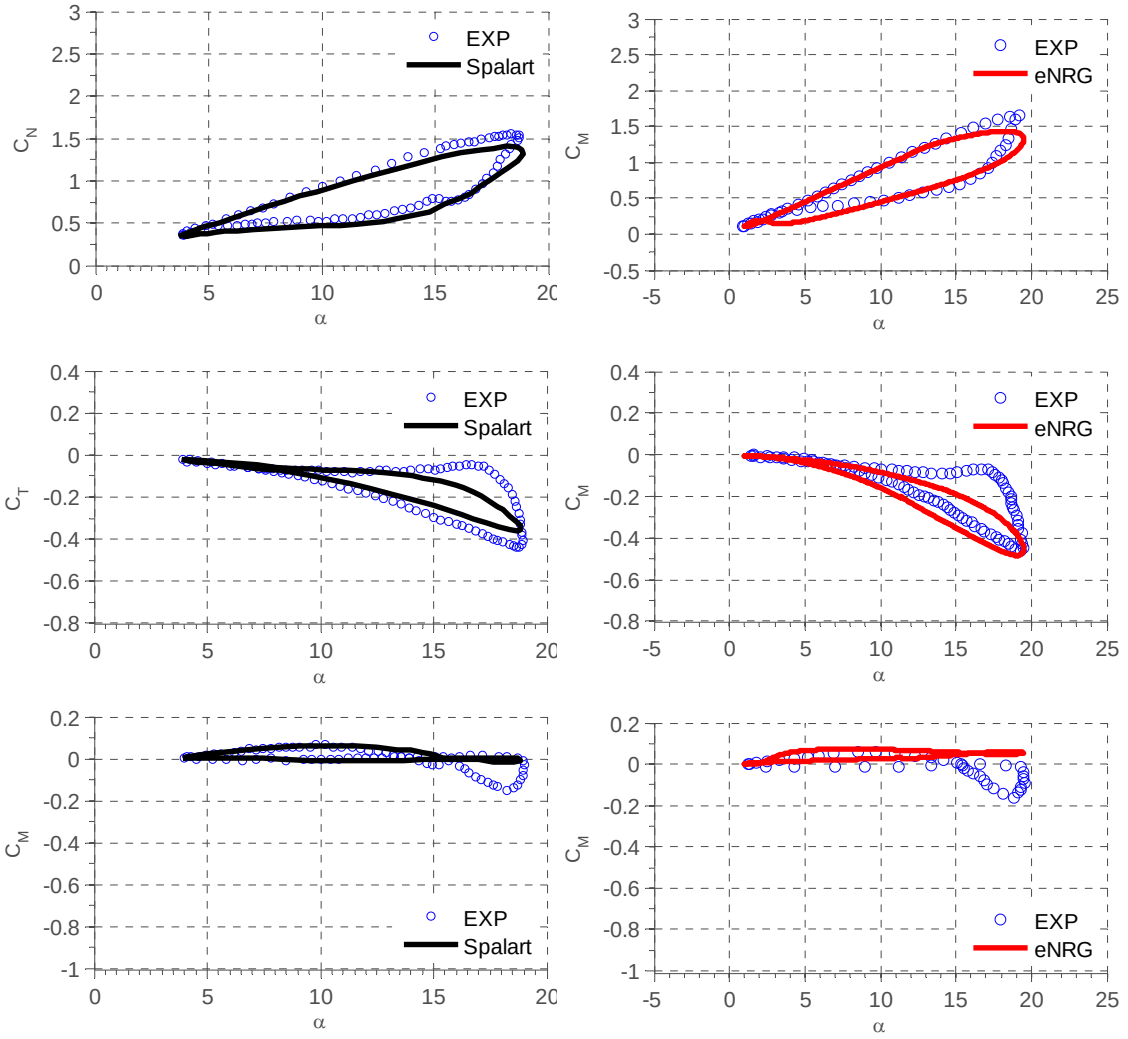

UNSTEADY VISCOUS COMPUTATIONS, SINGLE WAKE

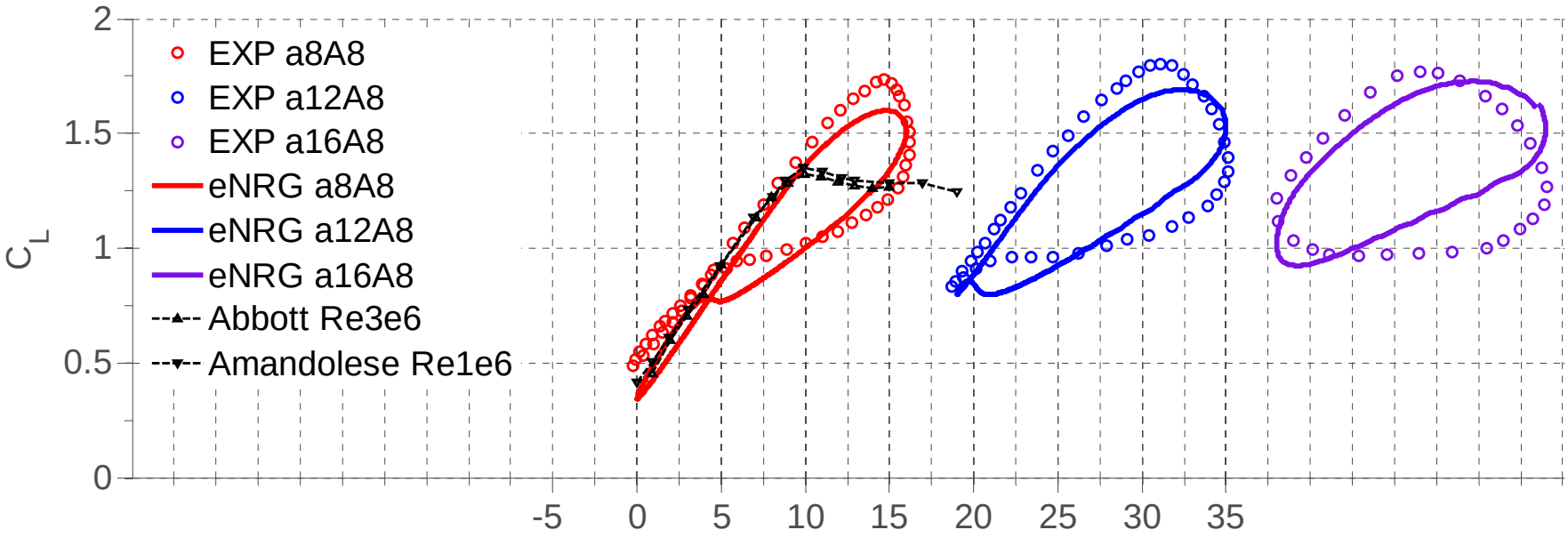

- **NACA 63421**
- **k = 0.0785**

- EXP, Unsteady experiments, *Institut AéroTechnique, S4 wind tunnel, TI = 1.1.*
- eNRG, Unsteady Viscous-Inviscid strong coupling code.

Q3D STEADY VISCOUS INVISCID SOLVER

QUASI-3D BOUNDARY LAYER EQUATIONS

- Dimensional variables of interest in rotational study: c, r, Ω , V_w

- In order to proceed with a parametric study of the rotational effects in a wind turbine blade, two variables are defined:

1. The ratio between the chord length and the radial position,

$$ls = \frac{c}{r}$$

2. The ratio between the rotational speed an the relative velocity,

$$RO = \frac{\Omega r}{U_{rel}}$$

Where Ω is the blade angular velocity, U_{rel} is defined typically,

$$U_{rel} = \sqrt{\left((1+a')\Omega r\right)^2 + \left((1-a)V_w\right)^2}$$

The four dimensional variables of interest are reduced to two adimensional parameters ls & RO, base for our parametric study.

QUASI-3D BOUNDARY LAYER

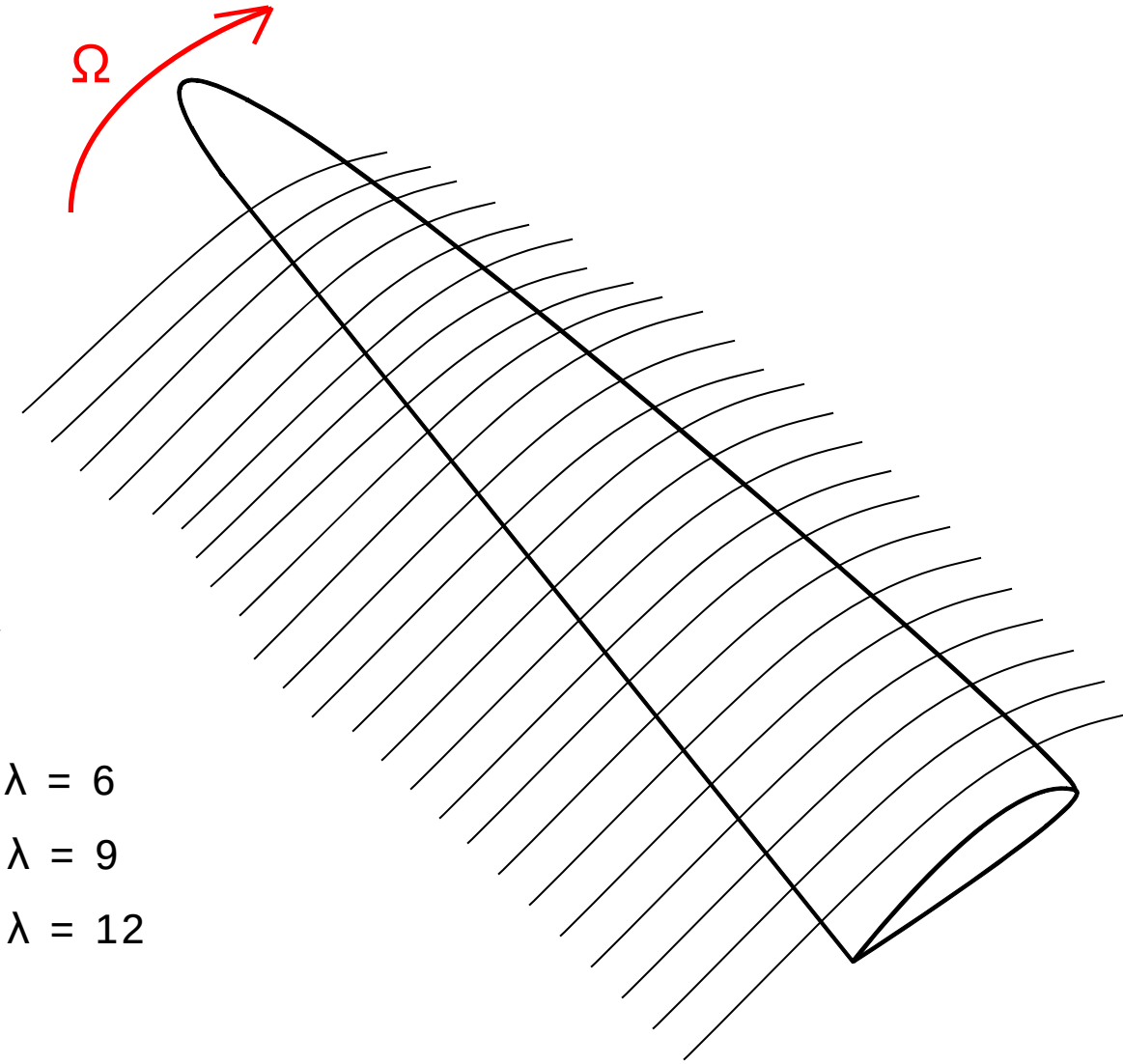

- Artificial rotor.
- S809 Airfoil.
- Re 1e6.
- R = 10 m.
- Ω = 70 rpm.

- Tip speed ratio, $\lambda = \frac{\Omega R}{Q_w}$

  - Q_W = 12.20 m/s → λ = 6
  - Q_W = 8.14 m/s → λ = 9
  - Q_W = 6.11 m/s → λ = 12

QUASI-3D BOUNDARY LAYER

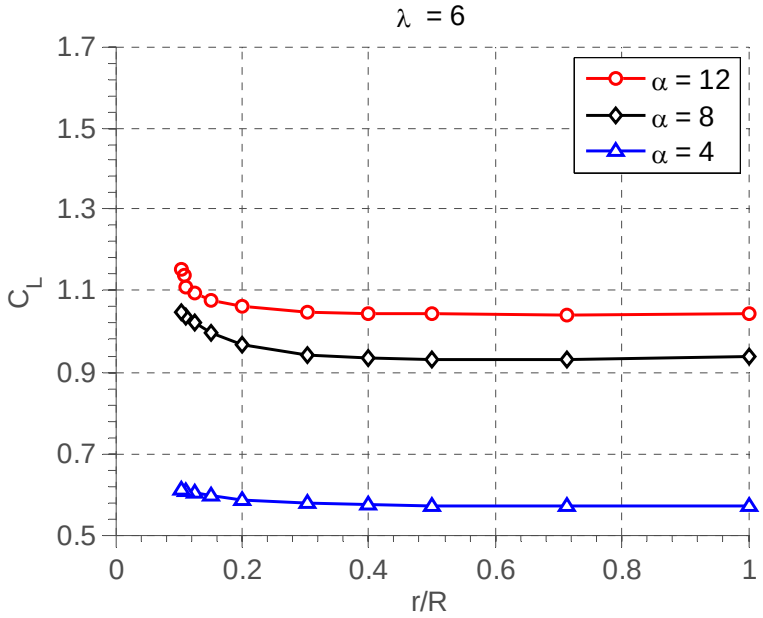

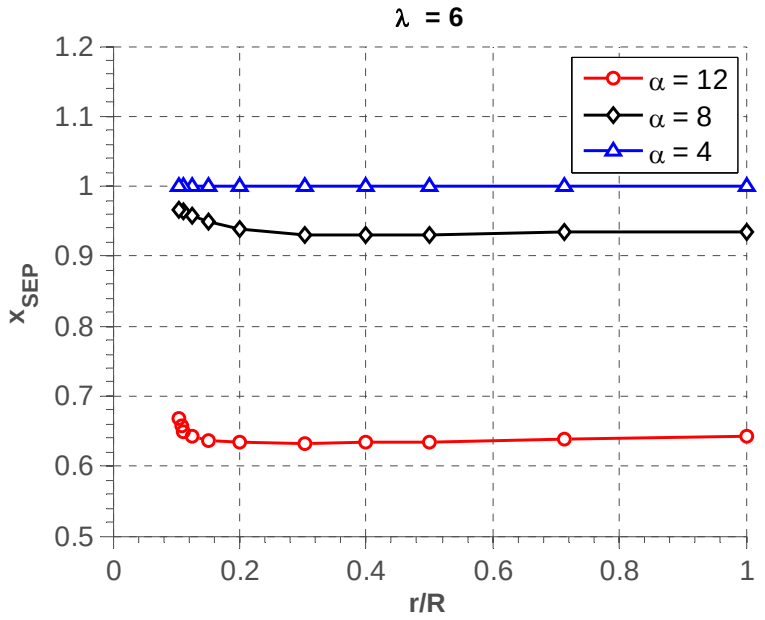

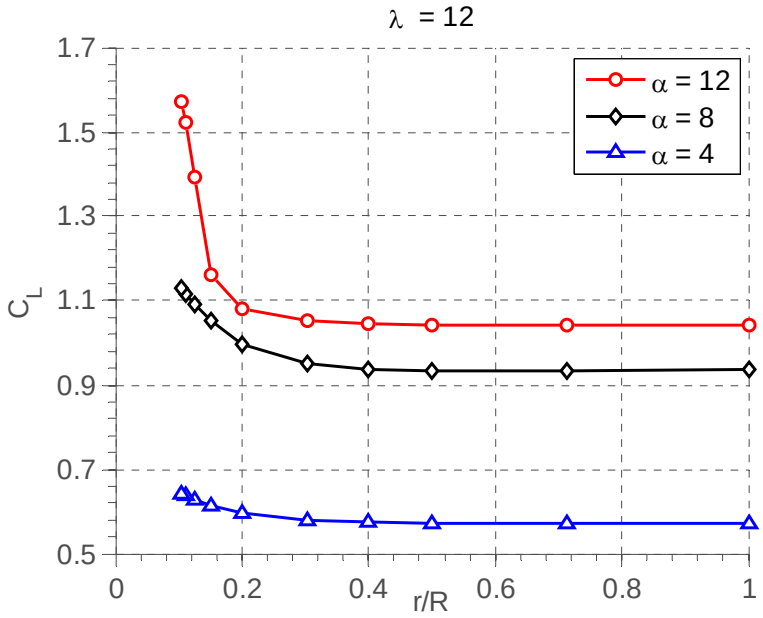

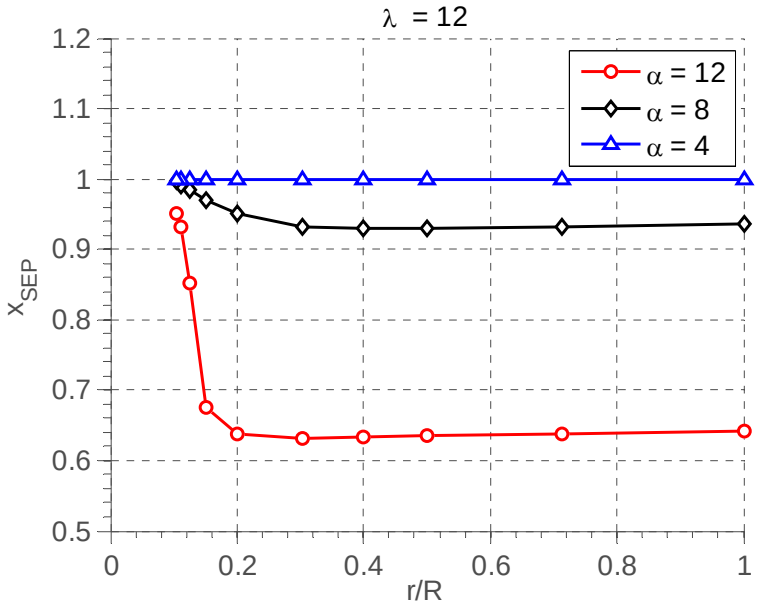

QUASI-3D BOUNDARY LAYER

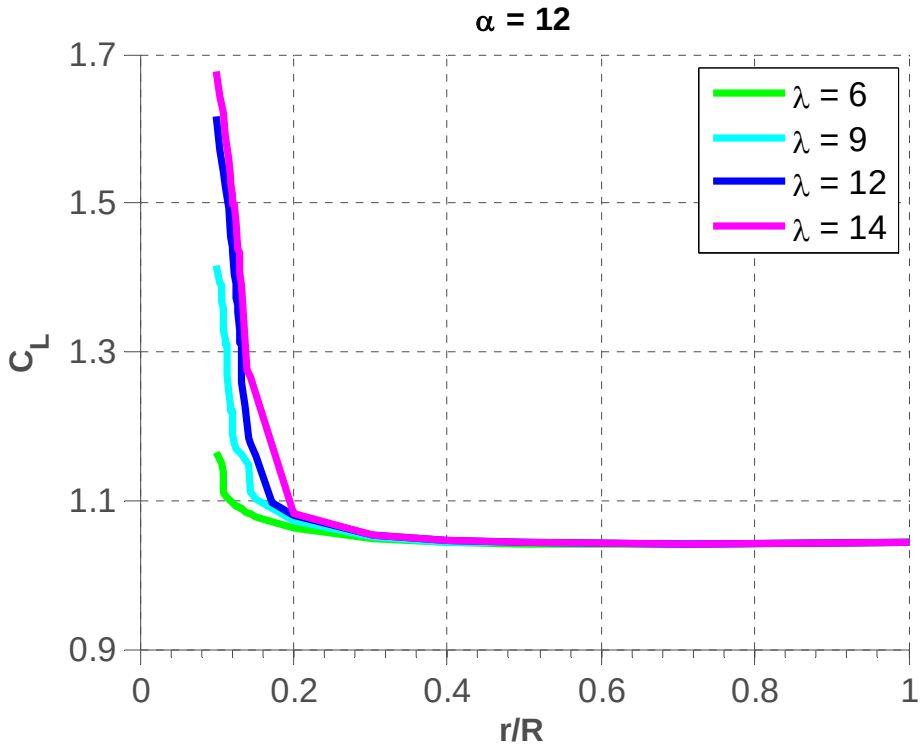

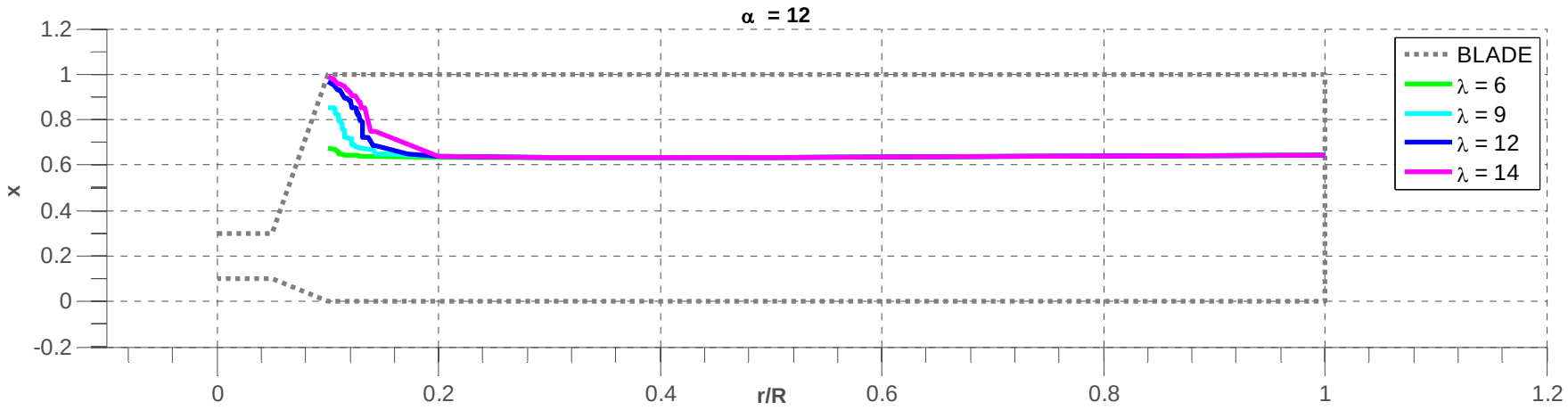

DOUBLE WAKE POTENTIAL SOLVER

DOUBLE WAKE MODEL

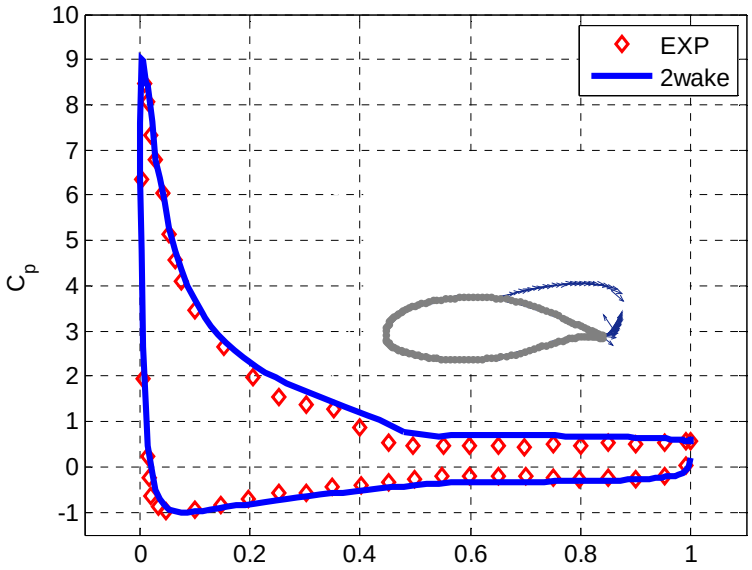

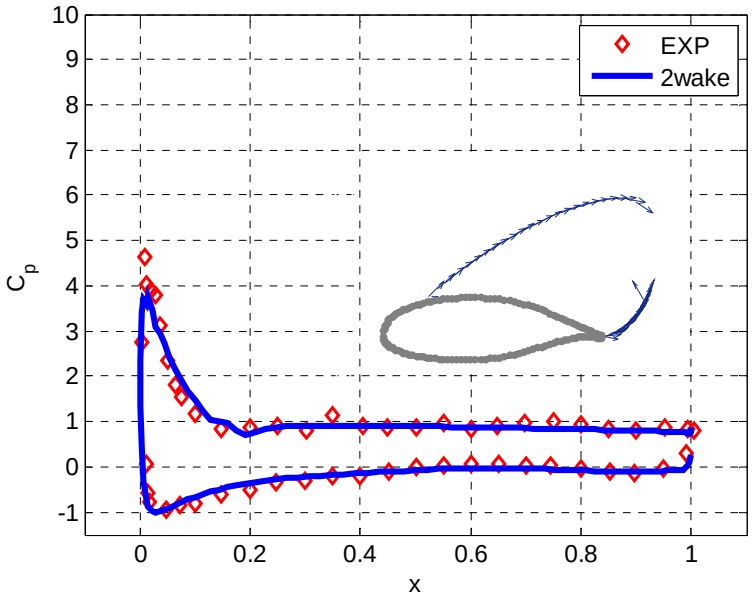

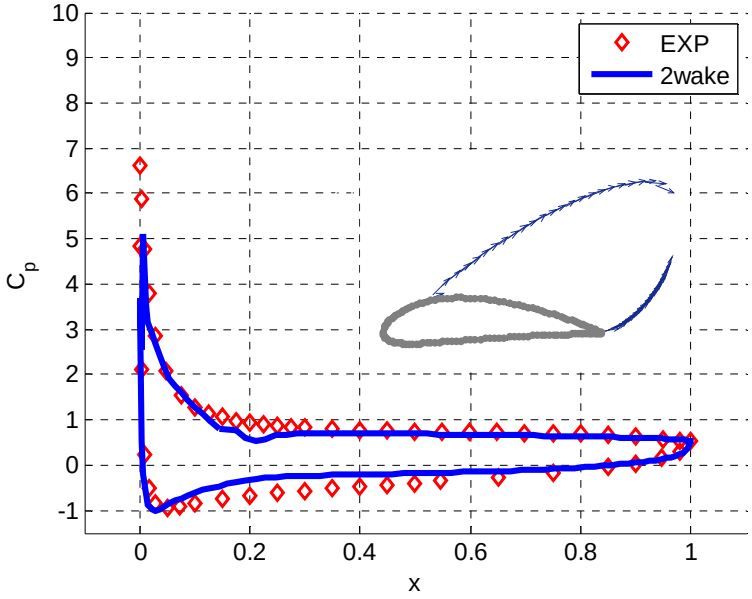

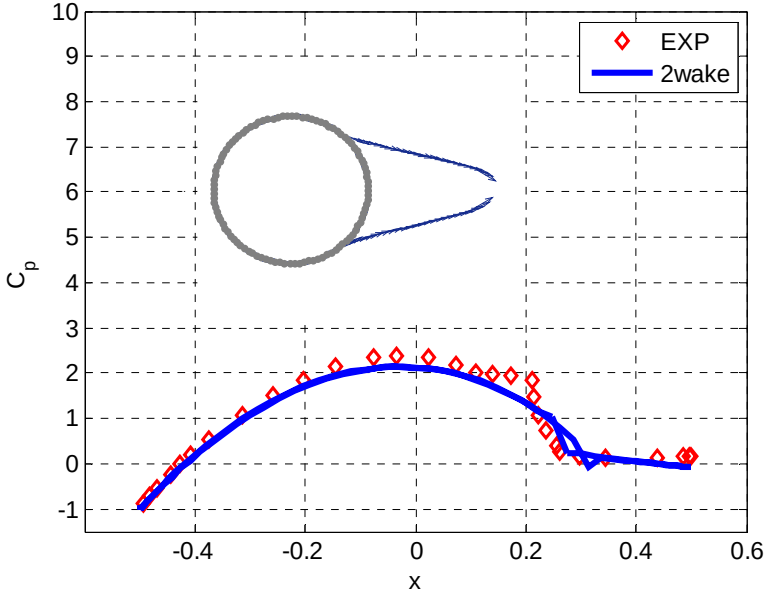

DOUBLE WAKE MODEL

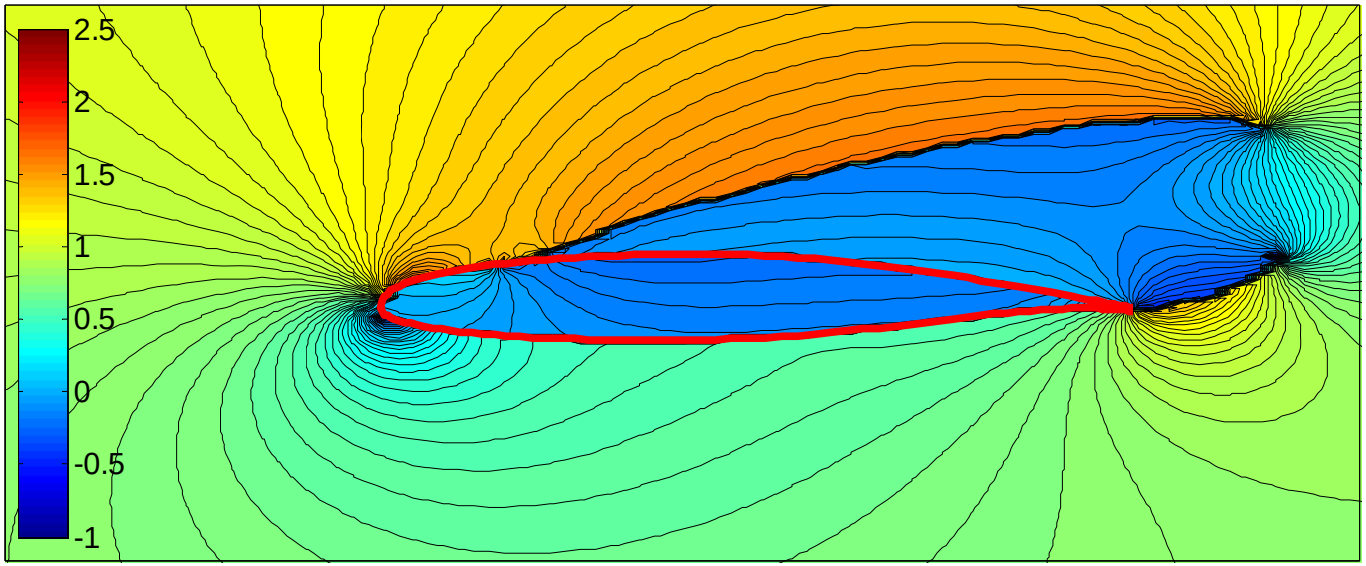

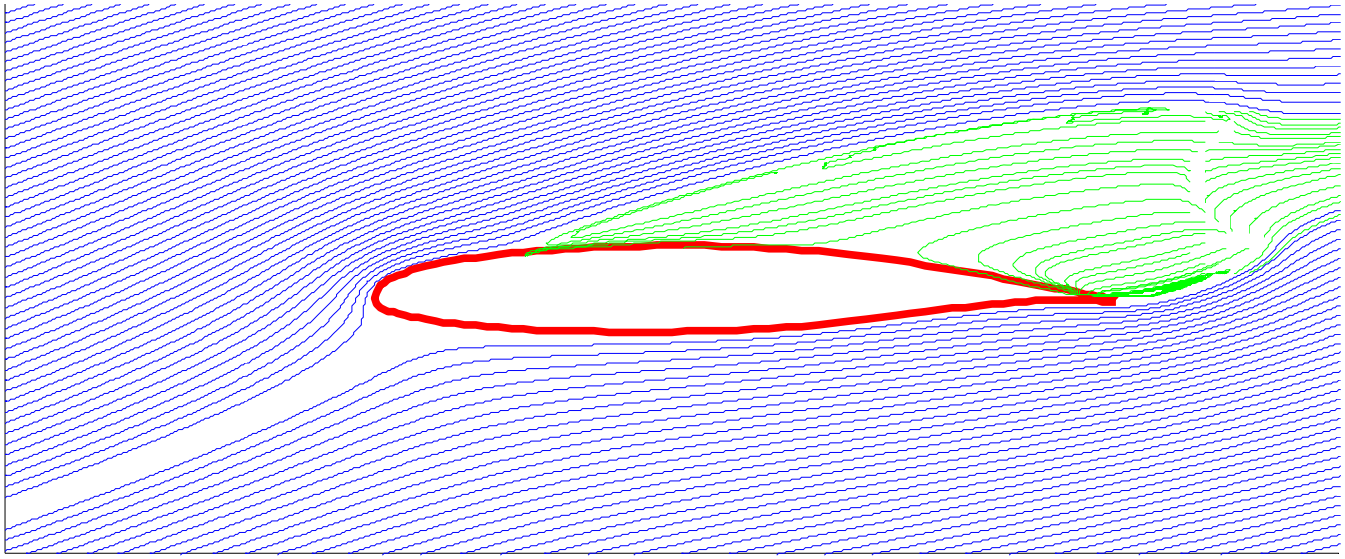

CONCLUSIONS

- **VISCOUS INVISCID SOLVER IMPLEMENTED**
  - **STEADY 2D**
  - **UNSTEADY 2D**
  - **STEADY Q3D**
  - **STEADY / UNSTEADY 2D/Q3D WITH FLAP**
- **DOUBLE WAKE POTENTIAL SOLVER IMPLEMENTED**
  - **DEEP STALL CONDITIONS**

THANK YOU FOR YOUR ATTENTION.

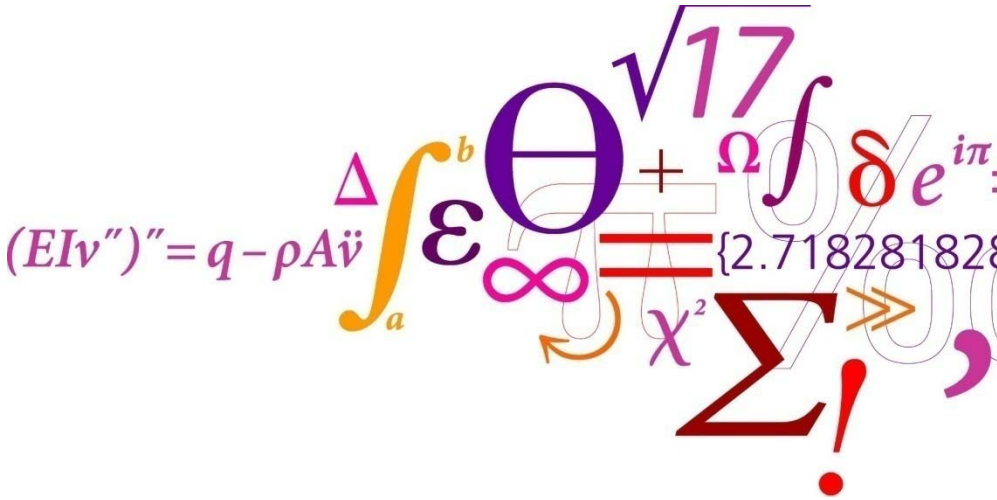

DTU Mekanik
Institut for Mekanisk Teknologi

5 PIV measurements on model scale turbine

PIV measurements on a wind turbine in a water flume

by
Robert Mikkelsen, Svend Petersen, Kasper Damkjær

Content

- Setup in flume
- Some results
- Summary

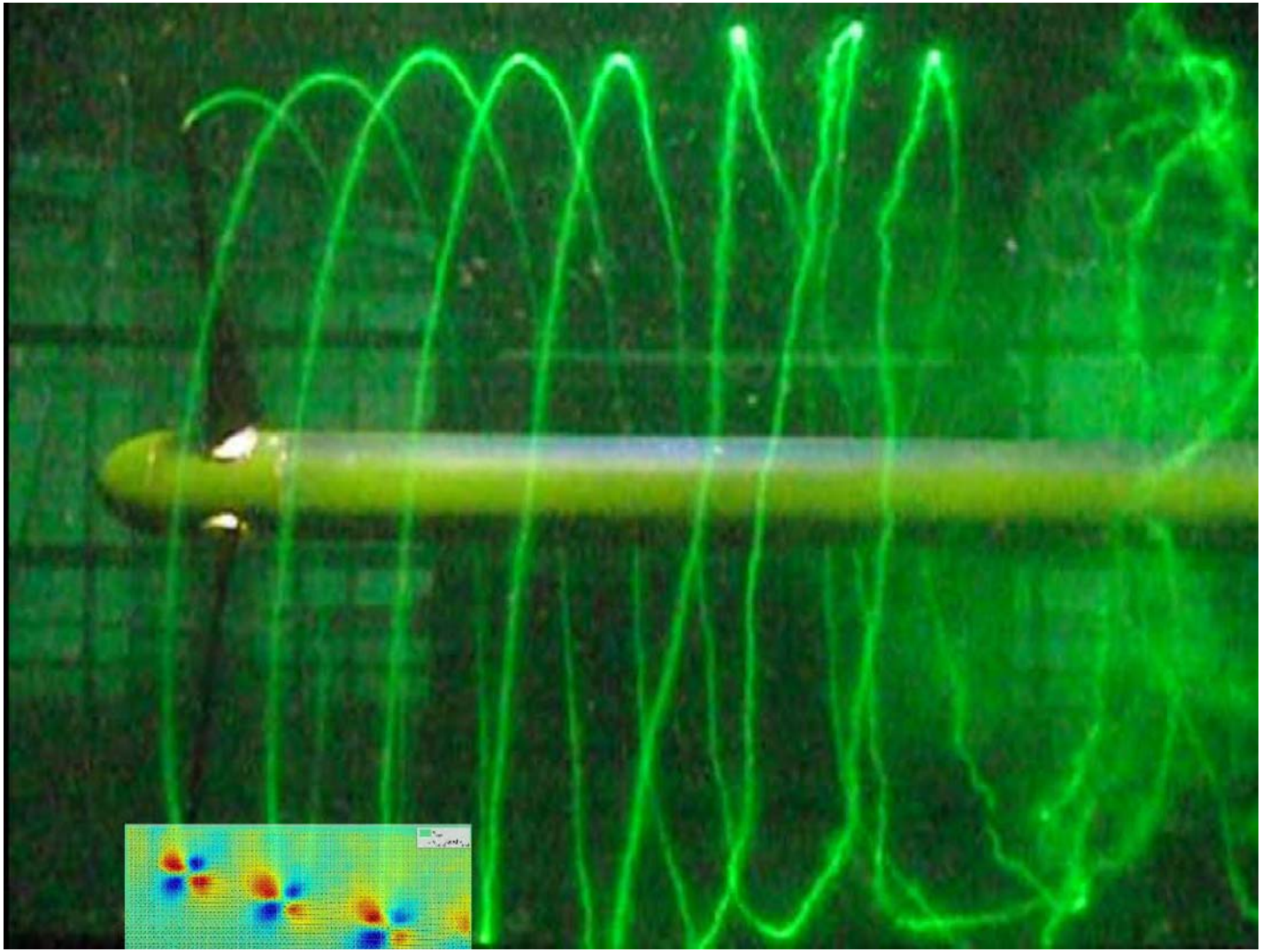

Flume

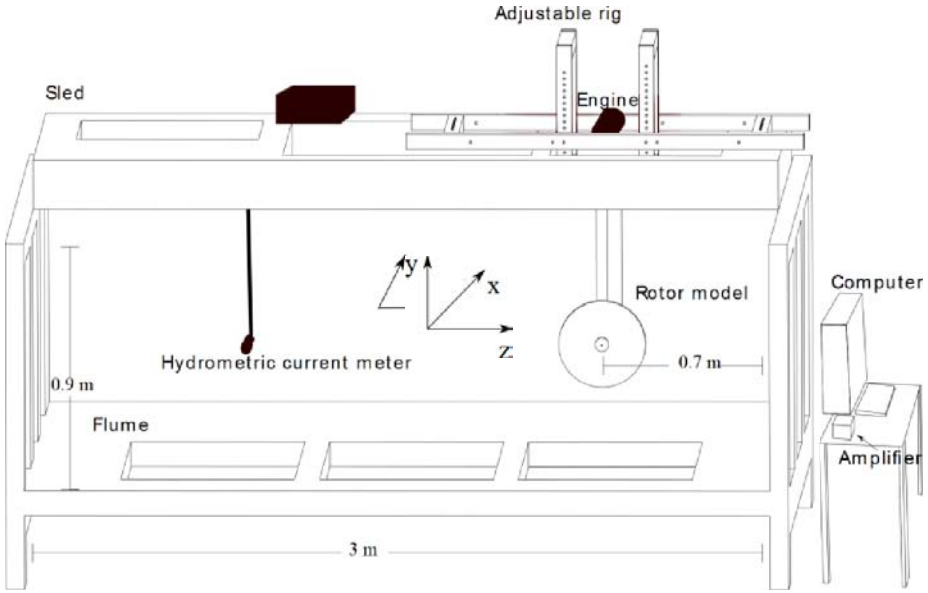
Adjustable rig
Sled
Engine
y
x
z
Rotor model
Computer
Hydrometric current meter
0.9 m
0.7 m
Flume
Amplifier
3 m

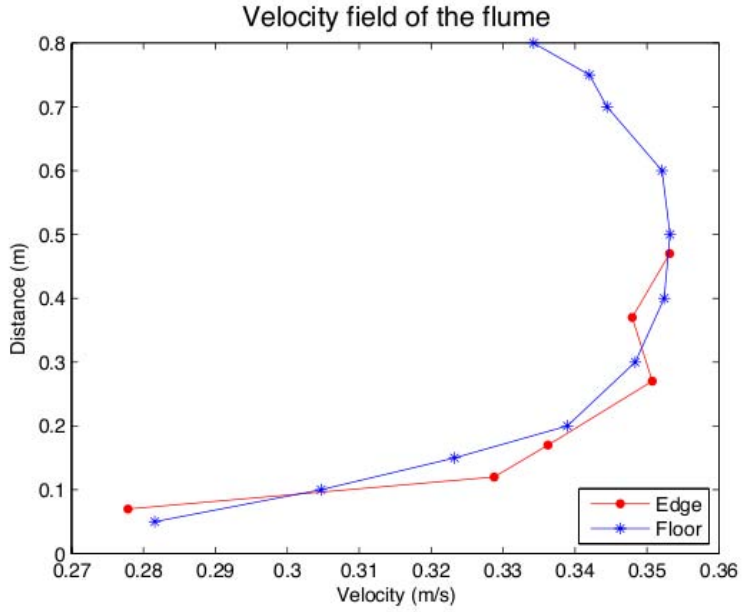
Velocity field of the flume
Distance (m)
Velocity (m/s)
0
0.1
0.2
0.3
0.4
0.5
0.6
0.7
0.8
0.27
0.28
0.29
0.3
0.31
0.32
0.33
0.34
0.35
0.36
Edge
Floor

The turbine – Glauert opt. λ=5

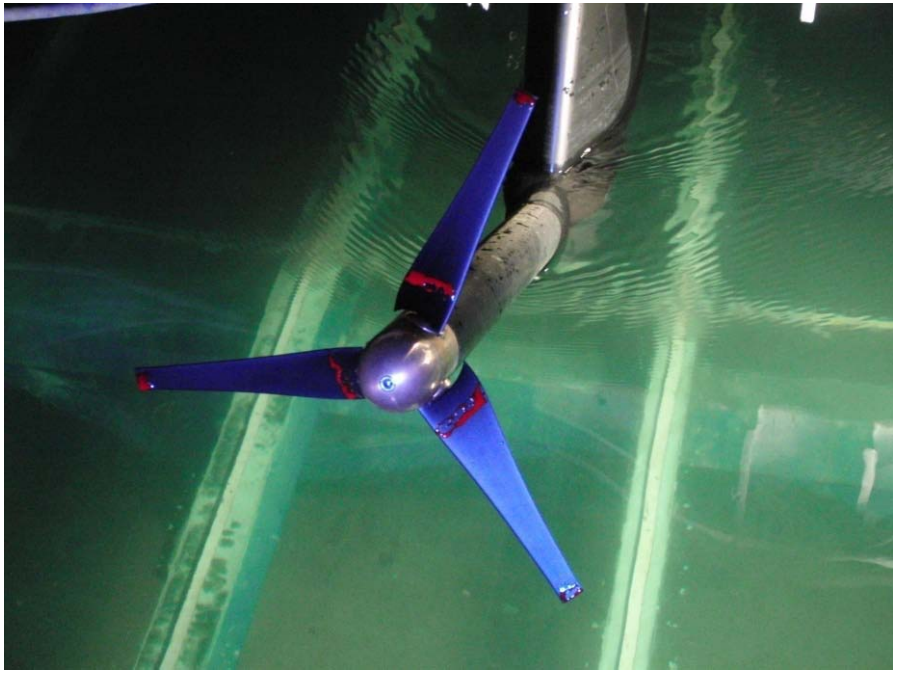

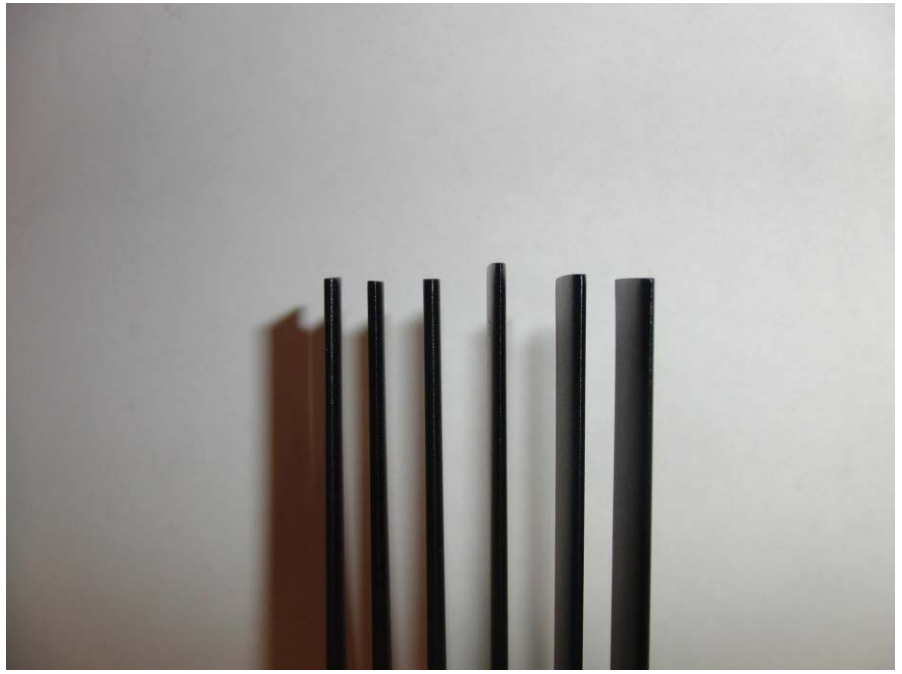

- D=0.35m
- SD7003 aerofoil

Fluorescein on tips - TSR 5

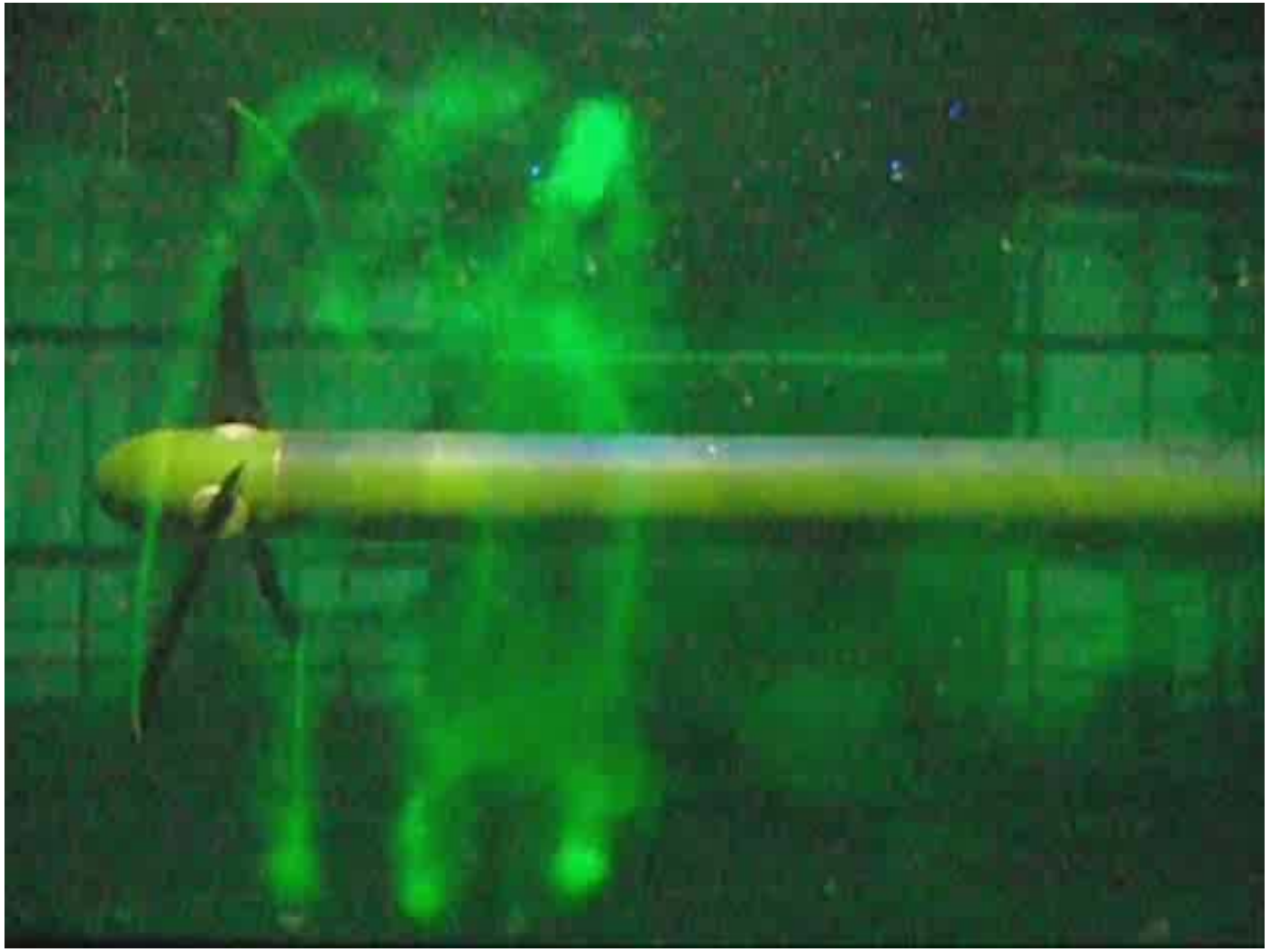

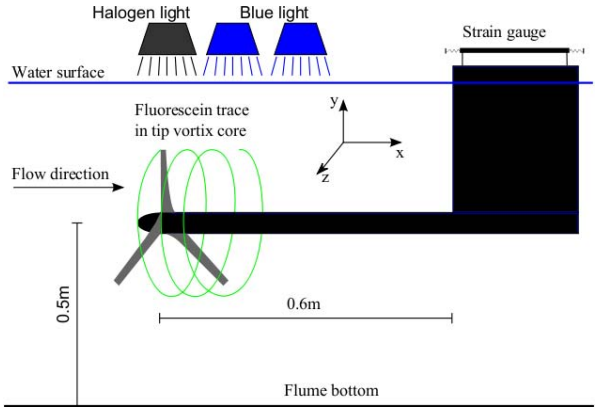

Fluorescein on tips -TSR 4

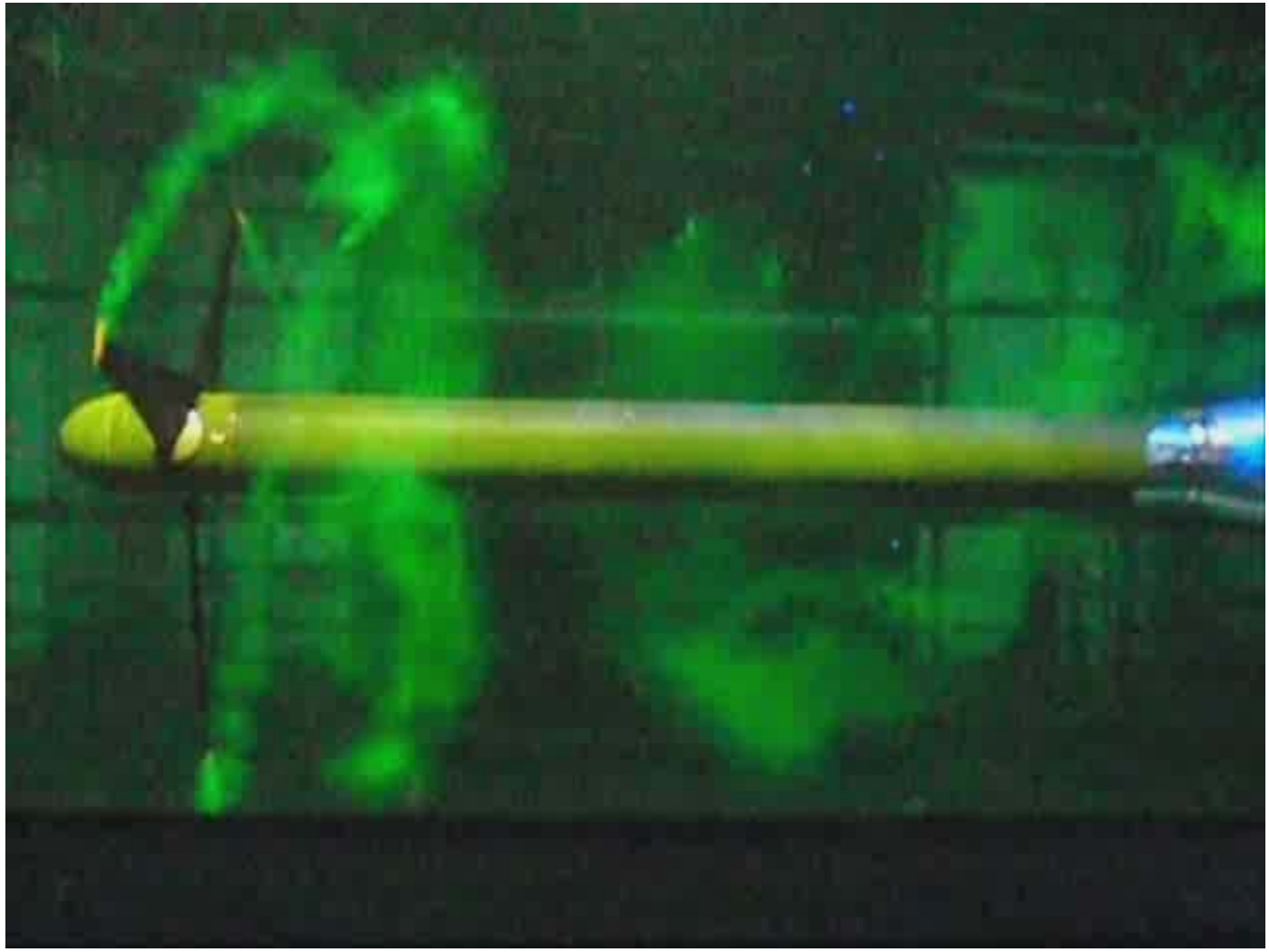

Fluorescein on tips - TSR 7

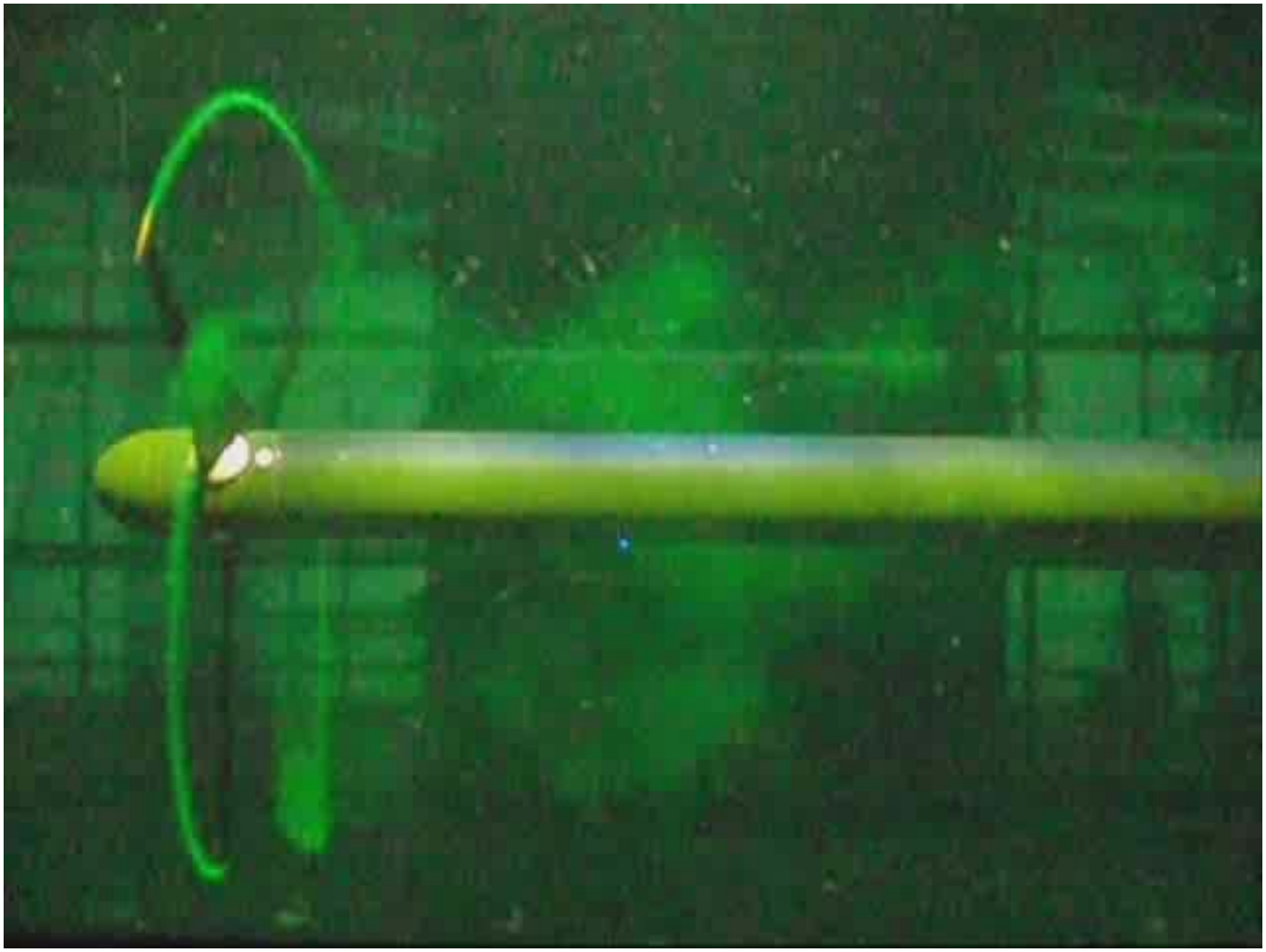

PIV set-up

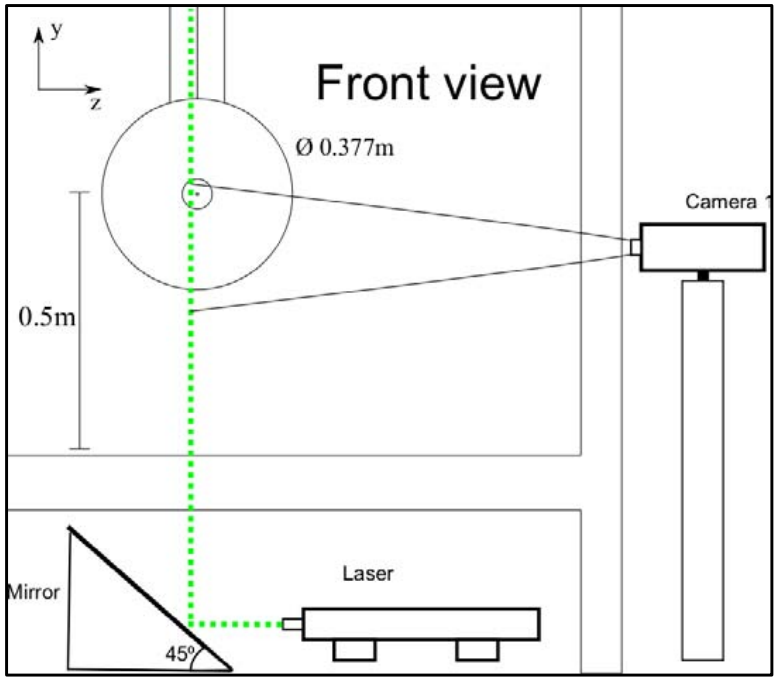
y
z
Front view
Ø 0.377m
Camera
0.5m
Mirror
Laser
45°

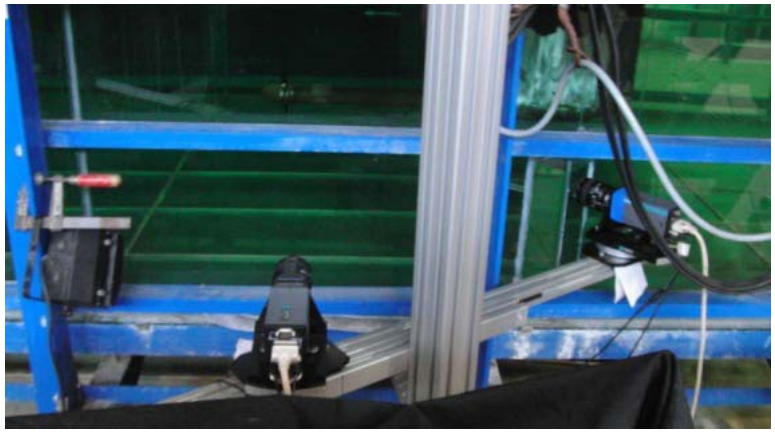

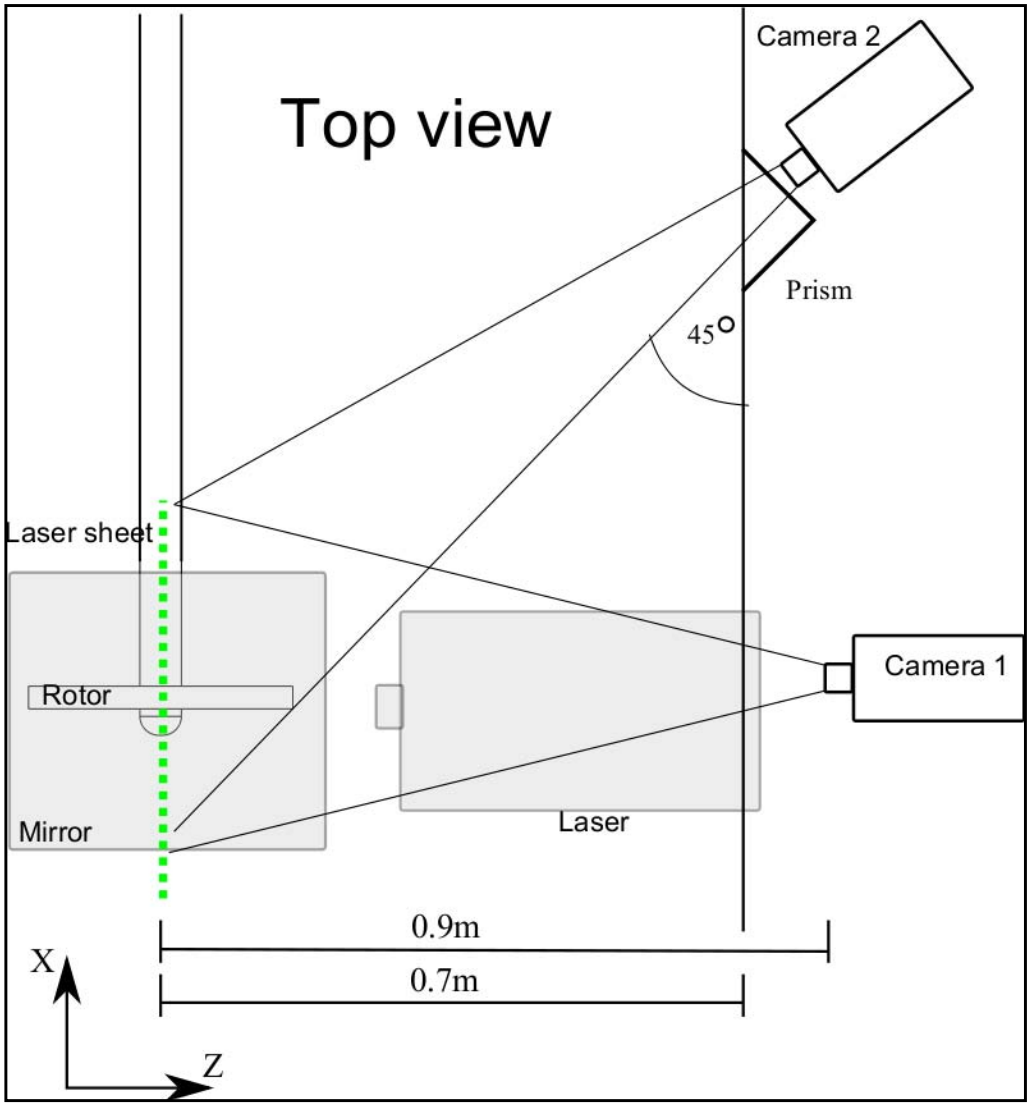
Top view
Camera 2
Prism
45°
Laser sheet
Rotor
Camera 1
Mirror
Laser
0.9m
0.7m
X
Z

Focus areas

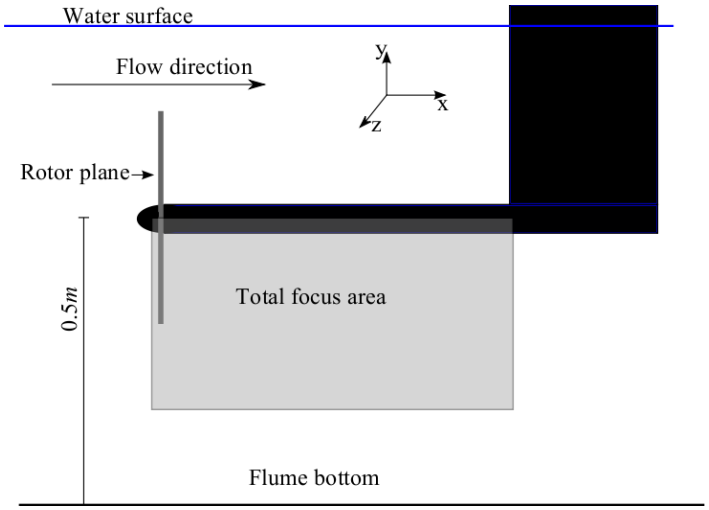
Water surface
Flow direction
y
x
z
Rotor plane
0.5m
Total focus area
Flume bottom

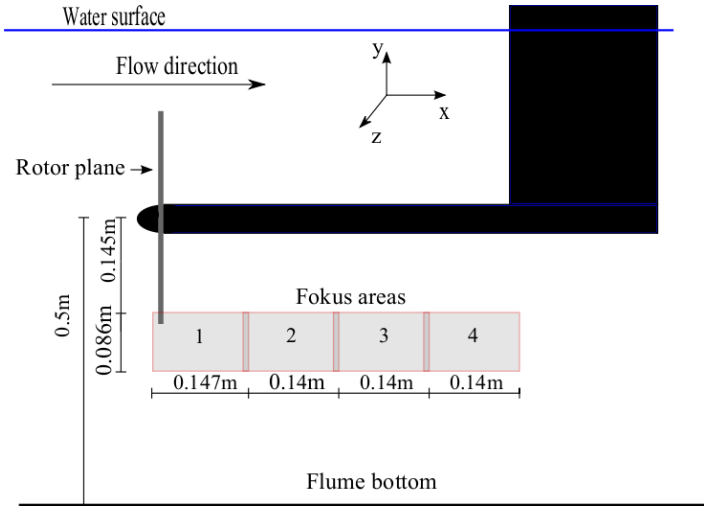
Water surface
Flow direction
y
x
z
Rotor plane
0.5m
0.145m
0.086m
Fokus areas
1
2
3
4
0.147m
0.14m
0.14m
0.14m
Flume bottom

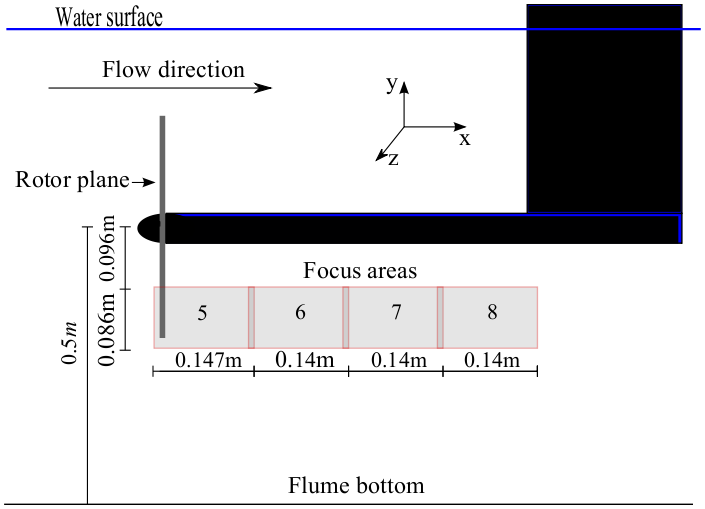
Water surface
Flow direction
y
x
z
Rotor plane
0.5m
0.096m
0.086m
Focus areas
5
6
7
8
0.147m
0.14m
0.14m
0.14m
Flume bottom

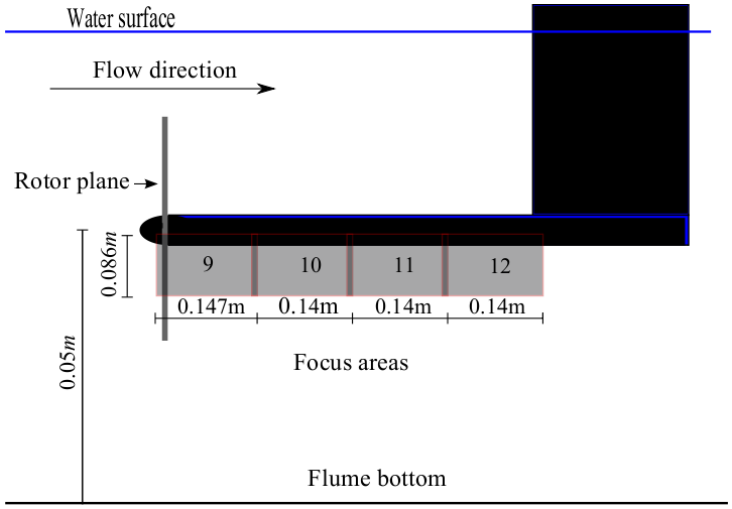
Water surface
Flow direction
Rotor plane
0.086m
9
10
11
12
0.147m
0.14m
0.14m
0.14m
Focus areas
0.05m
Flume bottom

PIV, Mean(500) Axial Velocity, TSR 4-7

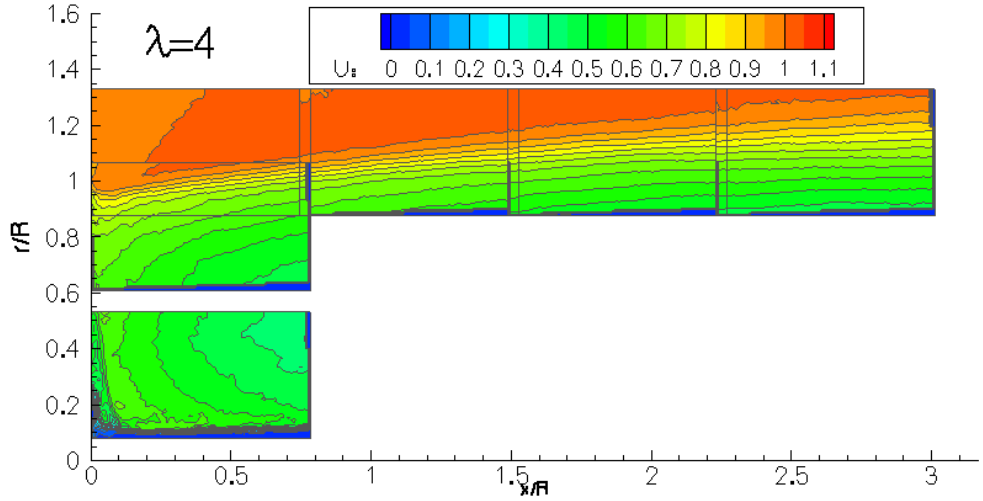

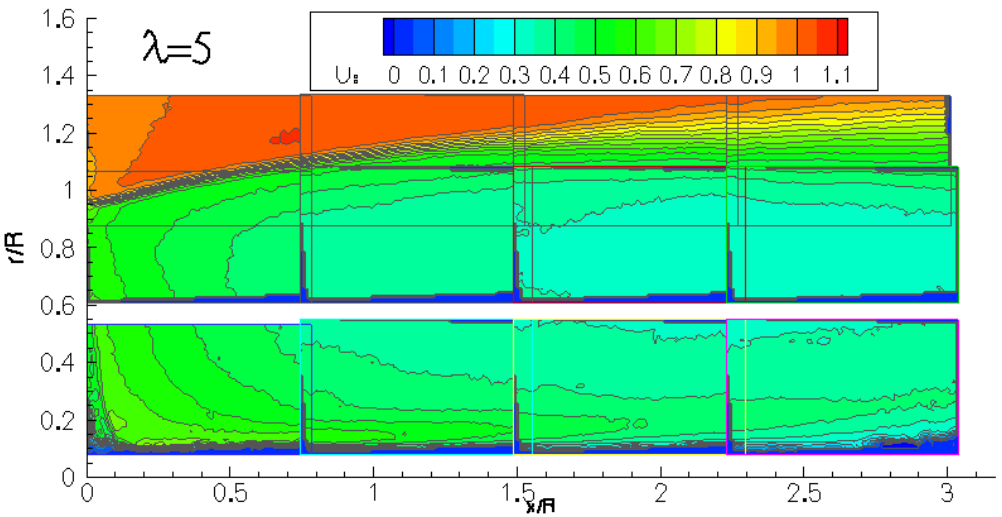

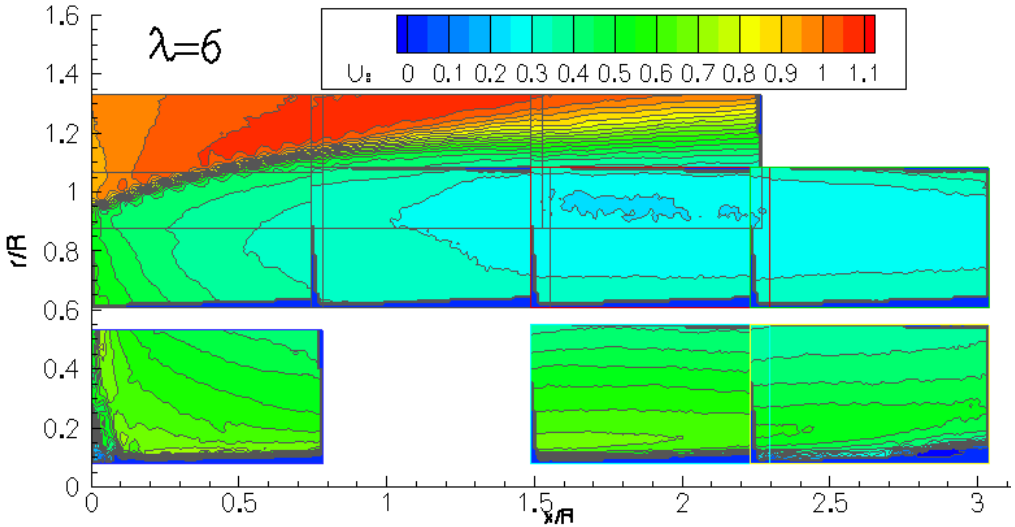

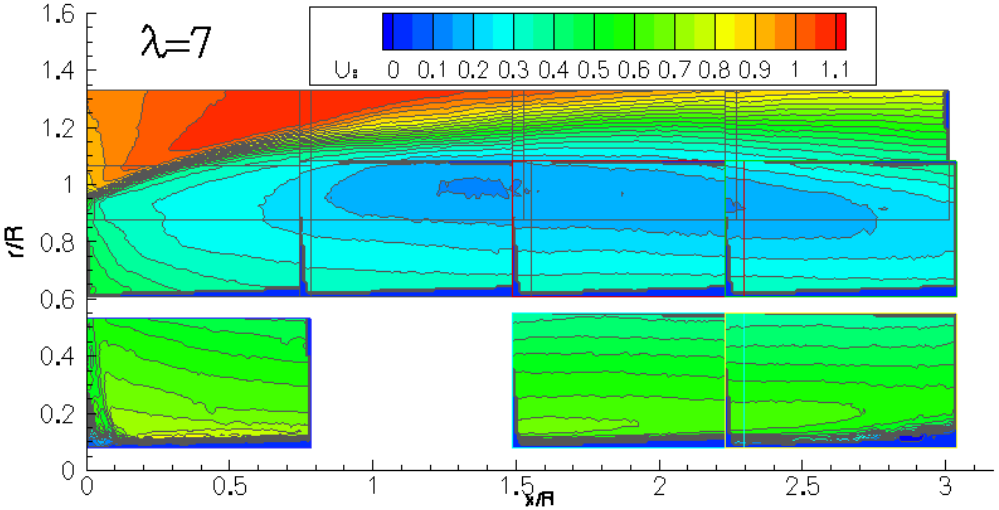

PIV, Mean Axial Velocity Urms TSR 4-7

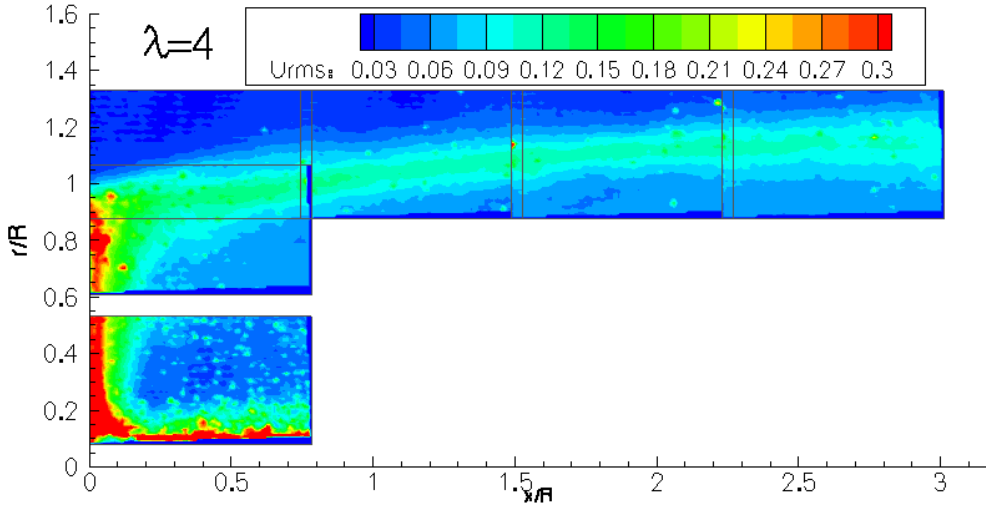

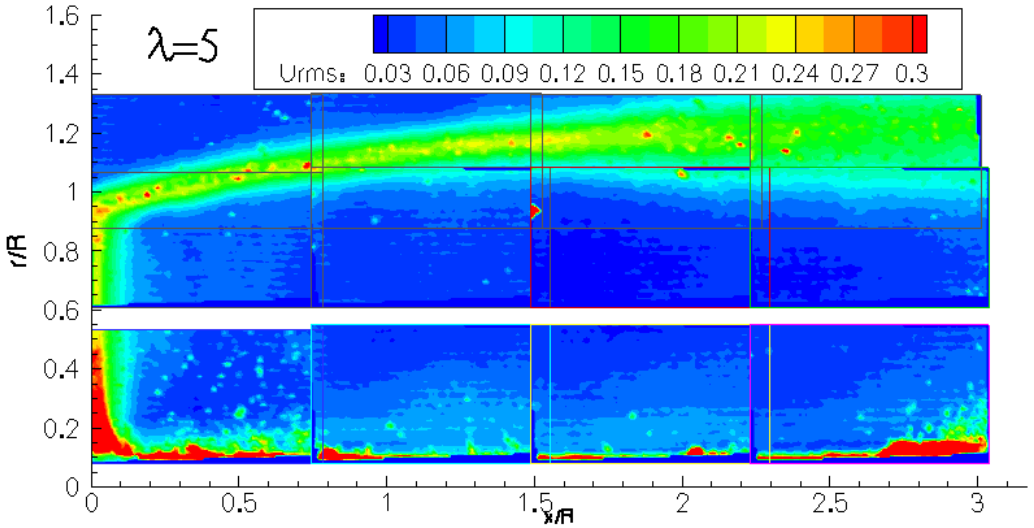

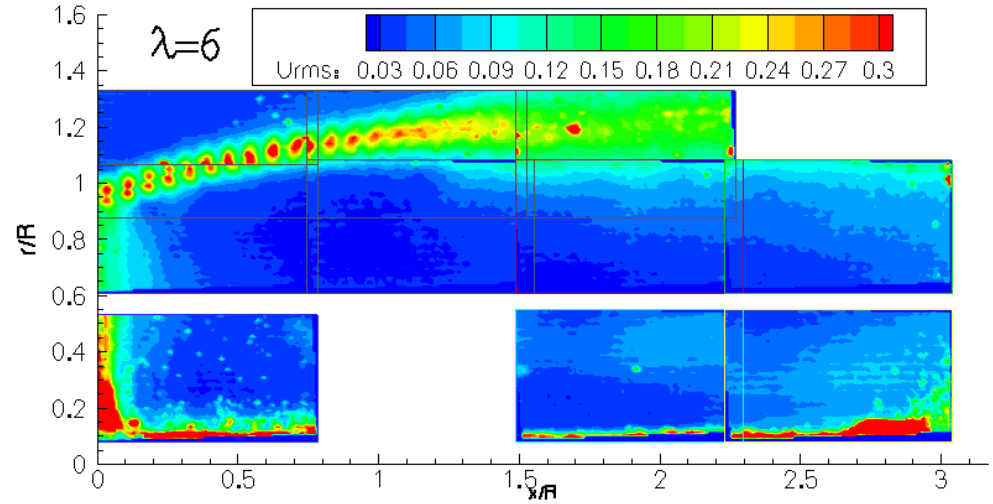

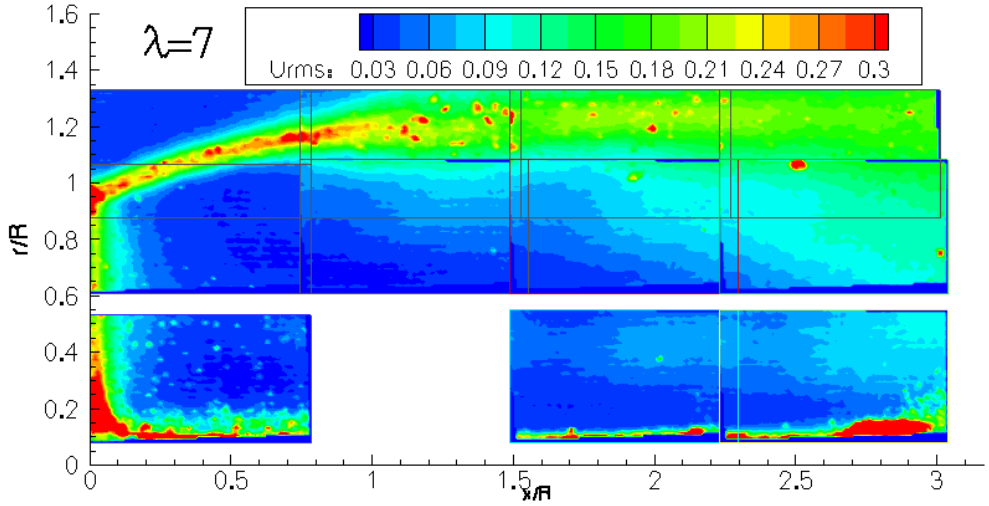

PIV, Mean Axial Velocity U TSR 4-7

4

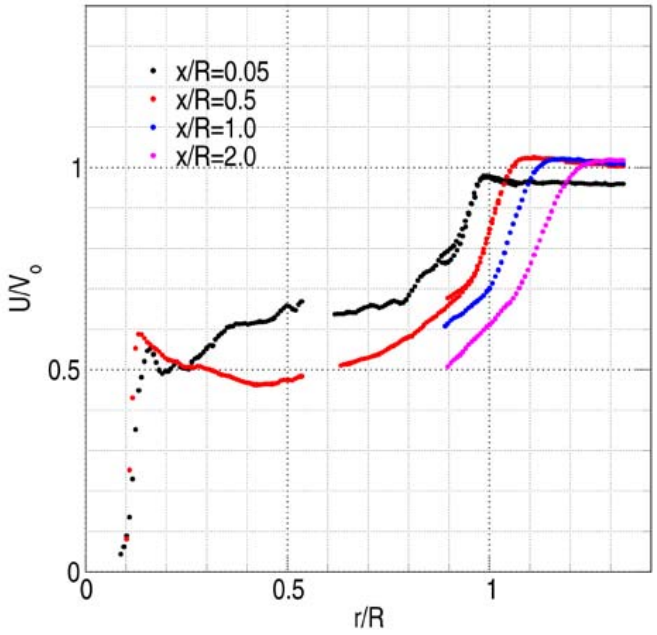

5

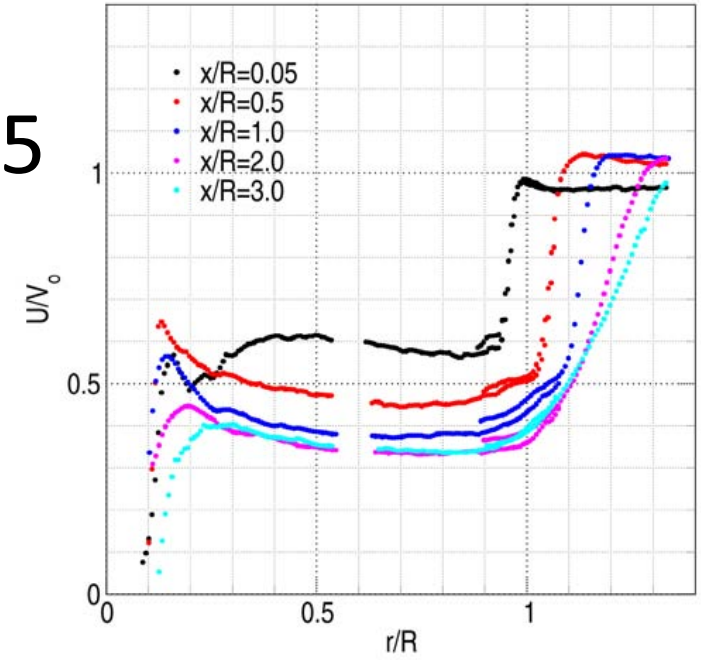

6

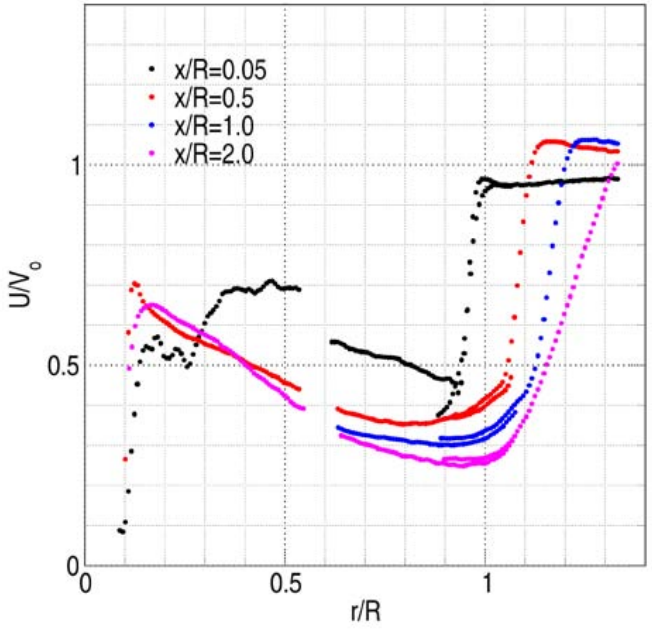

7

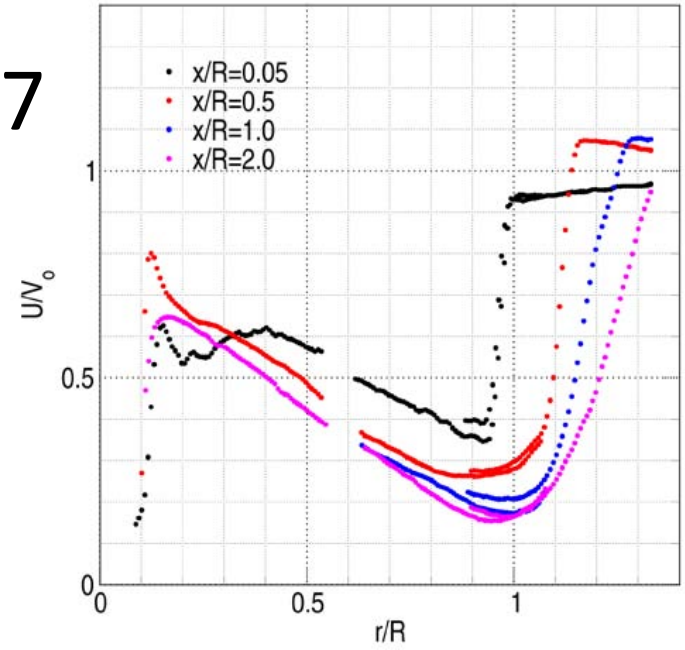

PIV, Phase ave., U-vel, TSR 6

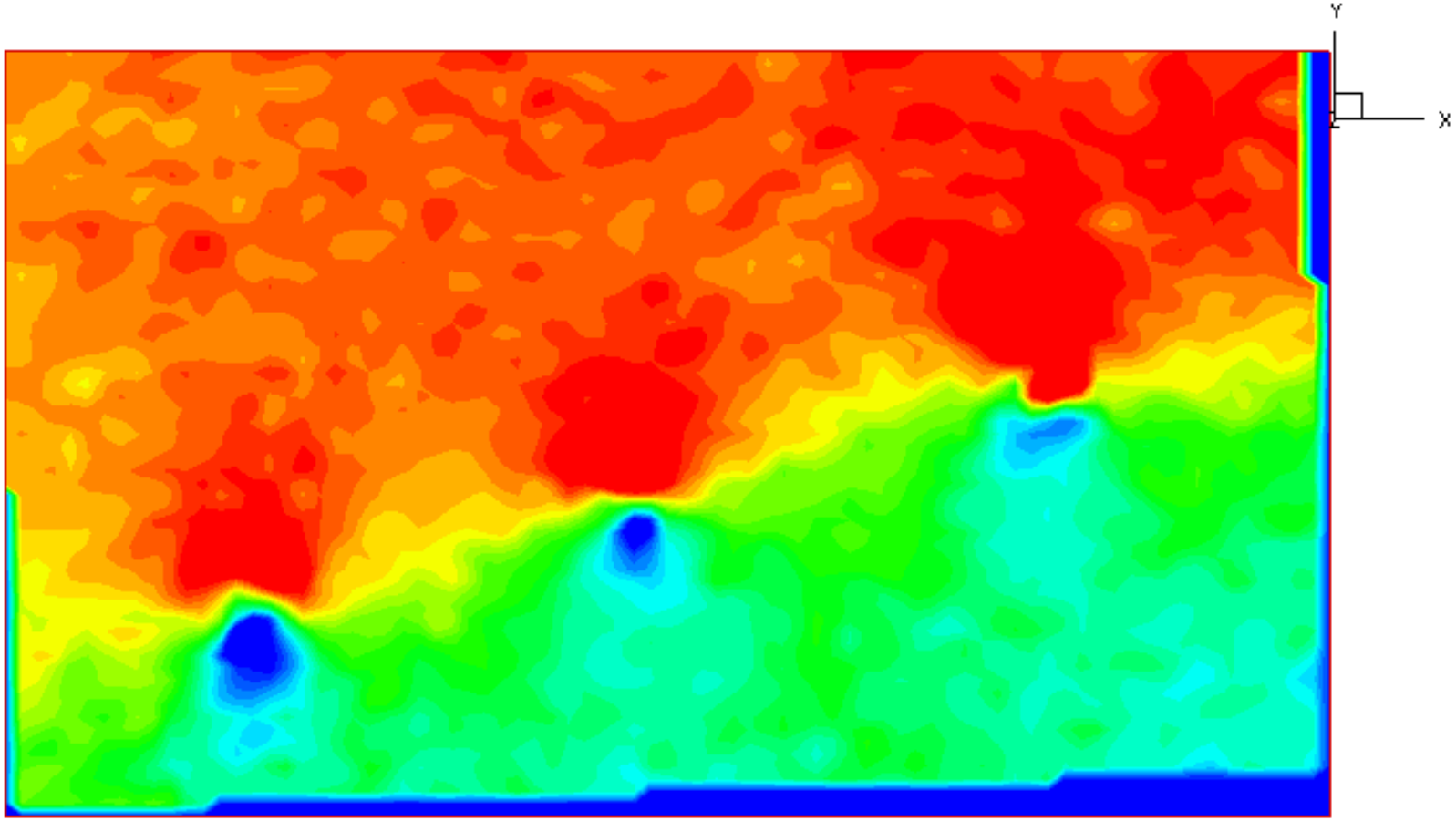

PIV, Phase Average(100) Uax TSR 4-7

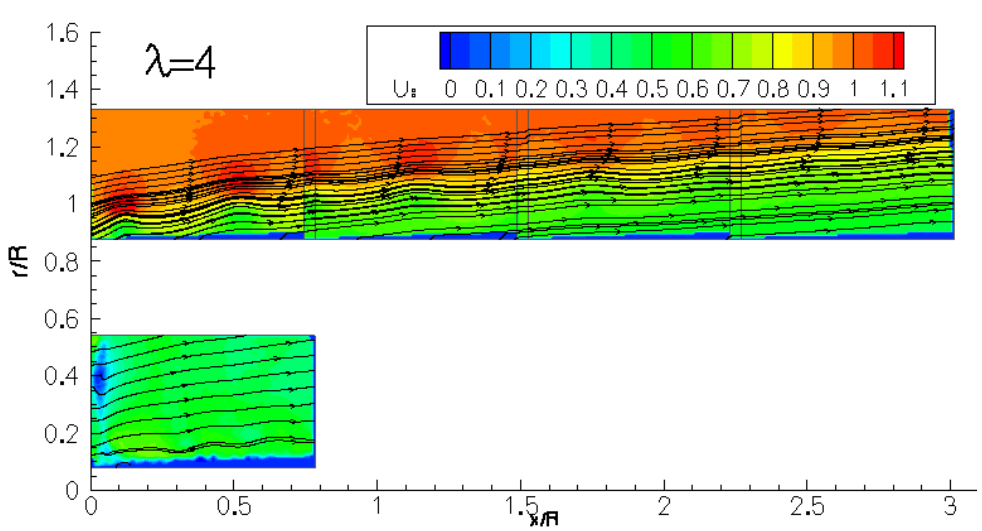

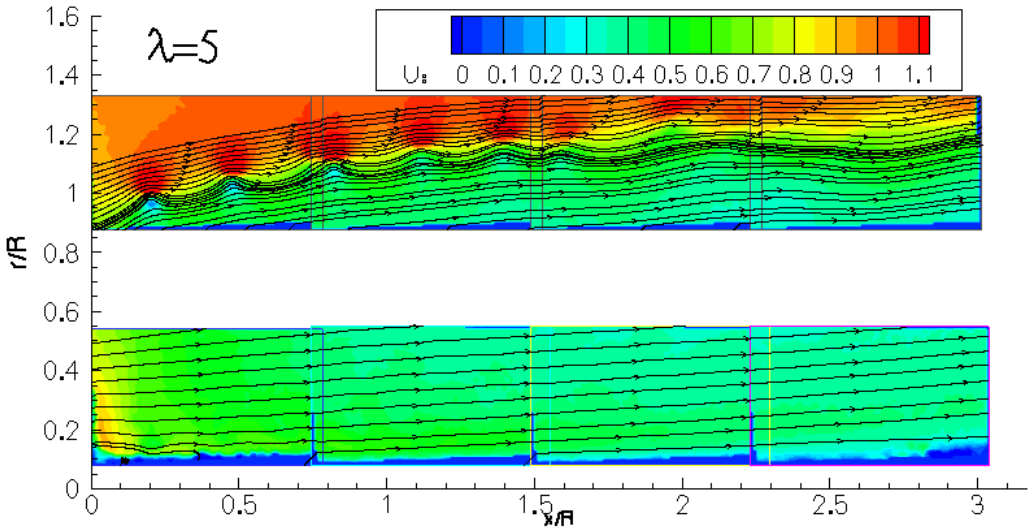

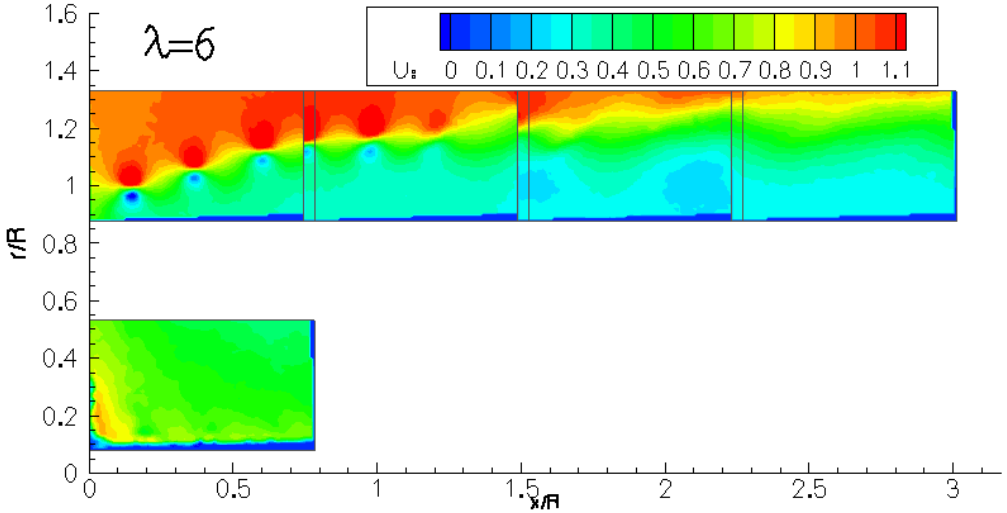

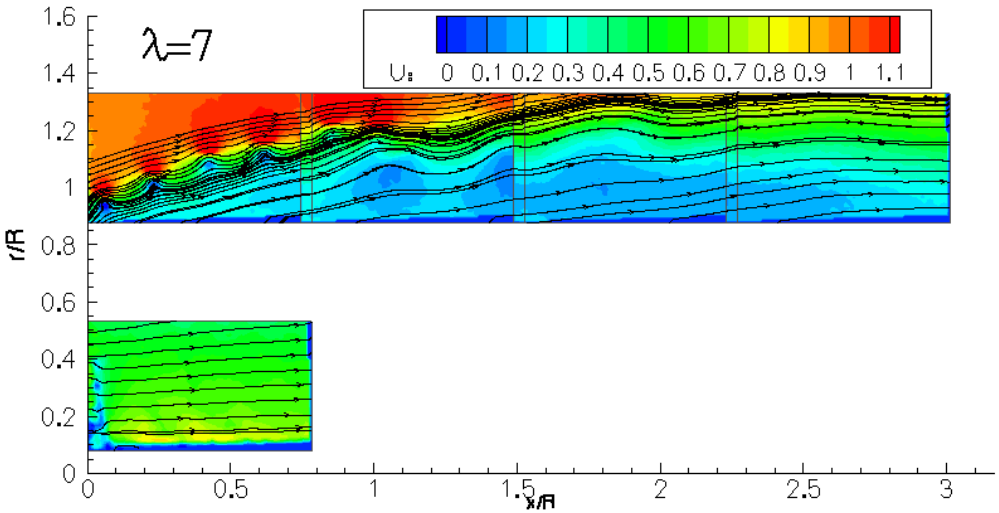

MEXICO PIV, Phase Ave., Uax

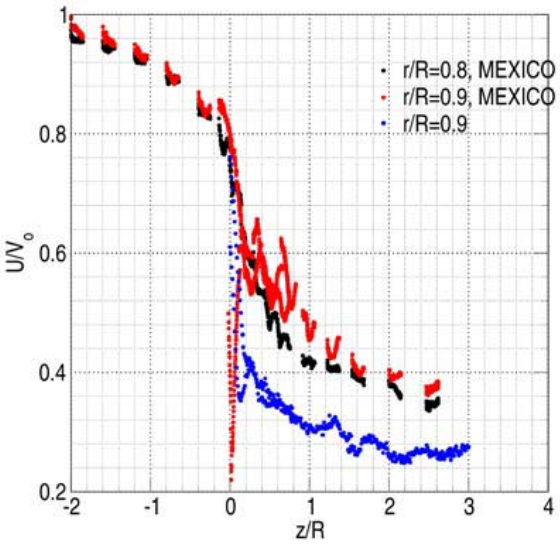

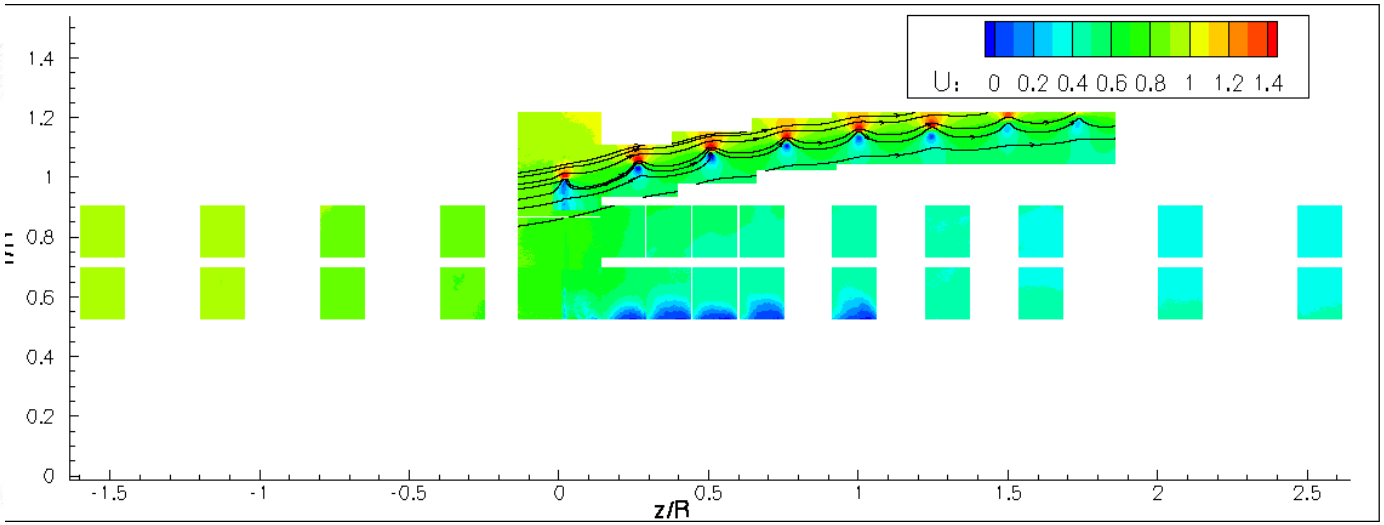

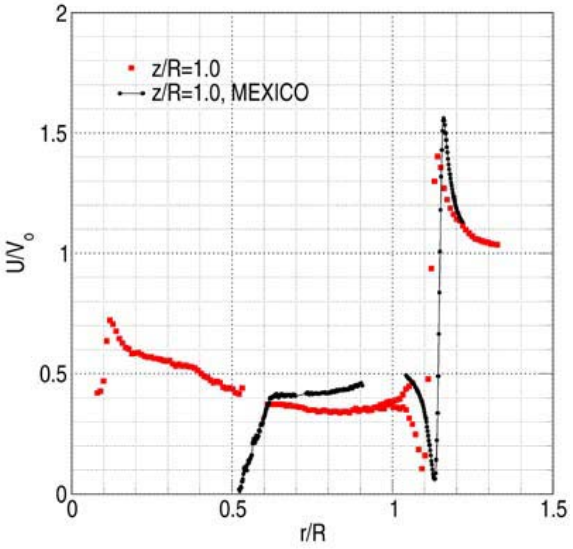

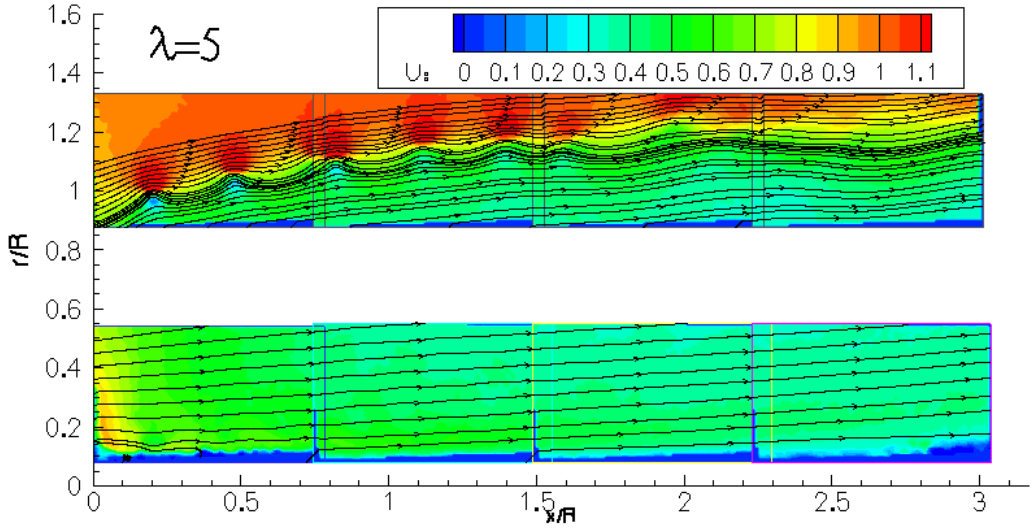

MEXICO PIV, Phase Ave., W

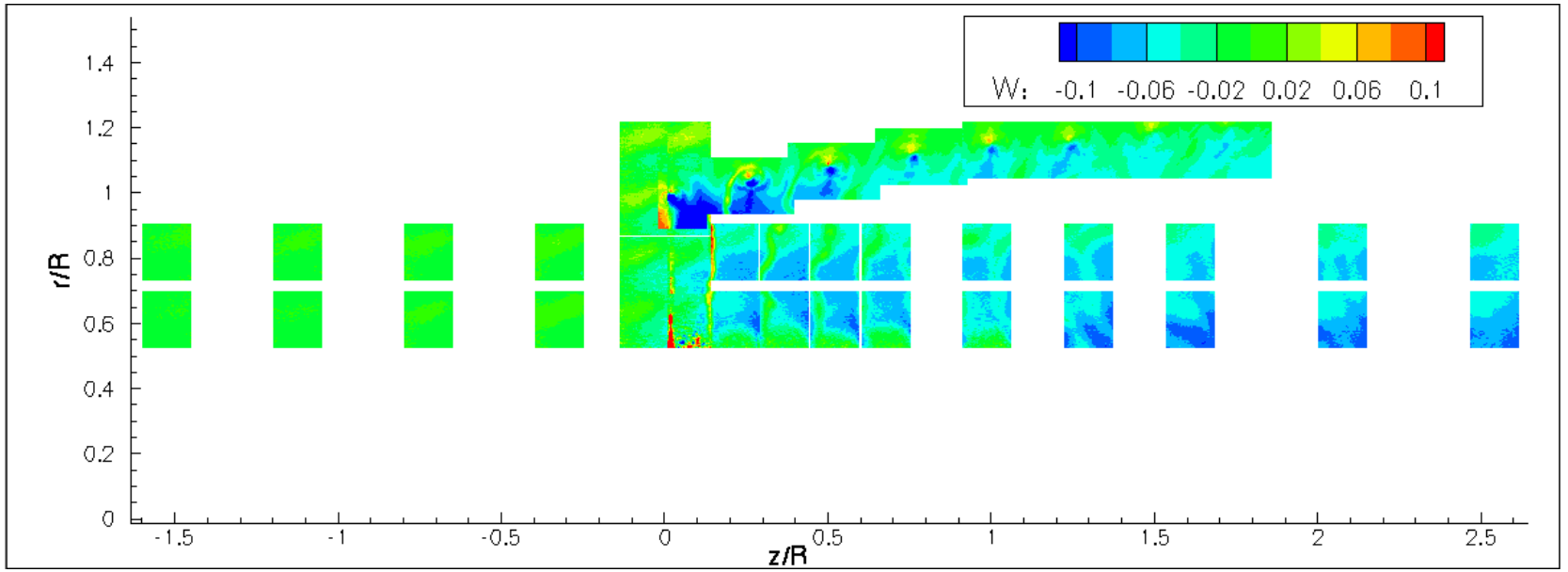

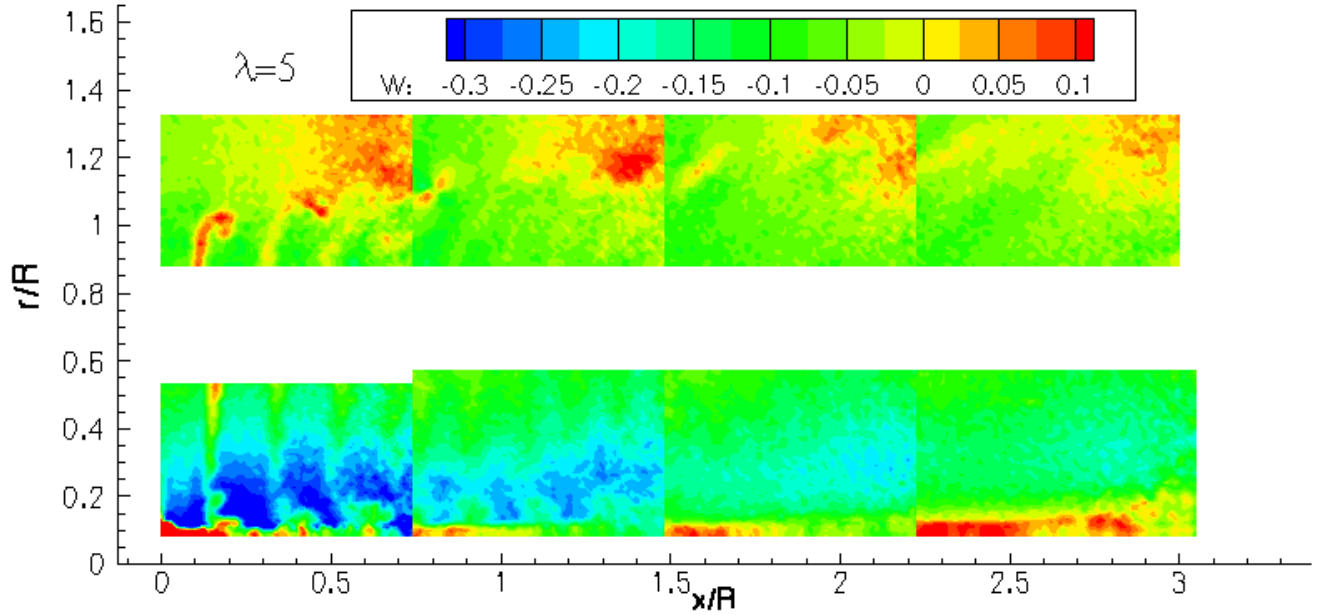

PIV, Tangentiel Vel, W-mean TSR 4-7

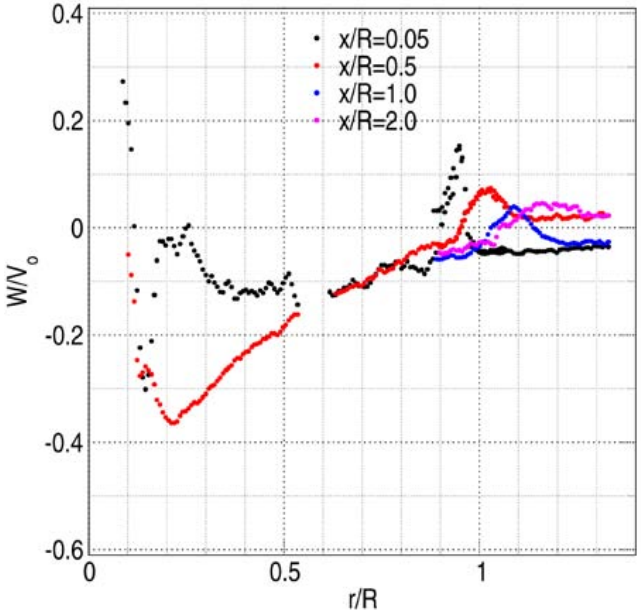

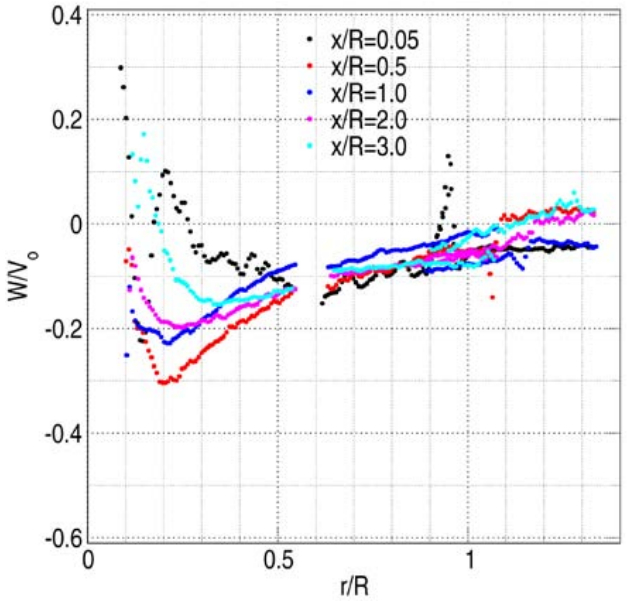

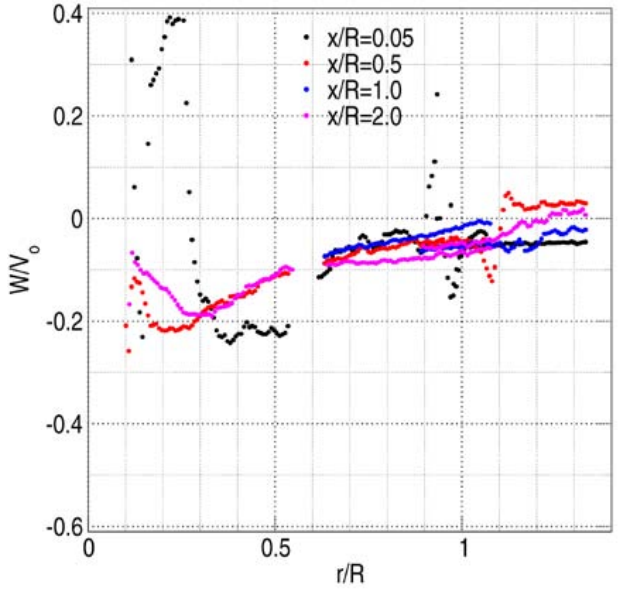

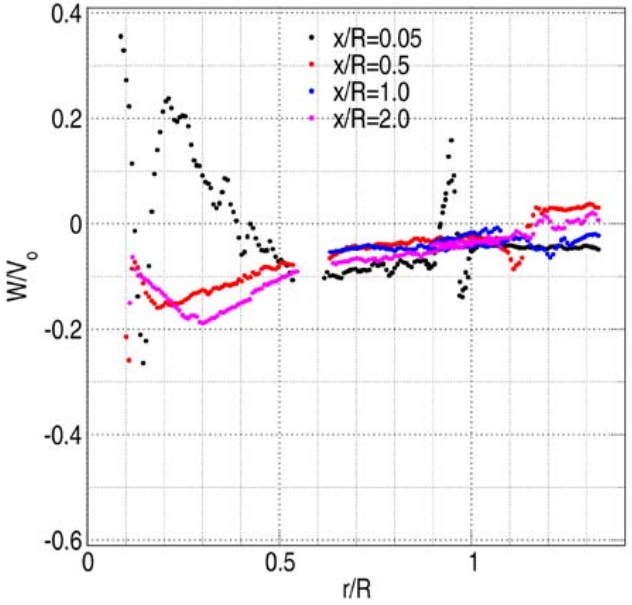

PIV, Phase ave., U-rms, TSR 4-7

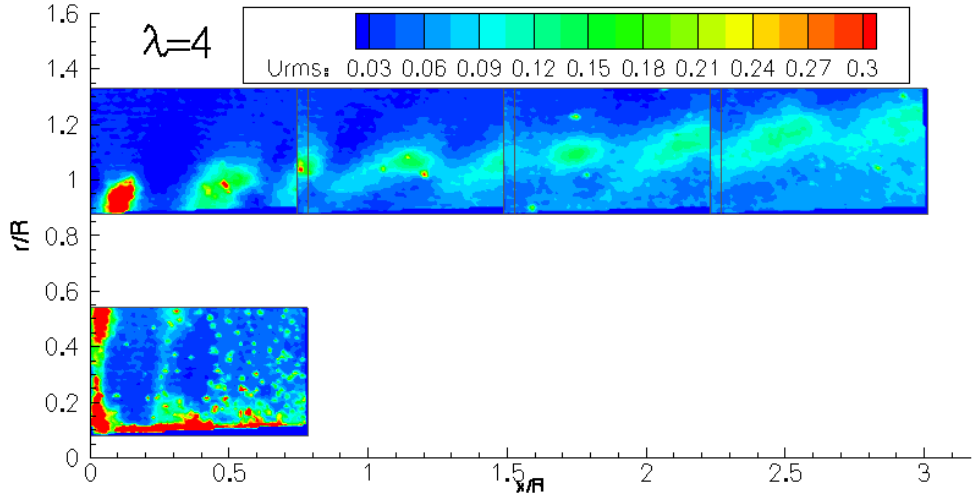

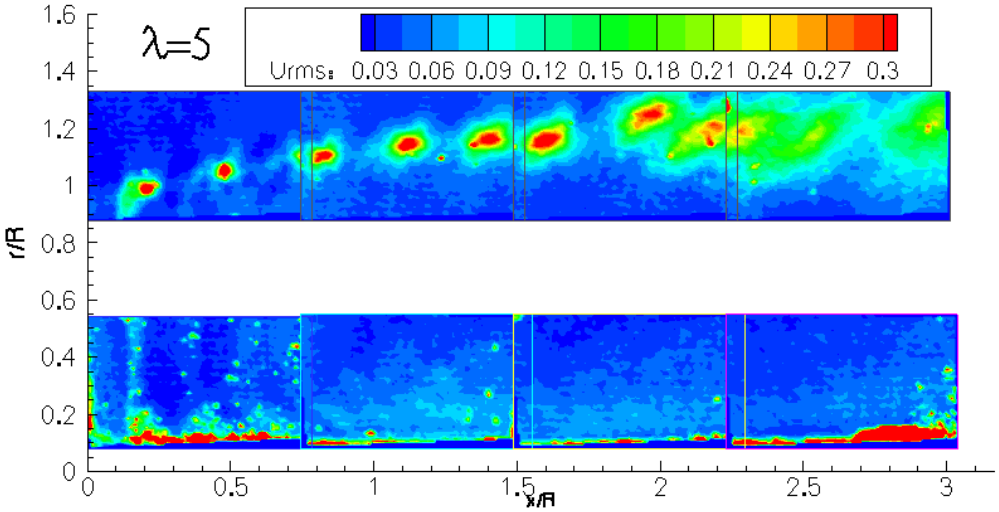

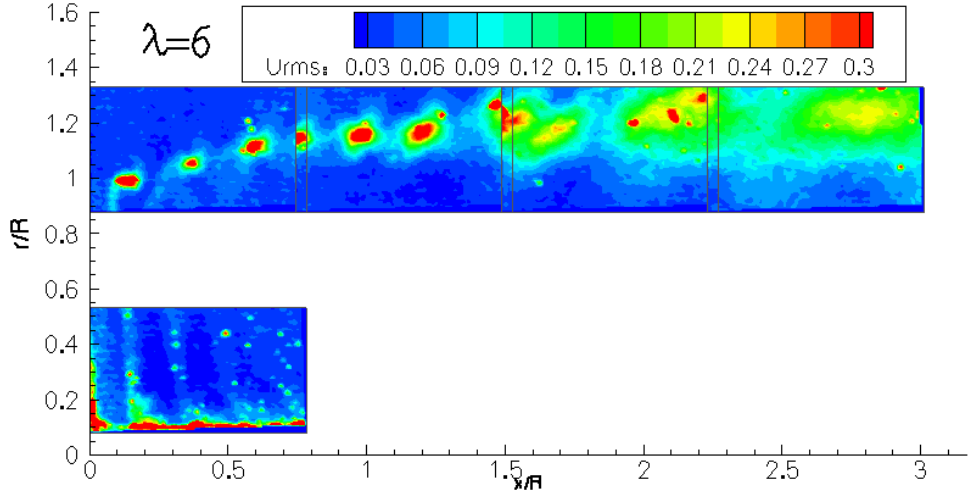

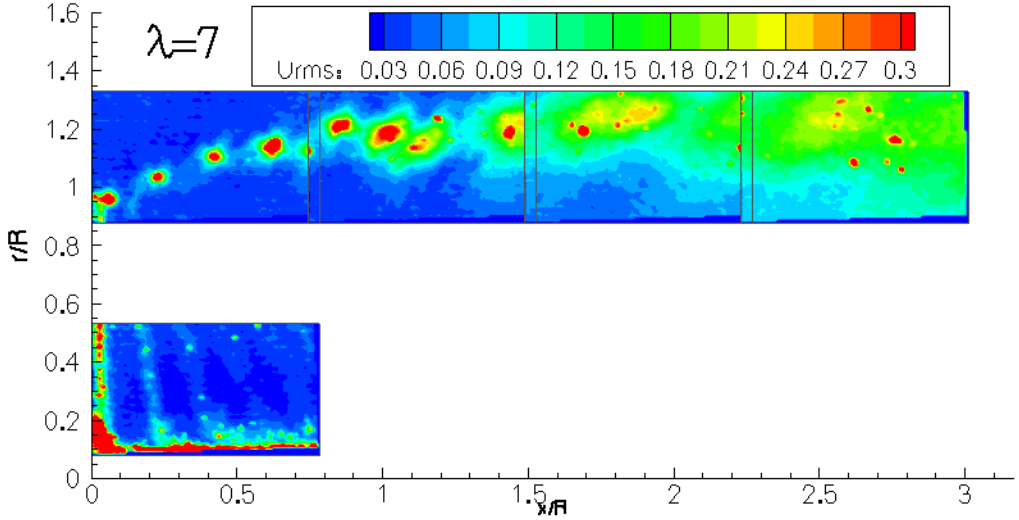

PIV, U-vel, TSR 6 unfolded, 5deg/s

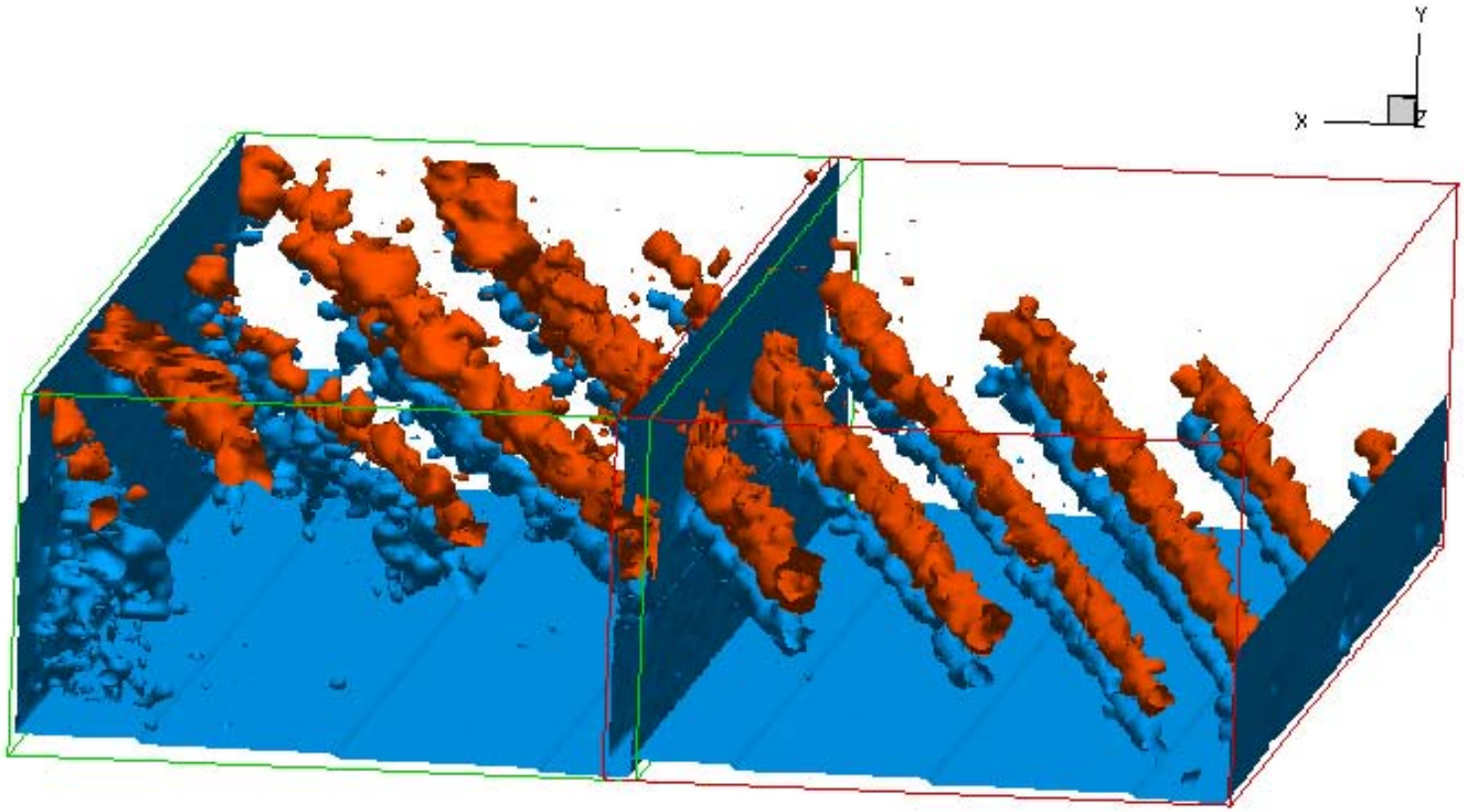

Expansion of the wake

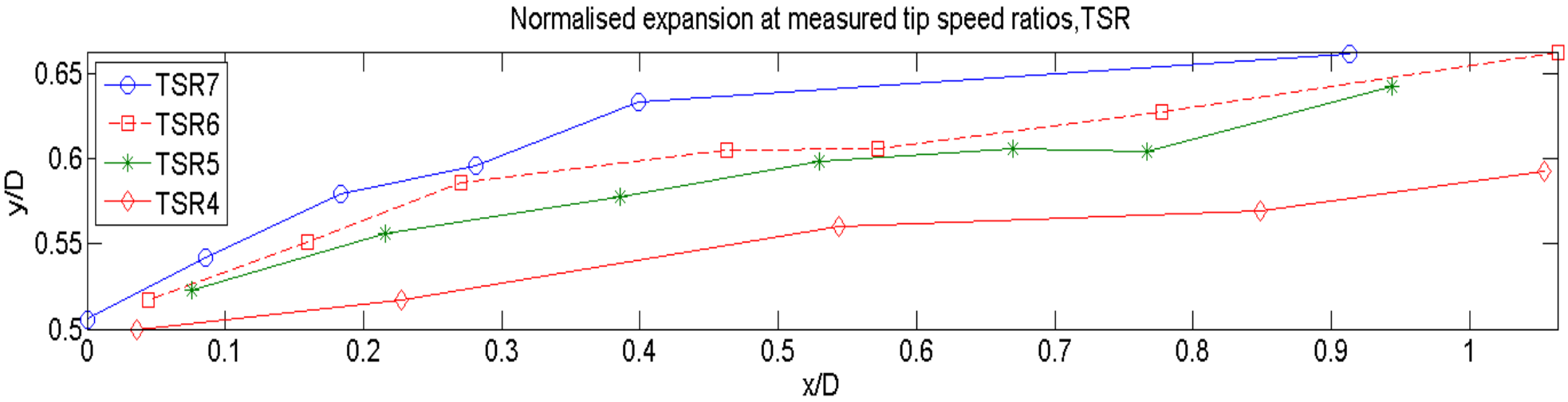

PIV, U-vel, TSR 6 unfolded, 5deg/s

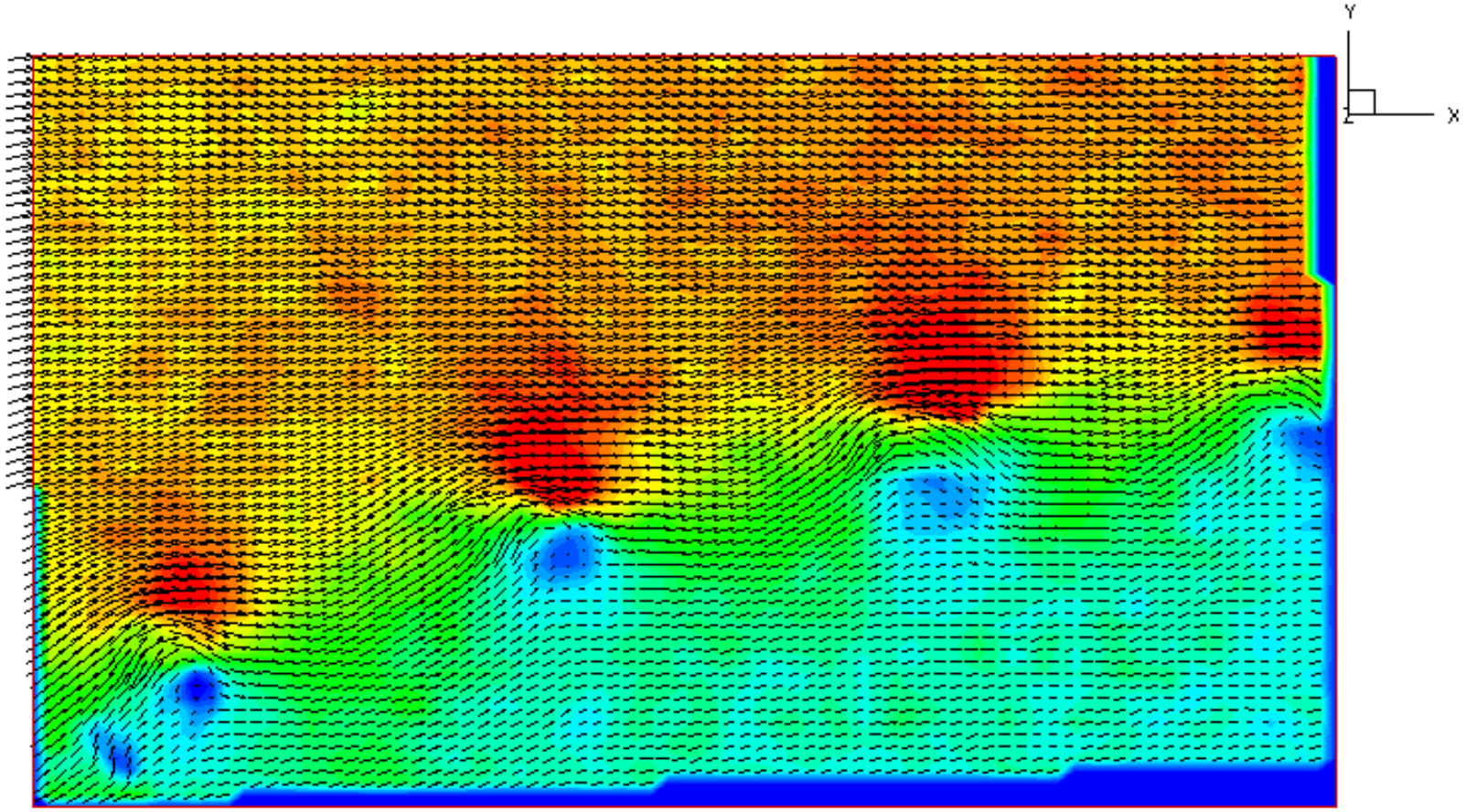

Rotation of the wake

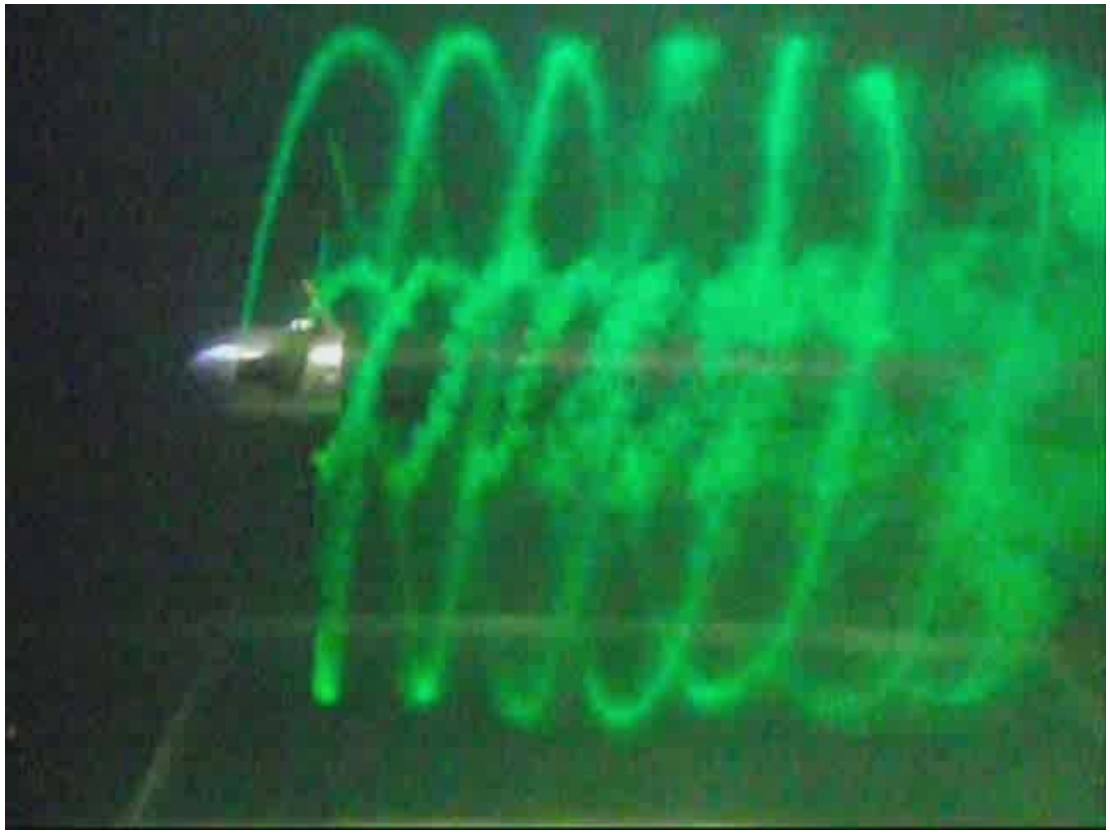

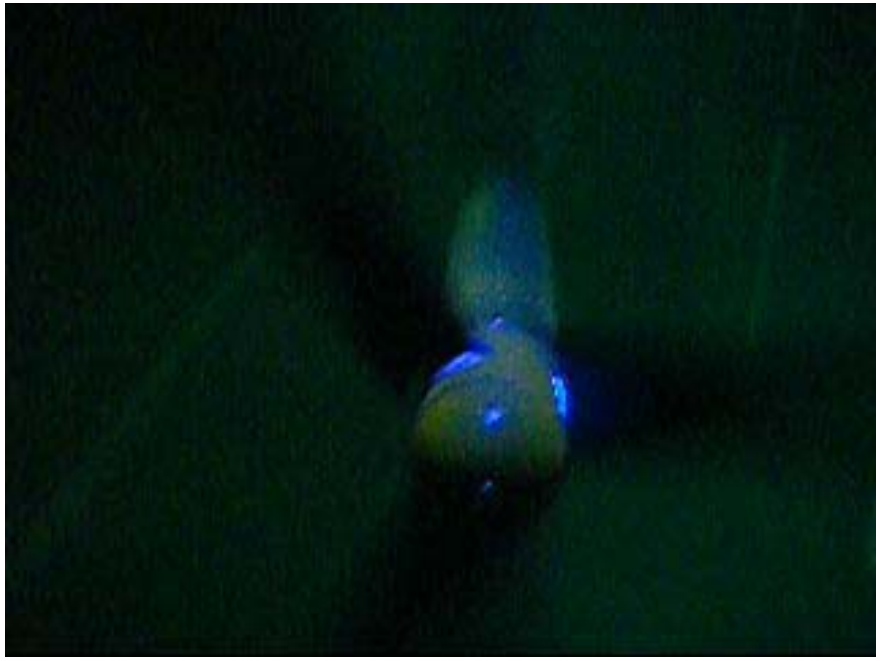

Thrust measurements

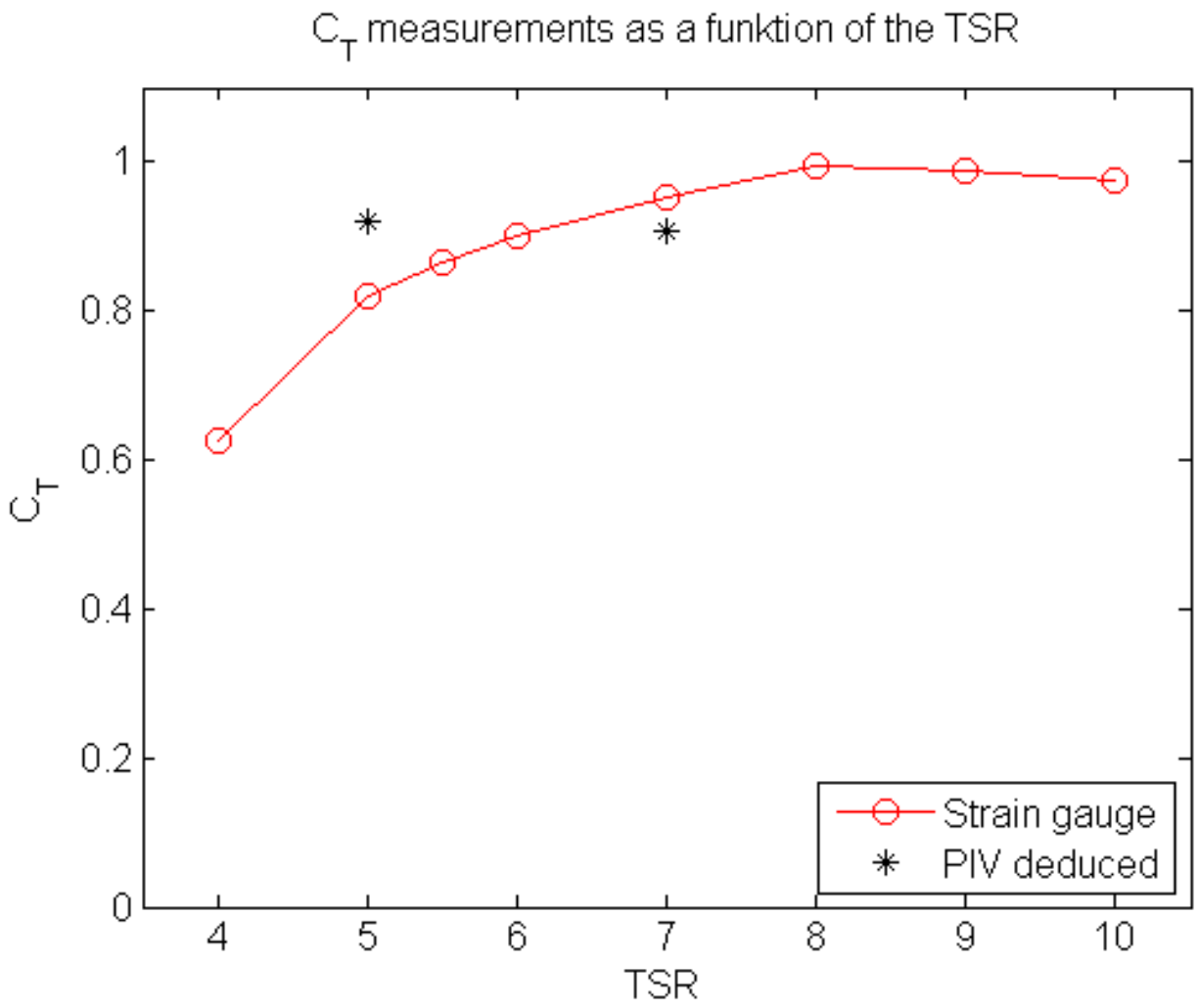

$$T = \dot{m}(V_0 - u_1)$$

$$C_T = \frac{T}{\frac{1}{2}\rho V_0^2 A}$$

Visualisation with upstream injection

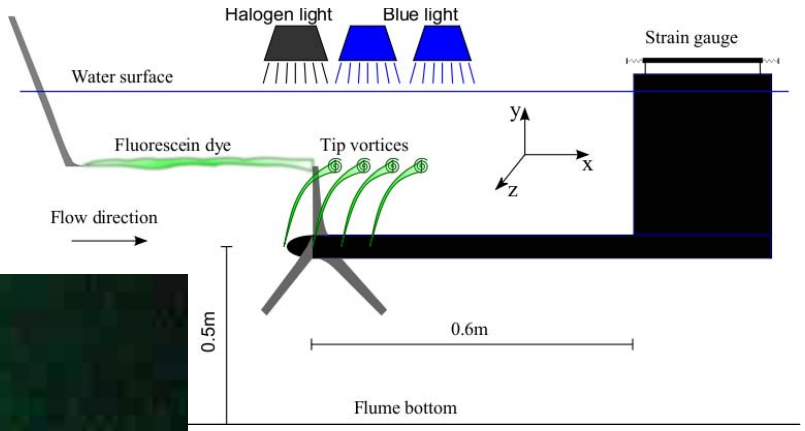

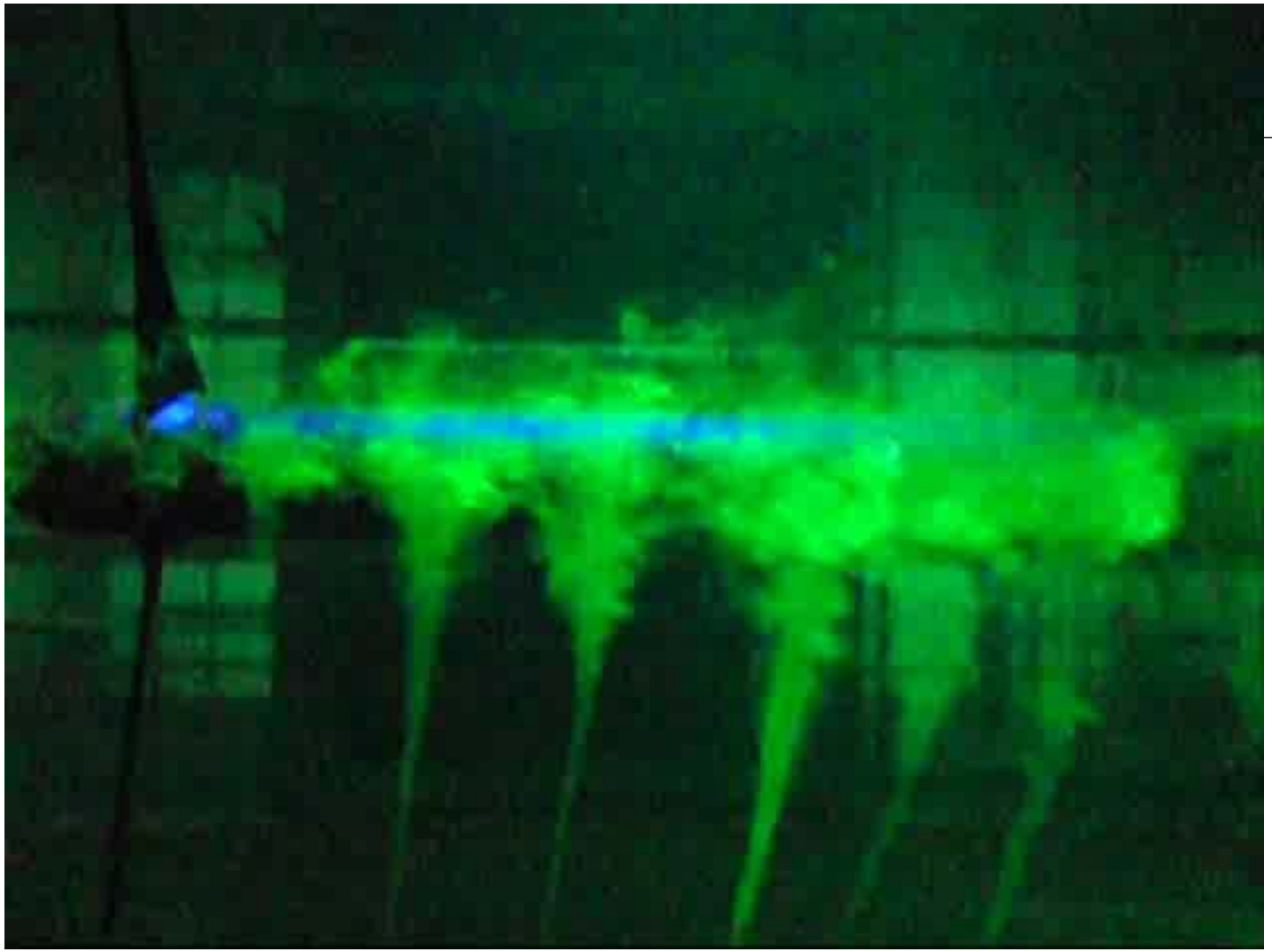

Summary

- Experimental facilities were found useable
- Visualization captures dynamics of helical structures
- Full mapping of the mean flow in the wake at TSR 4-7
- Wake expansion at different TSR’s
- 3D mapping of the wake near the rotor plane
- Strain gauge measurements needs improvment
- Improvement of PIV data
  - More measurements planed 2011
  - Out of plane vel.
  - Upstream measurements
  - Phase triggering

6 Simulations of backward swept blade

Potential of fatigue and extreme load reductions on swept blades using HAWC2

David Verelst

RISØ DTU

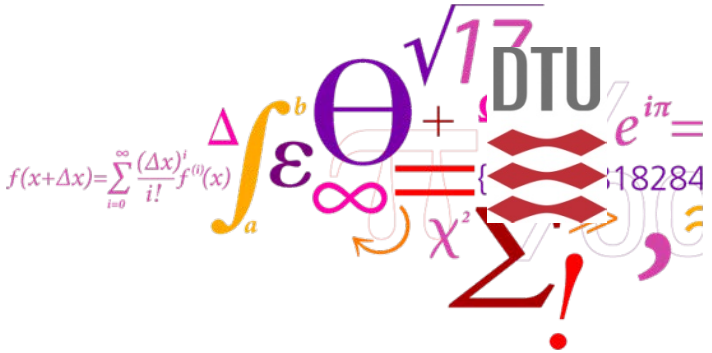

Risø DTU
National Laboratory for Sustainable Energy

UPWIND Turbine: 5MW NREL

Reference turbine by J. Jonkman et al (NREL 2009)

Rating	5 MW
Configuration	Upwind, 3 blades
Control	Variable speed, collective pitch
Drivetrain	High speed, Multiple-stage gearbox
Rotor, Hub diameter	126m, 3m
Cut-in, Rated, Cut-out wind speed	3 m/s, 11.4 m/s, 25 m/s
Cut-in, Rated rotor speed	6.9, 12.1 RPM
Rated tip speed	80 m/s
Overhang, Shaft tilt, Precone	5m, 0 deg, 0 deg

Previous swept blade studies

- This presentation is based on a public Risø report:
  Load Consequences when Sweeping Blades – A Case Study of a 5 MW Pitch Controlled Wind Turbine, D.R.S. Verelst, T.J. Larsen, 2010
- Sandia – Night & Karver STAR blade
  - Objective: increase energy consumption on Zond 750 turbine for low wind speed sites (average wind speed around 5.8 m/s)
  - Zond 750 is a variable speed pitch controlled machine
  - Larger swept blade but load level maintained (blade root bending moments)
  - Increased energy capture in below rated conditions. Full scale tests shows energy increase of 10-12%
  - Thomas Ashwill et al., *Development of the Swept Twist Adaptive Rotor (STAR) Blade*, AIAA-2010-1582).

Why sweep?

- Sweep adds a geometric coupling between bending and twist deformations of the blade
- Increase blade size while maintaining blade root bending moment load levels. As a result, increased energy capture due to larger rotor
- For backward sweep, pitch to feather decreases angle of attack variations over one rotor revolution (cfr. turbulence, shear): passive cyclic pitch
- Preliminary results indicate decreased yawing moments (work in progress for EWEC 2011)

Methodology

- 5 sweep curve exponents combined with 24 tip offsets = 120 + 1 (ref.) blade variants
- 2 different controller implementations (Risø and NREL)
- Steady wind speeds (4..26 m/s, 1m/s steps)
- Turbulent wind speeds (4..26 m/s, 2m/s steps, 10 min series) same seed number, TI=0.18
- Equivalent loads for standard wind speed distribution and 20 years

$$x = a\left(\frac{z - z_0}{z_e - z_0}\right)^b$$

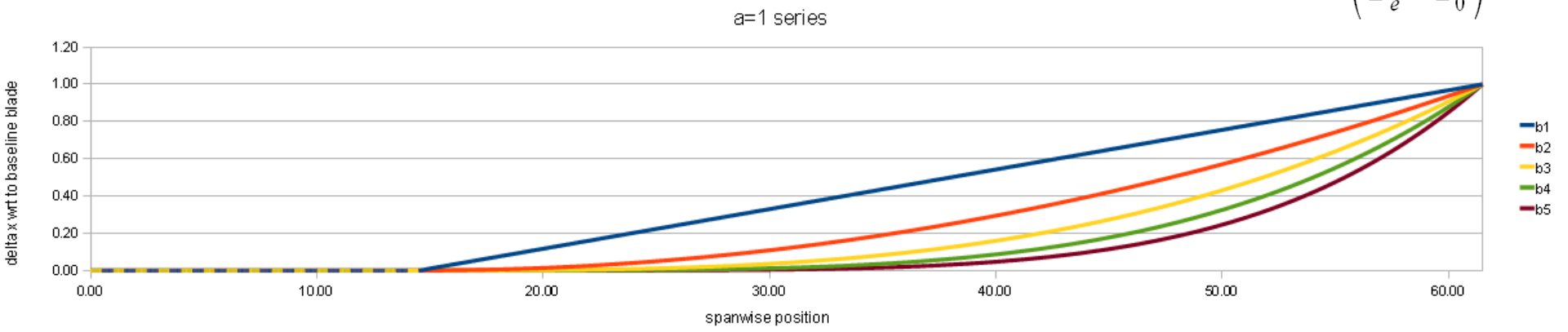

Blade structural characteristics

Start sweep curve at 14.35m (blade radial pos)

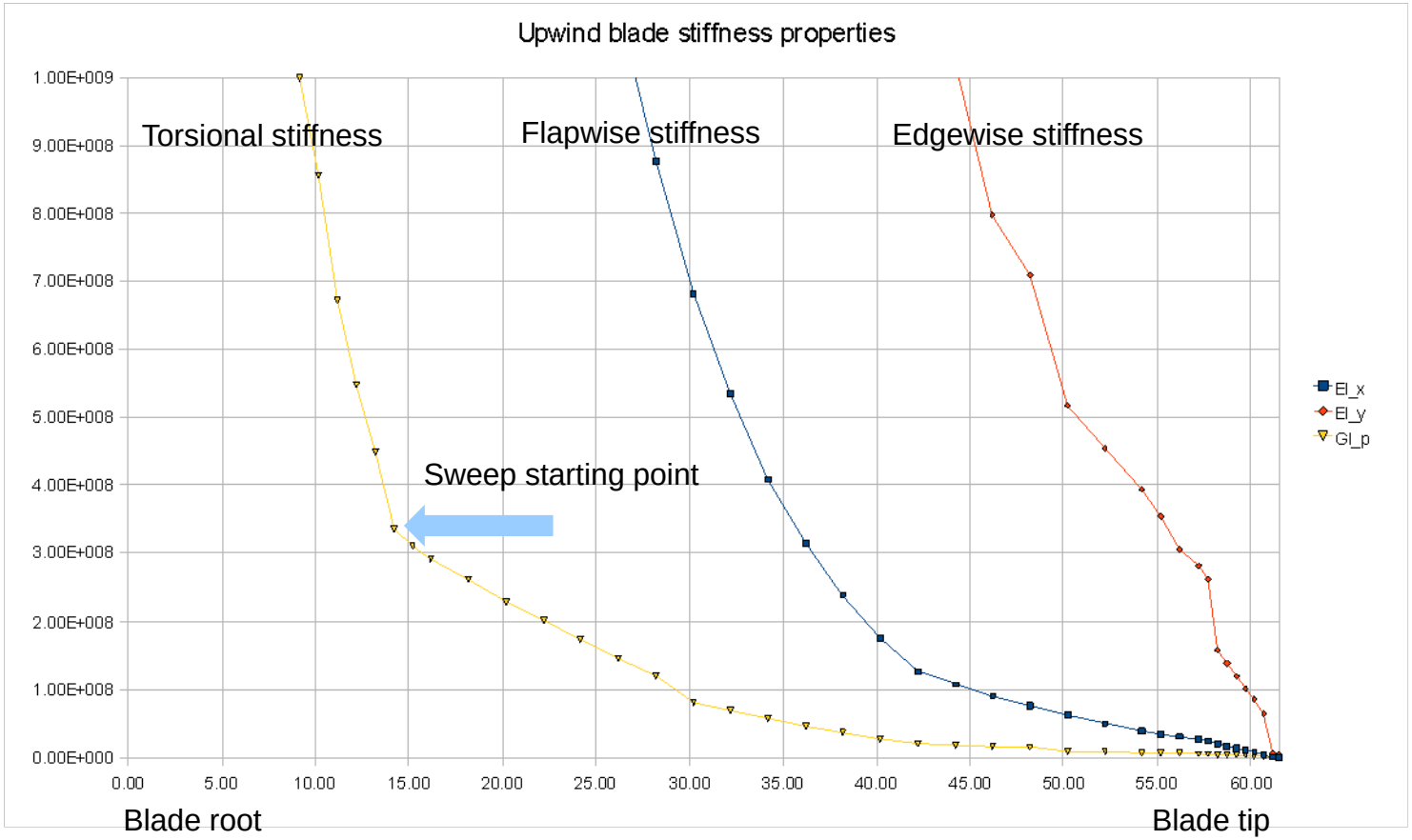

Equivalent loads – blade flap

Forward sweep

No sweep

Backward sweep

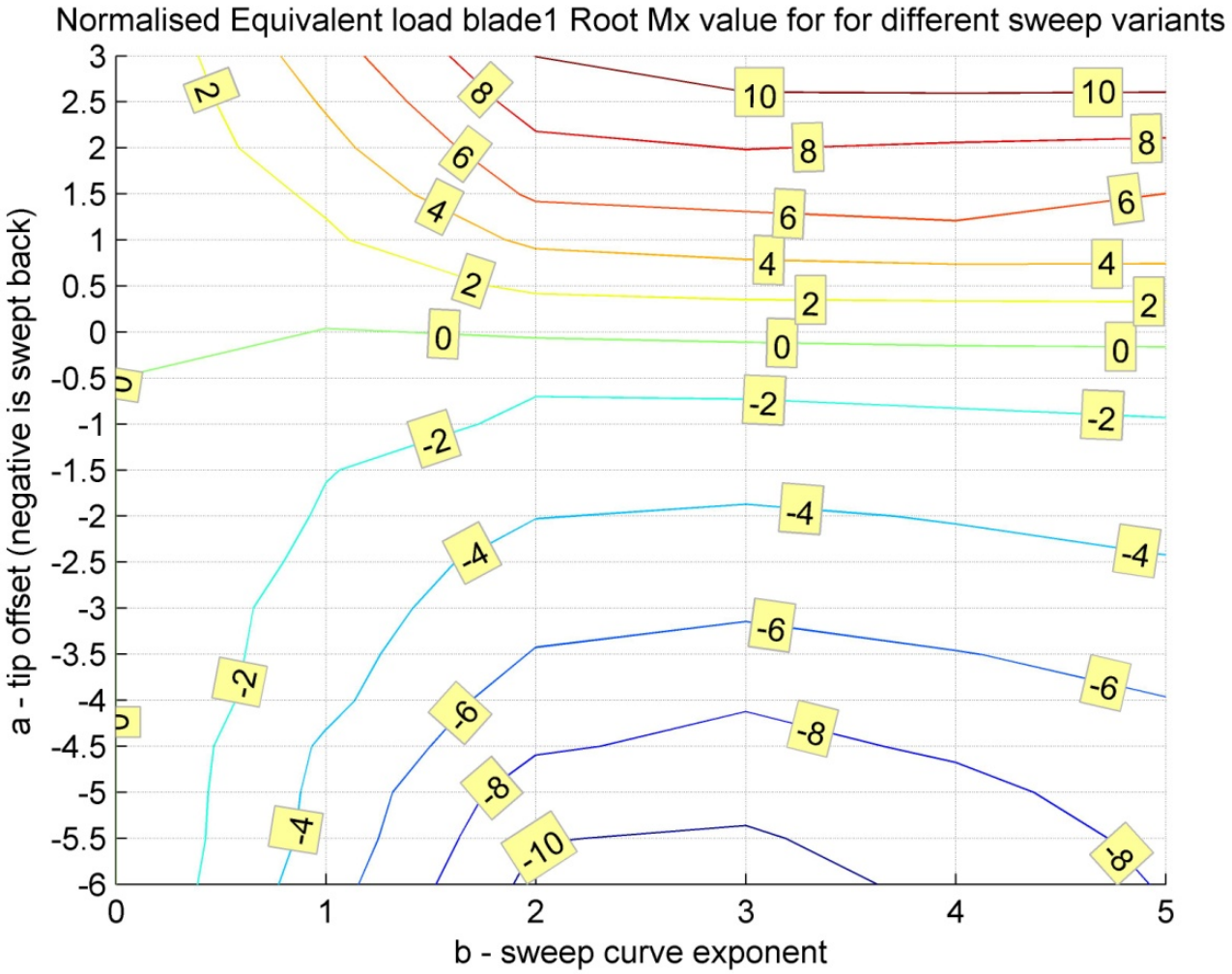

Equivalent loads – blade edge

Forward sweep

No sweep

Backward sweep

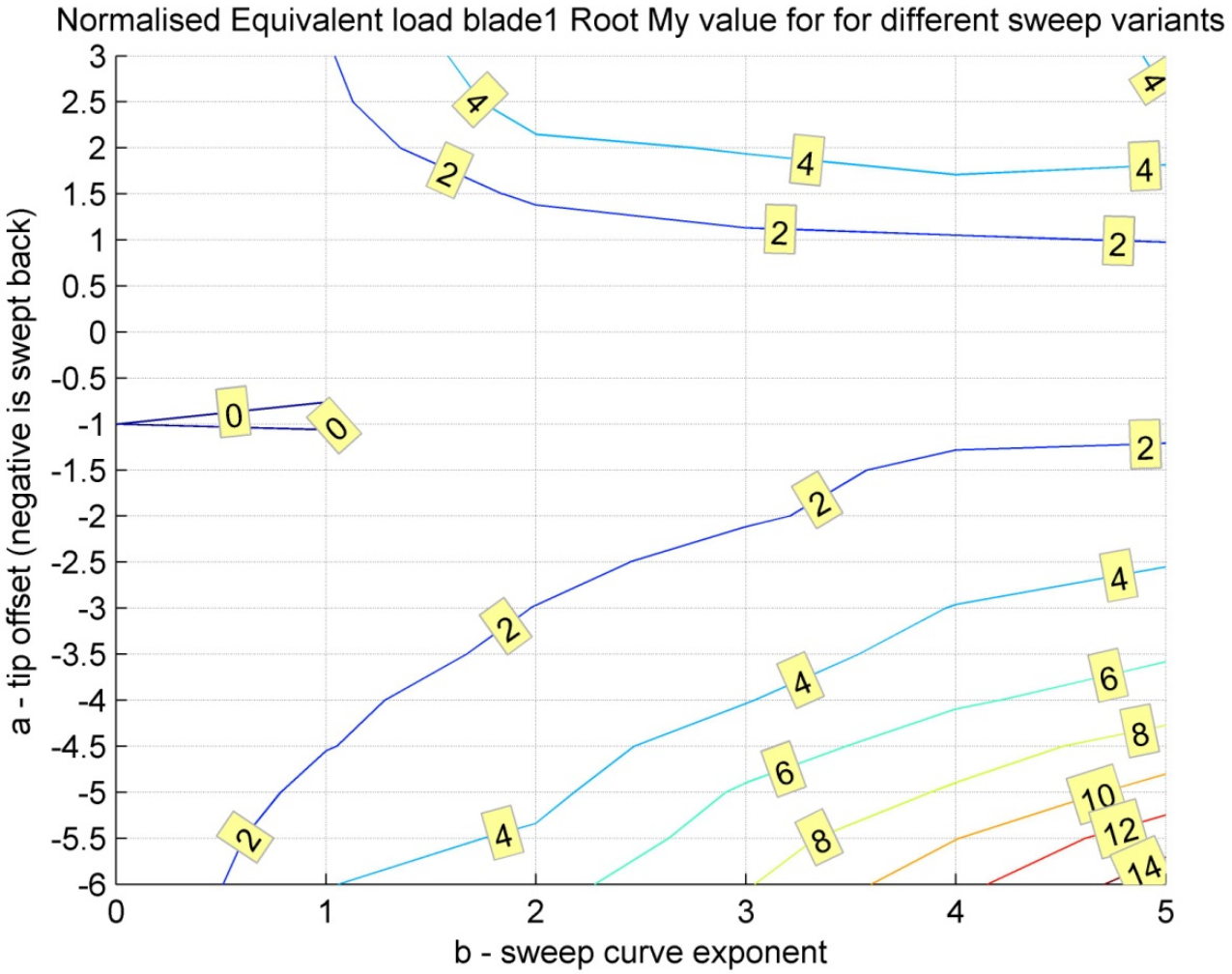

Equivalent loads – blade torsion

Forward sweep

No sweep

Backward sweep

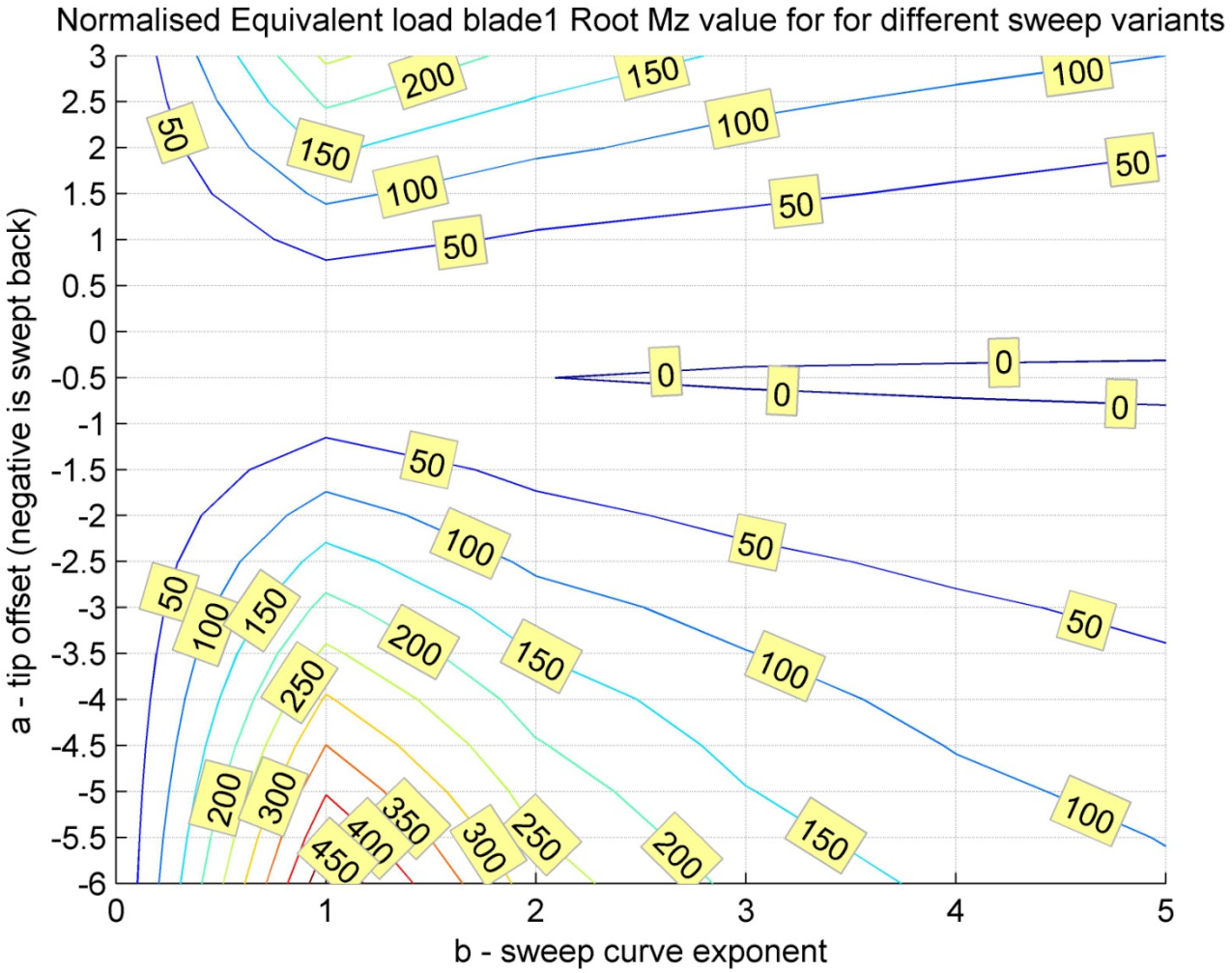

Extreme loads – blade flap

Forward sweep

No sweep

Backward sweep

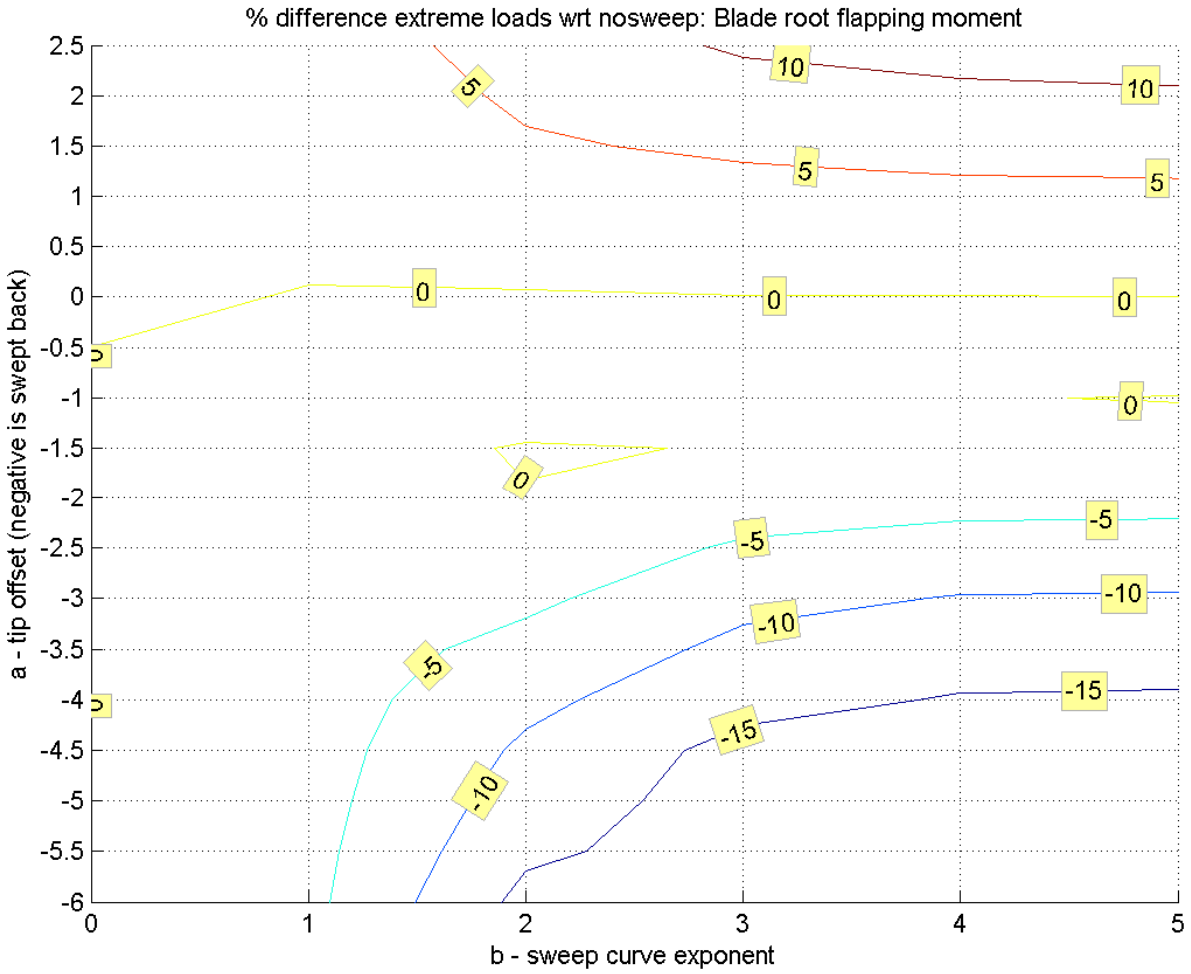

Extreme loads – blade edge

Forward sweep

No sweep

Backward sweep

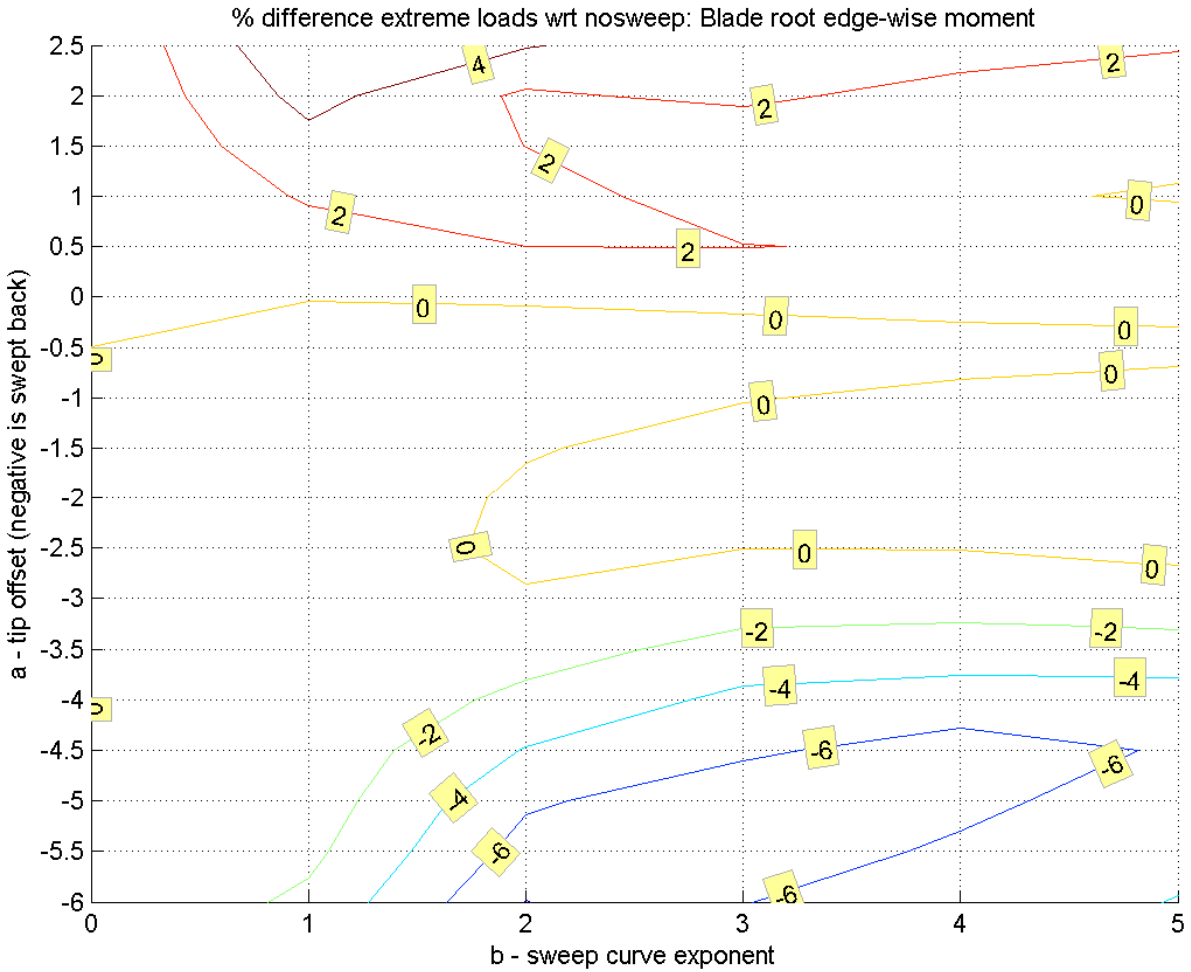

Overview of Approximate Load Consequences

Load consequences backward sweep wrt no-sweep					**Risø**	
Controller	**Risø**		**NREL**		**wrt NREL**	
Loads	fat.	ext.	fat.	ext.	fat.	ext.
Blade root flap	-8 %	-15 %	-10 %	-15 %	0 %	+2 %
Blade root edge	+7 %	+6 %	+3 %	-4 %	+3 %	+12 %
Blade root torsion	+50 %	+50 %	+50 %	+50 %	+1 %	+2 %
Tower base FA	-3 %	-8 %	-3 %	-4 %	na	-3 %
Tower base SS	+2 %	-12 %	+4 %	-6 %	na	-10 %
Tow. base torsion	-10 %	-15 %	-8 %	-15 %	na	-2 %
Shaft-end tilt	-10 %	-2 %	10 %	-10 %	na	+20 %
Shaft-end yaw	-15 %	-20 %	-14 %	-20 %	na	-3 %
Shaft-end torsion	+ 1.5 %	0.5 %	+ 1.0 %	-2.5 %	na	+1.5 %

Table 3. Overview of approximate load consequences for a pitched controlled, extreme swept wind turbine

Energy Yield – steady wind

Forward sweep

No sweep

Backward sweep

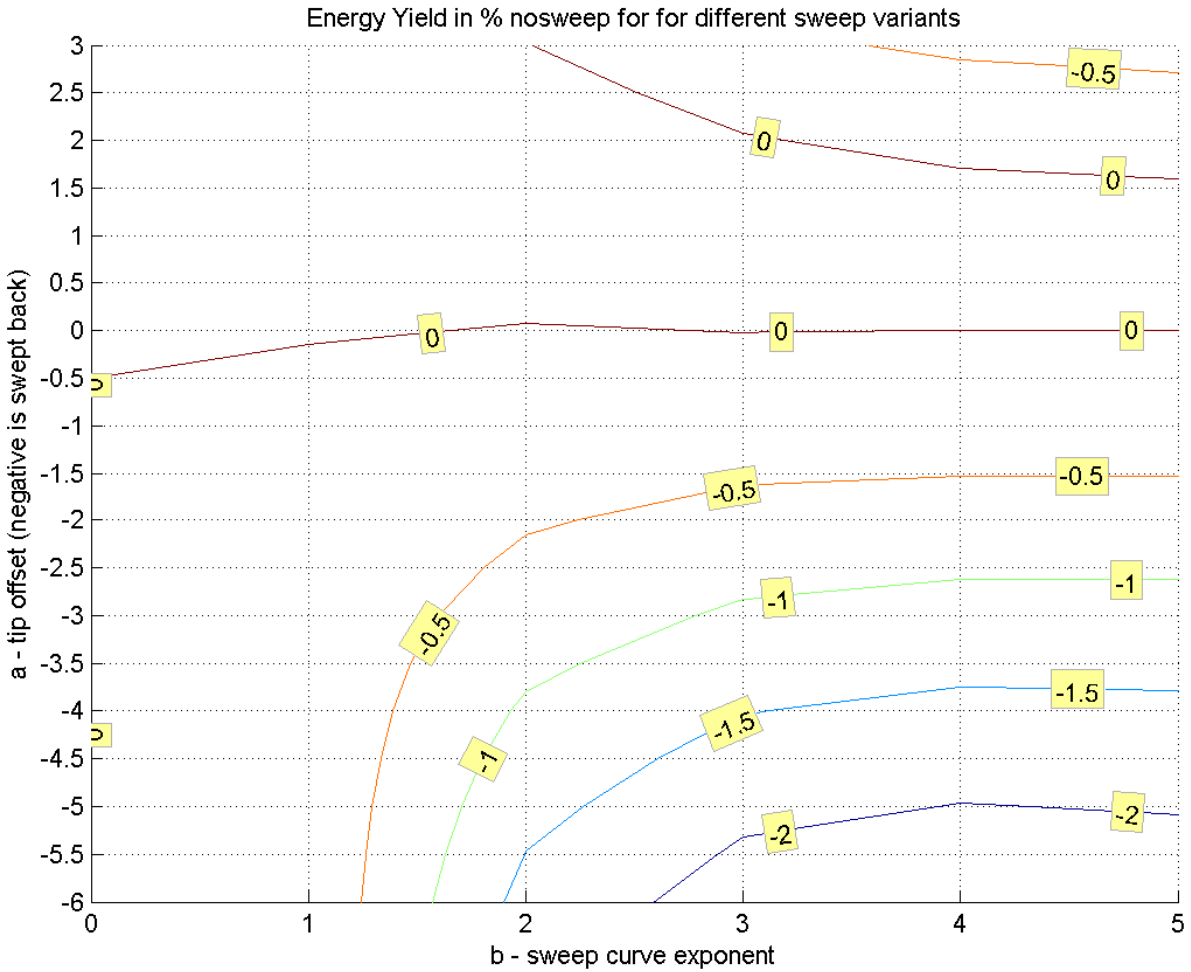

Power Curve

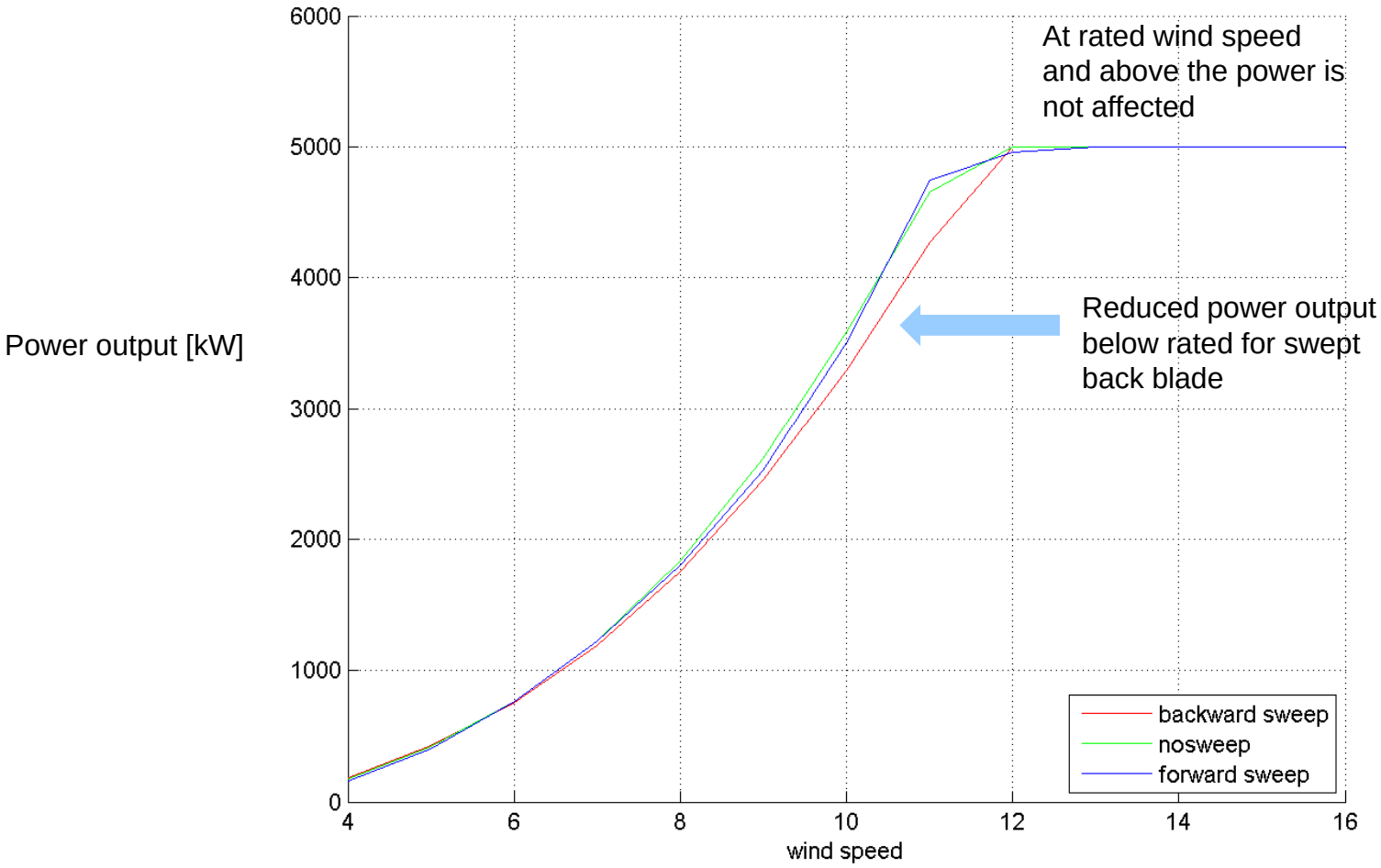
Power output [kW]
6000
5000
4000
3000
2000
1000
0
4
6
8
10
12
14
16
wind speed
At rated wind speed and above the power is not affected
Reduced power output below rated for swept back blade
backward sweep
nosweep
forward sweep

Tip Twist and Pitch Angle

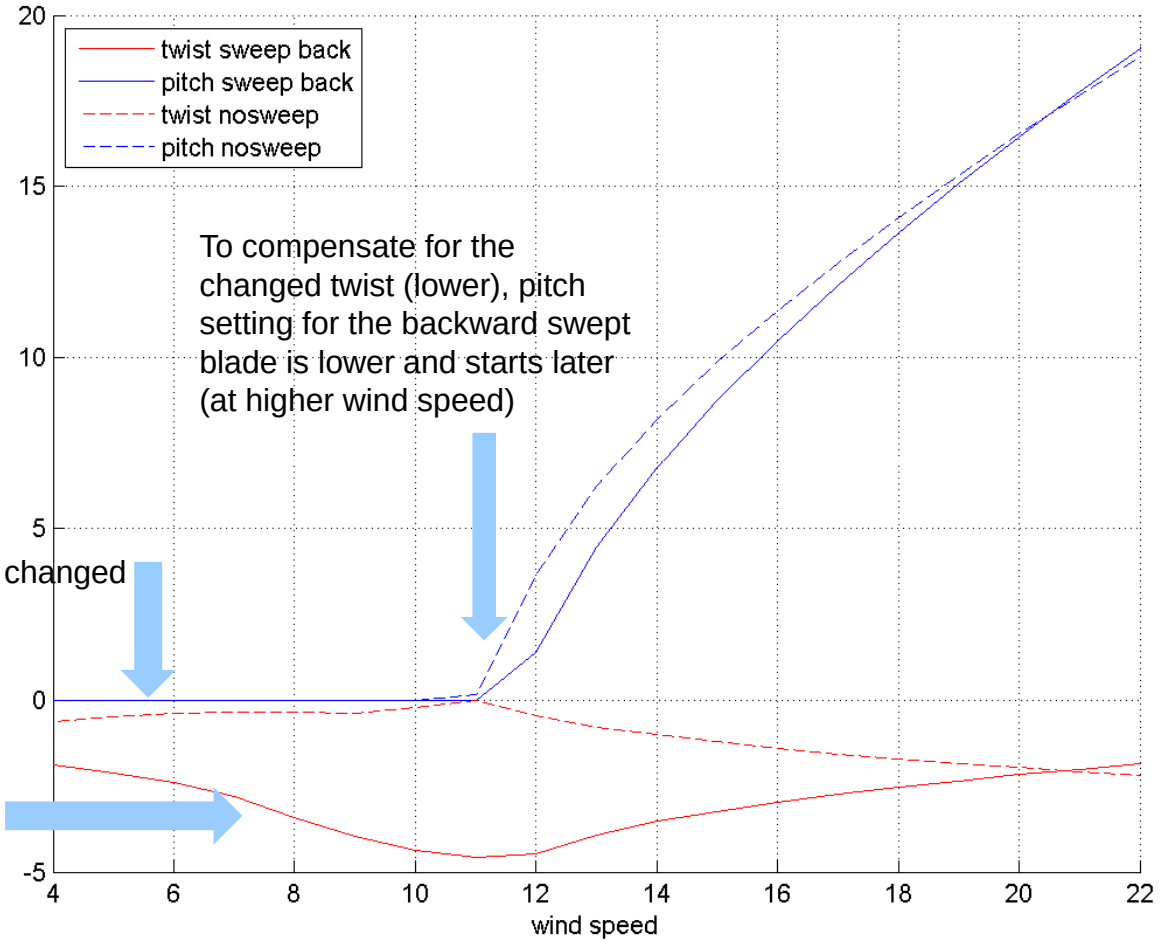

Conclusions

- Forward sweep (pitch to stall):
  - Edge- and flap-wise blade loading increases
  - Pitch control induced instabilities
- Backward sweep (pitch to feather):
  - Flap-wise blade loading decreased, edge-wise increased
- Blade root torsional moment increased significantly
- Decreased tower and shaft loadings
- Sensitive for sweep shape (exponent) and controller
- Passive load shedding mechanism is expected to be relevant for even larger wind turbines

7 Eigenvalue analysis of backward swept blades

Aeroelastic modal analysis of backward swept blades using HAWCStab2

Morten Hartvig Hansen

Old findings: - Lower flapwise loads for backward sweep

New findings: - Lower flapwise damping but higher flapwise stiffness
- Flutter limit decreases

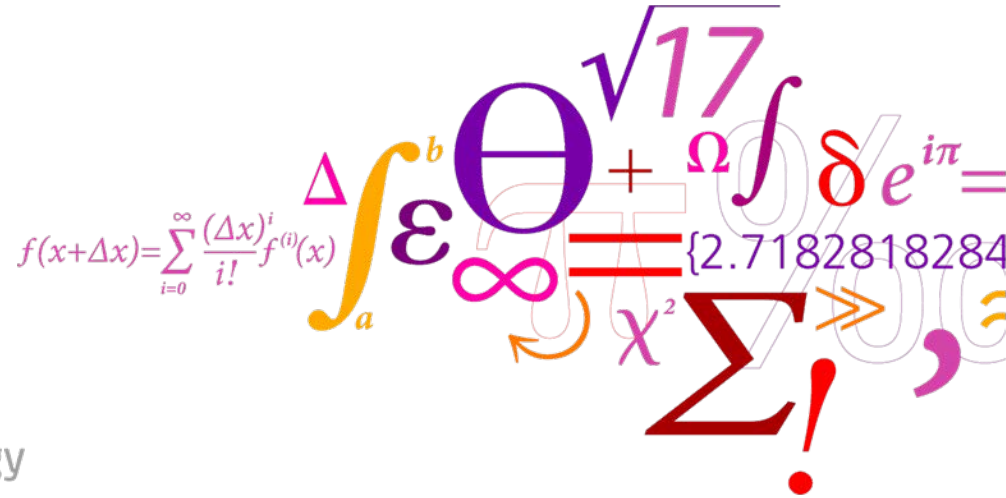

Risø DTU
National Laboratory for Sustainable Energy

Field test at Sandia Nat. Lab.

- Ashwil *et al.*, “Development of the swept twist adaptive rotor (STAR) blade”, In Proc. of the 48th AIAA Aerospace Sciences Meeting, 2010:
  - 26.1 m STAR prototype blade can increase the annual energy capture by 10-12% compared to a baseline 23.5 m blade without increasing the blade root bending moments

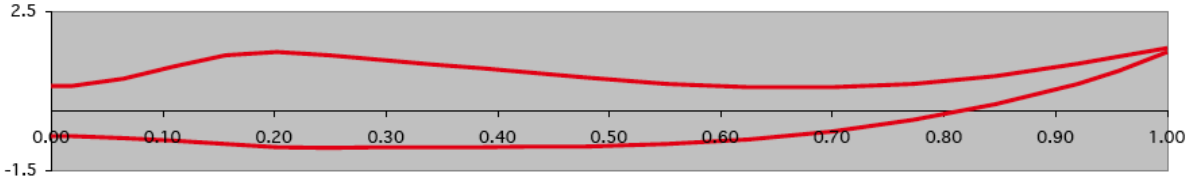

What is HAWCStab2?

Linear aeroelastic model for eigenvalue and frequency domain analysis of wind turbines and blades

Nonlinear kinematics based on co-rotational elements with possibility of bearings e.g. generator and pitch.

Uniform inflow to give a stationary steady state.

Analytical linearization about the stationary steady state.

Unsteady aerodynamics based on Leishman-Beddoes. A two state (per calc. point) model of dynamic inflow will soon be included.

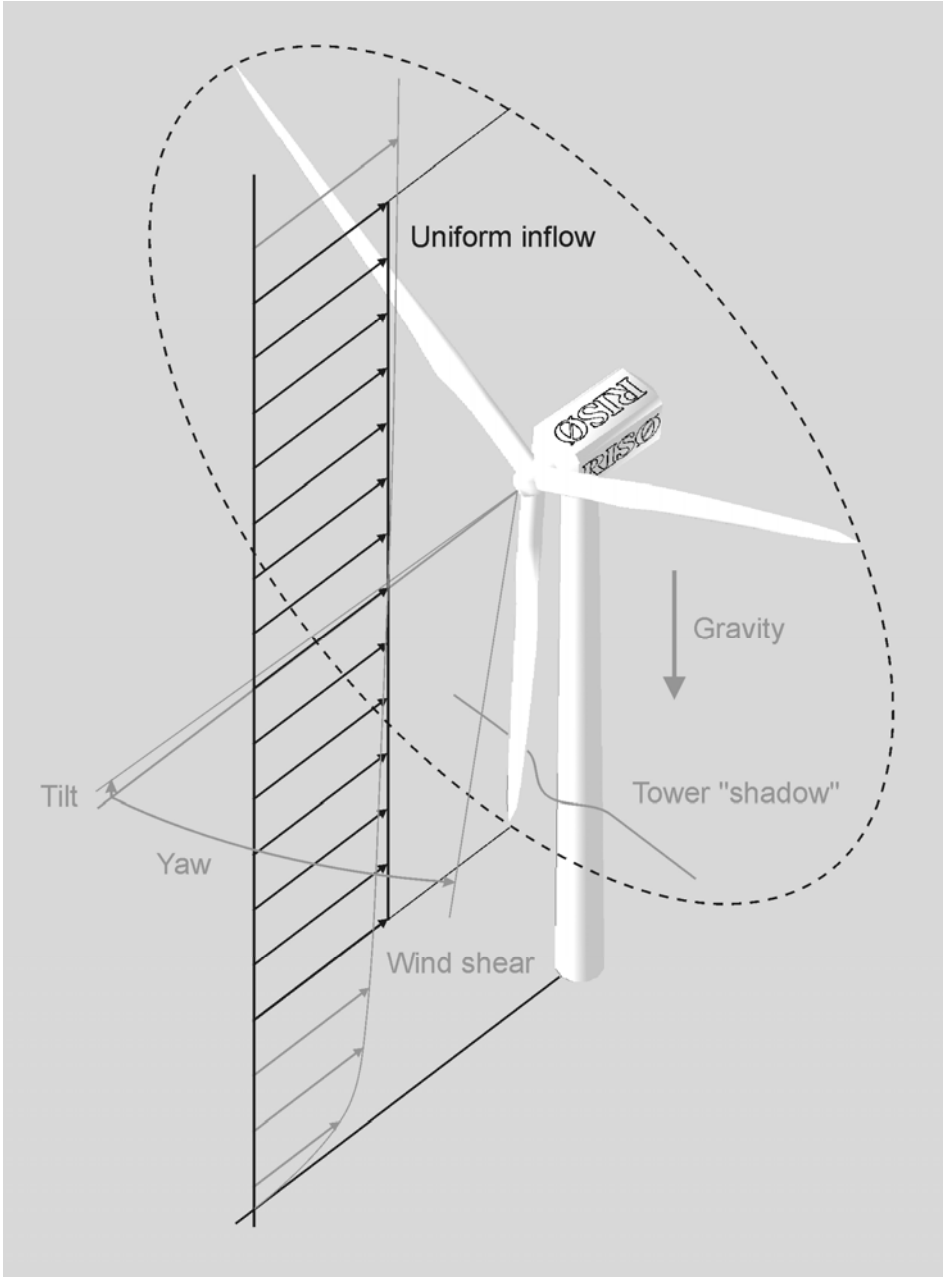

Nonlinear kinematic formulation for blade

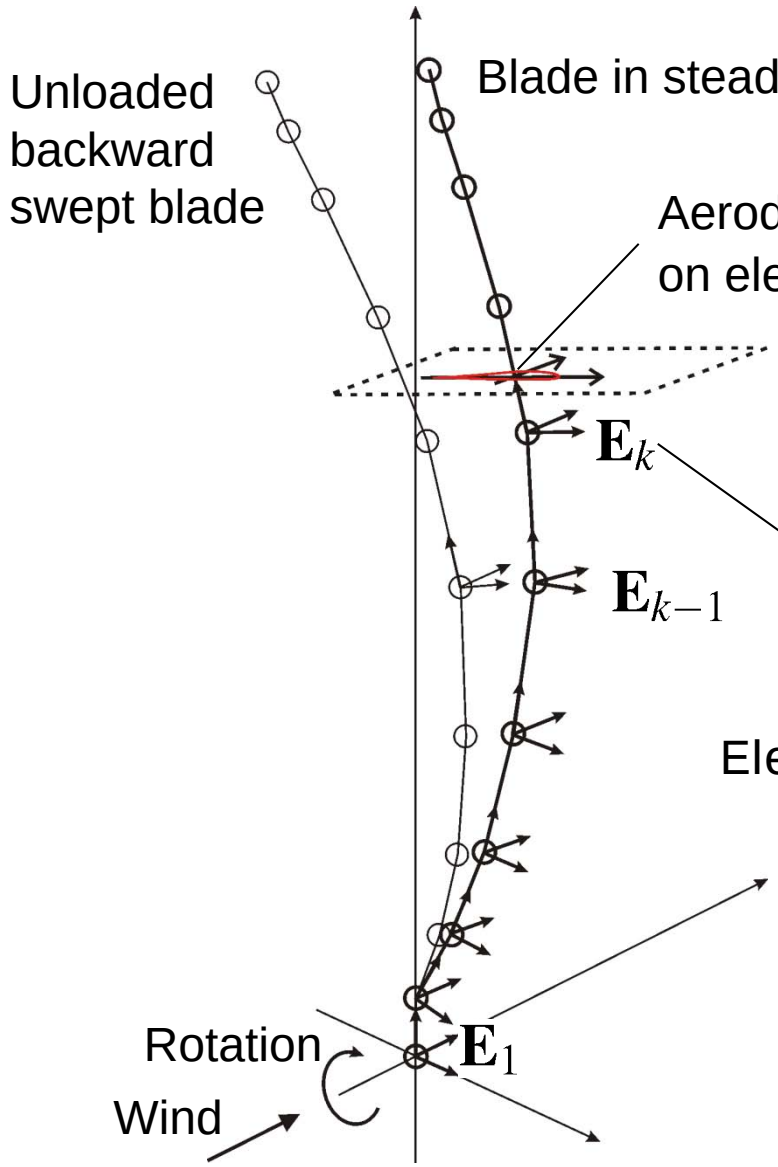

Element positions and orientations

$$\mathbf{r}_{e,k} = \sum_{n=1}^{k-1} \mathbf{T}_{e,n} \left(\delta \mathbf{u}_n + (l_n + \Delta l_n)\, \mathbf{e}_3 \right)$$

$$\mathbf{T}_{e,k} = \left(\prod_{n=1}^{k-1} \mathbf{E}_n \mathbf{T} \left[\delta \boldsymbol{\theta}_n \right] \right) \mathbf{E}_k$$

Nonlinear steady state

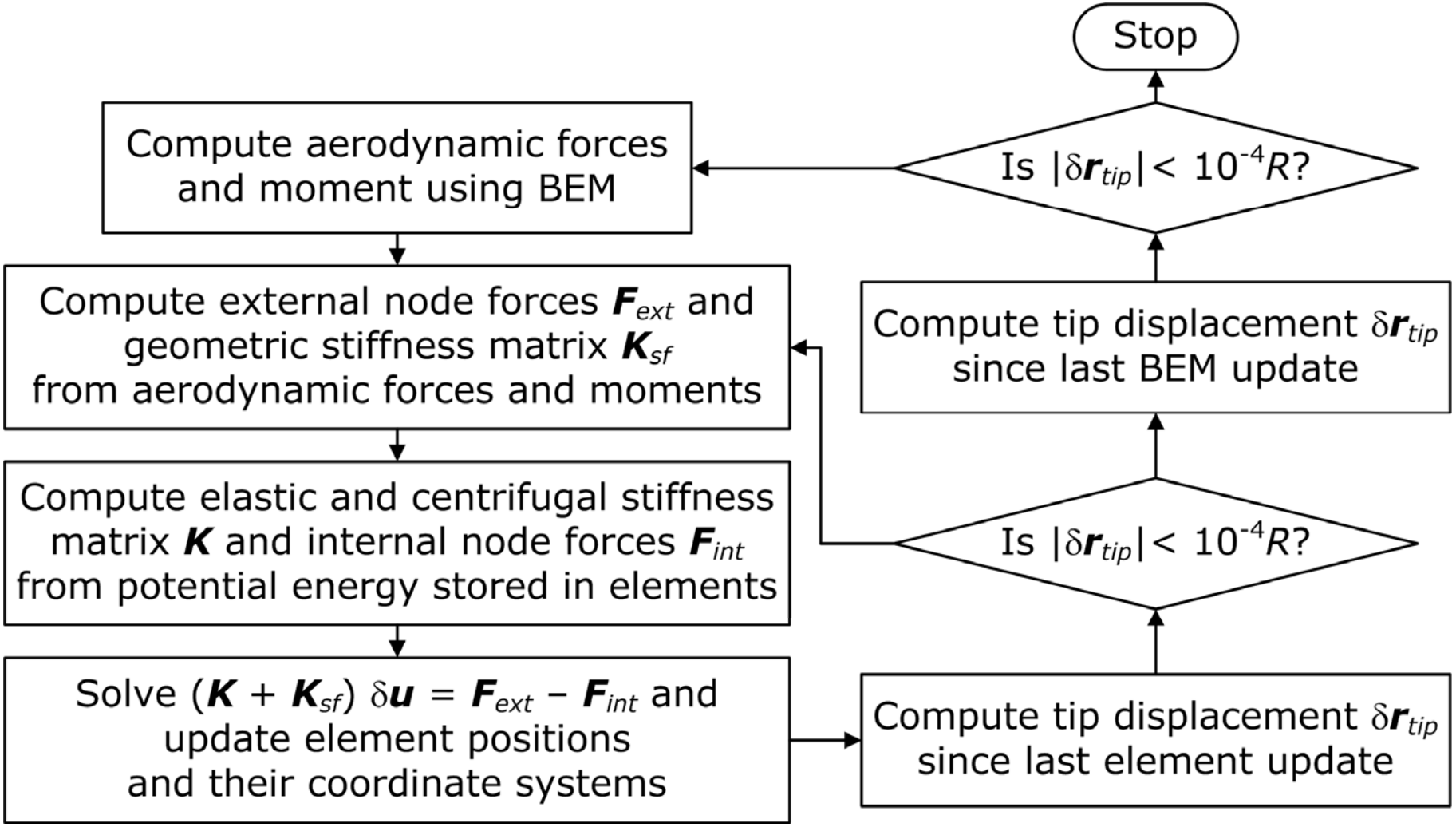

Linear equations for small vibrations about the nonlinear steady state

Structural mass
Structural damping
Gyroscopic forces
Aerodynamic damping
Elastic stiffness
Geometric stiffness of steady state force
Aerodynamic stiffness
Coupling to aerodynamic states

$$\mathbf{M}\ddot{\mathbf{x}}_s + (\mathbf{C} + \mathbf{G} + \mathbf{C}_a)\,\dot{\mathbf{x}}_s + (\mathbf{K} + \mathbf{K}_{sf} + \mathbf{K}_a)\,\mathbf{x}_s + \mathbf{A}_f\mathbf{x}_a = \mathbf{F}_s$$

$$\dot{\mathbf{x}}_a + \mathbf{A}_d\mathbf{x}_a + \mathbf{C}_{sa}\dot{\mathbf{x}}_s + \mathbf{K}_{sa}\mathbf{x}_s = \mathbf{F}_a$$

Time lags matrix

Coupling to structural states

$\mathbf{x}_s$ = elastic (and bearing) degrees of freedom

$\mathbf{x}_a$ = aerodynamic state variables

$\mathbf{F}_s, \mathbf{F}_a$ = forces due to actuators and wind disturbance

Backward swept blades
Baseline – NREL 61.5m with CG at EA

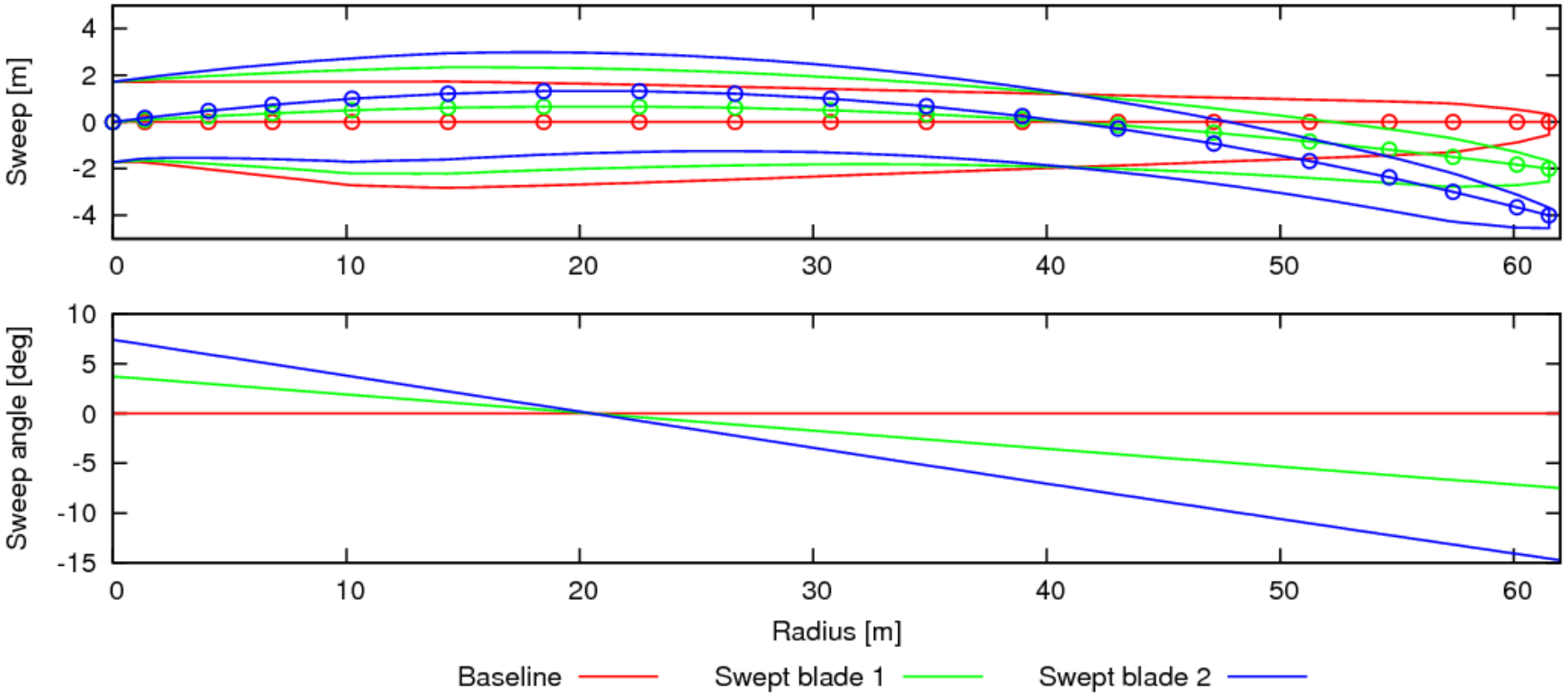

Steady state power and pitch angle & torque

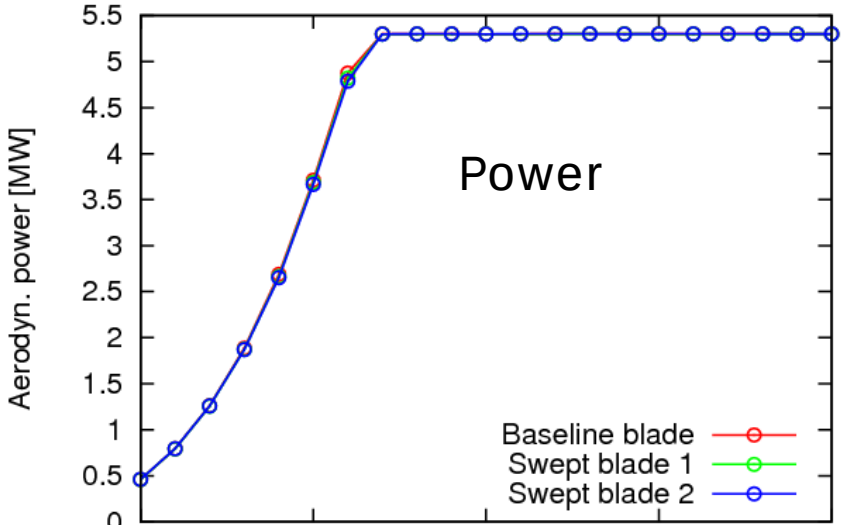

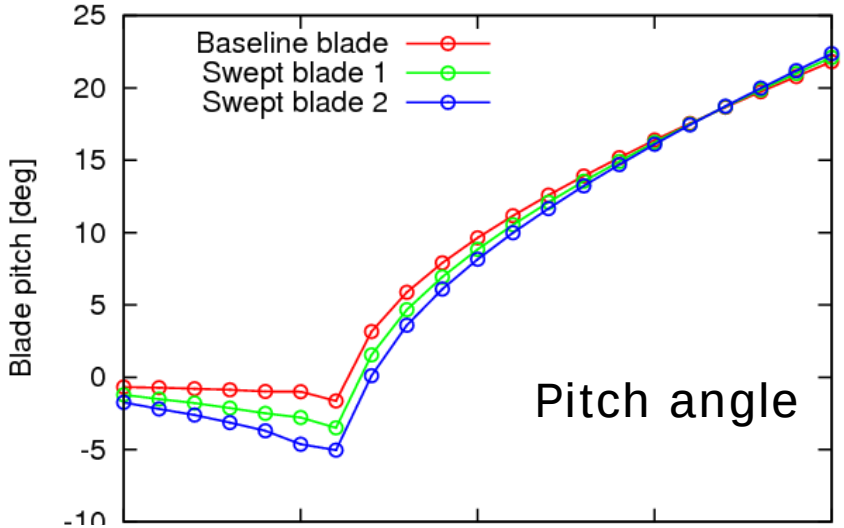

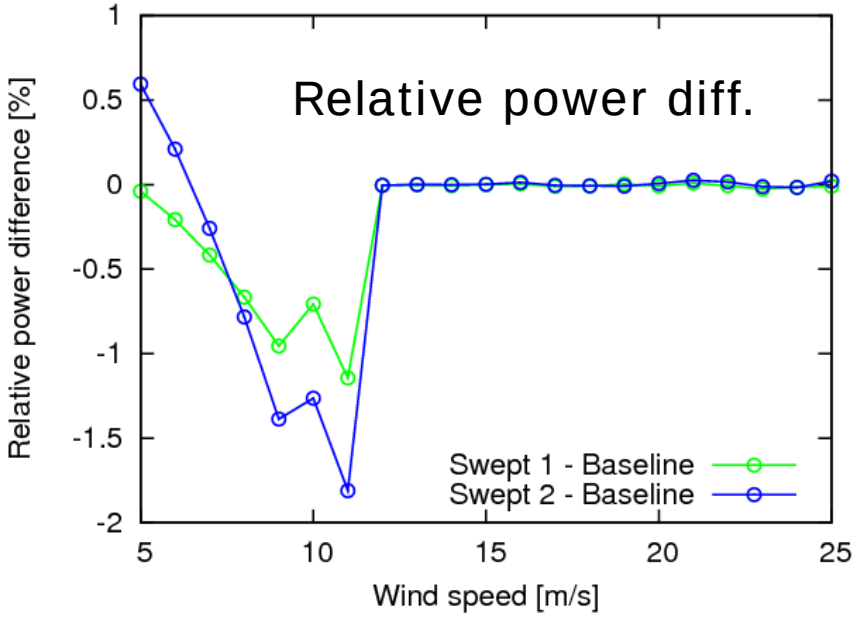

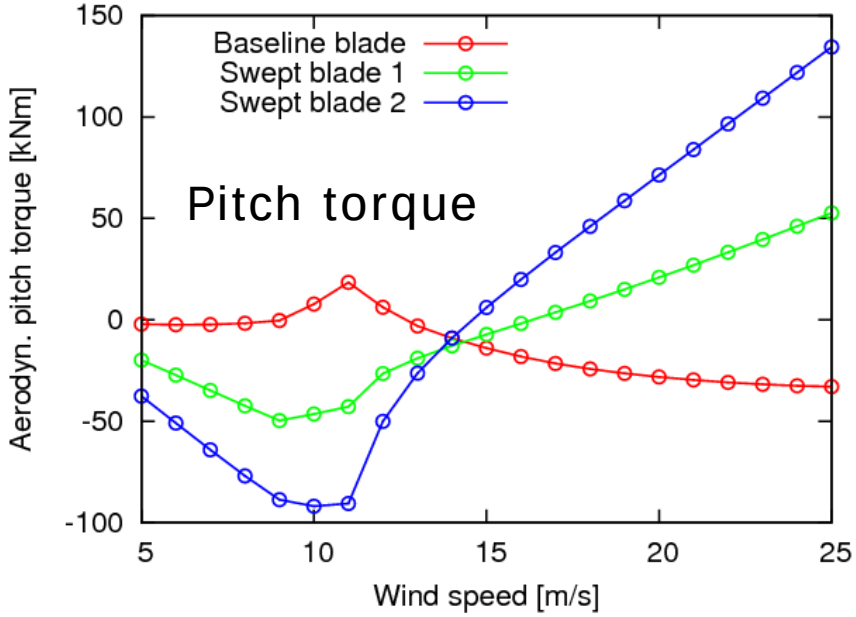

Steady state thrust and tip deflection

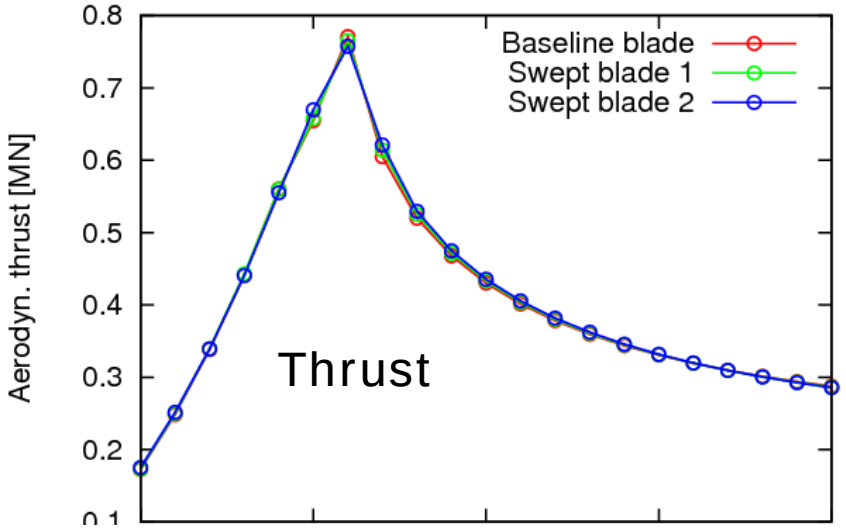

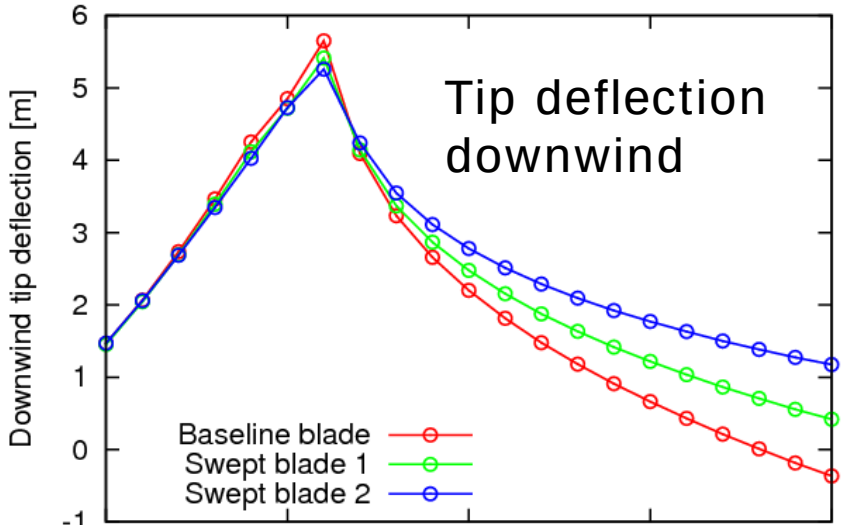

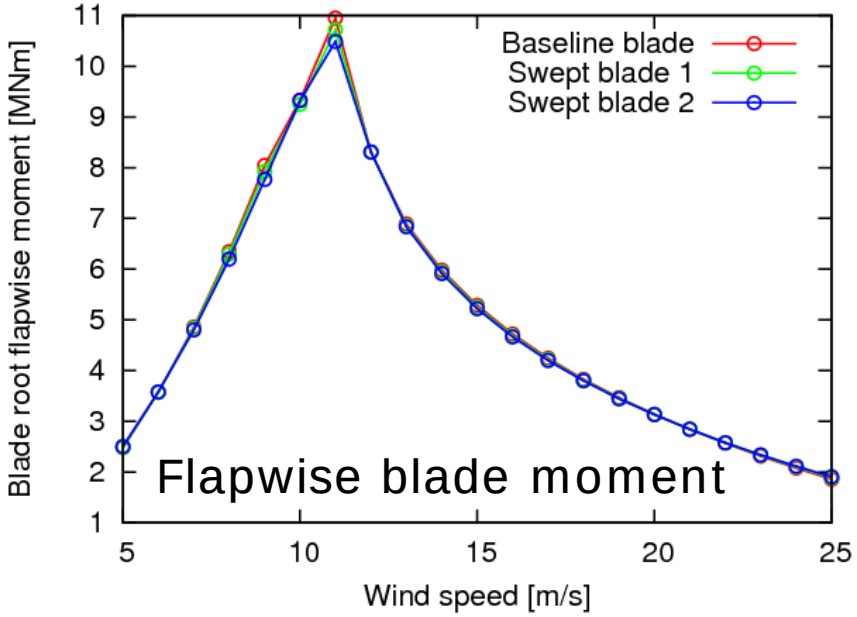

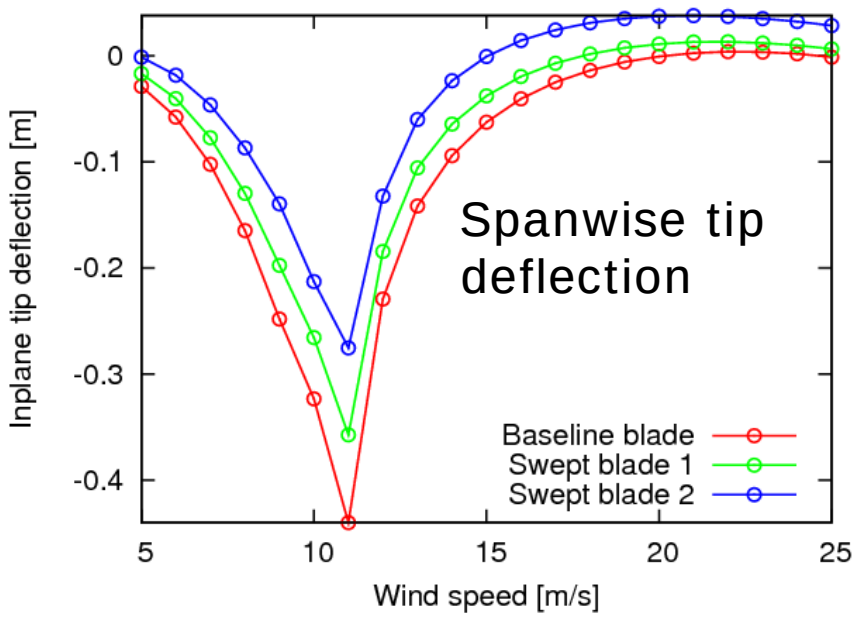

Modal frequencies and damping – 1st flap

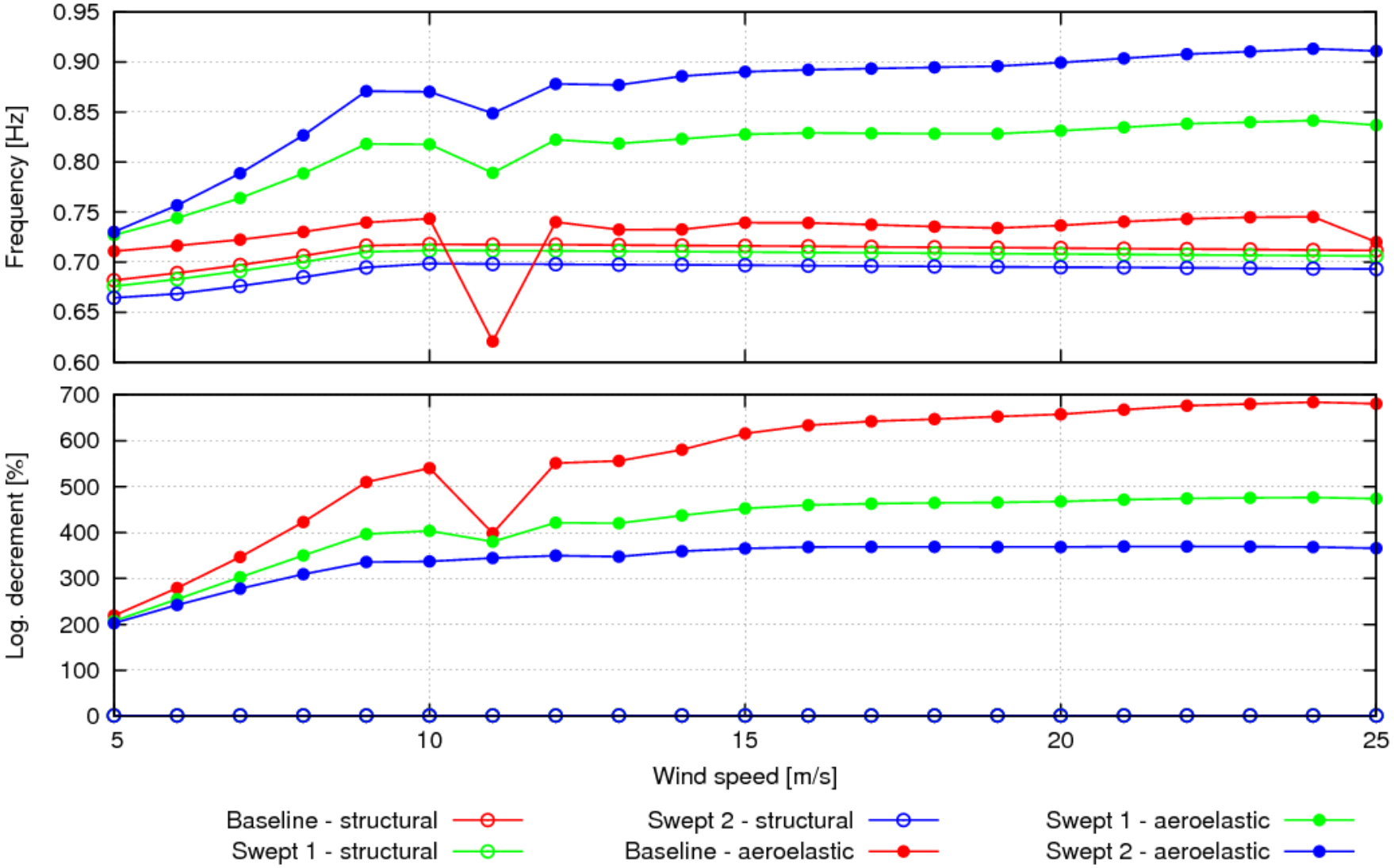

Mode shapes at 12 m/s – 1st flap

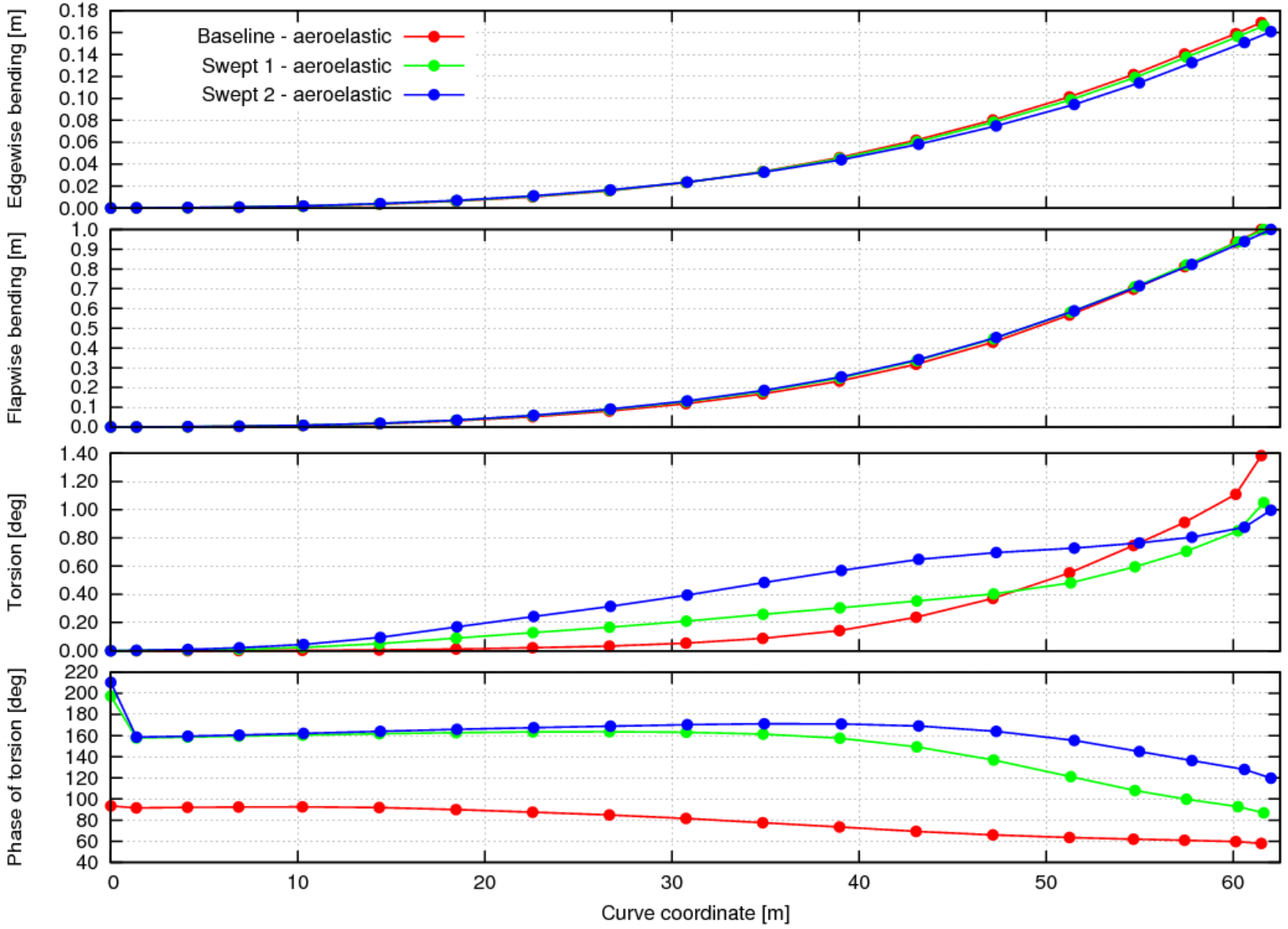

Blade section motion at 75% radius – 1st flap

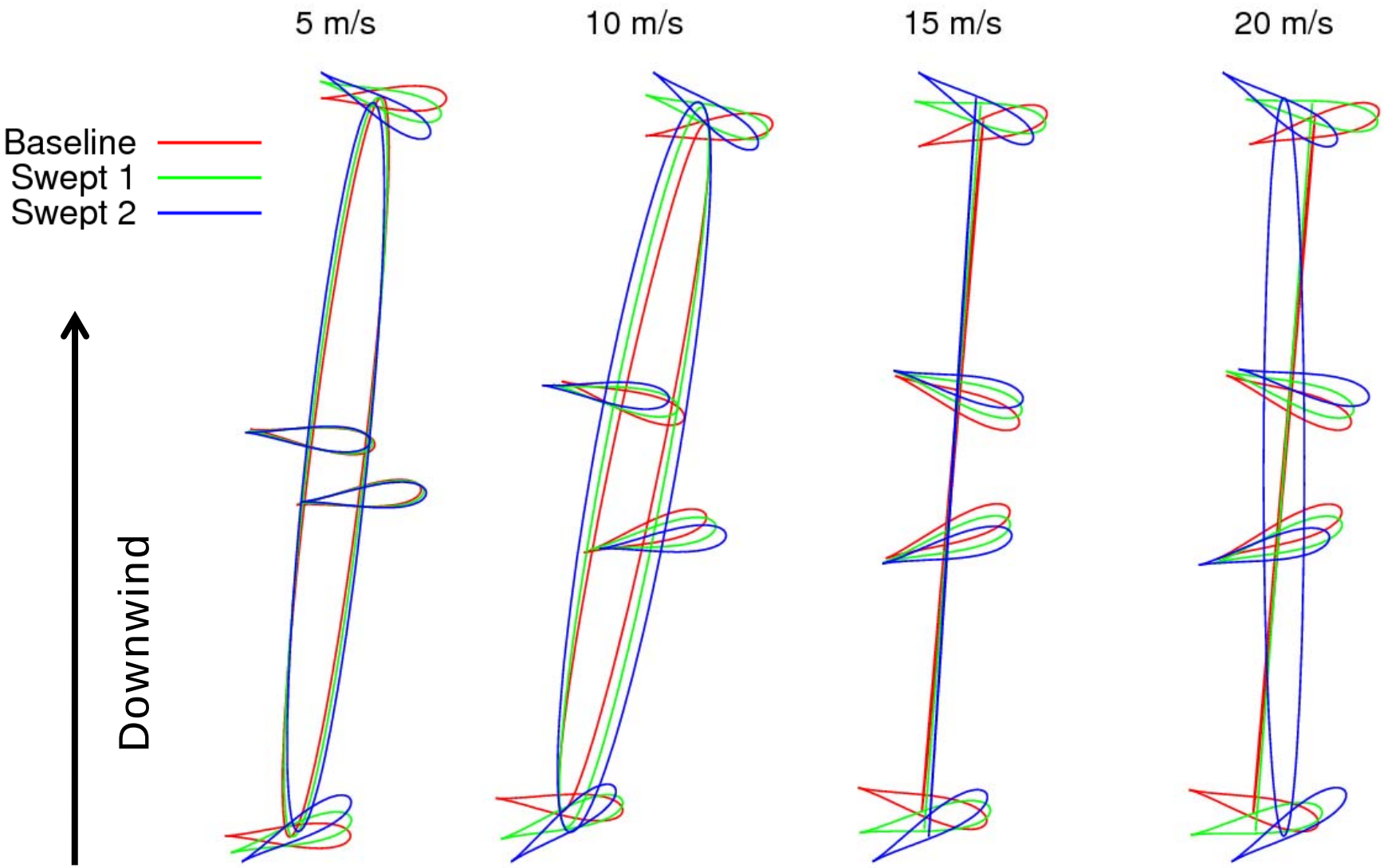

Flapwise blade root moment

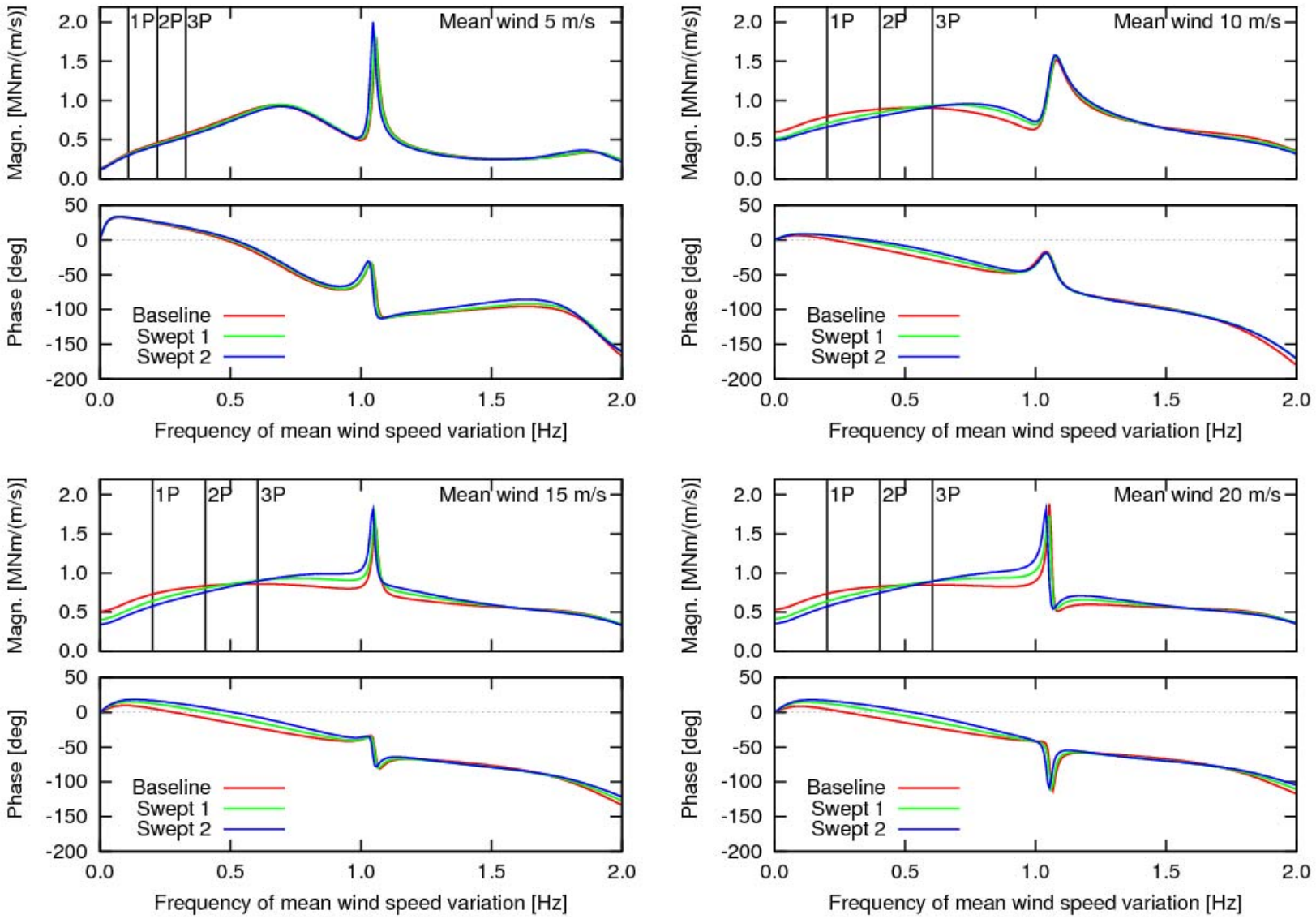

Edgewise blade root moment

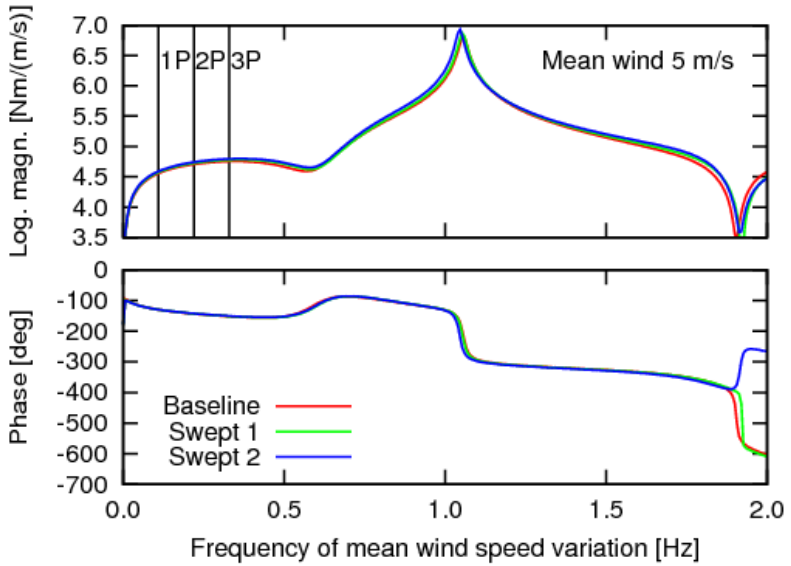

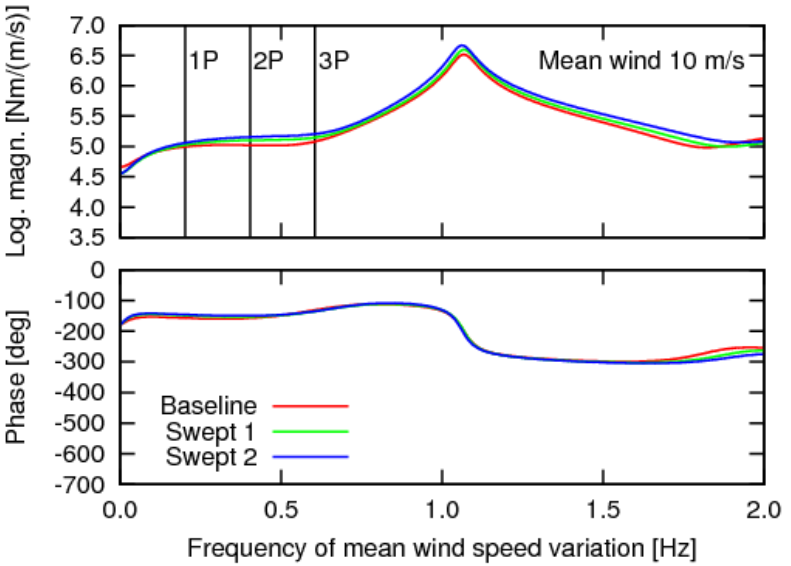

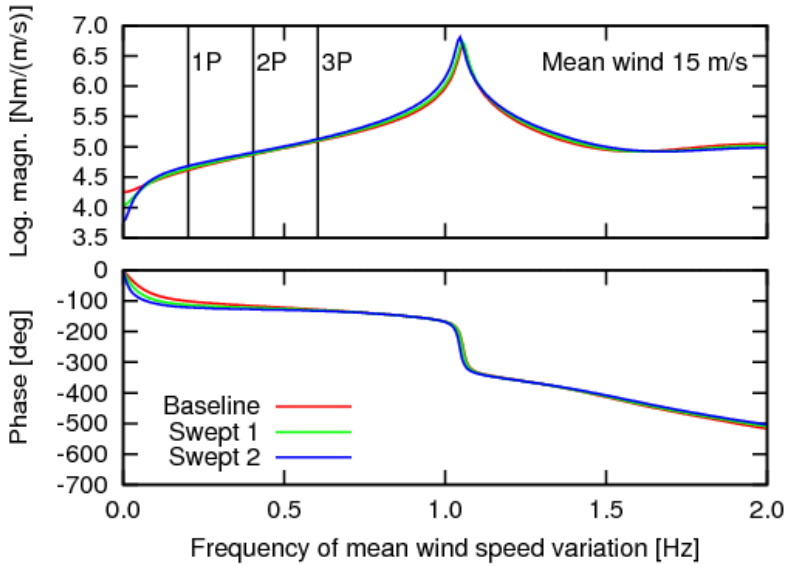

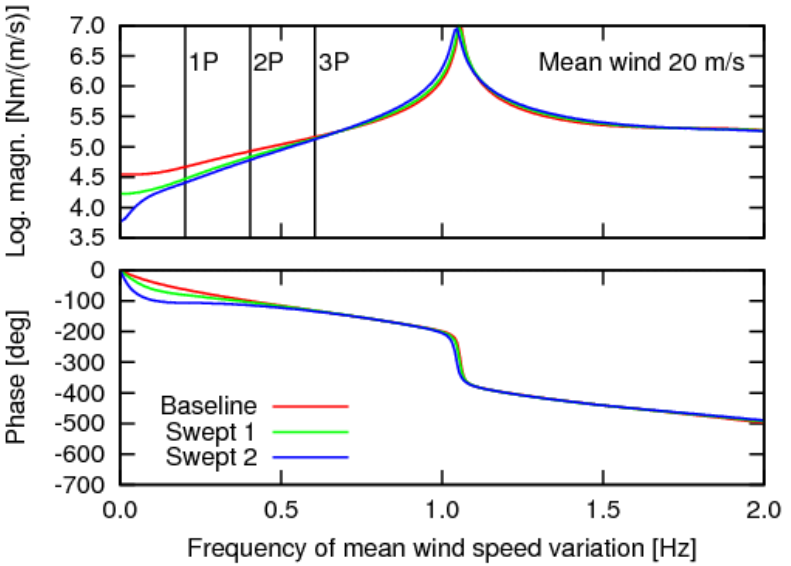

Conclusions

- Backward swept blades twist towards feathering for flapwise bending in both structural and aeroelastic first flapwise bending modes
- This structural coupling of bending and torsion leads to higher aeroelastic modal frequency and lower aeroelastic damping of this mode
- The increased flapwise frequency of a backward swept blade is caused by added aerodynamic flapwise stiffness due to the twisting towards feathering when bending downwind
- This increased flapwise stiffness lowers the frequency response of backward swept blades at frequencies below the first flapwise frequency which can explain the reduced fatigue loads observed in previous studies
- The previously reported slight increase in edgewise blade root loads of backward swept blades can be explained by a slight reduction of aeroelastic damping of the first edgewise bending mode

Flutter test case – Typical Section analogy

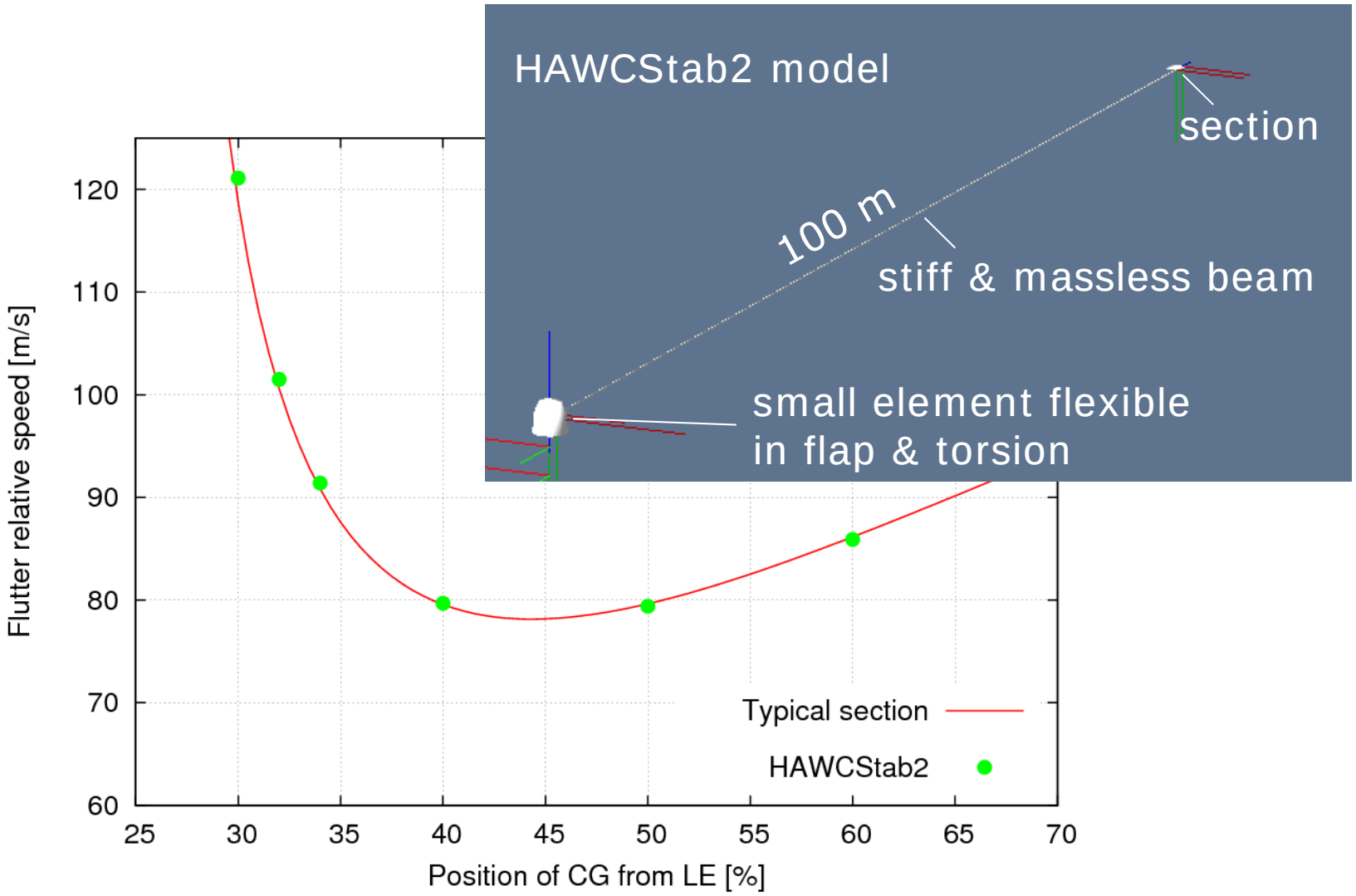

Lowest damped modes for 0 deg pitch and increasing relative speed ($\lambda = \sqrt{99}$)

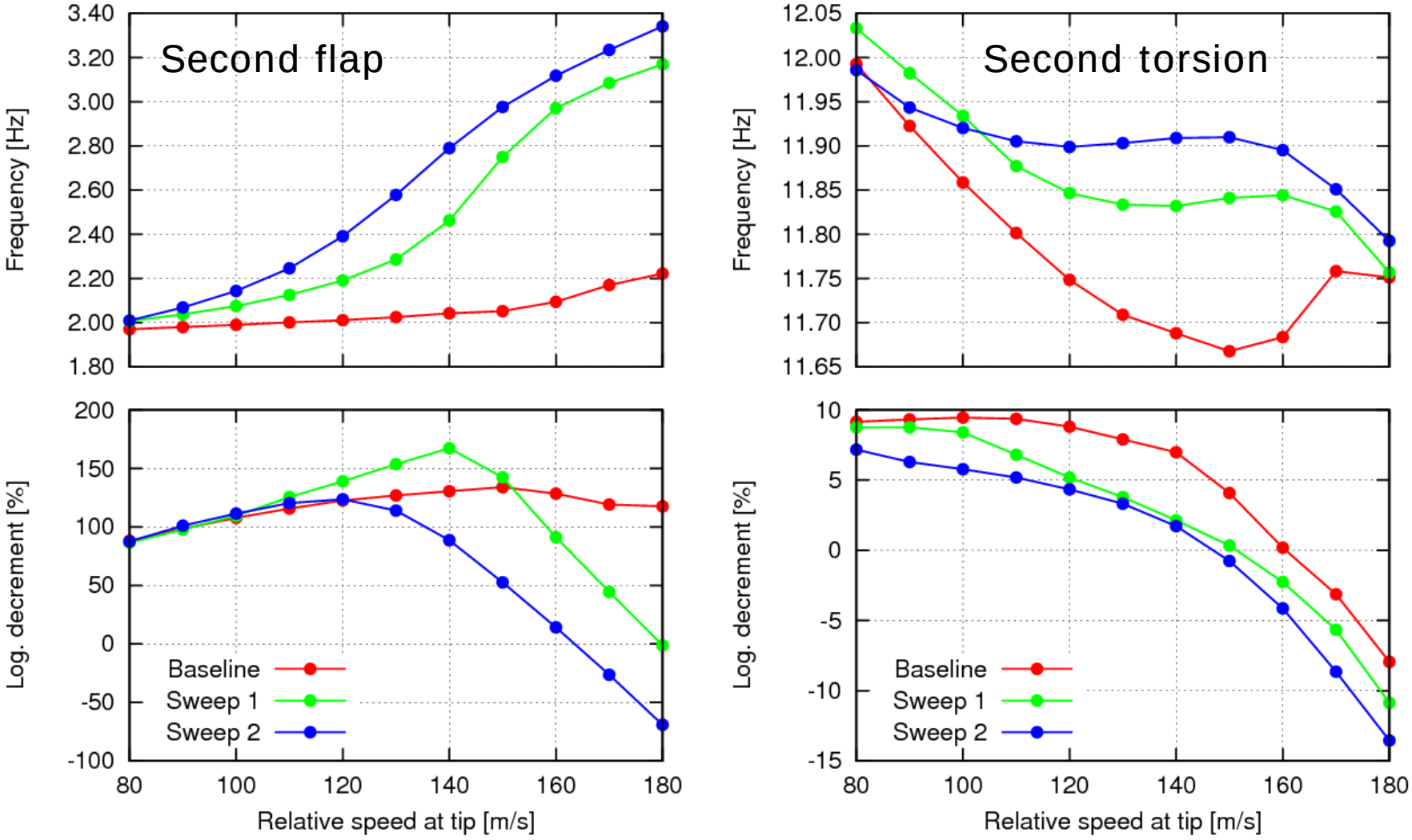

8 Aeroelastic rotor design minimizing the loads

Aeroelastic rotor design minimizing the loads

Mads Døssing, Christian Bak

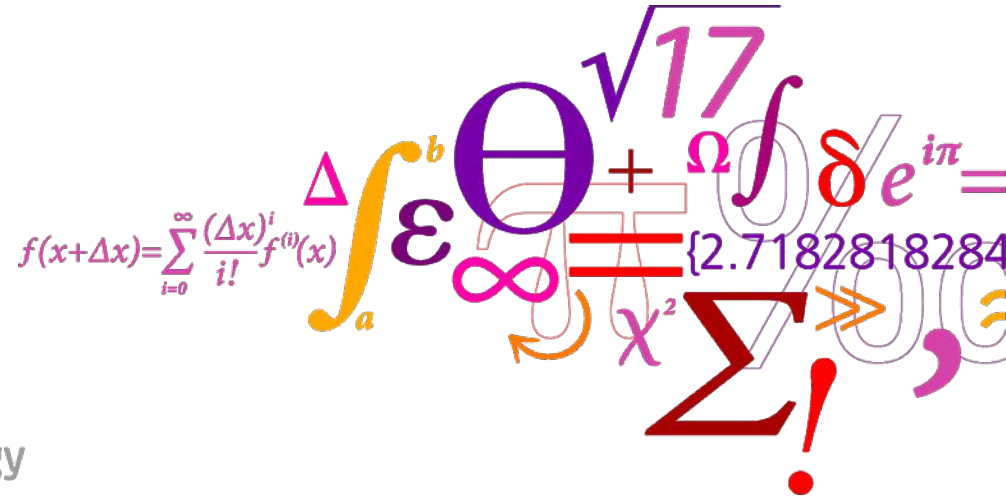

Risø DTU
National Laboratory for Sustainable Energy

Outline

- Background
- Simplified structural model
- Simplified fatigue model
- Influence of wide/slender blade on loads
- Optimization procedure
- Blade with DU airfoils (NREL 5MW)
- Blade with Risø-B1 airfoils (NREL 5MW)
- Conclusions

Background

- Design of rotors purely based on aerodynamics have been carried out several times e.g. by Johansen et al.

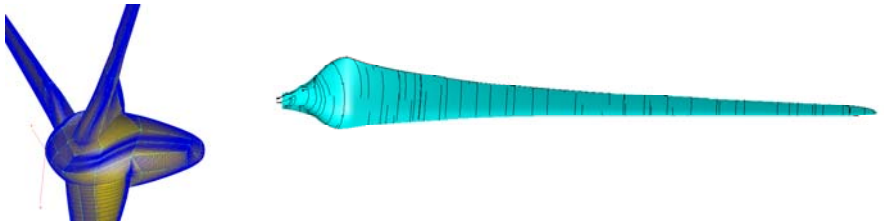

- Design of rotors and the influence on loads have been investigated e.g. by Fuglsang in Reasearch in Aeroelasticity, EFP2002. However, constant structural layout was assumed.

- Also, design of rotors and the influence on loads have been investigated e.g. by Fuglsang et al in the EU project SITEOPT. However, structural correlation to rotor design was very simple.

- In this work more advanced models (however still simple) are developed to take into account mass and stiffness variations

Simplified structural model

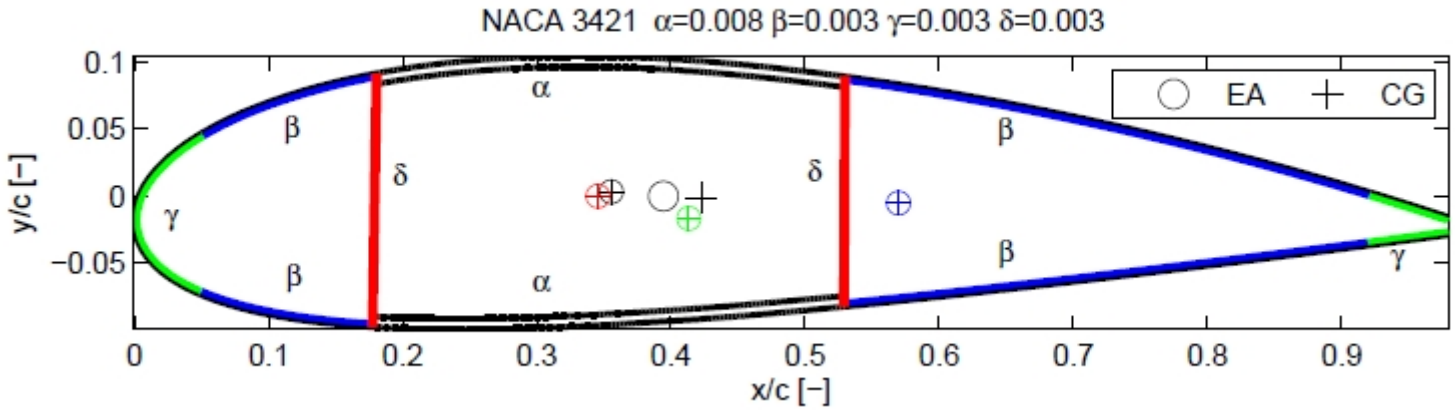

Simplified structural model

Section area (closed section)	$A_0 = c^2 C_{A_0}$
Section mass	$m = c^2 \sum_i \alpha_i \rho_i C_{A_i}$
Longitudinal stiffness	$EA = c^2 \sum_i \alpha_i E_i C_{A_i}$
Moment of stiffness about the x axis	$ES_x = c^3 \sum_i \alpha_i E_i C_{S_{x\,i}}$
Moment of stiffness about the y axis	$ES_y = c^3 \sum_i \alpha_i E_i C_{S_{y_i}}$
Moment of mass about the x axis	$\rho S_x = c^3 \sum_i \alpha_i \rho_i C_{S_{x\,i}}$
Moment of mass about the y axis	$\rho S_y = c^3 \sum_i \alpha_i \rho_i C_{S_{y_i}}$
Moment of stiffness inertia about the x axis	$EI_x = c^4 \sum_i \alpha_i E_i C_{I_{x\,i}}$
Moment of stiffness inertia about the y axis	$EI_y = c^4 \sum_i \alpha_i E_i C_{I_{y_i}}$
Moment of centrifugal stiffness	$ED_{xy} = c^4 \sum_i \alpha_i E_i C_{D_{xy_i}}$

$$
\begin{aligned}
C_{A_0} &= \int_i \operatorname{sgn}(y^*) y^* \, dx^* \\
C_{A_i} &= \int_i ds^* \\
C_{S_{x\,i}} &= \int_i y^* \, ds^* \\
C_{S_{y_i}} &= \int_i x^* \, ds^* \\
C_{I_{x\,i}} &= \int_i y^{*2} \, ds^* \\
C_{I_{y_i}} &= \int_i x^{*2} \, ds^* \\
C_{D_{xy_i}} &= \int_i x^* y^* \, ds^*
\end{aligned}
$$

Simplified fatigue model

$$R_{eq} \propto (1-a)^{1/m} \Omega^{1+1/m} \int_r^R (r'-r) r' C_l' c \, dr'$$

$$R_{eq} \propto c_1 = \Omega \int_r^R (r'-r) r' c \, dr'$$

Influence of wide/slender blade on loads

	M [kg]	AEP [GWh]	f_1 [Hz]	f_2 [Hz]	f_3 [Hz]
Increased chord (f_c=1.1)	16900	19.72	0.647	1.10	1.91
NREL 5MW	15100	19.51	0.665	1.05	1.94
Decreased chord (f_c=0.9)	13340	19.23	0.683	9.84	1.99

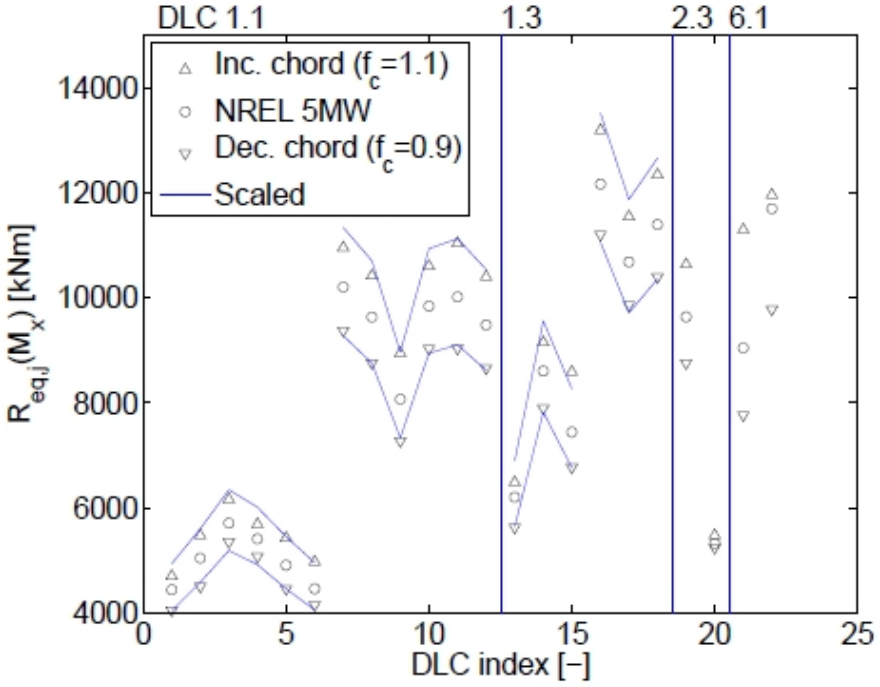

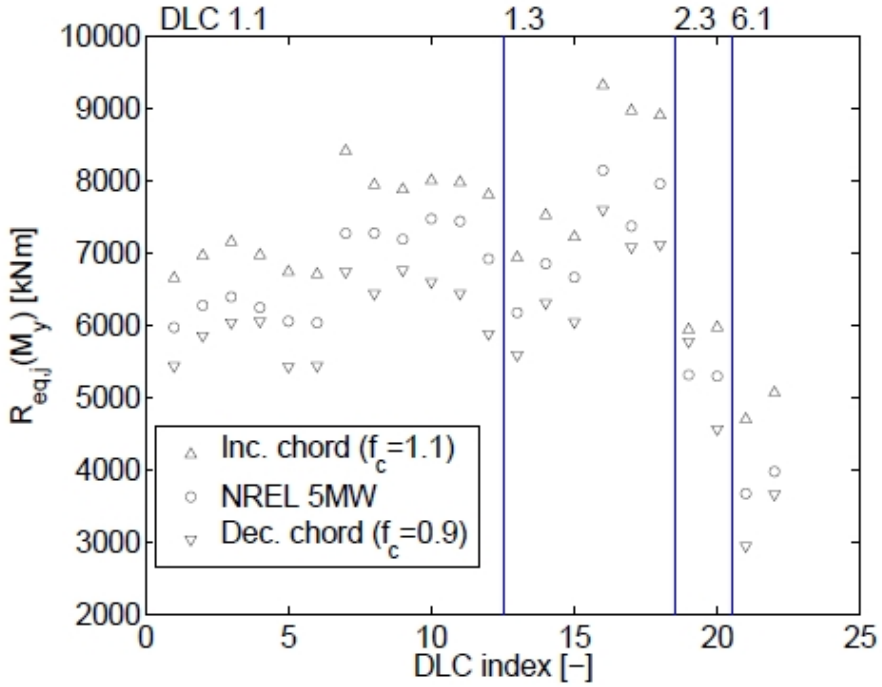

Optimization procedure

- Optimization using steady state aerodynamic design and simplified fatigue model to reduced blade root flap fatigue load. Constraints on power and blade mass in design point (design point: 11m/s i.e. at rated wind speed for load reduction)

- Optimization using aeroelastic computations (HAWC2) with reduced number of design load cases to reduce blade root flap fatigue load. Constraints on power and blade mass in design point (design point: 10m/s)
- The load cases should as far as possible be controller independent
- No power optimization

Blade with DU airfoils (NREL 5MW)

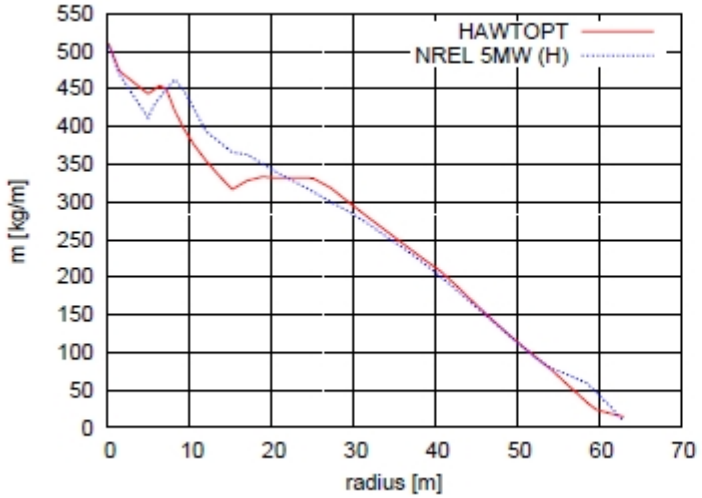

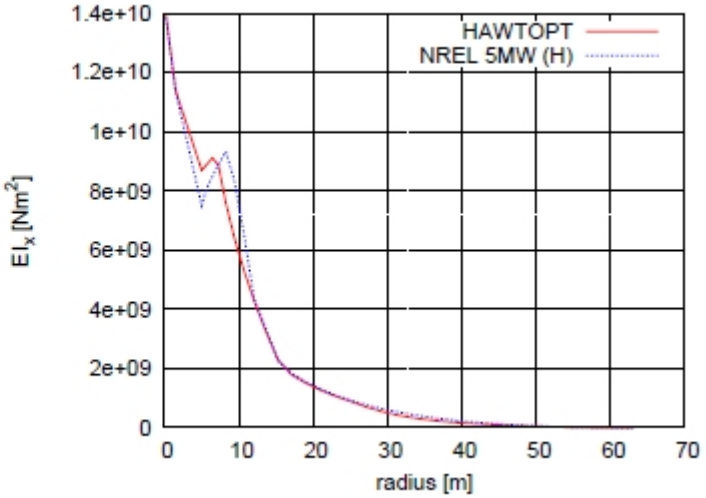

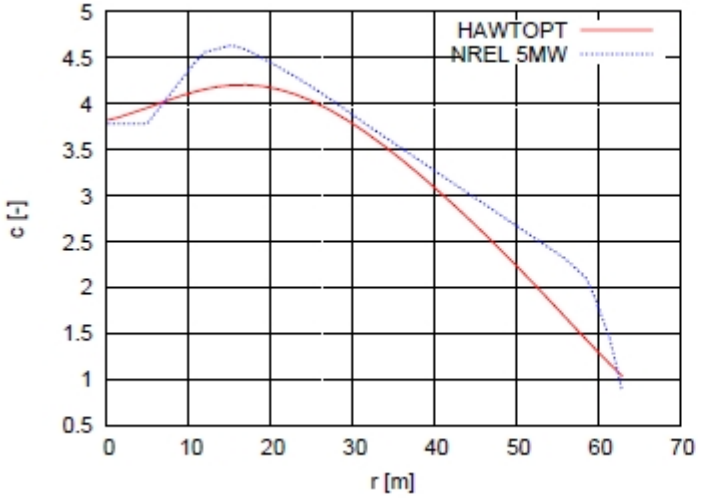

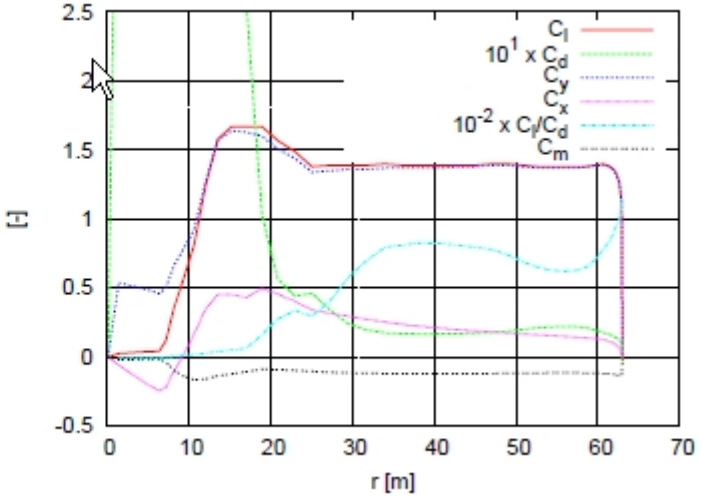

Blade with DU airfoils (NREL 5MW)

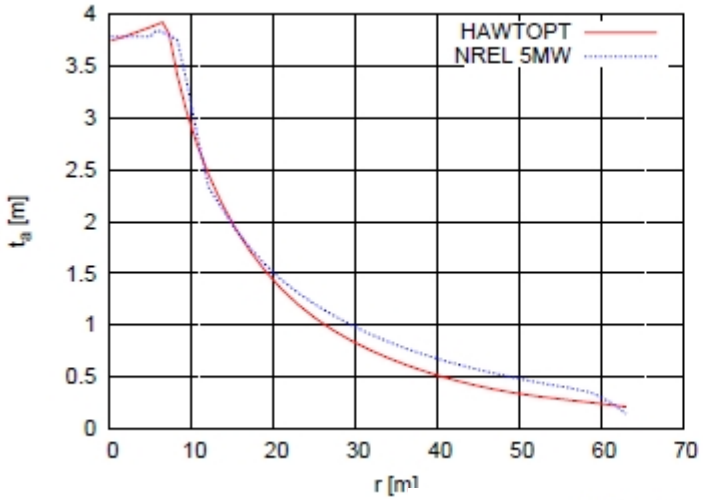

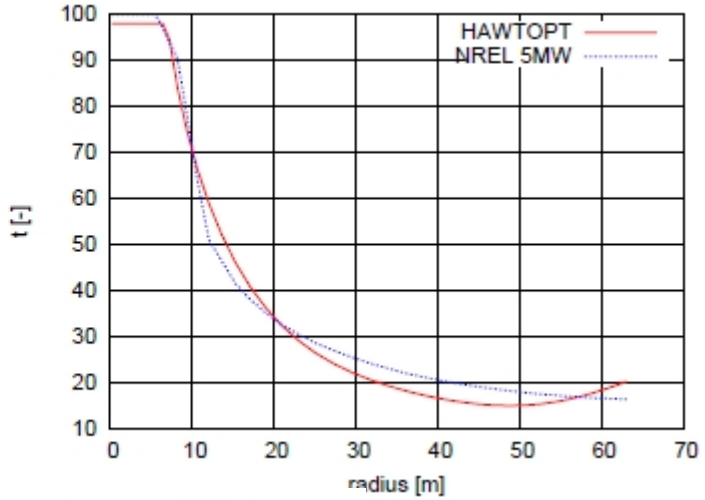

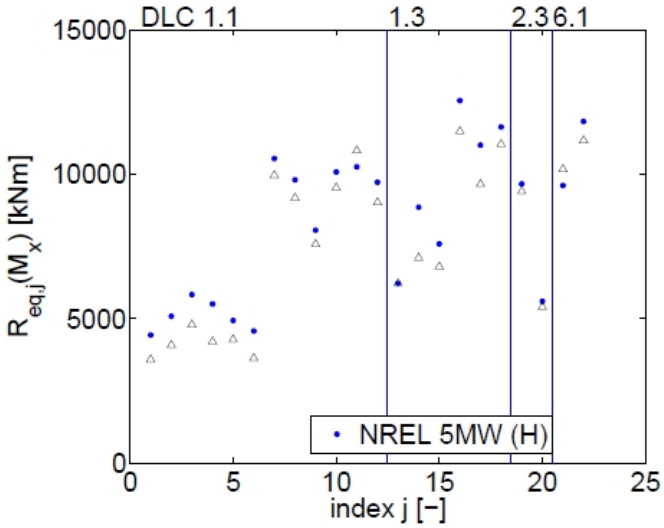

Blade with Risø-B1 airfoils (NREL 5MW)

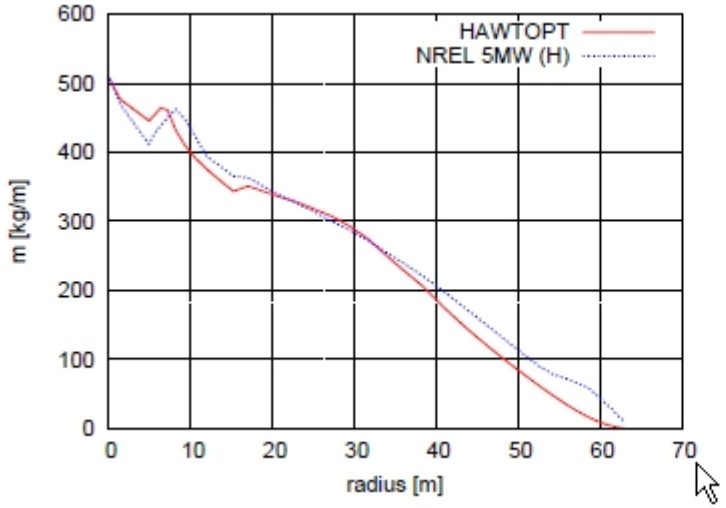

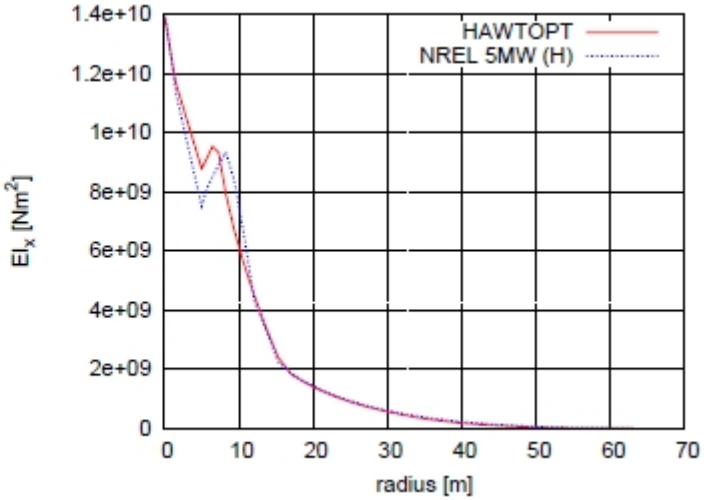

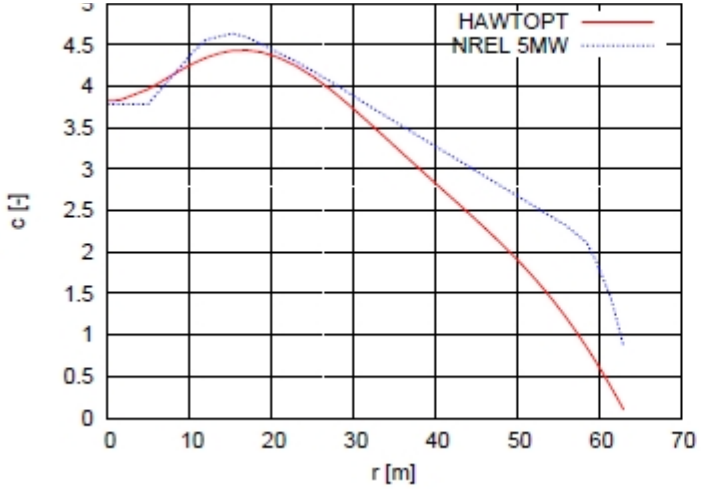

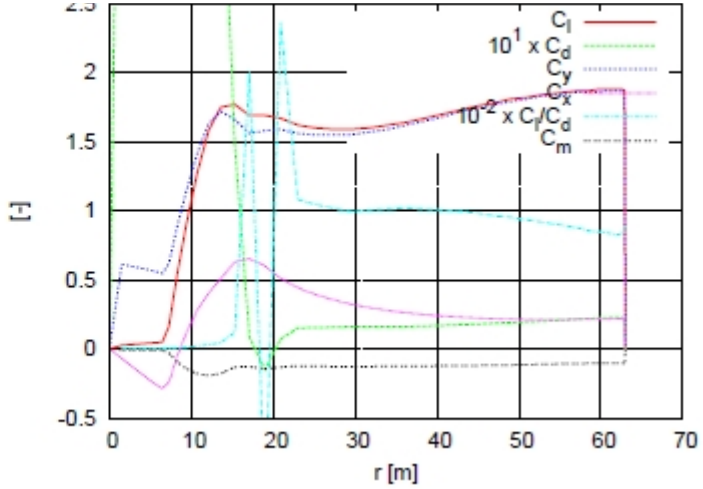

Blade with Risø-B1 airfoils (NREL 5MW)

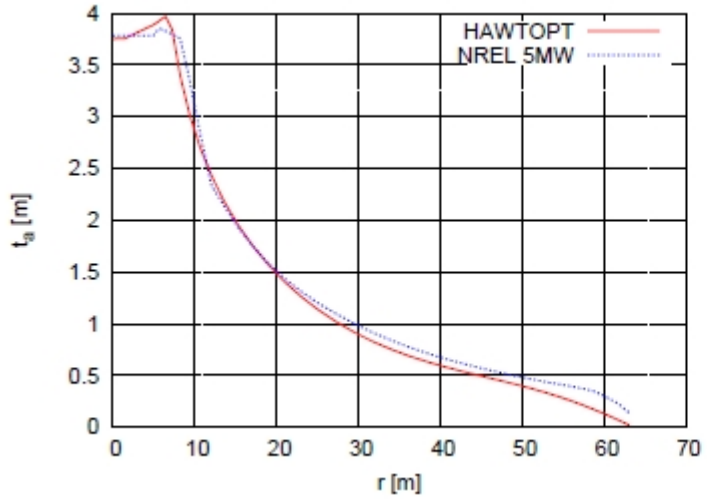

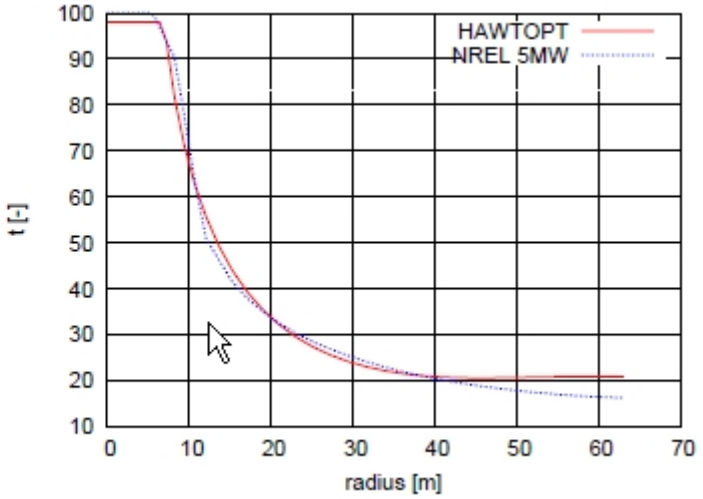

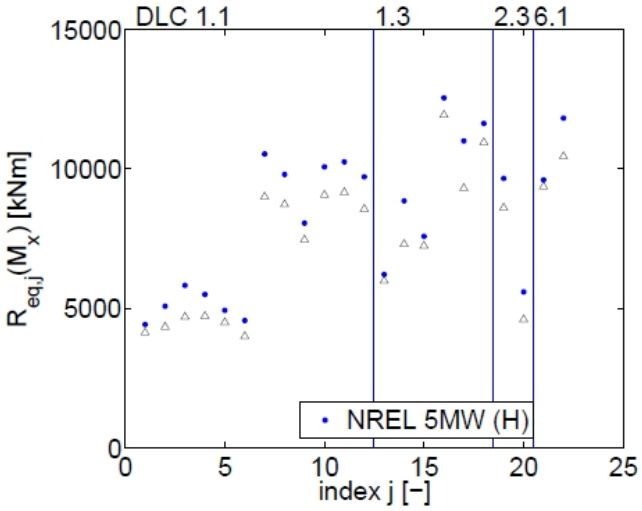

Comparing blades

		M [kg]	f_1 [Hz]	f_2 [Hz]	f_3 [Hz]
6.1	NREL 5MW	16880	0.672	1.05	1.95
6.2	NREL 5MW (H)	16330	0.665	1.06	1.94
6.4	Point Opti. (DUxx)	15945	0.658	1.03	1.89
6.5	Point Opti. (B1-xx)	15500	0.798	1.19	2.25

		AEP [GWh]	Airfoils	λ	C_l
6.1	NREL 5MW	21.3425	DUxx	7.7	0.95
6.4	Point Opti. (DUxx)	21.0414	DUxx	6.4	$\approx$1.4
6.5	Point Opti. (B1-xx)	20.9682	B1-xx	6.4	$\approx$1.6-1.8

		$R_{eq,1(100s)}(M_x)$	$R_{eq}(M_x)$	$R_{eq}(M_y)$
6.1	NREL 5MW	-	-	-
6.2	NREL 5MW (H)	4202.0	5983.0	5270.9
6.4	Point Opti. (DUxx)	3142.0	5787.5	5376.2
6.5	Point Opti. (B1-xx)	3466.0	5258.1	4966.1

Conclusions

- A simplified structural model has been formulated
  - Comparison to existing blades show good agreement
- A simplified fatigue model has been formulated
  - Comparison to aeroelastic calculations show good agreement
  - Slender blades show lower loads
- Design with DU airfoils showed
  - 3.3% reduction in fatigue loads
  - 2.4% reduction in mass
  - 1.4% reduction in AEP
- Design with Risø B1 airfoils showed
  - 12.1% reduction in fatigue loads
  - 5.1% reduction in mass
  - 1.8% reduction in AEP

9 A small study of flat back airfoils

A Small Study of Flatback Airfoils

Niels N. Sørensen

Wind Energy Division · Risø DTU

RISØ-DTU, 27-01-2011

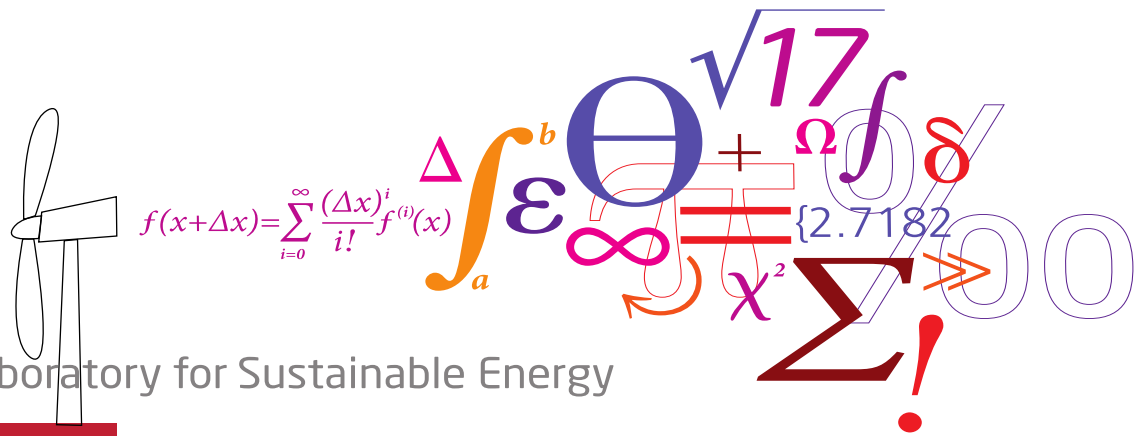

Risø DTU
National Laboratory for Sustainable Energy

Outline

1. Introduction
2. Flow solver settings
3. Grid Generation
4. Evaluation of Performance, 2D
5. 3D Investigation
6. Parametric Study, 2D
7. Conclusion and Further Work

Background

- Why are ’flatback’ airfoils interesting for rotor root design
  - They may be desirable from a structural point of view
  - They are claimed to be more roughness insensitive
  - They can provide relatively high lift (Cl > 2)
  - The drag penalty of the thick trailing edge may not be important at the inboard sections
  - They are sometimes claimed to be more efficient than traditional truncated airfoils

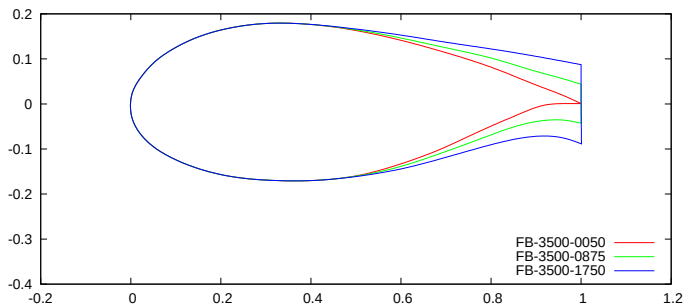

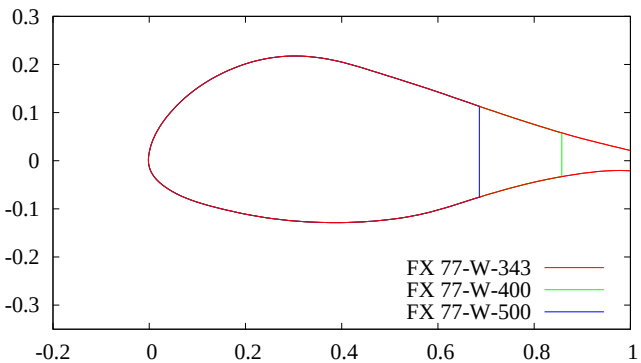

Niels N. Sørensen,
Risø DTU

Challenges

- What problems must be foreseen when designing ’flatback’ airfoils, designed for the root section where the thickness is larger than 30%
  - Typical design codes as the Xfoil code will eventually fail to give answers due to the trailing edge thickness
  - The validity of CFD codes for these airfoils must be checked
  - Wind tunnel testing of thick airfoils at high Re and AOA may be difficult
  - What should the design philosophy be
- How will the flatback airfoils work during operational conditions
  - How will the 3D effects often referred to as ’Stall Delay’ influence the performance
  - How are there dynamical behaviour in stall

Present Study

The present study will not answer all these questions, but is the first step towards the design and testing of a flatback airfoil.

- We will evaluate the capability of our in-house CFD solver (EllipSys) to predict flatback and truncated airfoils
- We will briefly investigate possible wall junction problems for thick airfoils in tunnels
- We will do a small parametric study of possible ways to generate truncated airfoils

Flow solver settings

EllipSys2D/3D

- Two dimensional simulations and a few three dimensional simulations are performed
- Both steady and transient runs $\Delta t = \Delta \tilde{t} \frac{c}{U_\infty} = 1 \times 10^{-2}$
- For the 2D simulations we use both fully turbulent and transitional computations based on the $k - \omega$ SST model
- For the 3D simulations we use a so called Delayed Detached Eddy Simulation technique based on the SST model, along with the transition modeling
- Transition modeling is based on the $\gamma - Re_\theta$ model
- The diffusive terms are model using central differences
- In 2D the third order accurate QUICK scheme is used for the convective terms
- In 3D a hybrid fourth order central/QUICK scheme is used to resolve the DES areas

Grid Generation 2D

All grids are generated with the hyperbolic grid generation code HypGrid2D

- The grid has 320 cells in chordwise direction, and 128 cells in the wall normal direction
- The height of the first cell is $1 \times 10^{-6} \times$ Chord
- The outer boundary are placed 45 Chords away from the airfoil

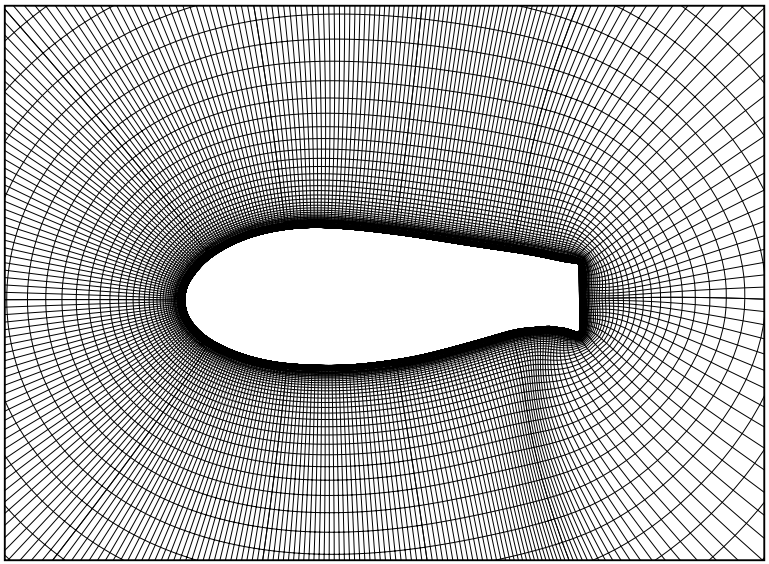

Grid Generation 3D

All grids are generated with the hyperbolic grid generation code HypGrid2D

- The inner O-grid has 320 cells in chordwise direction, and 128 cells in the wall normal direction
- The inner O-grid is embedded in a stretched square grid
- The height of the first cell is $1 \times 10^{-6} \times$ Chord
- The upstream and downstream boundaries are placed 9 chords away, while the bottom and lid are approximately 5 chords away
- In the spanwise direction, the domain is 1 Chord long and 128 cells are used

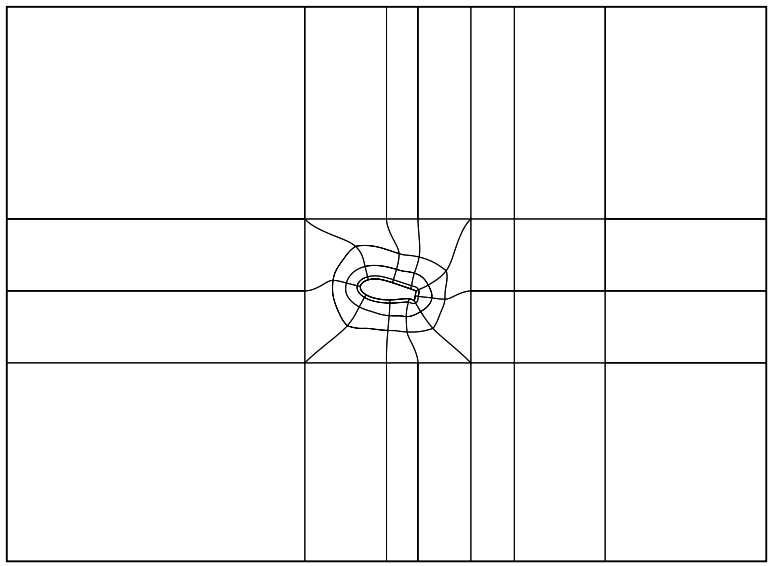

Grid Generation 3D (2)

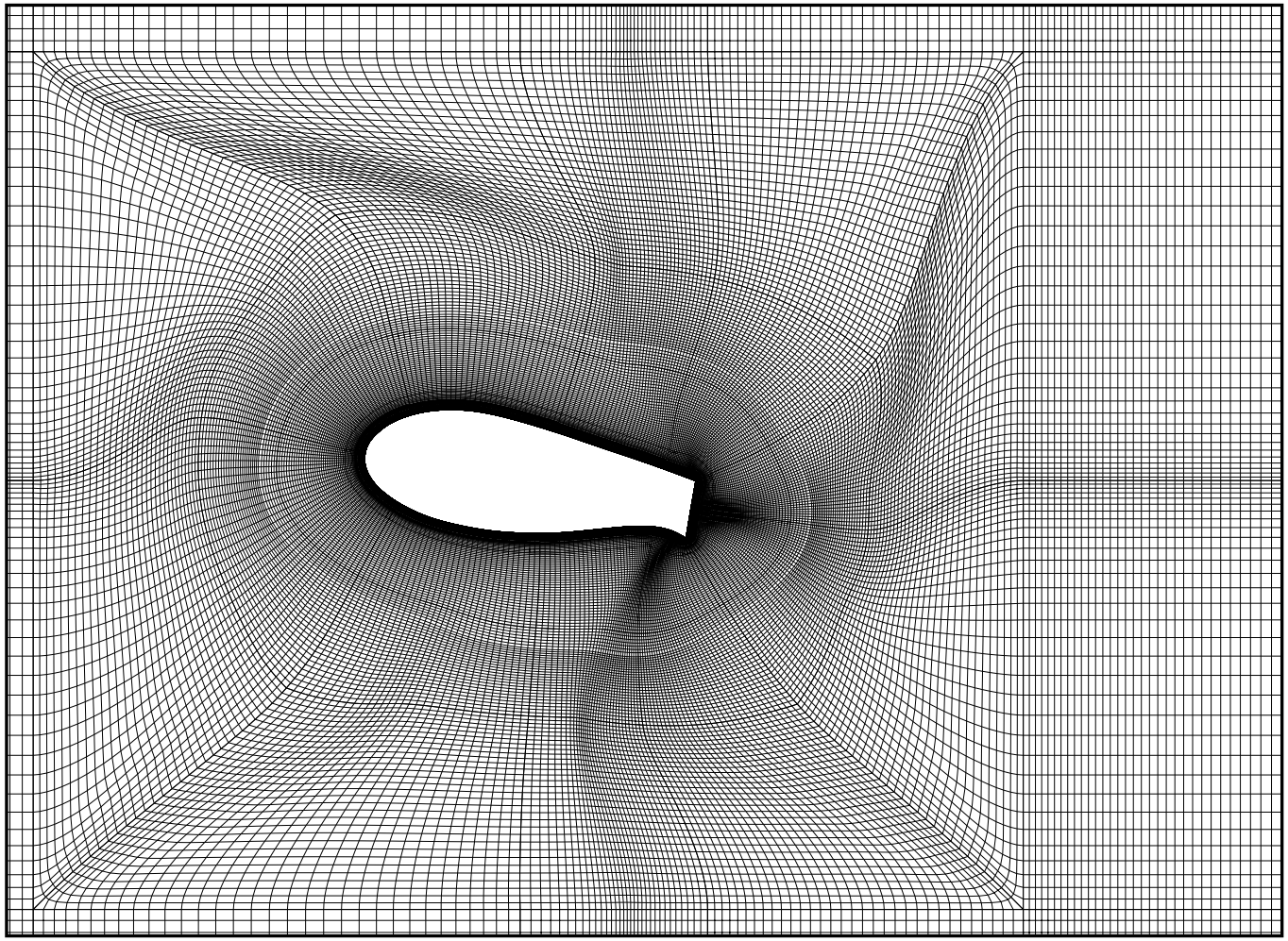

Niels N. Sørensen,
Risø DTU

Grid Generation 3D (2)

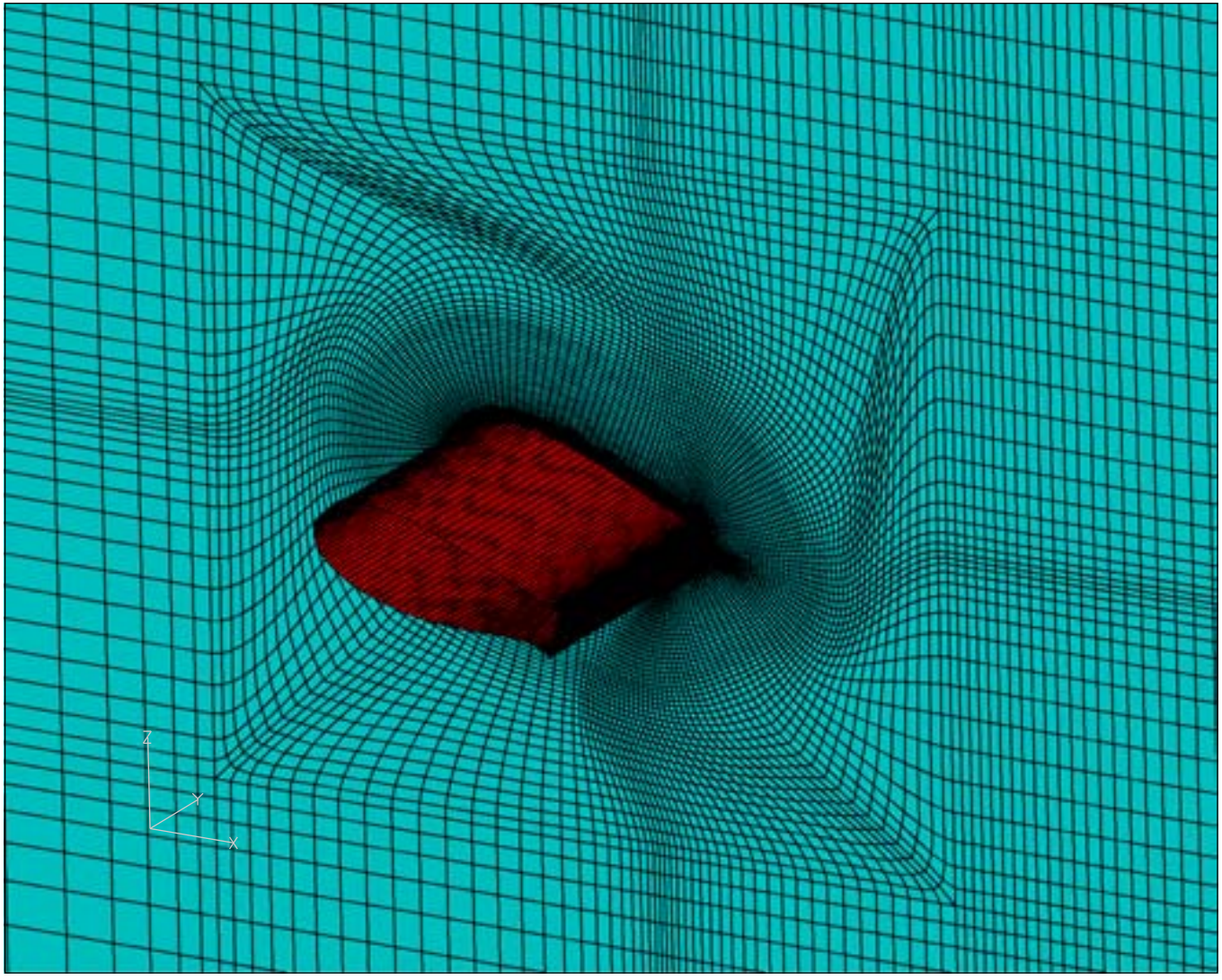

Niels N. Sørensen,
Risø DTU

Grid Generation 3D (2)

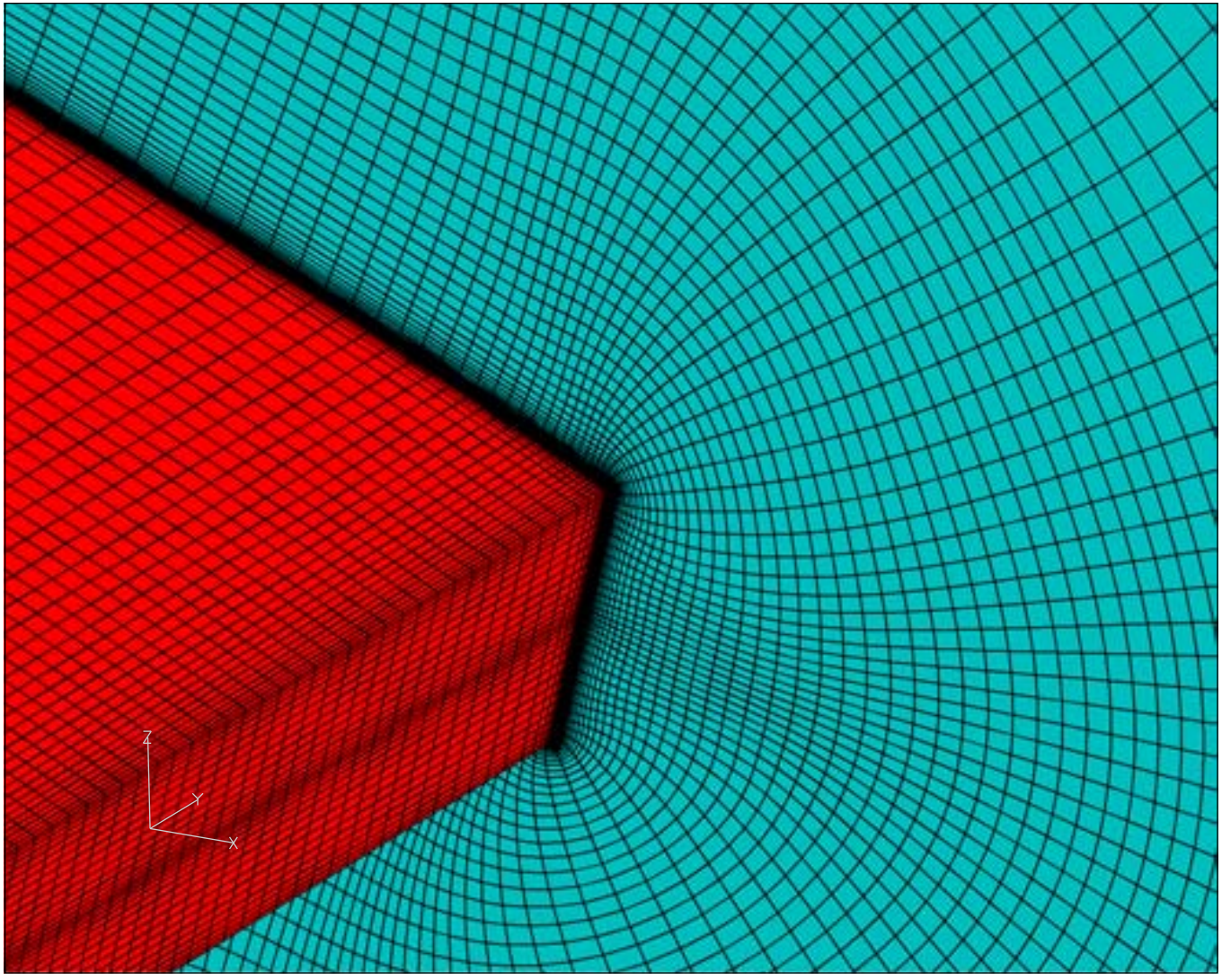

Niels N. Sørensen,
Risø DTU

Evaluation of Performance, 2D

FX-77-W-343

Conditions: $Re = 3 \times 10^6$, free transition
Data from University of Stuttgart

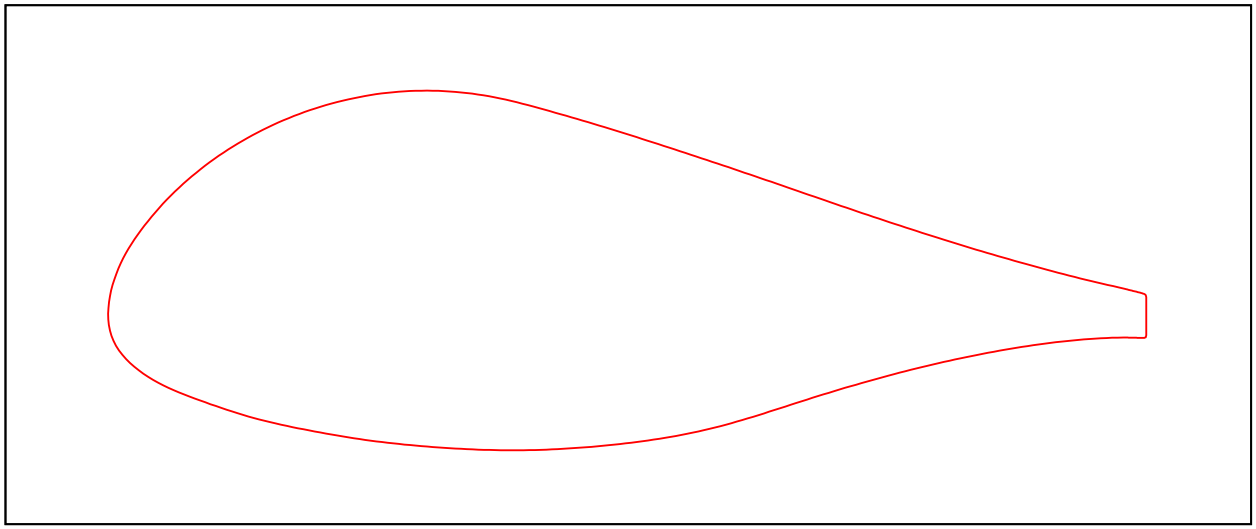

Niels N. Sørensen,
Risø DTU

Evaluation of Performance, 2D

FX-77-W-343

Conditions: $Re = 3 \times 10^6$, free transition
Data from University of Stuttgart

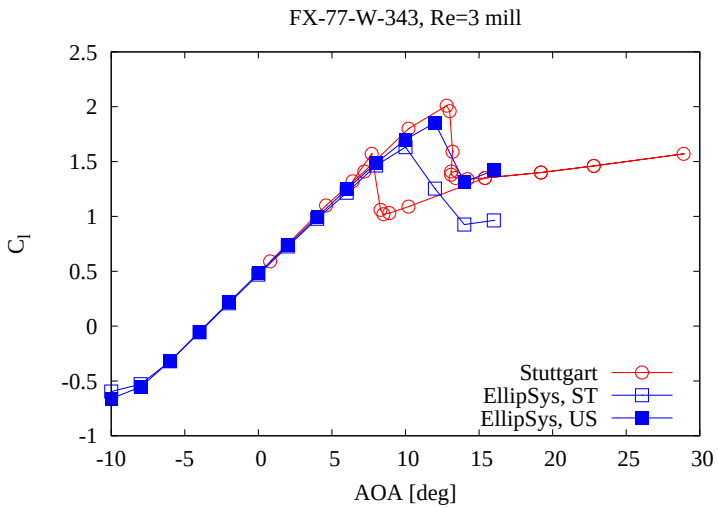

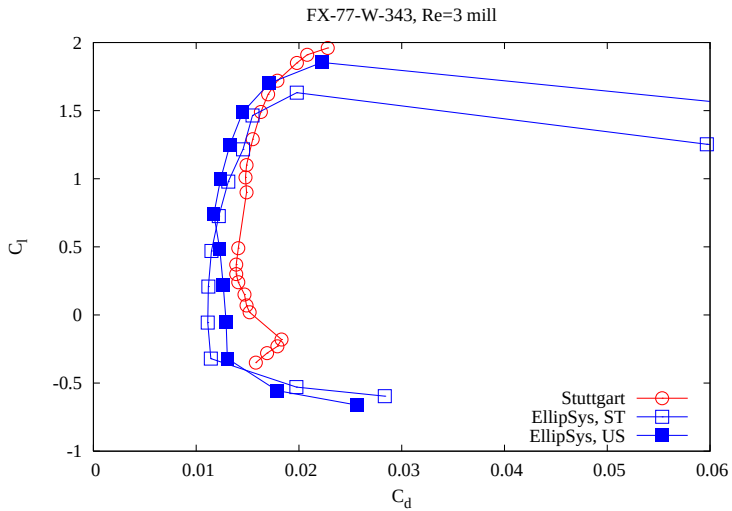

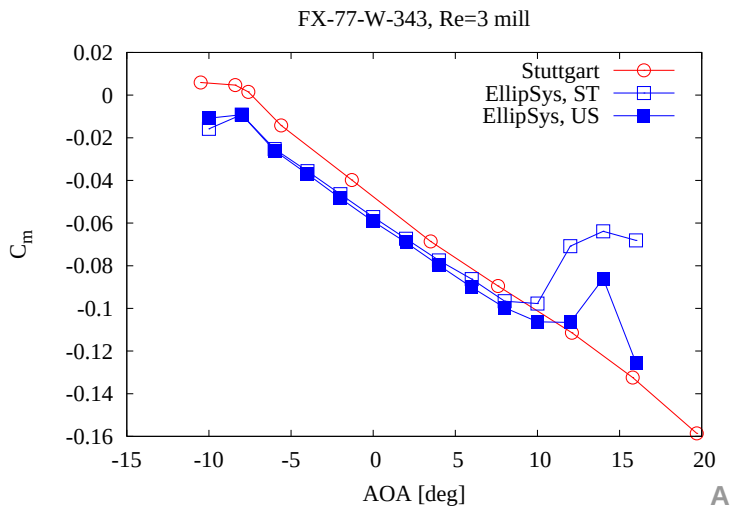

Niels N. Sørensen,
Risø DTU

Evaluation of Performance, 2D

FX-77-W-400

Conditions: $Re = 4 \times 10^6$, free transition

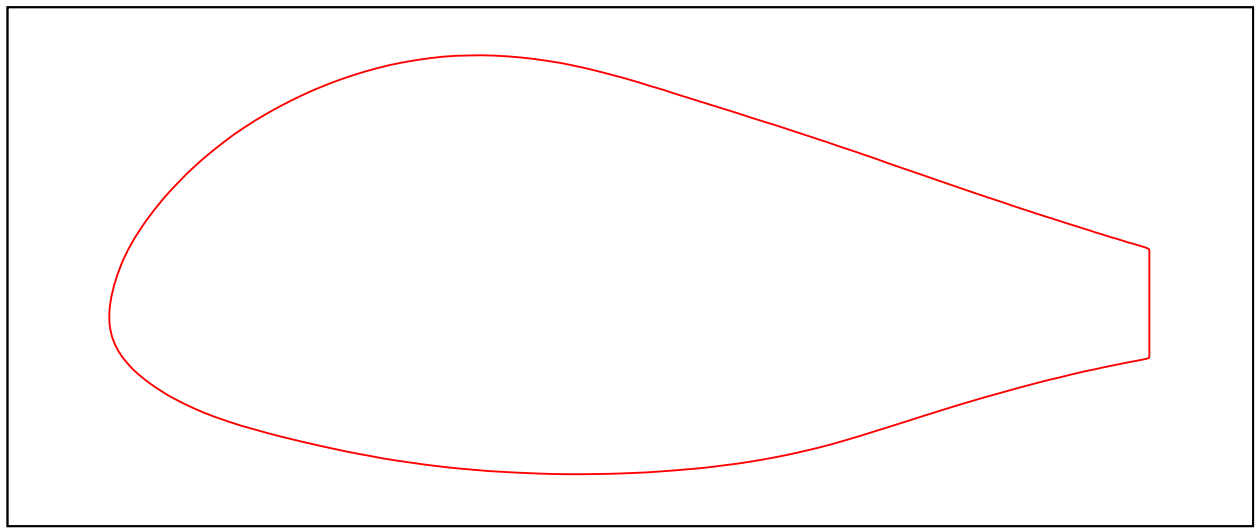

Niels N. Sørensen,
Risø DTU

Evaluation of Performance, 2D

FX-77-W-400

Conditions: $Re = 4 \times 10^6$, free transition

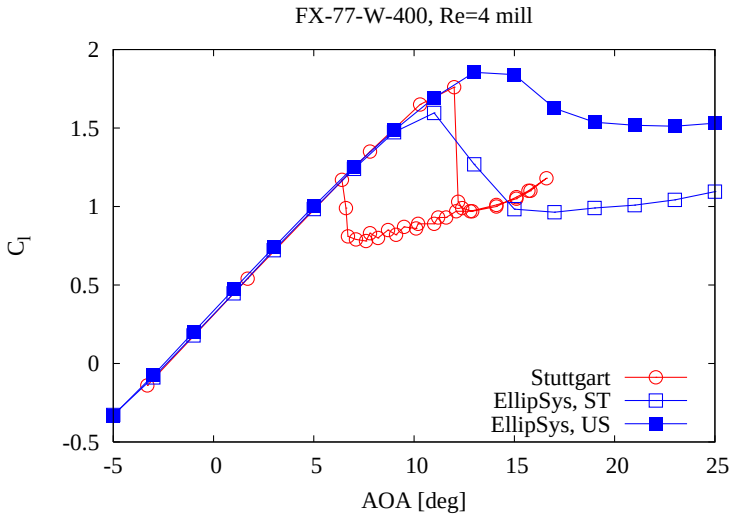

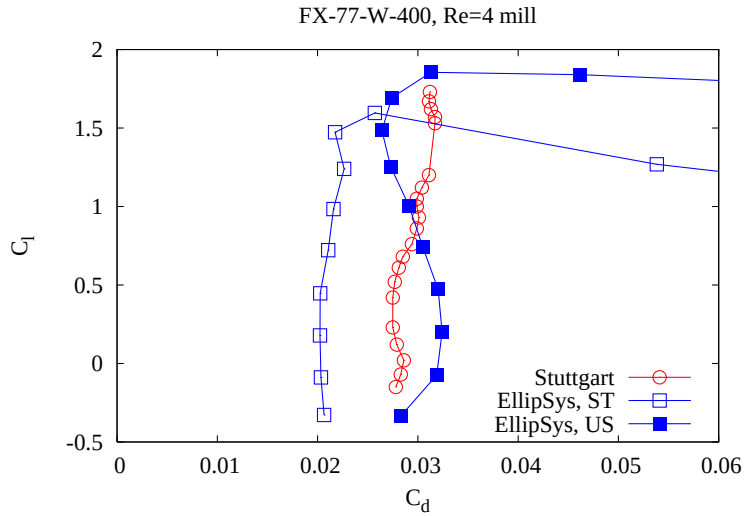

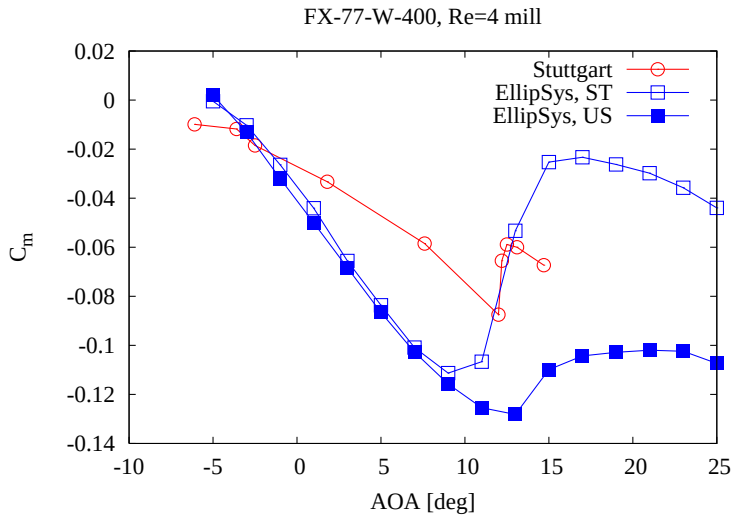

Niels N. Sørensen,
Risø DTU

Evaluation of Performance, 2D

FX-77-W-500

Conditions: $Re = 2.75 \times 10^6$, free transition

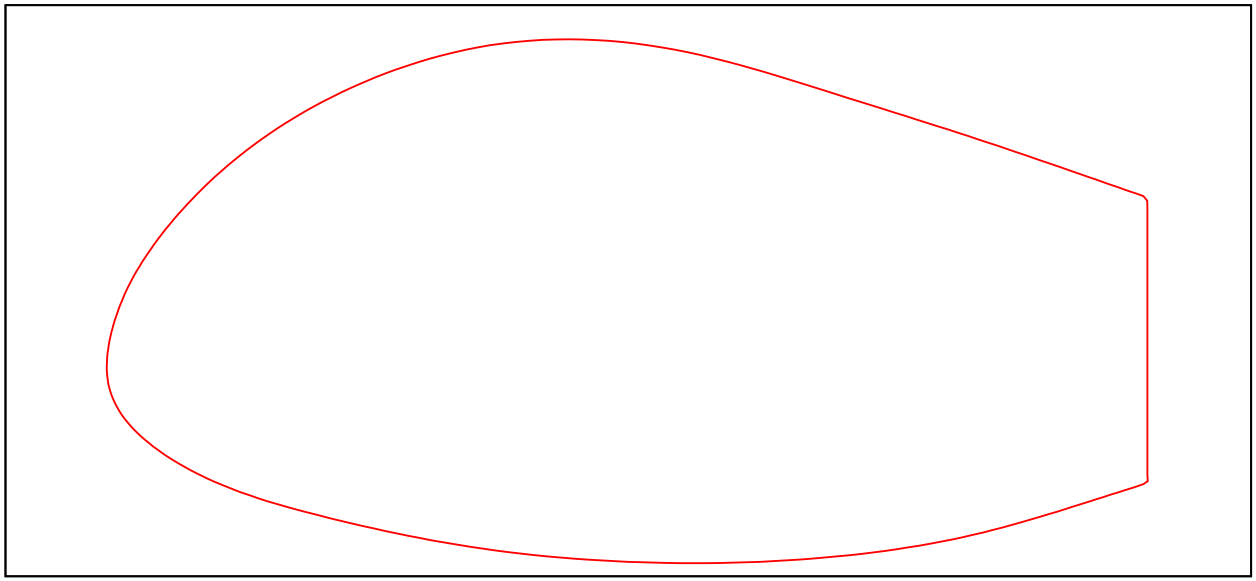

Niels N. Sørensen,
Risø DTU

Evaluation of Performance, 2D

FX-77-W-500

Conditions: $Re = 2.75 \times 10^6$, free transition

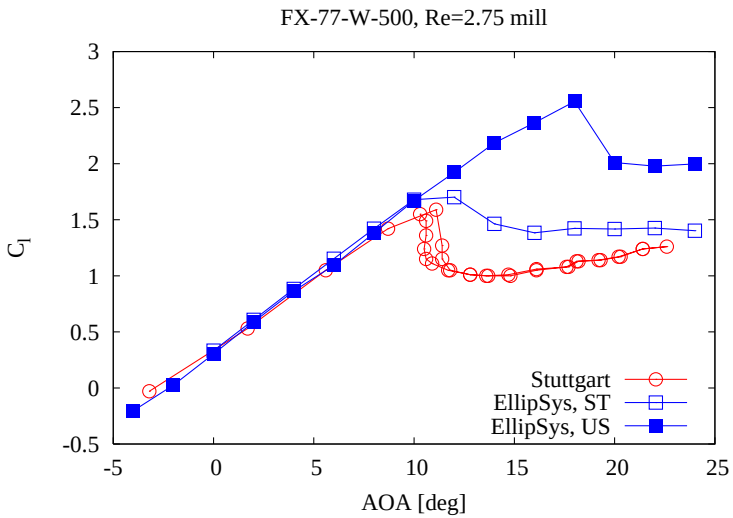

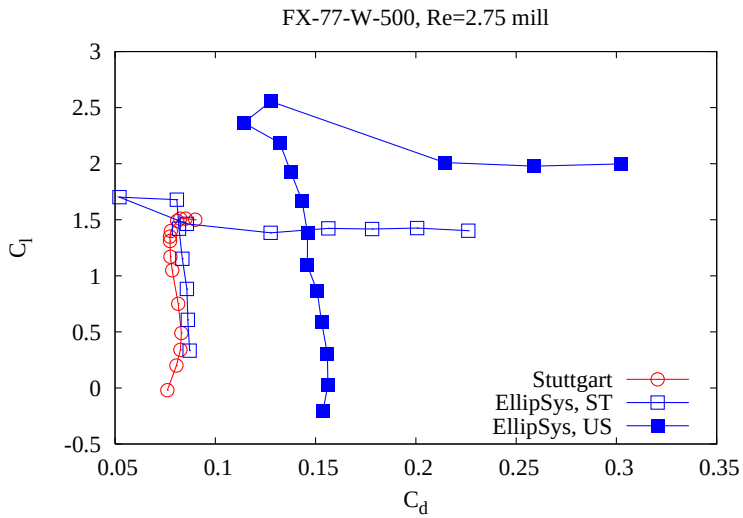

Niels N. Sørensen,
Risø DTU

Evaluation of Performance, 2D

FB-3500-0050

Conditions: $Re = 666.000$, free transition left and fixed right
Data from University of California (UC Davis)

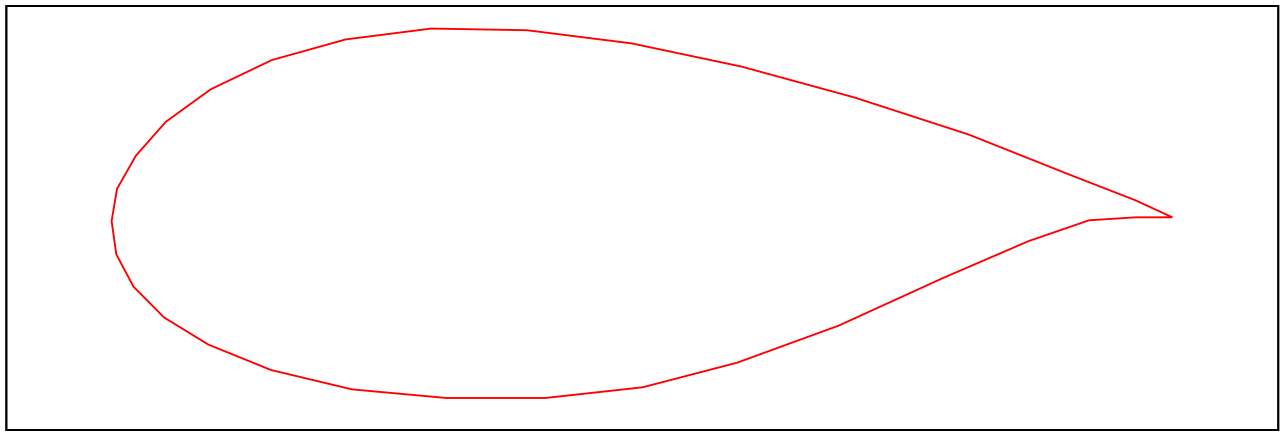

Niels N. Sørensen,
Risø DTU

Evaluation of Performance, 2D

FB-3500-0050

Conditions: $Re = 666.000$, free transition left and fixed right
Data from University of California (UC Davis)

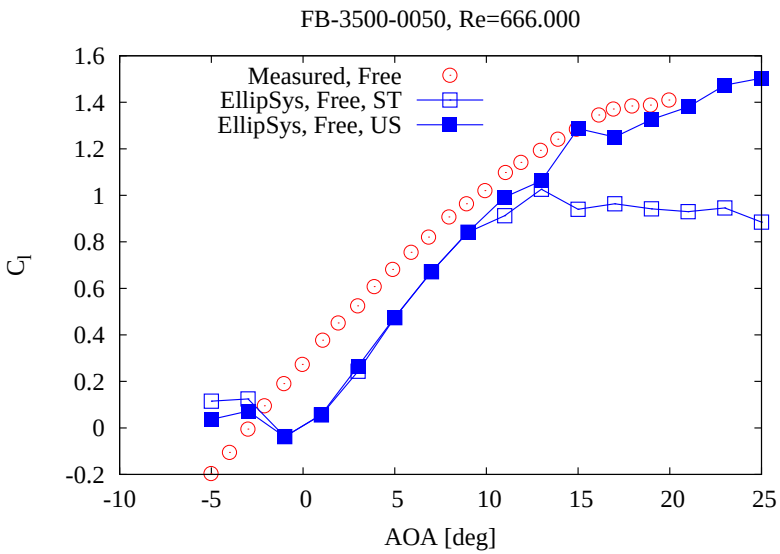

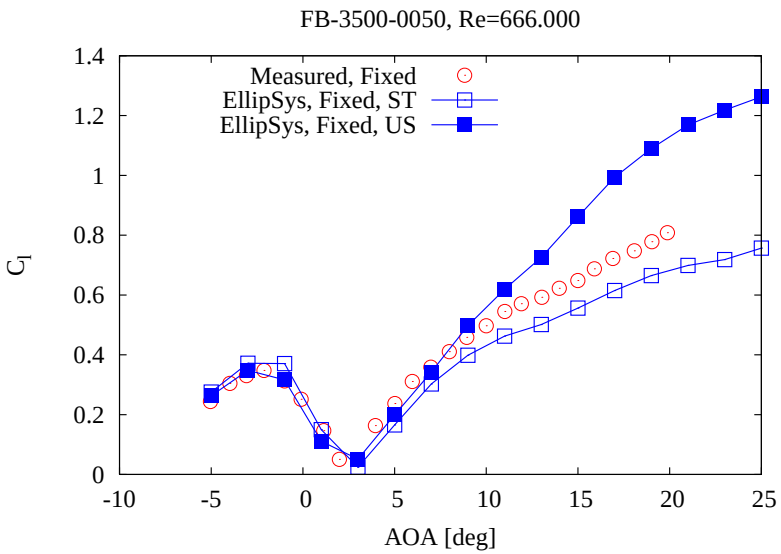

Niels N. Sørensen,
Risø DTU

Evaluation of Performance, 2D

FB-3500-0050

Conditions: $Re = 666.000$, free transition left and fixed right
Data from University of California (UC Davis)

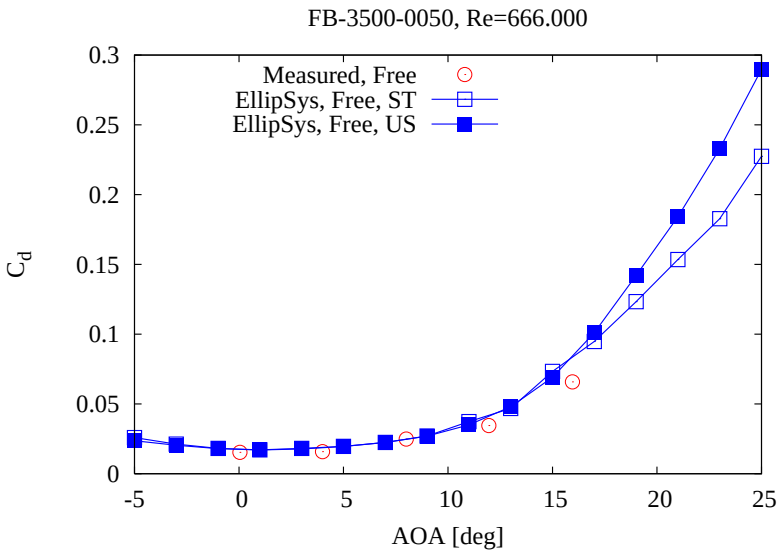

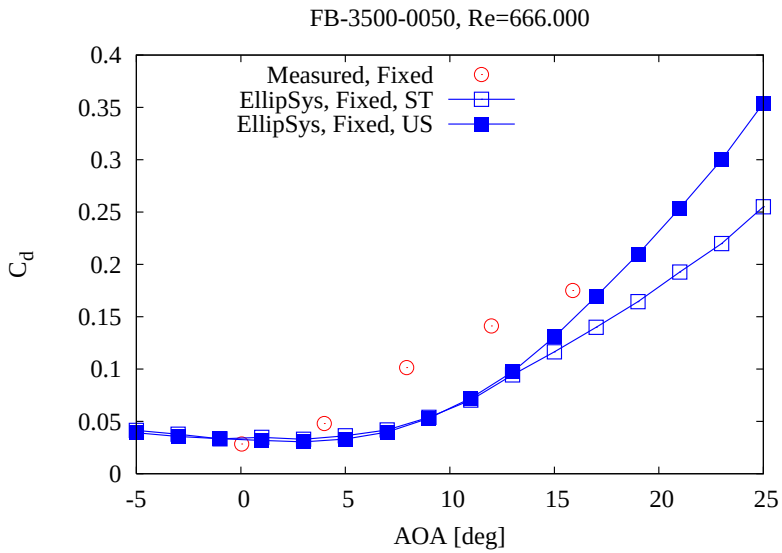

Niels N. Sørensen,
Risø DTU

Evaluation of Performance, 2D

FB-3500-0875

Conditions: $Re = 666.000$, free transition left and fixed right

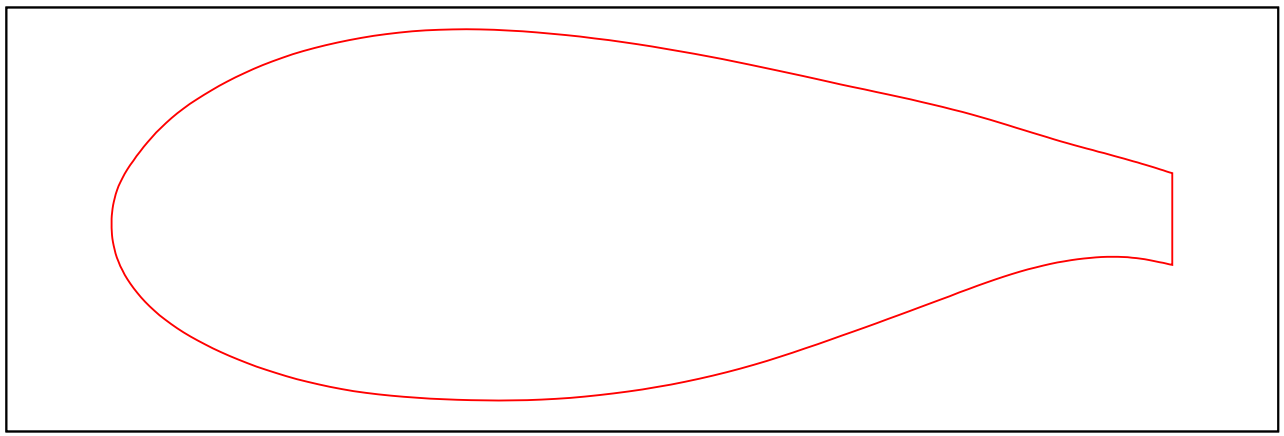

Niels N. Sørensen,
Risø DTU

Evaluation of Performance, 2D

FB-3500-0875

Conditions: $Re = 666.000$, free transition left and fixed right

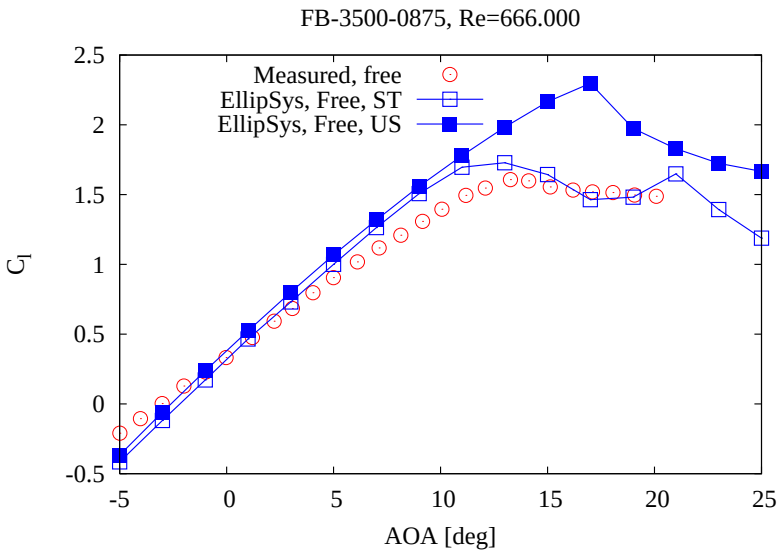

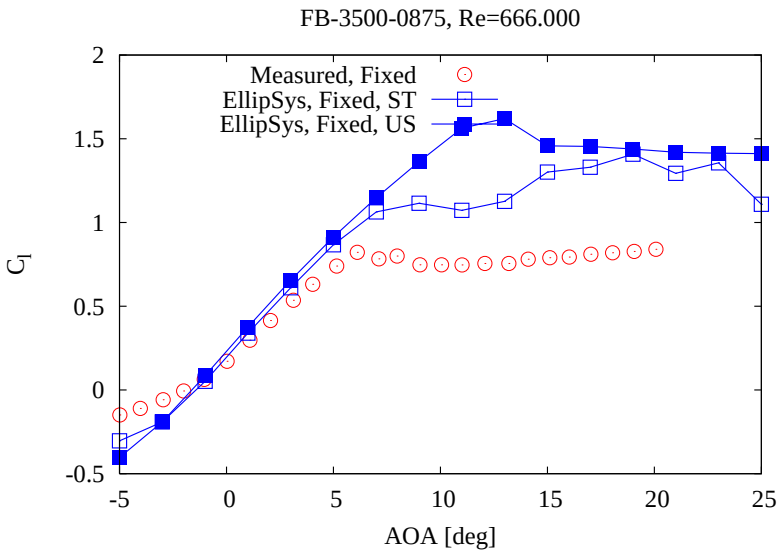

Niels N. Sørensen,
Risø DTU

Evaluation of Performance, 2D

FB-3500-0875

Conditions: $Re = 666.000$, free transition left and fixed right

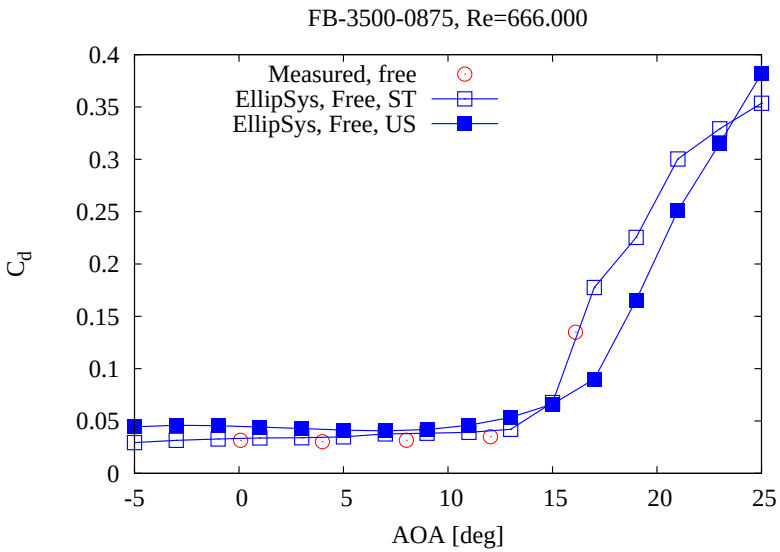

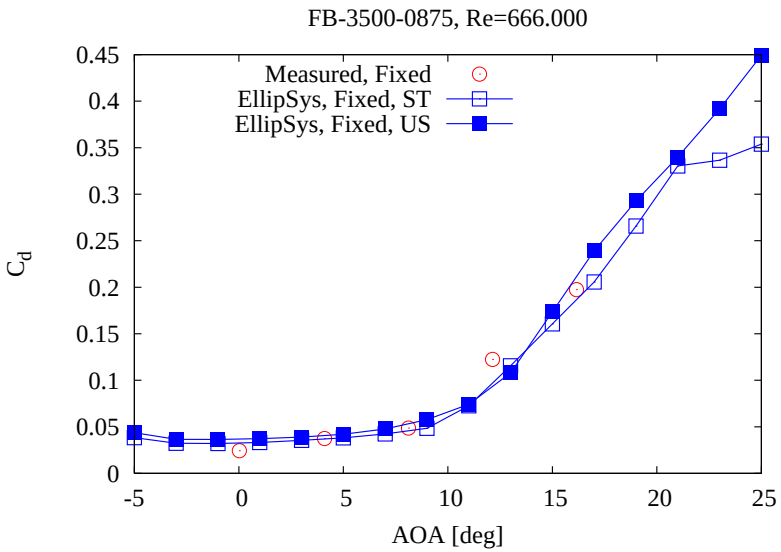

Niels N. Sørensen,
Risø DTU

Evaluation of Performance, 2D

FB-3500-1750

Conditions: $Re = 666.000$, free transition left and fixed right

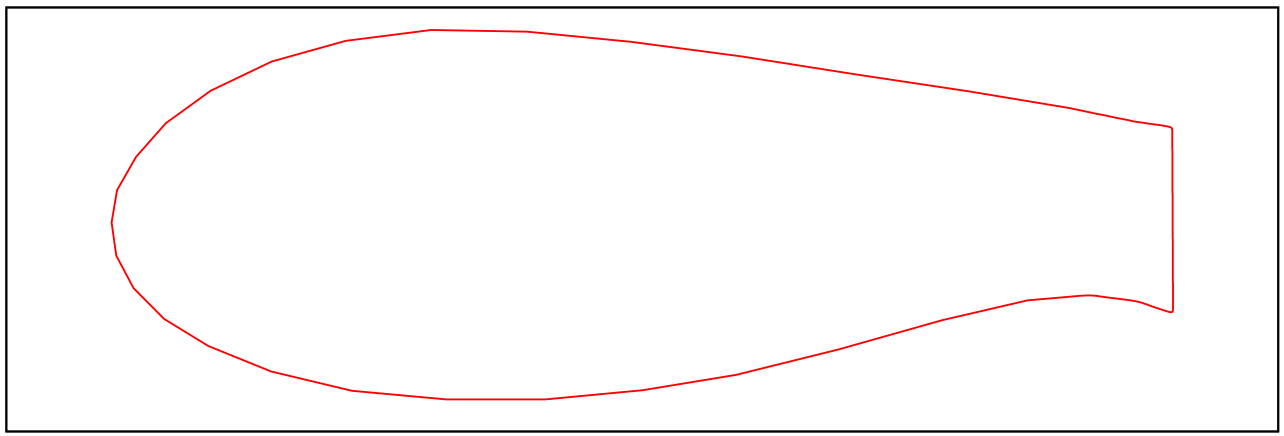

Niels N. Sørensen,
Risø DTU

Evaluation of Performance, 2D

FB-3500-1750

Conditions: $Re = 666.000$, free transition left and fixed right

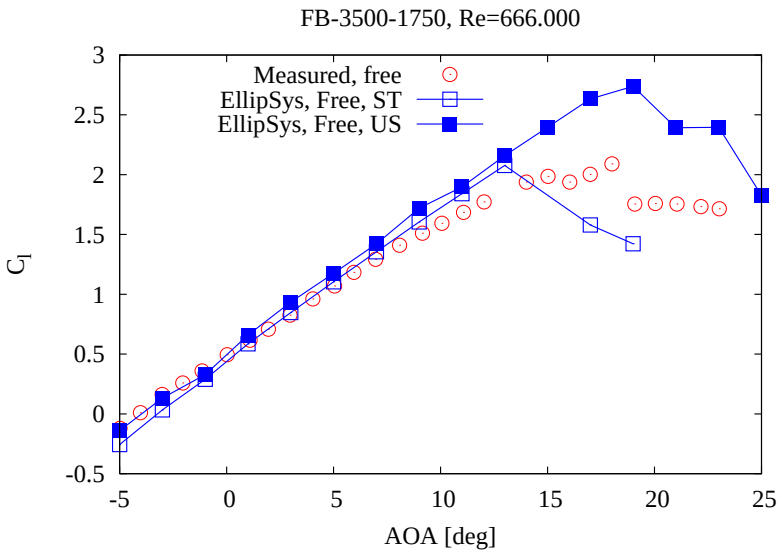

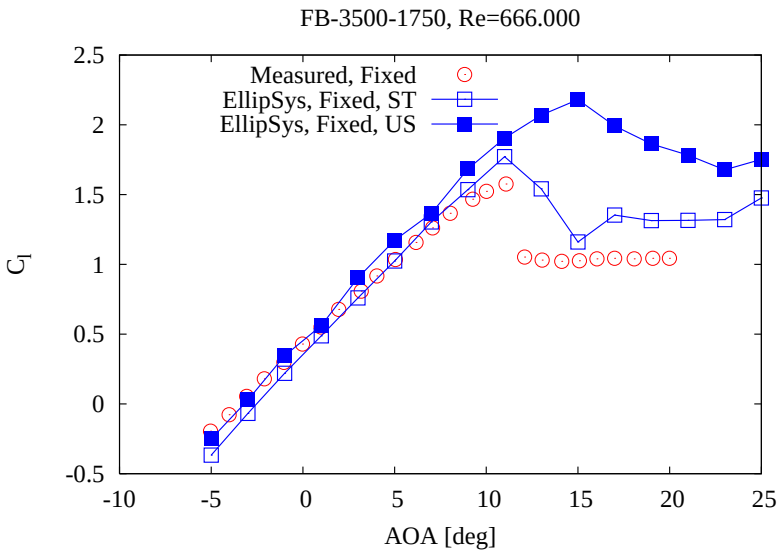

Niels N. Sørensen,
Risø DTU

Evaluation of Performance, 2D

FB-3500-1750

Conditions: $Re = 666.000$, free transition left and fixed right

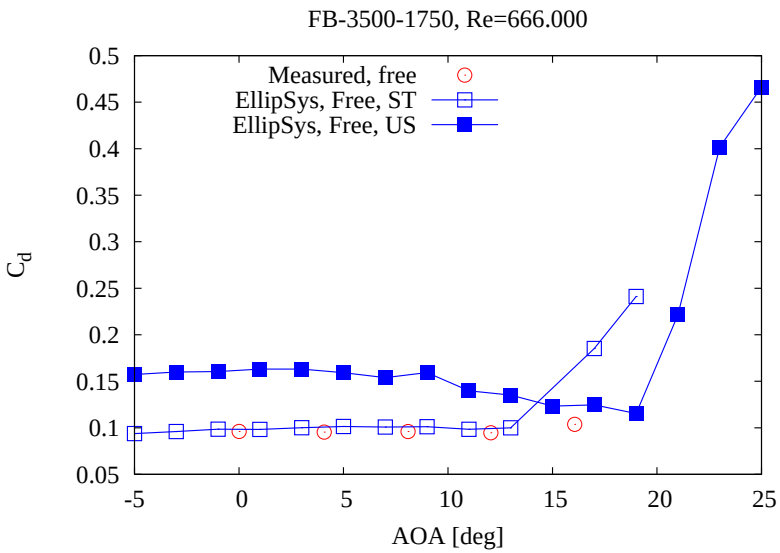

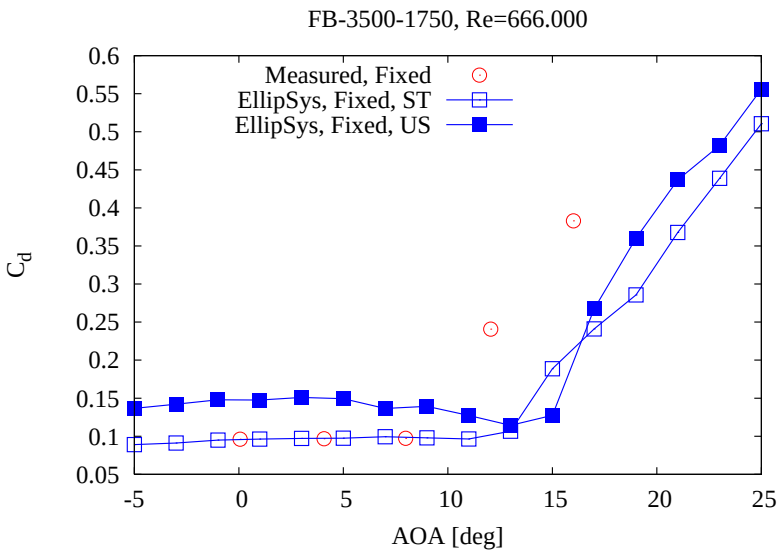

Niels N. Sørensen,
Risø DTU

Evaluation of Performance, 2D

FB-3500

Comparison of the three flat back airfoils

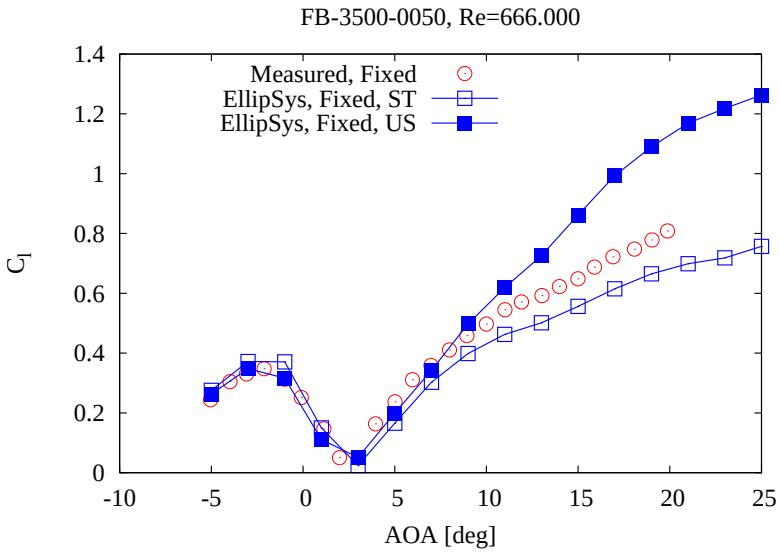

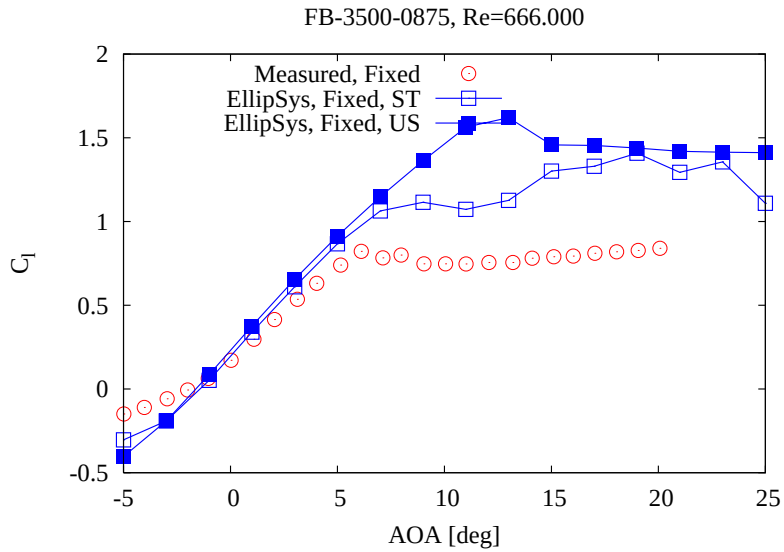

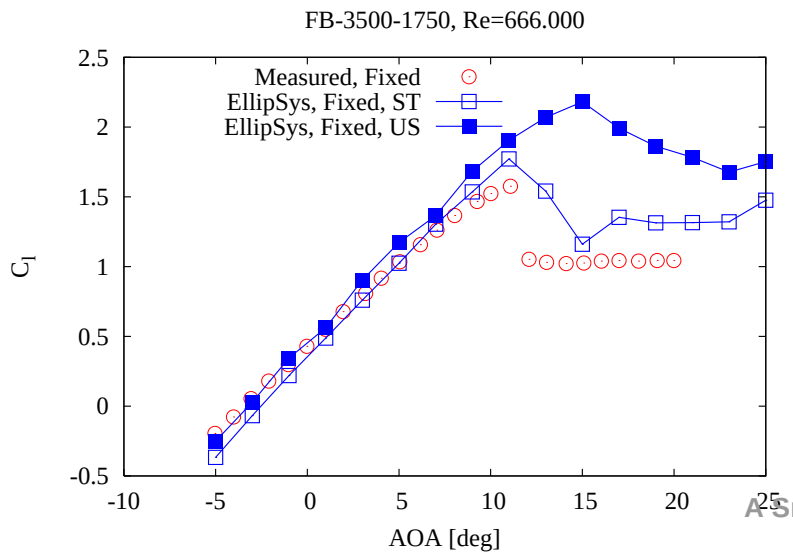

Niels N. Sørensen,
Risø DTU

Evaluation of Performance, 2D

FB-3500

Comparison of the three flat back airfoils

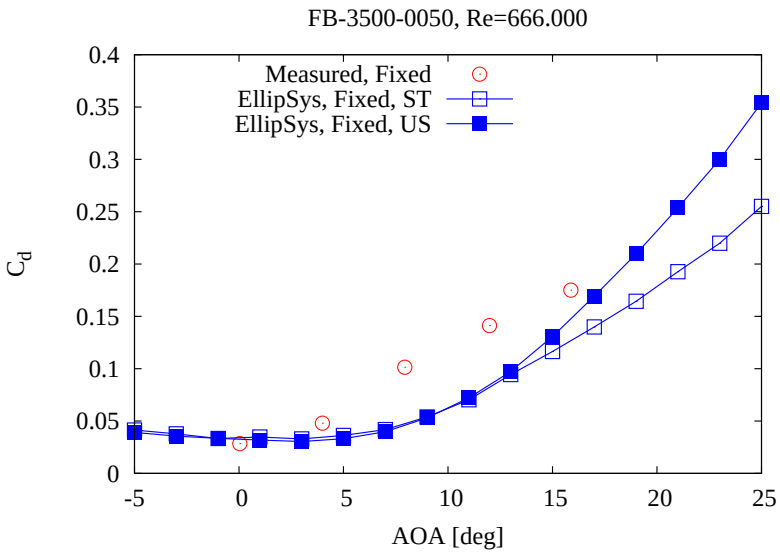

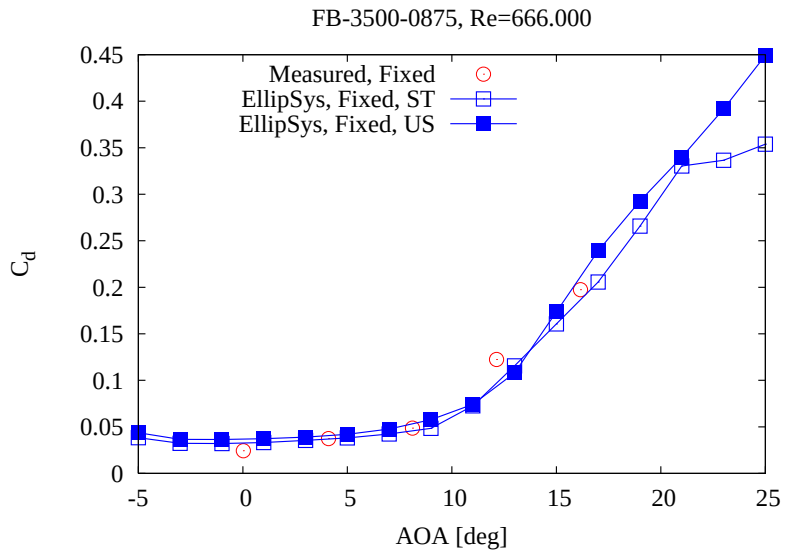

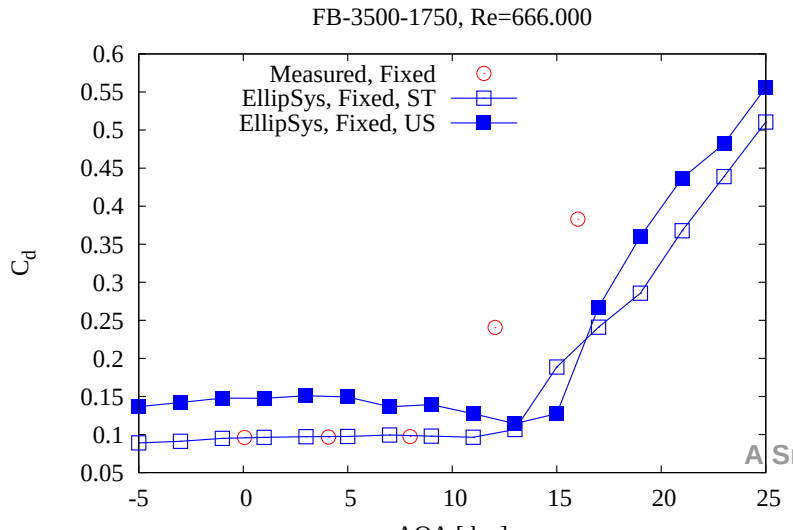

Niels N. Sørensen,
Risø DTU

Resume of performance evaluation

- The solver is capable of reproducing effect of changing from free to fixed transition
- Generally the drag is well captured for the flatback airfoils, (it is mainly pressure based)
- In all 2D cases the steady state results are closer to the measured lift (slightly surprising)
- The tendency of the drag is not as clear, in some cases the unsteady agrees better
- We can use CFD to compare the quality of different designs

3D Investigation

- How will the flatback airfoils behave in the tunnel
- Is the fact that 2D steady computations perform better due to some 2D artifact
- Can 3D provide improved insight?

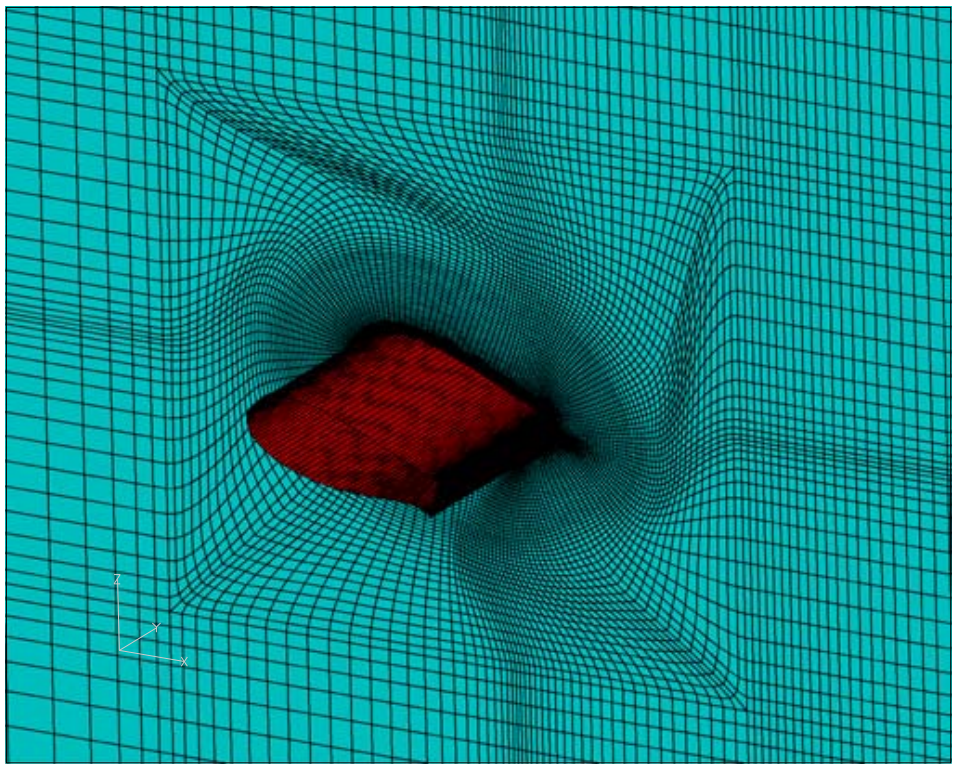

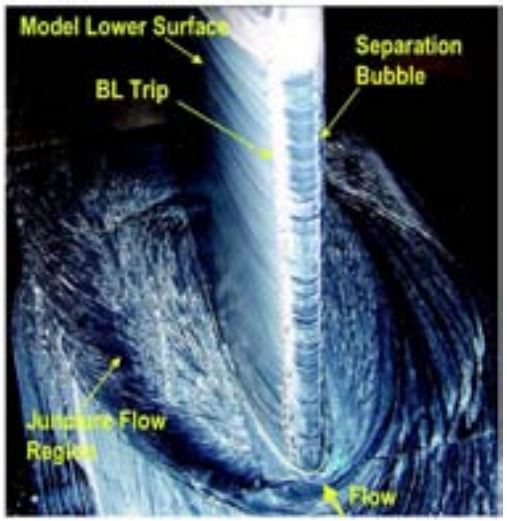

Niels N. Sørensen,
Risø DTU

3D Flow Patterns

Operational conditions

- $Re = 666.000$
- Free transition
- Span length is equal to 2 chords

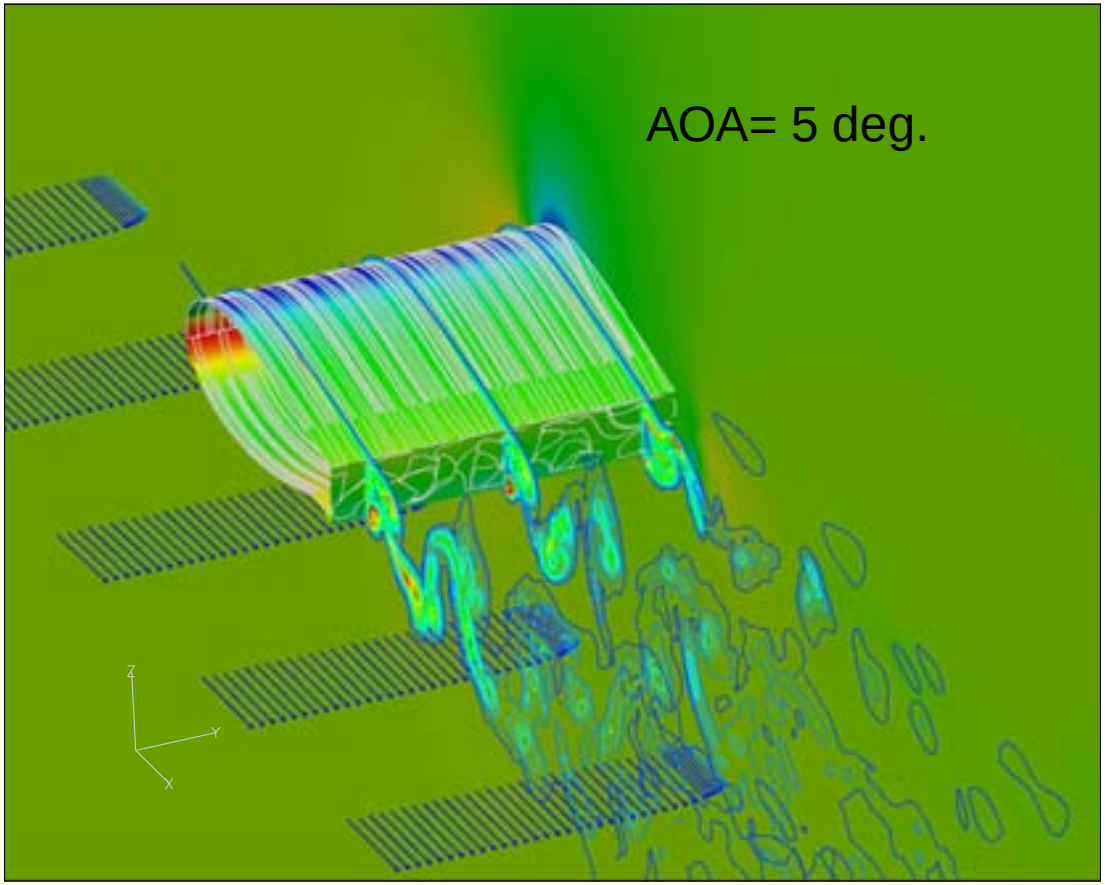

Niels N. Sørensen,
Risø DTU

3D Flow Patterns

Operational conditions

- $Re = 666.000$
- Free transition
- Span length is equal to 2 chords

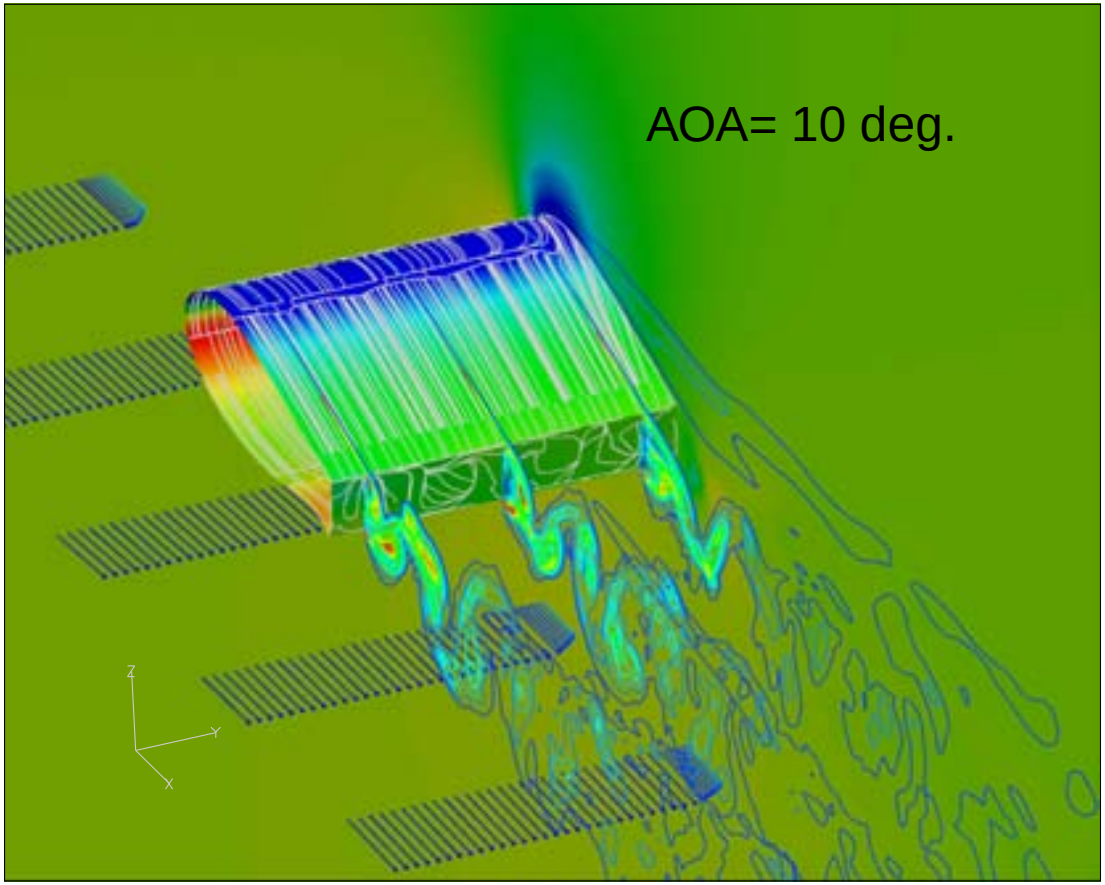

Niels N. Sørensen,
Risø DTU

3D Flow Patterns

Operational conditions

- $Re = 666.000$
- Free transition
- Span length is equal to 2 chords

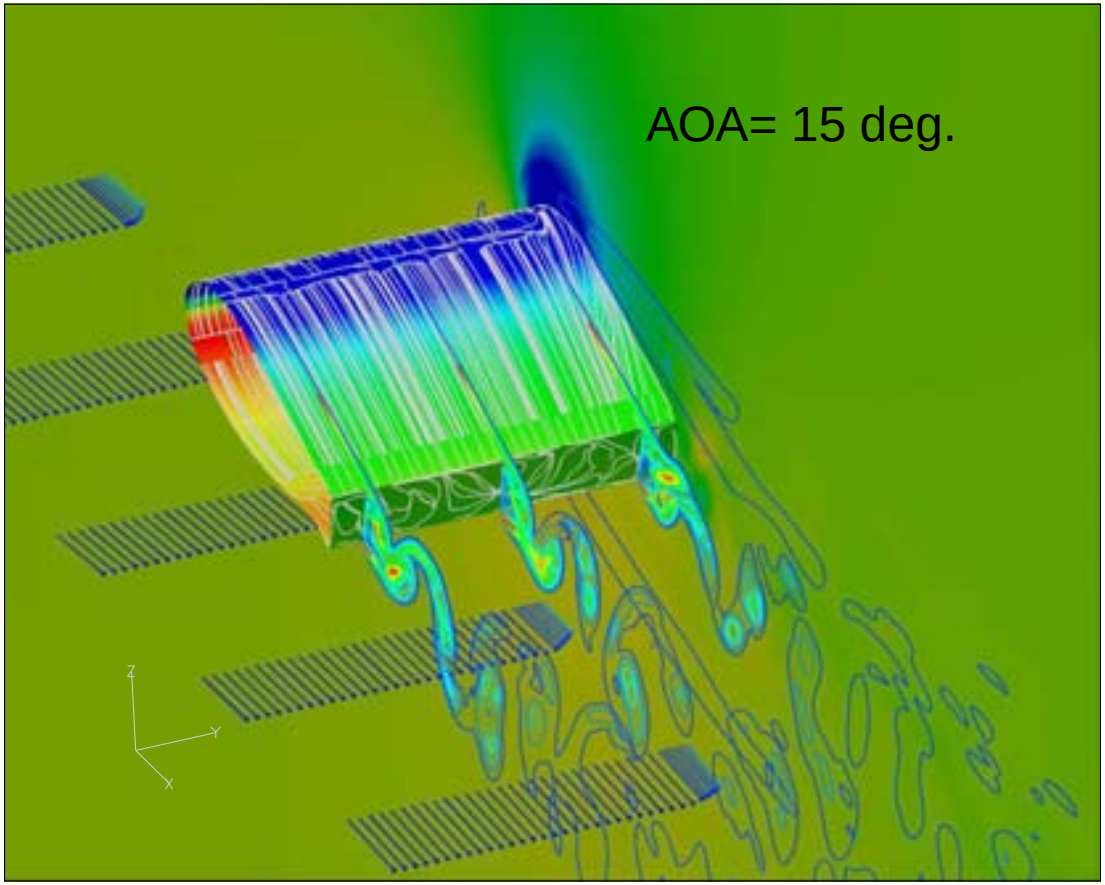

Niels N. Sørensen,
Risø DTU

3D Flow Patterns

Operational conditions

- $Re = 666.000$
- Free transition
- Span length is equal to 2 chords

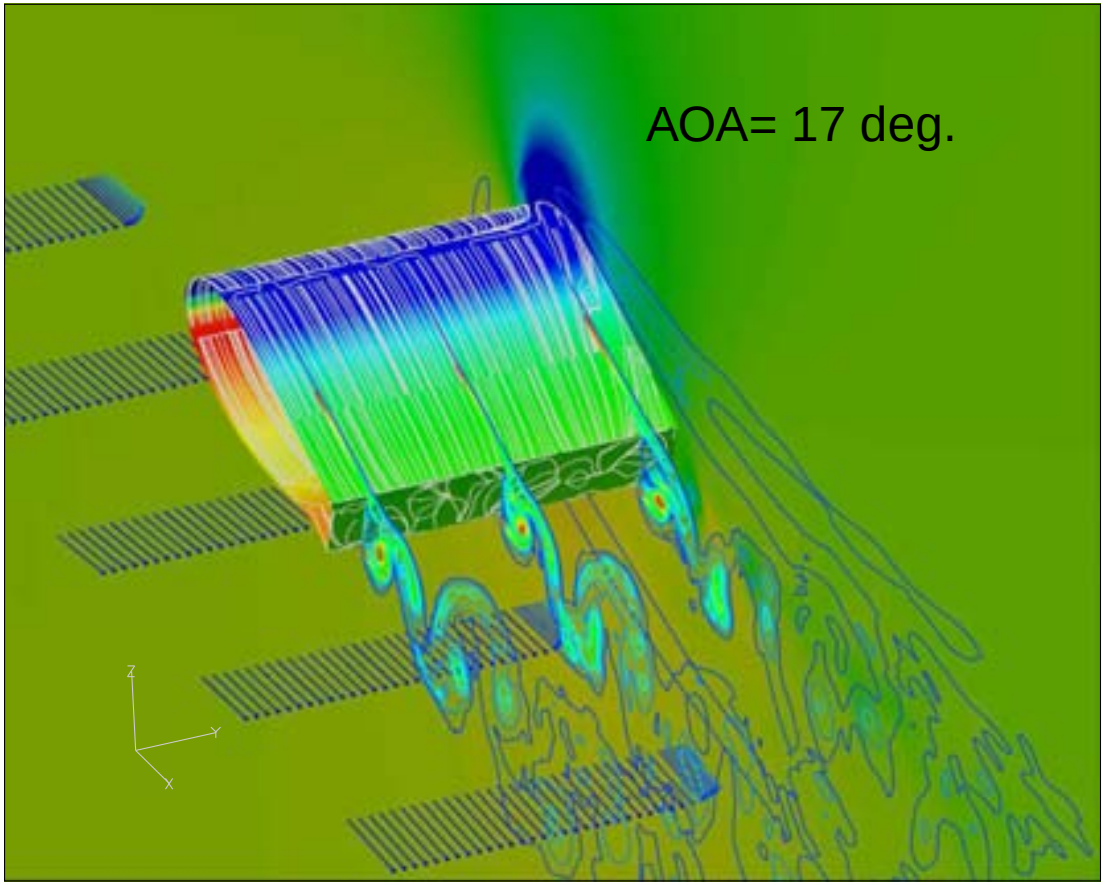

Niels N. Sørensen,
Risø DTU

3D Flow Patterns

Operational conditions

- $Re = 666.000$
- Free transition
- Span length is equal to 2 chords

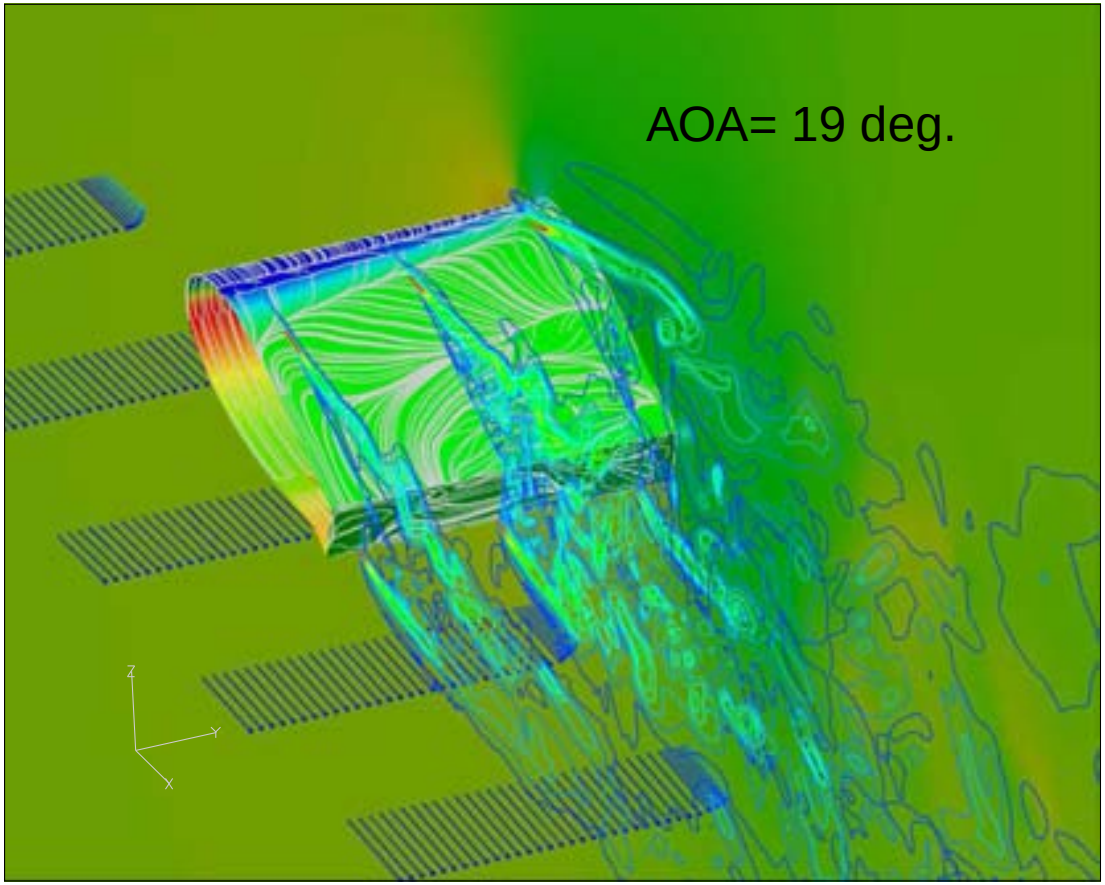

Niels N. Sørensen,
Risø DTU

Comparison between different techniques

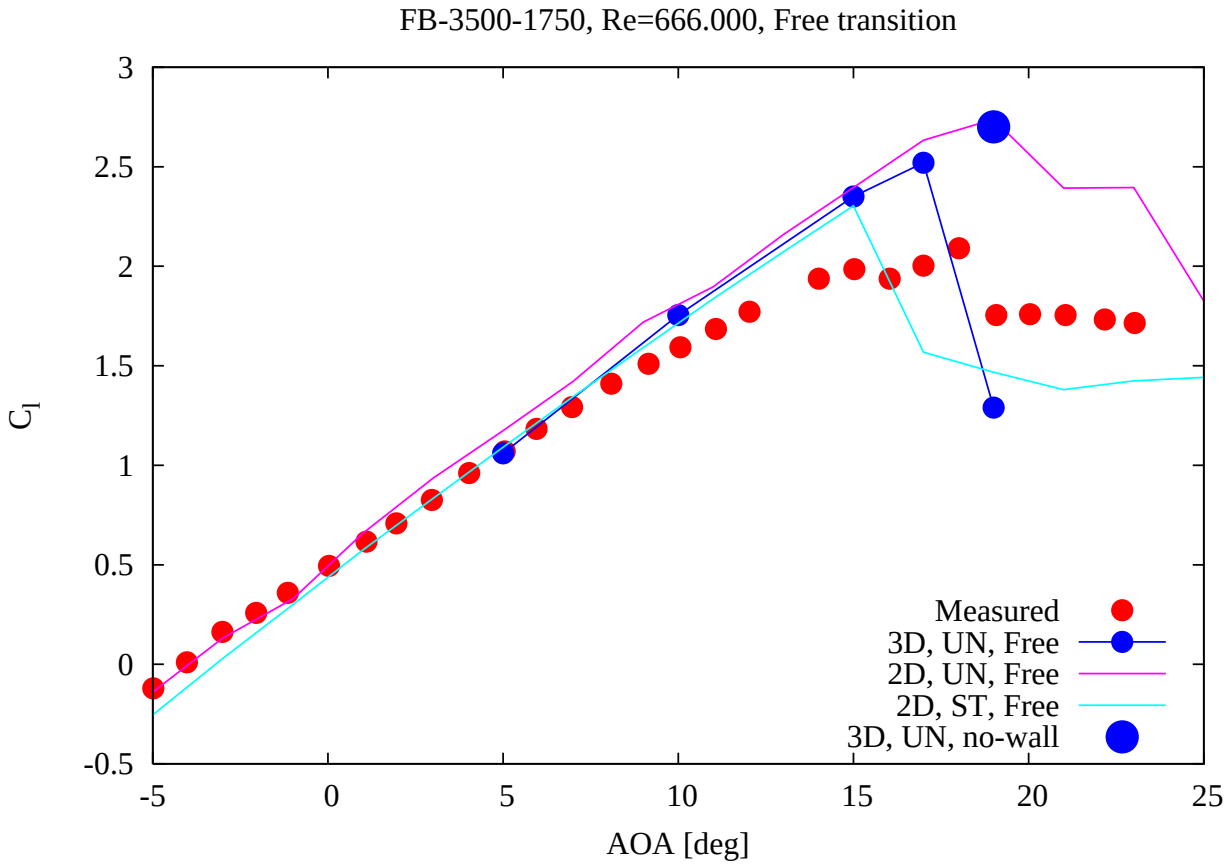

- 3D unsteady comp. agrees better than 2D unsteady comp
- By coincidence 2D steady captures nearly the same value as 3D unsteady

Niels N. Sørensen,
Risø DTU

Comparison between different techniques

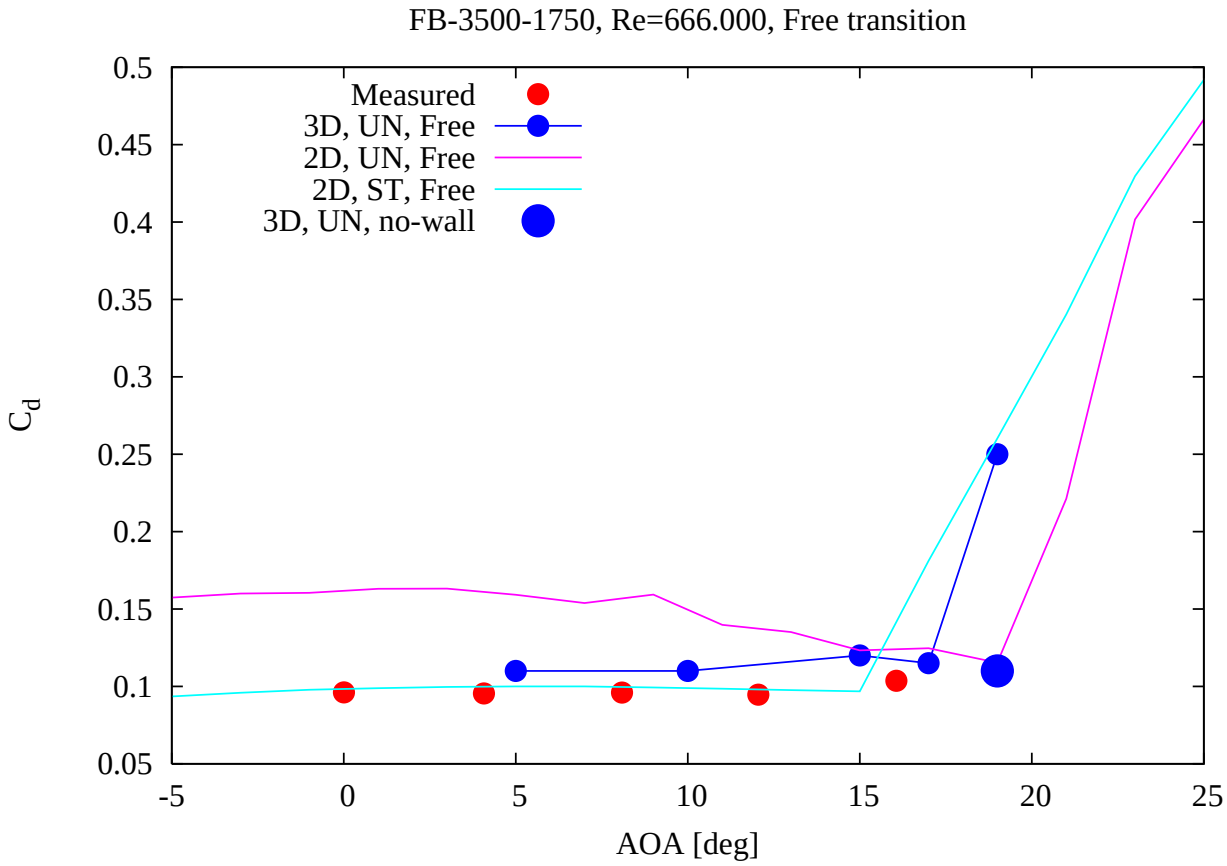

- 3D unsteady comp. agrees better than 2D unsteady comp
- By coincidence 2D steady captures nearly the same value as 3D unsteady

Niels N. Sørensen,
Risø DTU

Resume of 3D computations

Results for the FB-3500-1750 Airfoil

- At low angles of attack (<17 degrees) the inclusion of the wall junction only caused minor changes
- At high angle of attack (>17 degrees) the wall junction induces severe 3D flow and low lift
- Tunnel effects may play an important role in experimental and computational evaluation of FB airfoils

Flatbacking the DU-97-W-300

Operational conditions, $Re = 3.2 \times 10^6$, Free transition
Opening the trailing edge, towards suction or pressure side

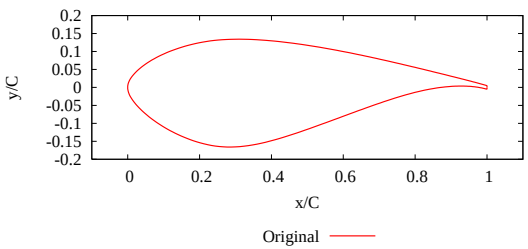

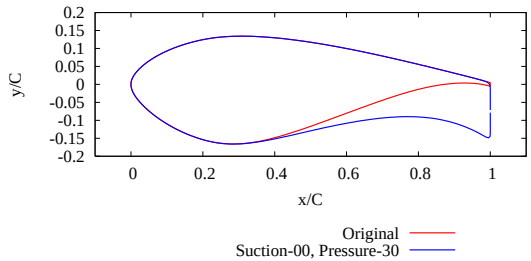

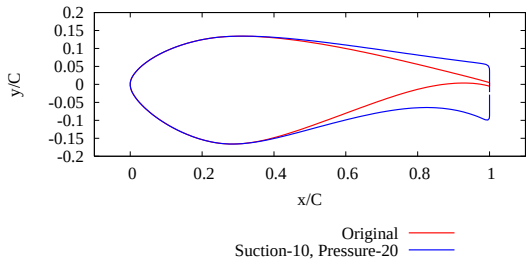

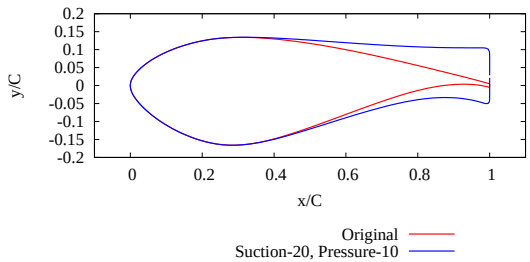

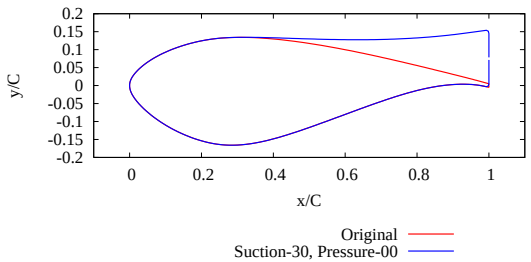

Niels N. Sørensen,
Risø DTU

Airfoil performance

Operational conditions, $Re = 3.2 \times 10^6$, Free transition
All generated flatback airfoils have higher max lift

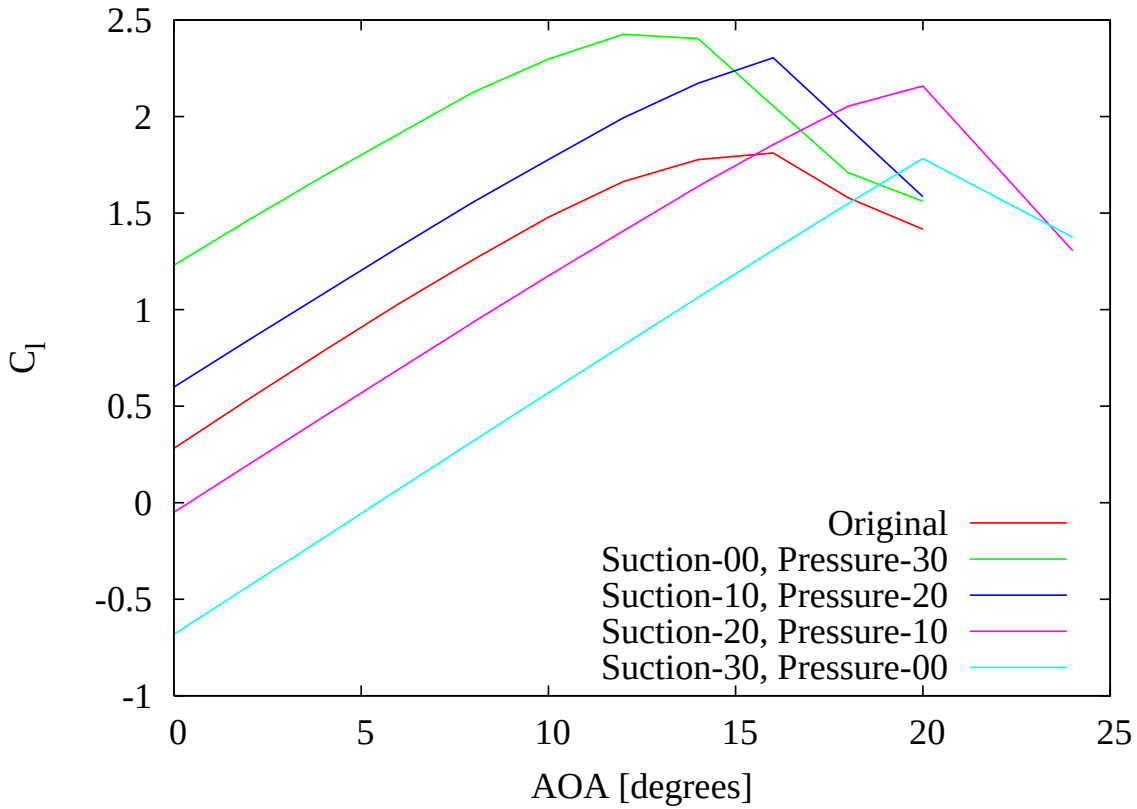

Niels N. Sørensen,
Risø DTU

Airfoil performance

Operational conditions, $Re = 3.2 \times 10^6$, Free transition

All generated flatback airfoils have higher drag

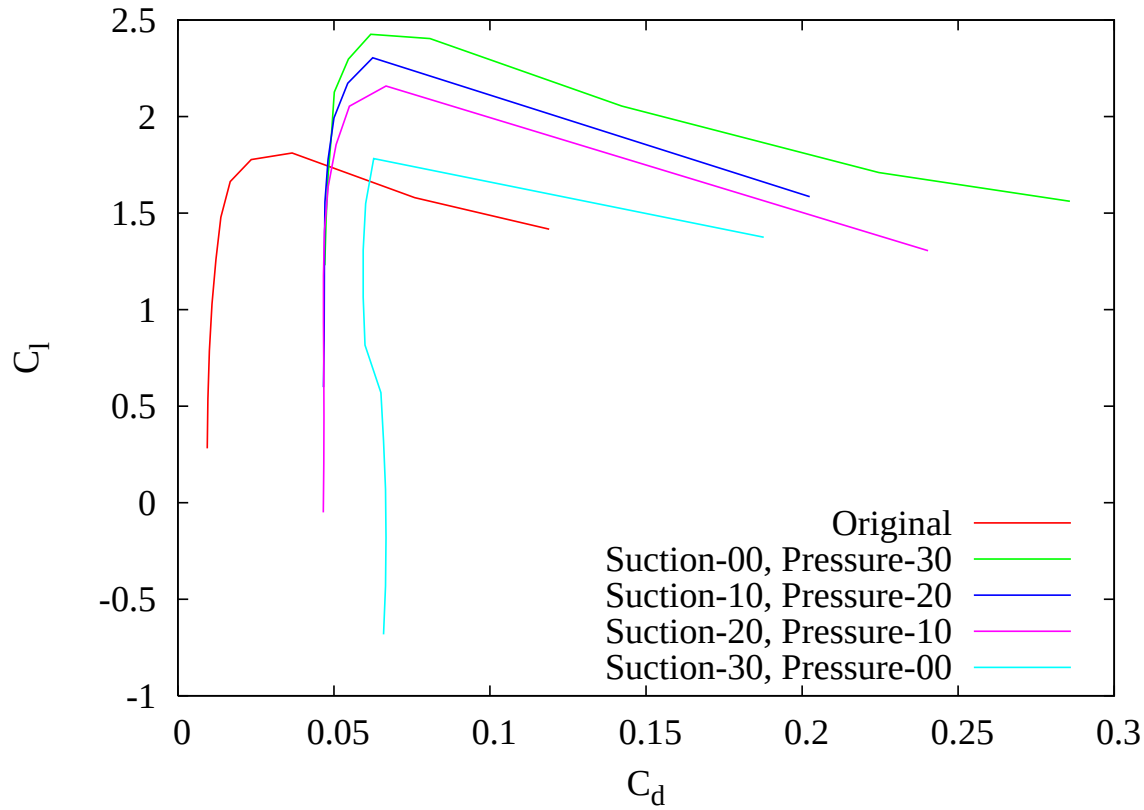

Niels N. Sørensen,
Risø DTU

Resume of parametric study

- The flatback version has a higher lift
- The most efficient one is the one opened solely to the pressure side
- The drag increases for all airfoils, and generally to the same level

Conclusion and Further Work

Conclusions:

- We believe that both the 2D/3D CFD solvers can be used to evaluate flatback airfoils
- Computations indicate that high lift can be obtained, and the exp. of FB-3500-1750 indicates that this may be true
- It is clear from the parametric study that to increase the lift the opening of the trailing edge most be done towards the pressure side

Further work:

- We need to design an airfoil for tunnel test
- We need to evaluate the dynamic performance (3D dynamic stall comp.)
- We need to evaluate the performance of flatback in rotational environment
- Noise issues from the vortex shedding at the thick trailing edge

10 Status of airfoil design

Status of airfoil design and plans for wind tunnel tests of new thick airfoils

Christian Bak, Mac Gaunaa, Niels Sørensen, Franck Bertagnolio

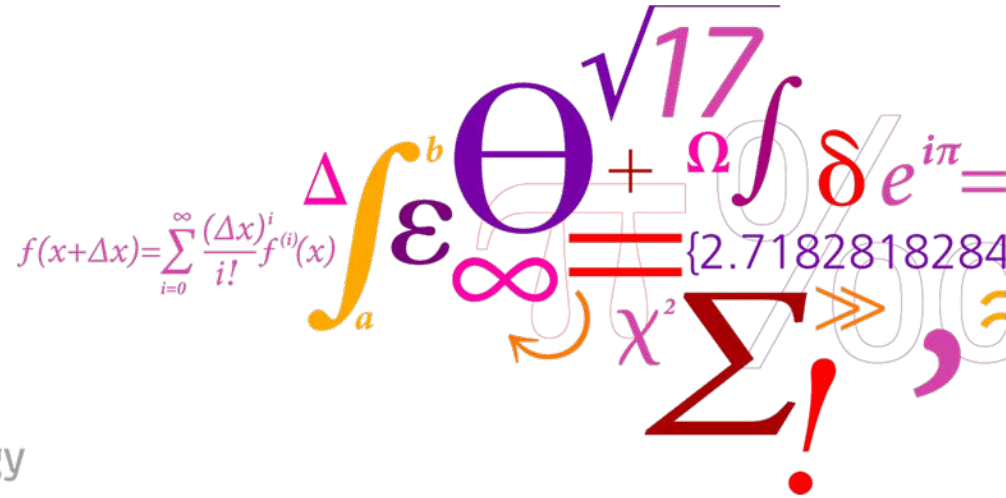

Risø DTU
National Laboratory for Sustainable Energy

Background
Airfoils designed and tested in the past

- **Risø-A1**: **High cl-cd-ratio, good stalling characteristics, good roughness sensitivity**
- **Risø-P**: High cl-cd-ratio, **very good stalling characteristics**, good roughness sensitivity
- **Risø-B1**: Medium cl-cd-ratio, **high lift**, **very good roughness insensitivity**
- **Risø-C2**: High cl-cd ratio, high lift, very good roughness insensitivity, **high moment of resistance**

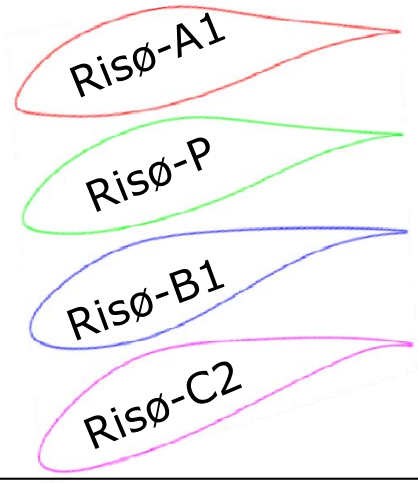

Stall regulation, t/c 12% to 24%

Pitch regulation, t/c 15% to 24%

Pitch reg var speed, t/c 15% to 53%

Pitch reg var speed, t/c 15% to 36%

Status
Recent designs

- New aspects taken into account:
  - Trailing edge noise (mainly thin and medium thick airfoils)
    - TNO model
    - Glegg model
  - Thick airfoils with high lift and low sensitivity to roughness
    - Flat back airfoils
    - Multielement airfoils

Thick multielement airfoils
Slat size investigation

Big slats

0.3c and 0.5c

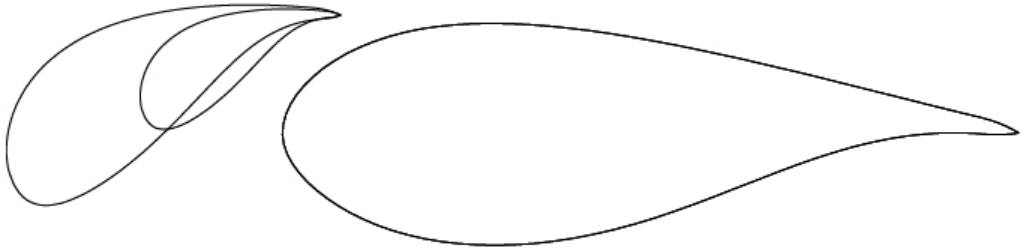

Small slats

0.1c and 0.2c

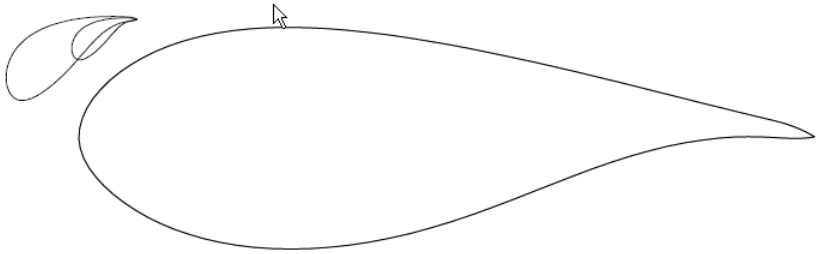

Thick multielement airfoils
Slat size investigation

Slat/main chord length ratio	c_{slat}/c_{main}	0.1	0.2	0.3	0.5
Relative angle of slat	β	-30.0^o	-30.0^o	-27.5^o	-27.5^o
Position of slat TE along main airfoil	$s_{TE,slat}$	0.15	0.15	0.15	0.15
Distance between slat TE and main airfoil	$n_{TE,slat}$	0.05	0.05	0.05	0.05
Slat additional parabolic camber	$k_{camber,slat}$	0.1	0.1	0.1	0.1
Lift ratio slat/main airfoil at max l/d	L_{slat}/L_{tot}	1%	33%	50%	64%
Max lift ratio multiple/isolated main airfoil	L_{mult}/L_1	~ 1	~ 1.5	~ 2.2	$>\sim 2.5$

Further work

- Airfoil designs
  - Thin low noise airfoil will be designed (in EUDP 2009 Low Noise Airfoil project)
  - Final multielement airfoil will be designed
  - Flat back airfoil will be designed
- Wind tunnel tests
  - Multielement airfoil and flat back airfoil will likely be tested in the LM LSWT around summer 2011

Risø DTU is the National Laboratory for Sustainable Energy. Our research focuses on development of energy technologies and systems with minimal effect on climate, and contributes to innovation, education and policy. Risø has large experimental facilities and interdisciplinary research environments, and includes the national centre for nuclear technologies.

Risø DTU
National Laboratory for Sustainable Energy
Technical University of Denmark

Frederiksborgvej 399
PO Box 49
DK-4000 Roskilde
Denmark
Phone +45 4677 4677
Fax +45 4677 5688

www.risoe.dtu.dk